UNIVERSITY OF KENT

A Study of the Synergies Between Control Mechanisms in the Immune System and the Variable Structure Control Paradigm

by

Anet Jorim Norbert ANELONE

Supervisors

Professor Sarah Spurgeon OBE

Dr. Xinggang Yan

A Thesis Submitted to The University of Kent
For The Degree of Doctor of Philosophy
in Electronic Engineering

in the
School of Engineering and Digital Arts

January 2017

Abstract

This thesis argues that variable structure control theory finds application in immunology. The immune system maintains a healthy state by using feedback to switch on and off immune responses. Experimental and mathematical work has analysed the dynamics of the immune response of T cells, relatively little attention has been paid to examine the underlying control paradigm. Besides, in modelling and simulation studies, it is necessary to evaluate the impact of uncertainty and perturbations on immunological dynamics. This is important to deliver robust predictions and insights. These facts motivate considering variable structure control techniques to investigate the control strategy and robustness of the immune system in the context of immunity to infection and tolerance. The results indicate that the dynamic response of T cells following foreign or self-antigen stimulation behaves as a naturally occurring switched control law. Further, the reachability analysis from sliding mode control highlights dynamical conditions to assess the performance and robustness of the T cell response dynamics. Additionally, this approach delivers dynamical conditions for the containment of Human Immunodeficiency Virus (HIV) infection by the HIV-specific CD8+ T cell response and antiretroviral therapy by enforcing a sliding mode on a manifold associated with the infection-free steady-state. This condition for immunity reveals particular patterns for early diagnosis of eventual success, marginal and failure cases of antiretroviral therapy. Together, the findings in this thesis evidence that variable structure control theory presents a useful framework to study health and disease dynamics as well as to monitor the performance of treatment regimes.

Acknowledgements

Thanks to GOD A

I would like to thank Professor Sarah K. Spurgeon OBE and Dr. Xinggang Yan for their supervision. My deepest gratitude to Sarah for her trust and care.

I am also grateful to Professor Yury Orlov, Dr. Harsal B. Oza, Dr. Tobias Von-der-Haar, Dr. Peter Lee, Dr. Markus Reichhartinger. Additionally, I would like to thank people from the School of Engineering and Digital Arts for their support during my doctoral research.

I will always be thankful for the financial support received from my dear country the Republic of Cote d'Ivoire, La GOSPA and from the University of Kent.

Great thanks to my parents. I want to thank my father Anelone Kouakououa Jean-Paul for his words of encouragements; Sois courageux, mon fils. Besides, this thesis would have not been possible without my mother Dr. Anelone Sawadogo Limnya and her phenomenal Faith in God Jesus-Christ. I would also like to thank my brothers, my sisters (gros bisou a Cindyn) and my extended family for their support.

Special thanks to Tonton Andre Marie Tuho for his help during my stay in the UK. In addition, I am grateful to my British family, David Miller and his family for their warm hospitality. With great joy, I want to say Merci a toutes mes Mamans. In particular, I am grateful to maman Rumbi, maman Liliane, maman Christine, manan Celine, maman Beatrice, maman Salmon just to name a few.

I want to express my sincere gratitude to all my dear friends around the world.

I cannot find words to express my gratitude to the catholic and salsa community in Canterbury. The catholic society (CATSOC) of the University of Kent has become my family in Canterbury. The Franciscan Study Center was home to me. I wish to thank Fr. Peter Geldard, Judith, Fr. Thom, and Fr. Peter C.

With all my heart, I want to thank and bless each person that God has put in my way to contribute to the joy and success of my pilgrimage in Canterbury.

I dedicate this thesis to my dear Chericoco Adjoua.

Glory to GOD Ω

Contents

Abstract i

Acknowledgements ii

Contents iii

List of Abbreviations v

List of Figures v

1 Introduction 1
- 1.1 Overview . . . 1
- 1.2 Thesis organisation . . . 5
- 1.3 Contributions . . . 7

2 Variable Structure Control Paradigm 10
- 2.1 Introduction . . . 10
- 2.2 Basic principles of switched control system . . . 13
- 2.3 Sliding mode control design and properties . . . 18
- 2.4 Robustness properties . . . 21
- 2.5 Conclusion . . . 26

3 Synergies Between the Dynamics of the Immune Response of T Cells and the Variable Structure Control Paradigm 27
- 3.1 Introduction . . . 27
- 3.2 Review of the specific T cell response . . . 29
- 3.3 Synergies between the dynamics of the immune response of T cells and the variable structure control paradigm . . . 32
- 3.4 Robustness analysis . . . 40
- 3.5 Conclusion . . . 46

4 Self-Tolerance Mechanism of T Cells, a natural VSC 48
- 4.1 Introduction . . . 48
- 4.2 Review of tolerance mechanisms . . . 50
- 4.3 Analysis of dynamics of self-tolerance . . . 52
- 4.4 Sliding mode control framework . . . 62
- 4.5 Conclusion . . . 72

5 Evaluation of the Conditions for the containment of HIV infection by the HIV-specific CD8+ T Cell response, a Variable Structure Control Perspective **74**

5.1 Introduction . . . 74
5.2 Model description . . . 81
5.3 Dynamical condition for immunity using the reachability analysis . . . 83
5.3.1 Candidate control function modelling the cytolytic killing mechanism 87
5.4 Steady-state condition for immunity provided by the reproductive ratio . . 90
5.5 Simulation experiments . . . 94
5.5.1 Constant cytolytic killing action . . . 97
5.5.2 Dynamical cytolytic killing action . . . 100
5.6 Conclusion . . . 105

6 Case Study: Prediction of the Containment of HIV Infection by Antiretroviral Therapy - a Variable Structure Control Approach **106**

6.1 Introduction . . . 106
6.2 System model . . . 109
6.2.1 The reproductive ratio, a steady-state condition for the success of antiretroviral therapy . . . 113
6.3 A reachability condition to monitor the containment of HIV infection . . . 114
6.4 Parameter identification . . . 116
6.4.1 The clinical data sets . . . 116
6.4.2 Parameter identification procedure . . . 117
6.4.3 Parameter estimation results . . . 121
6.5 Prediction of the outcome of antiretroviral treatment . . . 128
6.5.1 Effective treatment . . . 129
6.5.2 New insight into marginal cases . . . 130
6.5.3 Failure cases . . . 135
6.6 Conclusion . . . 137

7 Conclusions and Future work **139**

7.1 Conclusions . . . 139
7.2 Future work . . . 142

A Pseudo-code of the Multi-Point Identification Method **145**

B Estimates of HIV Dynamics Parameters following Antiretroviral Therapy **151**

Bibliography **156**

List of Publications **173**

List of Abbreviations

Acronym	What (it) Stands For
ART	**A**nti**R**etroviral **T**herapy
APCs	**A**ntigen **P**resenting **C**ells
DS	**D**ouble **S**aturation
HAART	**H**ighly **A**ctive **A**nti**R**etroviral **T**herapy
HIV	**H**uman **I**mmunodeficiency **V**irus
LCMV	**L**ymphocytic **C**horiomeningitis **V**irus
ODE	**O**rdinary **D**ifferential **E**quation
RNA	**R**ibonucleic **A**cid
SMC	**S**liding **M**ode **C**ontrol
VSC	**V**ariable **S**tructure **C**ontrol
VSCS	**V**ariable **S**tructure **C**ontrol **S**ystem

(1)

List of Figures

1.1 The approach and contributions 7

2.1 Phase portrait of the double integrator system (2.1) with a fixed structure control strategy (2.2). 14
2.2 An Electron 15
2.3 An Electron 16
2.4 Oscillator system (2.6) with a variable structure control law. $\alpha = 0.6$ and $m = 1.1$ from (2.9) (2.7). 17
2.5 Comparison of the output response $y(t)$ of the oscillator system (2.7) generated by the stable fixed structure control in Fig. 2.3 versus the switched control in Fig. 2.4. The output response of the oscillator system shows that the designed switched control law yields a faster settling time than the stable feedback alone. 18
2.6 Phase portrait of the unstable sub-system of (2.7) with the fixed control structure $u(t) = -0.6$ with poles at 0.5 and -1.2 19
2.7 Time evolution of the switching function (2.8) for the pendulum system (2.10) with $a_1 = 0.5$ under the switched control (2.14) with $m = 1$ and $\rho = 1$ 23
2.8 Phase portrait of the double integrator system (2.1) and the pendulum system (2.10) with a sliding mode 23
2.9 Pendulum system (2.10) produced by a smooth control (2.23). 25

3.1 Time evolution of the population dynamics of specific CD8+ T cells after acute infection from experimental data in [1, 2] 31
3.2 Phase portrait analysis of the T cell population dynamics of (3.1)-(3.3) with an activation function having a fixed structure. Top: the trajectory of the T cell response generated by $\mathcal{F}(t)) = 1$ is shown. This induces unstable dynamics and a motion away from the origin. The trajectory depicts an exponential and unbounded expansion of activated T cells. Bottom: the trajectory of the T cell response generated by $\mathcal{F}(t)) = 0$ is seen. The trajectory exhibits a stable motion towards the origin. This motion depicts the contraction of the population of activated T cells and the formation of memory T cells. . . 35
3.3 Population dynamics of the specific T cell response of the model (3.1)-(3.3) with a discontinuous immune response function (3.4). 37

3.4 Simulation of the scenario of CD8+ T cell population dynamics following acute infection. Top: Time evolution of the population dynamics of the antigen-specific T cell response, closed-loop system formed by (3.1)-(3.3),(3.6). Bottom: the time evolution of the antigen-dependent activation function eq (3.5). Following infection, the magnitude of the activation function is at a maximum. This induces the reduction of the state N and an increase of the state A. The state variable N decreases because naive T cells become activated T cells. The state variable A increases due to the expansion of the population of activated T cells. When the magnitude of the immune response function falls to zero, the expansion phase is interrupted. There is production of memory T cells, the state M increases whilst the activated T cells undergo contraction i.e the state A decreases. Consequently, the activation function prescribes the variation over time of the total population of the antigen -specific T cells $(N + A + M)$ following infection. 38
3.5 Phase portrait of the trajectories of the specific T cell response. Closed-loop system formed by (3.1)-(3.3),(3.6) with the sigmoidal antigen-dependent activation function (3.5) 39
3.6 Time evolution of the sliding surface and reachability condition for the dynamics of the specific T cell response described by the closed-loop system formed by (3.1),(3.3),(3.6) and (3.10) with the antigen-dependent activation function (3.5) 43
3.7 Time evolution of the reachability condition and total population of antigen-specific T cells in the presence of a strong biological perturbation. $d_u = -2A$ for $t > 8$ and $d_u = 0$ otherwise. Model of the specific T cell response described by the closed-loop system formed by (3.1),(3.3),(3.6) and (3.10) with the antigen-dependent activation function (3.5) 45
3.8 Time evolution of the reachability condition and total population of antigen-specific T cells following infection with an undesirable proliferation signal d_u at day 23. Model of the specific T cell response described by the closed-loop system formed by (3.1),(3.3),(3.6) and (3.10) with the antigen-dependent activation function (3.5) 47

4.1 Model (4.1) of self-tolerance/autoimmunity where the immune response function describes the dynamic response of self-reacting T cells after self-antigen stimulation 52
4.2 Variation of the poles with respect to an increase in the value of the open-loop control $0 \leq u \leq 2$ for the system (4.1) 55
4.3 Simulation of the open-loop system $u = 0$ in system (4.1). 56
4.4 Autoimmune disease scenario when the open-loop $u = 0.7$ in system (4.1) . 56
4.5 Different personal immune response curves (4.7)-(4.10): - linear, + Michaelis-Menten, o sigmoidal and x discontinuous. 62
4.6 3D plot of the dynamical behaviour of the immune system (4.1). Comparison of the transient dynamics resulting from the implementation of the candidate immune response functions (4.7)-(4.10). H.S.: Healthy tolerance steady-state (4.5), A.S.: Autoimmune disease steady-state. T: Target cells, D: damaged cells and C: self-reacting effector T cells. 63
4.7 Model (4.1) of self-tolerance/autoimmunity where the immune response function u (4.20) is an adaptive sliding mode control feedback which imposes a robust state of self-tolerance via inhibition of self-reacting T cells 67

4.8 Immunological dynamics driven to the tolerance steady-state (4.5). Closed-loop system (4.1) with the negative tolerance feedback (4.20) 68
4.9 Time course of the switching function (4.13). Closed-loop system (4.1) with the negative tolerance feedback (4.20). 69
4.10 Time course of the reachability condition (4.21). Closed-loop system (4.1) with the negative tolerance feedback (4.20). 70
4.11 Time course of u_{eq}, the equivalent control signal (4.22) $t > t_s = 5days$. Closed-loop system (4.1) with the negative tolerance feedback (4.20) 70
4.12 Comparison of the performance of control laws u_1 in (4.20) and $u_2 = kD$ with parameter disturbance: $\lambda = 2$, $\mu = 0.1$, $\beta = 0.45$, $\alpha = 0.145$, $\gamma = 0.01$ and $k = 0.002$ 72

5.1 Model (5.1) of HIV infection dynamics in which infected cells in the eclipse phase are killed by the cytolytic effect of CD8+ T cells 82
5.2 Open-loop system (5.1). Simulation of HIV infection in the absence of a killing action from the HIV-specific CD8+ T cell response. $T(0) = 2.10^6$; $I(0) = P(0) = 0$; $V(0) = E(0) = 1$. $f = 1; \mathcal{K} = g_{max} = 0$. 95
5.3 Time evolution of the dynamical condition for immunity (5.9) in absence of the HIV-specific CD8+ T cell response $u_C = 0$. 96
5.4 Time evolution of the sliding surface (5.5) with $u_C = 0$. 97
5.5 Time evolution of the dynamical condition for immunity (5.13) with the cytolytic killing mechanism of the HIV-specific CD8+ T cell response $u_{C1} = -10I$ 98
5.6 Time evolution of the sliding manifold (5.5) with $u_{C1} = -10I$ 99
5.7 Time evolution of the control action (5.12) with $u_{C1} = -10I$ 99
5.8 Closed-loop dynamics (5.1). Simulation of HIV infection with a potent HIV-specific CD8+ response with u_{C1}. $T(0) = 2.10^6$; $I(0) = P(0) = 0$; $V(0) = E(0) = 1$. $f = 1$; $h_k = 1$ 101
5.9 Time evolution of the control action (5.25) with u_{C3} $h_k = 1$ 102
5.10 Time evolution of the reproductive ratio using u_{C3} (5.25) with $h_l = 1$. . . . 102
5.11 Time evolution of the dynamical condition for immunity (5.16) with the cytolytic killing mechanism of the HIV-specific CD8+ T cell response u_{C3} (5.25) 103
5.12 Time evolution of the sliding surface (5.5) with u_{C3} (5.25). 104

6.1 Model (6.1) of HIV infection dynamics following antiretroviral therapy (ART) 110
6.2 Comparison of the time evolution of measured CD4+ T cell count and HIV load versus its estimates for pt_1 using the HIV model (6.7). 124
6.3 Comparison of the time evolution of measured CD4+ T cell count and HIV load versus its estimates for pt_8 using the HIV model (6.7). 125
6.4 Comparison of the time evolution of measured CD4+ T cell count and HIV load versus its estimates for pt_{11} using the HIV model (6.7). 125
6.5 Comparison of the time evolution of measured CD4+ T cell count and HIV load versus its estimates for pa_3 using the HIV model (6.7). 126
6.6 Comparison of the time evolution of measured CD4+ T cell count and HIV load for pt_1. Original data and the responses generated with parameters estimated in the presence of additional noise and without additional noise are presented. HIV model (6.7). 127

6.7 Comparison of the time evolution of measured CD4+ T cell count and HIV load for pa_3. Original data and the responses generated with parameters estimated in the presence of additional noise and without additional noise are presented. HIV model (6.7). 128
6.8 Comparison of the time evolution of measured CD4+ T cell count and HIV load versus its estimates for pa_{24} using the HIV model (6.7). 129
6.9 Time evolution of the dynamical condition for immunity (6.18) using simulation results for pt_1 130
6.10 Time evolution of the dynamical condition for immunity (6.18) using simulation results for pa_{13} 131
6.11 Time evolution of the switching function (6.15) and dynamical condition for immunity (6.18) for pt_8 132
6.12 Time evolution of the switching function (6.15) and dynamical condition for immunity (6.18) for pa_{34} 133
6.13 Time evolution of the switching function (6.15) and dynamical condition for immunity (6.18) for pt_{11} 133
6.14 Phase portrait of the sliding surface (6.15) for pt_8 134
6.15 Phase portrait of the sliding surface (6.15) for pt_{11} 134
6.16 Time evolution of the switching function (6.15) along with the dynamical condition for immunity (6.18) for pa_3 135
6.17 Time evolution of the dynamical condition for immunity (6.18) using simulation results for pa_3 136
6.18 Time evolution of the dynamical condition for immunity (6.18) using simulation results for pa_8 and pa_{10} 136
6.19 Phase portrait of the sliding surface (6.15) for pa_3, pa_8 and pa_{10} 137

B.1 Comparison of the time evolution of the estimated dynamics of CD4+ T cell count and HIV load with different precision. Results for pt_1. l (6.7). 154
B.2 Comparison of the time evolution of the estimated dynamics of CD4+ T cell count and HIV load with different precision. Results for pt_8. l (6.7). 155
B.3 Comparison of the time evolution of the estimated dynamics of CD4+ T cell count and HIV load with different precision. Results for pa_3. l (6.7). 155

Chapter 1

Introduction

1.1 Overview

This thesis presents an interdisciplinary research between control engineering and mathematical immunology. In this thesis, the variable structure control paradigm is applied to study the dynamics of the specific T cell response as well as to formulate dynamical conditions for the maintenance of desirable immunological outcomes. The main objective is to improve the understanding of health and disease dynamics by using a control approach in order to contribute to modelling and simulation in immunology.

Control theory is a mature discipline in the analysis of dynamical systems with uncertainty. Mathematical models of engineering or phenomenological processes are constructed to capture the essential dynamics of the system in order to produce realistic input-output behaviour. As an abstraction of reality, there are discrepancies between a model and the real system. Furthermore, different factors such as ageing of the real system, disturbances, neglected dynamics and variations in parameter values contribute to disparities between every model and the real system. It is common practice to begin analysing the stability and dynamical behaviour of the mathematical model at nominal conditions before considering potential uncertainties. In fact, it is important to design a control strategy which exhibits robustness properties in order to enforce the desired stability and performance despite uncertainty. Consequently, several analytical techniques have been developed to study uncertain dynamical systems and to formulate robust control strategies.

A fixed structure control approach consists in designing and imposing a single structure control strategy such as a proportional feedback for the given system to meet the design objectives and required robustness [3–5]. In contrast, a variable structure control approach allows the control structure to change so that in high frequency the system dynamics can achieve the desired dynamical behaviour and robustness properties [6–8]. This approach offers several benefits and has been applied successfully to mechanical, electrical and chemical systems [9–13]. Switching between different dynamics is advantageous because the desirable properties of several subsystems can be combined so that the overall system possesses new and enhanced dynamical behaviours, including properties that are not present in any of the individual subsystems alone. Moreover, implementing a variable structure control strategy has been demonstrated to yield strong robustness properties in the presence of parameter uncertainties [7, 10, 14–16].

Sliding mode control is a special type of variable structure control [7, 10, 17]. In sliding mode control, a switching function is chosen to ensure the system yields the desired stability and performances when the states of the system lie on this manifold. Using Lyapanov stability analysis [14–16, 18], a reachability condition, which represents a condition for the sliding manifold to be attractive to the states of the system is, formulated. Next, a variable structure control is designed to satisfy this reachability condition so that the system states lie in the vicinity of the chosen switching function. Typically, a discontinuous or sigmoidal control function is implemented [19–23]. The sliding mode control approach provides two fundamental benefits: reduced order dynamics and total invariance to a certain class of uncertainty implicit in the input channels [7, 10, 13, 24]. Furthermore, using the concept of equivalent control, which represents the theoretical injection to maintain the sliding motion, the dynamics of unknown input signals or disturbances can be reconstructed and estimated [25–28]. Hence, the variable structure control theory provides a suitable framework for the analysis of the systems with switching mechanisms, in addition to the impact of uncertainty and disturbances.

In immunology, there is a need to understand the dynamics of the immune system in various contexts, such as acute infection, chronic infection and autoimmunity [29–31]. This knowledge is important because it provides information on health and disease dynamics in vivo and contributes to the improvement of treatment and prevention strategies. In recent decades, mathematical studies have been conducted to investigate the dynamics of the immune system [30, 32, 33]. Typically, a system of Ordinary Differential Equations (ODEs)

inspired by Predator-Prey dynamics in ecology is constructed to model the immunological phenomenon of interest. In addition to experimental studies, the mathematical modelling of immune cells and virus dynamics in vivo has delivered relevant insights, including information on HIV dynamics in vivo [34–36]

In order to formulate useful and robust predictions from a given model, it is important to understand the impact of parameter and modelling uncertainty, as well as the discrepancies between the observed dynamics and the dynamics produced by the model. In fact, uncertainties in the model are associated with a number of different factors such as lack of biological data for parameter estimation, unmeasurable state variables, ageing or patient-to-patient variability. This motivates the use of tools from variable structure control in immunological modelling and simulation because they enable the assessment of the effects of uncertainty on the dynamics and predictions of the models.

Current findings in immunology present the immune system as a dynamical system with feedback to maintain a robust healthy state in the body [2, 31, 37]. In fact, the immune system can be regarded as a set of cellular and molecular feedback mechanisms which regulate and control the immune response in order to preserve a healthy immunological homeostasis [31, 38–40]. In [41], it was hypothesised that the population of immune cells and antibodies either increases or decreases depending upon the antigen stimulation. The development of experimental facilities has validated this hypothesis. Additionally, experimental studies have provided kinetic data showing sharp changes in the population dynamics of T cells following acute infection to achieve immunity and prevent tissue damage [1, 42, 43].

Following vigorous infection, the population of responding antigen-specific T cells increases exponentially from a small number to a large number of cells at the peak of the response. After this peak, which occurs a few days post-infection, a large number of T cells die and few cells survive [44, 45]. This dynamical behaviour is known as the immune response program. This immunological program dictates the expansion, contraction and memory phase of the T cell response. From an immunological perspective, this dynamic control of the population size of T cells occurs to contain the infection, as well as to prevent autoimmunity. Hence, the population dynamics of the specific T cell response exhibit an inherent switching law which underpins the observed cellular dynamics.

The cellular and molecular mechanisms driving the population dynamics of the specific T cell response remain the subject of active research. Consequently, different mathematical

approaches have been proposed to model the dynamics of the antigen-specific T cell response [29, 38, 46, 47]. In previous analyses of the population dynamics of the specific T cell response, experimental results on Lymphocytic Choriomeningitis Virus (LCMV) infection in mice have often been considered. Experimental studies on LCMV infection in [1, 2, 48] have provided information on the kinetic variation of the number of CD8+ T cells in the spleen over time after acute and chronic infection. These kinetic data have been useful in the parameterisations of ODE models of the specific CD8+ T cell response. The focus of previous modelling approaches was on formulating different biological hypotheses for the immune response paradigm in order to explain the observed cellular dynamics [1, 29, 39]. Nonetheless, the control features that these dynamics yield have not been investigated. Further, previous mathematical studies neglected to analyse the robustness of the expansion/contraction dynamics of the CD8+ T cell response following acute and chronic infection.

A reason to consider that a switched control paradigm is at play is due to the fact that despite the differences in mathematical expression and related biological assumptions, sensible models of the T cell response provide a switching mechanism to engender the required changes in T cell population dynamics to capture the expansion, contraction and memory phase of the immune response. Additionally, a number of approaches have used saturation functions to prescribe the required changes in T cell population [29, 46]. Interestingly, the work in [38] referred to the immune response program as a switching process which governs the dynamic response of T cells post-infection. Further, the authors in [38] investigated the characteristics of candidate immune response functions. From the viewpoint of control engineering, the use of saturation functions to model the immune response program engenders a dynamic change in feedback regimes. This motivates the investigation of the synergies between the variable structure control paradigm and the T cell immune response dynamics. These investigations are important to improve understanding of the dynamics and robustness properties of the antigen-specific T cell response.

Besides, the dynamic response of the total T cell population plays a major role in the maintenance of self-tolerance [31, 49, 50]. In mathematical studies, candidate immune response functions have been proposed to describe the dynamic response of self-reacting T cells in order to study the mechanism of self-tolerance and the onset of autoimmunity [40, 51, 52]. It is important to analyse means by which candidate immune response functions

establish a robust state of tolerance. This is useful to understand how self-tolerance is maintained in vivo as well as to inform for candidate treatment for autoimmunity.

In the study of Human immunodeficiency Virus infection dynamics in vivo, the impact of the HIV-specific CD8+ T cell response in the containment of the infection is a critical research topic because it yields the potential for developing immunotherapies which will relieve patients from the lifelong uptake of antiretroviral drugs [30, 36, 53]. It remains unclear how the killing mechanisms of CD8+ T cells enforces an asymptomatic state in HIV-infected patients. In the last three decades, different mathematical expressions have been proposed to model the impact of HIV-specific CD8+ T cell response [30, 54, 55]. The control of HIV infection is often evaluated by computing the reproductive ratio [34, 35, 56]. In effect, the reproductive ratio sets a static threshold condition to determine whether the infection will spread or not.

Although it was mentioned that the HIV-specific CD8+ T cell response might control HIV infection [56–58], no formal control analysis was conducted on this immunological control mechanism. This motivates the analysis of the containment of HIV infection in vivo using a control engineering approach. The objective is to improve the understanding of the control performance of the HIV-specific CD8+ T cell response and antiretroviral therapy during the progression of the infection.

1.2 Thesis organisation

The thesis is organized as follows:

Chapter 2 provides a background on the VSC paradigm. The purpose of this chapter is to introduce analytical tools from VSC theory. The phase portrait analysis of the trajectories of an oscillator system with different control strategies is used to illustrate the basic principles and benefits of the variable structure control approach. Subsequently, a pendulum system is used to present the framework of sliding mode control. The design procedure for a sliding mode along with the reachability condition and the concept of the equivalent control are discussed. Moreover, a particular attention is given to show the robustness of the closed-loop dynamics of the system, when a discontinuous or a sigmoidal control function is applied.

Chapter 3 begins with a background on immunology. Next, a VSC approach is used to analyse the dynamics of the antigen-specific T cell response following vigorous infection. Rather than formulating another candidate model, a variable structure control approach is used to investigate the control features and robustness of the T cell response dynamics. It is assumed that a dynamic control is at play because the immune system highly regulates the cellular dynamics of T cells post-infection [2, 44, 45]. This regulation operates in such a way that appropriate immunological feedback can be enforced in order to maintain health. In essence, various feedback mechanisms are triggered following antigen stimulation, and the outcome of the combined effects of these immunological feedback mechanisms which promote or inhibit the immune response yield the observed kinetics of the T cell population post-infection. Interestingly, the core of VSC consists of switching between different feedback regimes according to a predefined switching logic that allows the system to achieve the desired performance. A phase portrait analysis is conducted to assess the control strategy of the immune system to elicit desirable immune response dynamics. Moreover, a sliding mode control analysis is used to investigate the robustness of the immune response dynamics.

Chapter 4 focuses on the mechanism of self-tolerance. A background on the biology of the self-tolerance mechanism is provided at the beginning of this chapter. Afterwards, a simple mathematical model of self-tolerance/autoimmunity is considered. Next, the characteristics of a set of candidate immune response functions and their impact on the achievement of self-tolerance are investigated. Candidate immune response functions are examined as candidate control strategies. Thus, the stability and the dynamical behaviour of the resulting closed-loop systems is analysed to understand the maintenance of or loss of self-tolerance. Finally, a reachability analysis is performed to design an adaptive sliding mode controller which models the inhibition of self-reacting effector T cells to achieve a robust self-tolerance steady-state.

A VSC approach is used in Chapter 5 to study the containment of HIV infection by the HIV-specific CD8+ T cell response. The model of HIV infection dynamics formulated in [56] is chosen for analysis. The cytolytic killing mechanism of CD8+ T cells is treated as a control input which aims to enforce a stable infection free steady-state. Further, a manifold associated with the infection free steady-state is identified. A reachability analysis is used to investigate conditions for this manifold to be attractive to the states of the chosen system. This is used to examine the control of HIV infection in vivo.

A case study is conducted in Chapter 6 to study the dynamics of HIV following initiation of antiretroviral therapy. The basic model of HIV dynamics used in [35, 59, 60] is chosen. A manifold associated with the infection free steady-state is identified and a dynamical condition for the containment of HIV infection by antiretroviral therapy is formulated using the reachability paradigm from variable structure control. Next, measurement of CD4+ T cell count and HIV load in the peripheral blood are used to estimate all the parameters of the model for a set of HIV infected patients. Data points collected in the first month following initiation of antiretroviral drugs are used for the estimation. The reproductive ratio as well as the reachability condition are computed for each patient to monitor and predict the progression of HIV infection following initiation of antiretroviral therapy. The reported clinical outcomes are used to assess the correctness of the predictions.

The final chapter is divided in two parts. First, the conclusions of the thesis are presented. Then, future work to build on the main findings of the thesis are suggested.

1.3 Contributions

The contributions of this thesis lie within the realm of modelling and simulation in immunology. An overview is given in Fig. 1.1.. The novelty of the approach resides in the fact

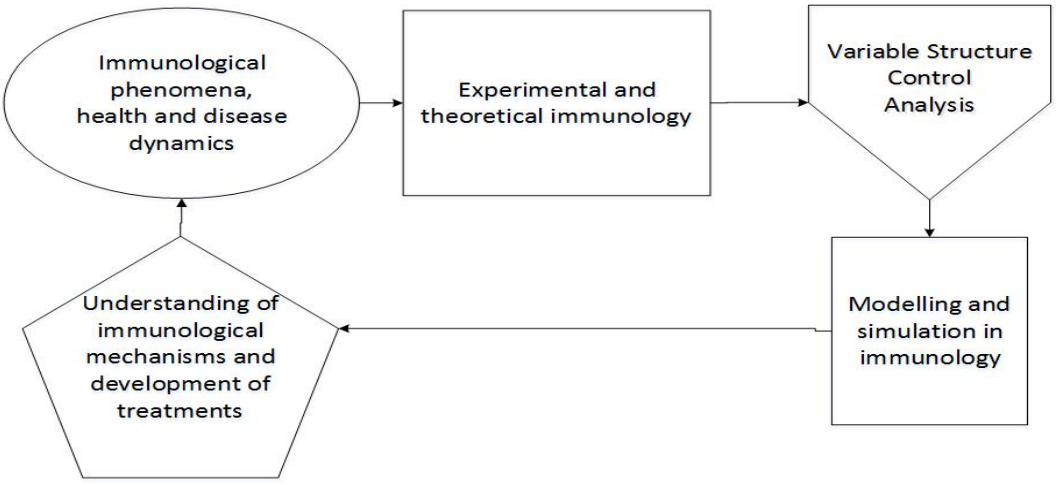

FIGURE 1.1: The approach and contributions

that variable structure control theory is utilised to investigate health and disease dynamics. The specific contributions are as follows:

- The work in Chapter 3 demonstrates the synergies between the observed cellular dynamics of the specific T cell response following vigorous infection and the variable structure control paradigm. The dynamic response of antigen-specific T cell following vigorous infection fits the variable structure control paradigm because changes in T cell population kinetics are underpinned by switching between different immunological feedback regimes in order to achieve immunity. In addition, the findings from the sliding mode analysis reinforce the notion that T cell response dynamics represent a closed-loop system, including a robust VSC law. Moreover, the reachability analysis is shown to be a suitable means to assess the impact of uncertainty and perturbations on the T cell response dynamics following acute and chronic infection.

- In Chapter 4, the VSC approach delivers further understanding of the impact of candidate immune response functions for the maintenance of self-tolerance. Candidate immune response functions reflect potential feedback regimes of the immune system to ensure self-tolerance. The transient dynamics and stability of the self-tolerance equilibrium are significantly dependent on the shape and characteristics of the immune response function. The framework of sliding mode control is used to demonstrate that a robust state of tolerance is achievable using an adaptive sliding mode control mechanism modelling an active suppression of self-reacting effector T cells.

- In chapter 5 the framework of sliding mode control is seen to deliver a dynamical condition for the containment of HIV infection by the HIV-specific CD8+ T cell response. The cytolytic killing mechanism modelled with a double saturation function is shown to operate as a boundary layer control strategy from the immune system to contain the infection in vivo. The time evolution of this dynamical condition for immunity indicates that the immunological requirements to contain HIV in vivo changes during the course of the infection.

- The case study conducted in Chapter 6 presents the reachability paradigm as a tool which delivers a time varying condition for the containment of HIV infection following initiation of antiretroviral therapy. Furthermore, the analysis of HIV patient data using the reachability condition reveals a dynamical signature associated with the outcomes of antiretroviral therapy. Together, the results show that the reachability paradigm is adequate to monitor and predict the progression of HIV infection following initiation of antiretroviral therapy.

The work in this thesis has produced the following articles:

1. Anelone, Anet J.N., Spurgeon, Sarah K., Modelling and simulation of the dynamics of the antigenspecific T cell response using variable structure control theory, 2016, PLOS ONE 11(11): e0166163. doi: 10.1371/journal.pone.0166163

2. Anelone, Anet J.N., Spurgeon, Sarah K., Prediction of the Containment of HIV Infection by Antiretroviral Therapy - a Variable Structure Control Approach, IET Systems Biology, 2016, DOI: 10.1049/iet-syb.2016.0028

3. Anelone, Anet J.N., Orlov, Yury, Spurgeon, Sarah K., Synergies between the dynamics of the immune response of T cells and the variable structure control paradigm, Recent Advances in Sliding Modes (RASM), 2015 International Workshop on , vol., no., pp.1,6, 9-11 April 2015

4. Anelone, Anet J.N., Oza, Harsal B., Spurgeon, Sarah K., The immune system: A variable structure control perspective, Proceedings of the 19th IFAC World Congress, 24-29 August 2014, Cape Town, South Africa.

5. Anelone, Anet J.N., Orlov, Yury, Spurgeon, Sarah K., Modelling the self-tolerance mechanisms of T cells: An adaptive sliding mode control approach, Control (CONTROL), 2014 UKACC International Conference on, vol., no., pp.573,578, 9-11 July 2014 doi: 10.1109/CONTROL.2014.6915203

In short, this introductory chapter has presented the central avenues of the thesis. The next chapter presents the methodology and the VSC paradigm in more detail.

Chapter 2

Variable Structure Control Paradigm

2.1 Introduction

The adaptive immune response is a set of cellular and molecular mechanisms which aim to destroy foreign pathogen and infected tissues as well as to prevent self damage within the host [37, 40]. Experimental studies have demonstrated that the specific response of T cells following infection with virus or bacteria engenders a number of changes in the metabolism, physiology, population and behaviour of the responding cells to clear the infection [2, 43, 61]. Interestingly, mathematical studies in [1, 29, 38] have shown that a sigmoidal or a discontinuous activation function can be used to prescribe realistic changes in the T cell population dynamics following vigorous infection. In effect, various immunological feedback mechanisms interact to activate or inhibit the T cell response to recover a healthy state. Thus, the immune system is intrinsically a dynamical system consisting of feedbacks and inherent immunological decision rules. Further, the dynamics of the specific T cell response has been shown to exhibit some robustness with respect to changes in various factors such as the initial number of responding cells or virus strains [29, 44, 45]. However, the presence of pathogen might impair the dynamics of the specific T response and induce undesirable outcomes [2, 37]. Consequently, it is important to quantify and analyse T cell and virus dynamics to understand how immunity is achieved in vivo and to inform the design of treatment [29, 30, 32].

The field of control engineering is a mature discipline involved with the study of uncertain dynamical systems. In fact, a set of tools have been developed to investigate how to maintain desired stability and performance in the presence of parameter and model uncertainty and disturbances. In the early 1960s in the Soviet union, the seminal work of Emelyanov and Barbashin introduced the concept of Variable Structure Control Systems (VSCS). The publication of a book by Itkis (1976) and a survey paper by Utkin (1977) in English allowed the VSC paradigm to be known outside of Russia. A VSCS is in essence a dynamical system with a set of feedback structures and a decision rule based on the states of the system [7]. The designed decision rule allows the system to switch between different feedback dynamics during its operation to achieve the desired performance. Besides, sliding mode control, a special type of VSC, has been developed to satisfy stability and performance requirements by designing a switched control law which confines the trajectories of the system to a chosen manifold of the state space. Importantly, systems with a VSC law have been demonstrated to possess some inherent robustness to uncertainty and disturbances [7, 13–16]. Further, techniques derived from VSC theory have been shown to deliver sensible insights on the impact of uncertainty and disturbances on the dynamical behaviour of systems [8, 62].

The design of a sliding mode control starts by defining a switching function which defines associated manifold to prescribe a stable dynamical behaviour which meets all the predefined constraints and requirements [7, 15, 22, 63]. Next, the existence condition for a sliding mode also known as the reachability condition is formulated. Afterwards, candidate control strategies are investigated to render the chosen manifold attractive to the trajectories of the system. It is common to have a discontinuous control such as the unit vector control [10, 14, 15, 22]. Fundamentally, the choice of the switching function and its parameters determine the dynamical behaviour of the system whilst the control gain ensures that the dynamics of the system reach and remain on the sliding manifold. The resulting closed-loop dynamics consist of a reaching phase in which the switching function moves towards the manifold of interest and a sliding phase in which the switching function is confined to the sliding manifold. During the reaching phase, the dynamics of the system are not robust to uncertainty and perturbations. However, when sliding motion starts the system exhibits reduced order dynamics and complete invariance to "matched uncertainty" i.e a class of uncertainty and perturbations present in the input channels. These advantages have motivated the development of sliding mode control strategies in various application such as furnace control, automotive engine control, control of electric motors and control

of chemical processes [8, 10]. in addition, the sliding mode control paradigm has been used to design robust regulators, state observers, model-reference control, adaptive schemes and fault detection techniques [62, 64–66].

Sliding mode control techniques have evolved to preserve the core benefits of reduced order dynamics and robustness to matched uncertainty whilst addressing new challenges brought by specific application requirements and constraints. In effect, it is often not possible to have measurements of all state variables. As a result, a framework has been developed to design sliding mode control in which the switching function has only a subset of state measurements as inputs [13, 16, 24, 67]. This subset of state measurements is usually called the system outputs. Additionally, a discontinuous control injection to enforce a sliding mode is undesirable in some practical implementations because the discontinuous control action generates chattering i.e high frequency switching around the sliding manifold [23]. From the literature on sliding mode control, several adaptation methodologies have been designed [23, 64]. An appropriate adaptation scheme needs to ensure the reachability condition holds with the minimum required amplitude of control gain. The adaptation method developed in [64] stops when ideal sliding motion occurs. In contrast, the method in [23] continues the adaptation process using an estimate of the equivalent control i.e the "average" action of the applied discontinuous control when ideal sliding mode occurs. Recently, an adaptation algorithm which provides the minimum possible magnitude of the discontinuous control under parameter uncertainty as well as reduction of chattering in first order sliding mode control has been introduced in [25].

Apart from adaptation strategies, the smoothing approach which consists of using a continuous approximation of the discontinuous control function eliminates chattering but does not allow the switching function to remain on the sliding manifold [15, 21, 22, 63]. Therefore, the resulting closed-loop dynamics lose some robustness. Next, an integral sliding mode control has been proposed in [17] to remove the non-robust reaching phase. Moreover, higher order sliding mode controllers in which the discontinuous control is found in higher order derivatives of the switching function have been developed to suppress chattering and achieve high performance [20, 25, 68].

This chapter reviews theory of VSC with a particular interest on some key notions which will be used later in this thesis to investigate T cell and virus dynamics in vivo.

The chapter is organized as follows: the basic philosophy of the VSC paradigm is presented in the first section. The next section, sliding mode control theory, a special class of VSC is reviewed. Next, the robustness properties of VSC are demonstrated in the third section. Finally, the last section summarizes the main features of VSC theory.

2.2 Basic principles of switched control system

The VSC paradigm consists of changing the control structures during the operation of the system according to a switching logic to force the system to exhibit desired stability and performance requirements. The following examples from [7, 10] are used to show cases in which switching between different control structure is beneficial to achieve the desired dynamical behaviour. Consider the second order dynamical system given as

$$\frac{d^2y(t)}{dt^2} = u(t) \tag{2.1}$$

which represents a double integrator system, a mass-spring damper with zero damping. The initial conditions are $y(0) = 1$ and $\frac{dy(0)}{dt} = 0$. The control objective is the establishment of a stable motion of the dynamics of the system towards the origin using the control input $u(t)$.

The outcome of a single structure control strategy is investigated using the candidate linear state feedback from [7]

$$u(t) = -ky(t) \tag{2.2}$$

where the parameter k is a strictly positive scalar, equivalent to the spring constant. The phase portrait of the dynamics of the closed-loop system generated by the negative feedback (2.2) for two different values of k i.e $k_1 = 0.5$ and $k_2 = 1.5$ shows that the trajectories do not move towards the origin, see Fig. 2.1. Therefore, this fixed structure control approach does not achieve the required stability and performance. A Lyapanov analysis is conducted to investigate the stability of the closed-loop system formed by the negative feedback (2.2). In simple terms, Lyapanov stability theory states that if a positive definite function V can be constructed using an algebraic combination of the state variables of the system, the equilibrium of interest is asymptotically stable if the corresponding derivative is a negative definite function of the state variables of the system [18]. From [10], a Lyapanov function

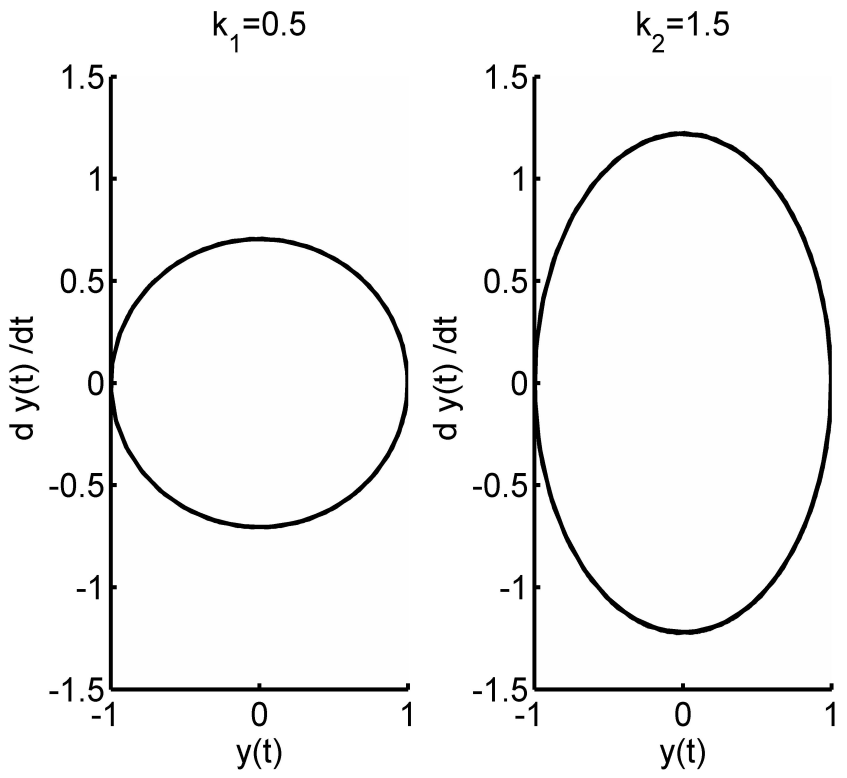

FIGURE 2.1: Phase portrait of the double integrator system (2.1) with a fixed structure control strategy (2.2).

for the system (2.1) is given as

$$V(y(t), \frac{dy(t)}{dt}) = y(t)^2 + \left(\frac{dy(t)}{dt}\right)^2 \tag{2.3}$$

Therefore, $V(y(t), \frac{y(t)}{dt})$ is positive definite as required. After simplifications, the first order derivative yields

$$\begin{aligned} \frac{dV(y(t), \frac{dy(t)}{dt})}{dt} &= 2y(t)\frac{dy(t)}{dt} + 2\frac{dy(t)}{dt}u(t) \\ &= 2y(t)\frac{dy(t)}{dt}(1-k) \end{aligned} \tag{2.4}$$

Consequently, to render $\frac{dV(y(t), \frac{dy(t)}{dt})}{dt}$ negative definite, when $y(t)\frac{dy(t)}{dt} < 0$, k must be less than unity but when $y(t)\frac{dy(t)}{dt} > 0$, k must be greater than unity. Thus, the expression (2.4) demonstrates that the magnitude of the gain k must change to allow the temporal derivative of the Lyapanov function $V(y(t), \frac{dy(t)}{dt})$ to be negative definite at all times so that the resulting dynamics are asymptotically stable.

This is a motivation for the use of a switched control approach to achieve the desired

control objective. In effect, the VSCS is characterized by a decision rule which purposefully switches between different feedback dynamics during the process to achieve desired stability and performance requirements. From (2.4), the following switching logic is suggested

$$u(t) = \begin{cases} -k_1 y(t) & \text{with } 0 < k_1 < 1 \text{ when } s(y(t), \frac{dy(t)}{dt}) < 0 \\ -k_2 y(t) & \text{with } 1 < k_2 \text{ when } s(y(t), \frac{dy(t)}{dt}) > 0 \end{cases} \tag{2.5}$$

where

$$s(y(t), \frac{dy(t)}{dt}) \quad = \quad y(t)\frac{dy(t)}{dt}$$

The phase portrait of the closed-loop dynamics resulting from this VSC law, see Fig. 2.2, shows that the trajectories of this VSCS exhibits an asymptotically stable motion towards the origin. In fact, this VSC law forces the trajectories to move closer to the origin in each quadrant. Thus, the desired stability and performance requirements are achieved by switching between two different feedback gain according to the evolution of the state variables. Hence, in this example, the VSC approach is shown to generate a dynamical behaviour which cannot be realized using a single control structure approach. Besides,

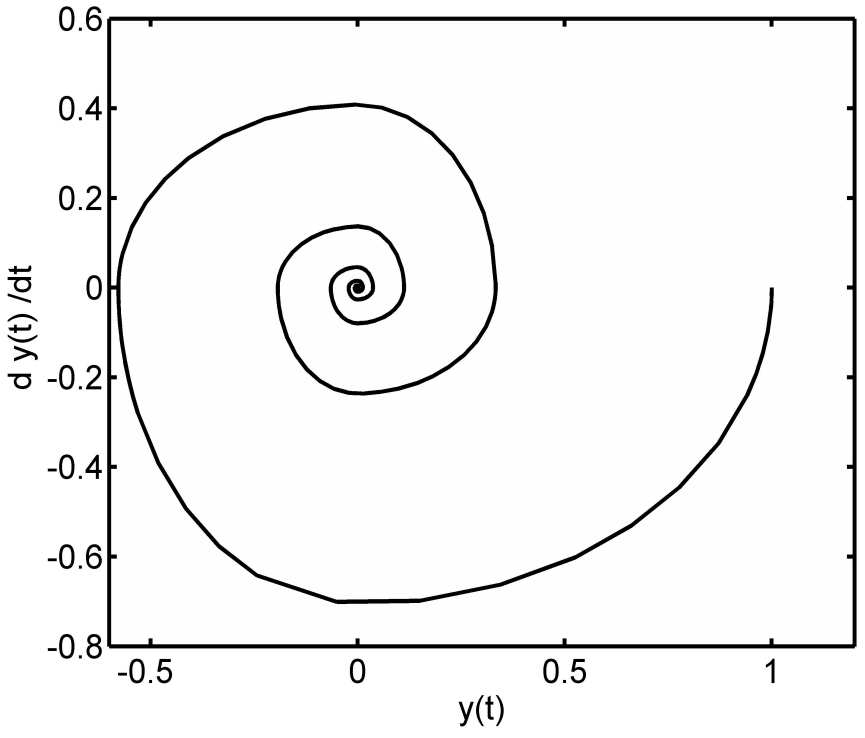

FIGURE 2.2: Phase portrait of the double integrator system (2.1) with a variable structure control (2.5).

consider the same control objective being imposed on an oscillator system given as

$$\frac{d^2y}{dt} - \xi\frac{dy}{dt} + u(t)y = 0 \tag{2.6}$$

where ξ is a constant and $u(t)$ is the control input. In the simulations, the parameter $\xi = 0.7$ and the initial conditions are $y(0) = 1$ and $\frac{dy(0)}{dt} = 1$. Here, a fixed structure control where $u(t) = 0.6$ is shown to generate stable dynamics and to satisfy the desired control objective, see the phase portrait in Fig. 2.3. Alternatively, the control objective can

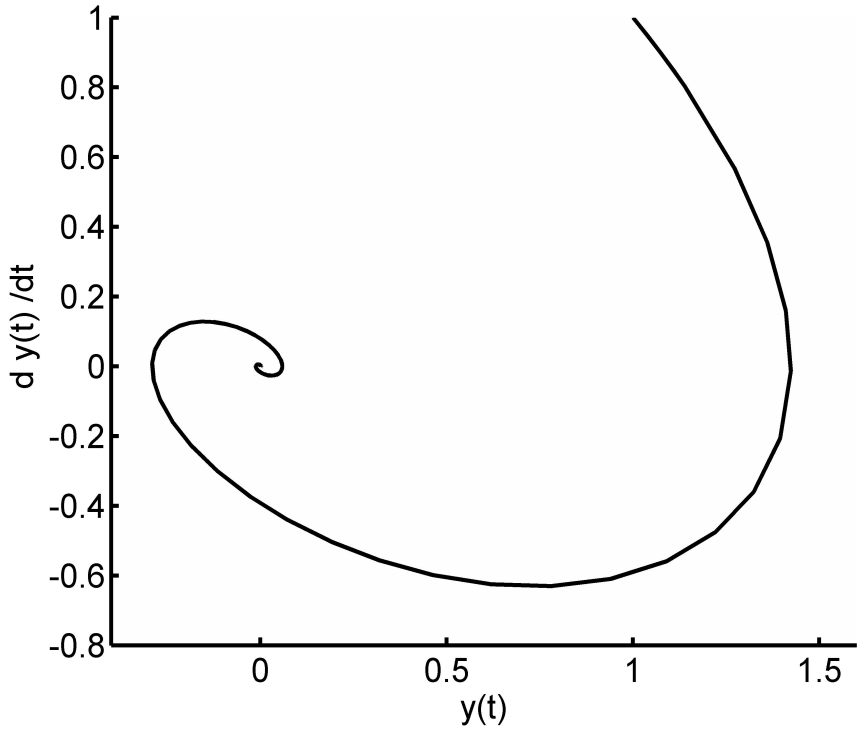

FIGURE 2.3: Phase portrait of the oscillator system (2.6) with a stable fixed structure control $u(t) = 0.6$ with poles at $(-0.35 + 0.69i)$

also be achieved using the following VSC law:

$$u(t) = \begin{cases} \alpha & \text{if } y(t)s(y(t), \frac{dy(t)}{dt}) > 0 \\ -\alpha & \text{if } y(t)s(y(t), \frac{dy(t)}{dt}) < 0 \end{cases} \tag{2.7}$$

where α is the chosen controller gain and the switching function

$$s(y(t), \frac{dy(t)}{dt}) = my(t) + \frac{dy(t)}{dt} \tag{2.8}$$

with

$$0 < m < -\frac{\xi}{2} - \left(\frac{\xi^2}{4} + \alpha\right)^{\frac{1}{2}} \tag{2.9}$$

where m is a positive scalar designed using the stable poles of the system (2.6).

Importantly, the phase portrait of the closed-loop dynamics imposed by the VSC law (2.7) with $m = 1$, see Fig. 2.4, shows that after a short transient the trajectories of the oscillator system move in a straight line i.e "slide" towards the origin whilst being confined to a manifold i.e $s(y(t), \frac{dy(t)}{dt}) = 0$ of the state-space. This specific dynamical motion, conventionally called a sliding mode [7, 10, 13, 16, 22], will be discussed in the next section. In comparison,

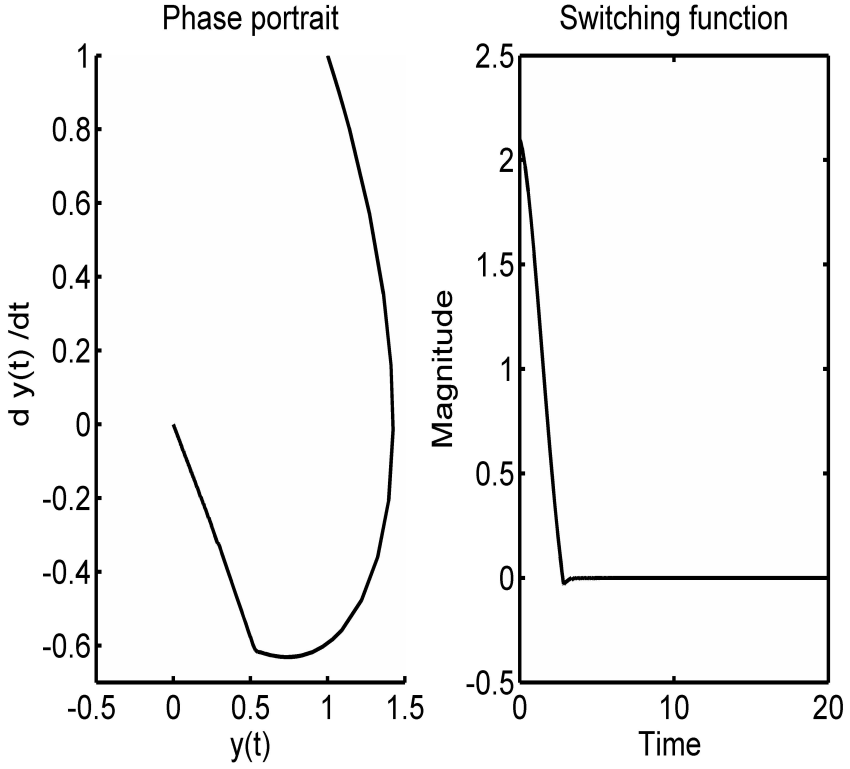

FIGURE 2.4: Oscillator system (2.6) with a variable structure control law. $\alpha = 0.6$ and $m = 1.1$ from (2.9) (2.7).

the time evolution of the output $y(t)$ in Fig. 2.5 shows that the VSCS with (2.7) produces a faster motion to reach and remain at the origin as compared to the ones produced by the stable fixed structure control strategy. In fact, the VSC (2.7) has been designed to exploit the fact that the unstable subsystem with $u = -0.6$ possesses some rapid transient towards the origin, see Fig. 2.6.

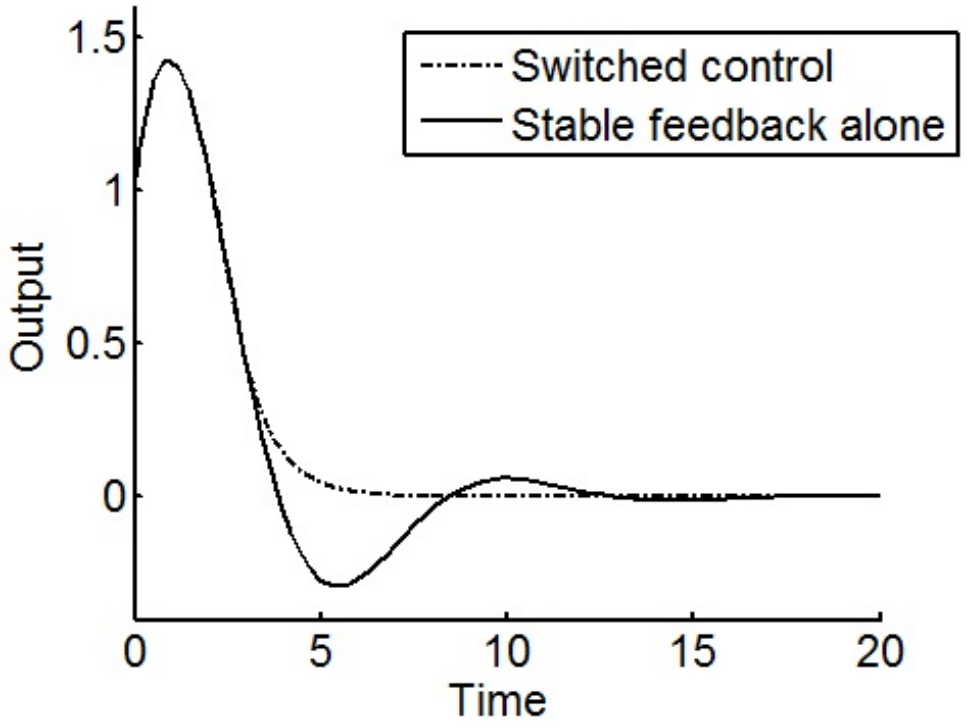

FIGURE 2.5: Comparison of the output response $y(t)$ of the oscillator system (2.7) generated by the stable fixed structure control in Fig. 2.3 versus the switched control in Fig. 2.4. The output response of the oscillator system shows that the designed switched control law yields a faster settling time than the stable feedback alone.

Together these findings evidence the ability of the VSC approach to generate new dynamical properties and behaviour which are not inherent in any of the sub-systems. Changing the dynamic structure of a system during its operation using an appropriate decision rule is seen to be beneficial to achieve desired stability and performance requirements.

2.3 Sliding mode control design and properties

The pendulum system is selected to present the basic design principles and properties of sliding mode control, a special class of VSC. In fact, the pendulum system is relatively simple and has been used in the literature to review the theory and benefits of SMC [10, 13, 14, 16]. Although, a single input single output system has been used to demonstrate the basic principles of sliding mode control, these results hold for multiple input multiple output systems. The dynamical equations modelling a pendulum system can be written as

$$\frac{d^2y(t)}{dt^2} = -a_1 sin(y(t)) + u(t) \tag{2.10}$$

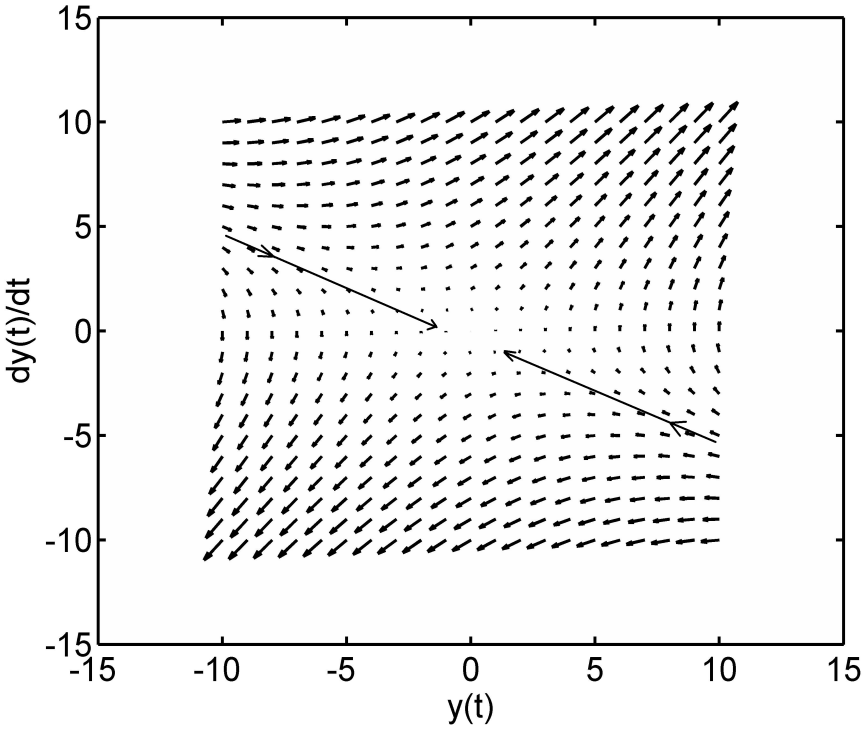

FIGURE 2.6: Phase portrait of the unstable sub-system of (2.7) with the fixed control structure $u(t) = -0.6$ with poles at 0.5 and -1.2

where a_1 is a positive scalar. The state variable $y(t)$ is the variation over time of the angular displacement of the attached object from the vertical. The chosen control input is $u(t)$, the force applied at the point of suspension. Consider that the states variables $y(t)$ and $\frac{dy(t)}{dt}$ are measurable and the initial conditions are $y(0) = 0$ and $\frac{dy(0)}{dt} = 0$. The control objective remains to force the trajectories of the system to attain and stay at the origin.

The design process starts by analyzing a linear approximation of the pendulum system (2.10). In effect, in the study of dynamical systems, it is sensible to study the dynamics of a system without its nonlinearities to have an initial understanding of its dynamical behaviour [10, 14, 51, 69]. By neglecting the nonlinear term $sin(y(t))$ in (2.10), the dynamical equations collapses to form a second order dynamical system corresponding to the double integrator system in (2.1).

A sliding mode control strategy for the system (2.1) is designed using the switching function (2.8). For the sake of simplicity, the following notation is adopted in the rest of the chapter:

$$s = s(y(t), \frac{dy(t)}{dt}) \quad \dot{s} = \frac{ds}{dt}$$

When the trajectories of the system (2.1) lie on the manifold formed by the switching line $s = 0$,

$$\frac{dy(t)}{dt} = -my(t) \tag{2.11}$$

As a result, the dynamics of the system (2.1) exhibit a first-order decay towards the origin. Therefore, the choice of the switching function (2.8) together with the switching line $s = 0$ is appropriate to generate the desired dynamical behaviour. Importantly, this motion is independent of any applied control signal. It is worth noting that the double integrator system (2.1) exhibits reduced order dynamics (2.11) during sliding motion.

Knowing that desirable dynamics are achieved when the trajectories of the system (2.1) exhibit a sliding mode, the next step consists in defining sufficient conditions to force the switching function to reach and to remain in the chosen sliding manifold. In the literature of sliding mode control, this process is known as defining the reachability condition for a sliding mode [7, 10, 13, 14, 16, 70]. In essence, to render the manifold $s = 0$ attractive,

$$\lim_{s\to 0^+} \dot{s} < 0 \quad and \quad \lim_{s\to 0^-} \dot{s} > 0 \tag{2.12}$$

Conventionally, this expression is written as

$$s\dot{s} < 0 \tag{2.13}$$

Both expressions (2.12) and (2.13) are termed reachability conditions [7, 13, 14, 16]. To satisfy this condition, the following candidate switched control law is proposed:

$$u(t) = -m\frac{dy(t)}{dt} - \rho sign(s) \tag{2.14}$$

where $0 < \rho$ is a scalar and $sign(.)$ is the signum function.

From (2.13),

$$s\dot{s} = s\left(m\frac{dy(t)}{dt} + u(t)\right) < 0 \tag{2.15}$$

Fundamentally, this inequality reveals a dynamical condition to confine the trajectories of the system to lie on the desired manifold and to enforce the desired stability and performance requirements. Alternatively, a stronger condition called the η-reachability condition given as

$$s\dot{s} \leq -\eta|s| \tag{2.16}$$

where η is a small positive constant which is called reachability constant to guarantee that a sliding mode will be reached in finite time [7, 13, 14, 16]

The $\eta-$reachability condition (2.16) becomes

$$s\dot{s} = -\rho|s| < -\eta|s| \tag{2.17}$$

since $s\ sign(s) = |s|$. Consequently , for $0 < \eta < \rho$ the candidate control (2.14) satisfies the reachability condition (2.17) and ensures that the states reach the manifold $s = 0$ in finite time and remains on it.

2.4 Robustness properties

Forcing the dynamics of the system (2.1) to lie on the switching manifold (2.8) is seen in this case to prescribe a linear, first order dynamics (2.11) to the system where the choice of the dynamical behaviour is entirely specified by the selection of the parameter m. In terms of VSC, robust performance is synonymous with attainment of the dynamics prescribed by the choice of switching surface despite the presence of model and parameter uncertainty [15, 21, 22, 63, 67]. Dynamical equations constructed to model phenomenological or mechanical systems are intrinsically abstractions of real system. Besides, systems can change due to ageing, accumulated damage, or perturbations. Further, the constructed model might be simplified or linearized to facilitate the use of existing mathematical tools to analyse its dynamics.

Let $\omega(t)$be an unknown function of a time varying disturbance and $M > \|\omega(t)\|$. The dynamical equation of the system (2.1) with this disturbance is given as

$$\frac{d^2y(t)}{dt^2} = \omega(t) + u(t) \tag{2.18}$$

Subsequently,

$$\begin{aligned} s\dot{s} = &\quad s\left(m\tfrac{dy(t)}{dt} + \omega(t) + u(t)\right) \\ s\dot{s} < &\quad -(\rho - M)\,|s| \qquad < -\eta|s| \end{aligned} \tag{2.19}$$

and the η-reachability condition is satisfied for $\rho > M$ and $0 < \eta < \rho - M$.

The nonlinear component of the pendulum system (2.10) has been ignored in the design of the sliding mode control (2.14) to achieve stability and performance requirements. For the pendulum system, $\omega(t) = -a_1 sin(y(t))$. The robustness of the control (2.14) applied to the pendulum system (2.10) is ensured when

$$\begin{aligned} s\dot{s} = &\quad s\left(m\tfrac{dy(t)}{dt} - a_1 sin(y(t)) + u(t)\right) \\ = &\quad s\left(-a_1 sin(y(t)) - \rho sign(s)\right) \qquad < 0 \end{aligned} \tag{2.20}$$

This suggests that the feedback gain ρ must have sufficient magnitude to satisfy the reachability condition (2.20) to enforce a sliding mode for the pendulum system (2.10), see Fig. 2.7. Consequently for these settings, the dynamics (2.11) enforced by the switching function are rendered insensitive to the effects of the unknown disturbances during the sliding motion. In effect, when (2.20) holds, $s = 0$ after some fine time t_{s1} then $\dot{s} = 0$ for all $t > t_{s1}$. Interestingly, the expression of the dynamics of the pendulum system in the sliding mode becomes (2.11). Thus, the dynamical behaviour of the pendulum system is identical to the one of the double integrator system after sliding motion takes pace (see the phase portrait in Fig. 2.8). This evidence that sliding mode system exhibits total invariance to a particular class of uncertainty, the so-called matched uncertainty, which acts in channels where the control feedback acts directly [7, 10, 13–16, 63]. Fundamentally, to achieve robustness, the magnitude of the applied control signal must be sufficiently large to guarantee that the reachability condition holds in the presence of matched parameter and uncertainty. Knowledge of the likely bound of the uncertainty rather than its exact dynamical behaviour is sufficient to design a robust sliding mode control law.

To demonstrate the inherent robustness of VSCS, the notion of the equivalent control introduced in [7] is presented. By definition [10, 16, 25], the equivalent control, usually denoted u_{eq} is the unique solution to the algebraic equation formed by equating the temporal derivative of the switching function to zero. In essence, the equivalent control action is the

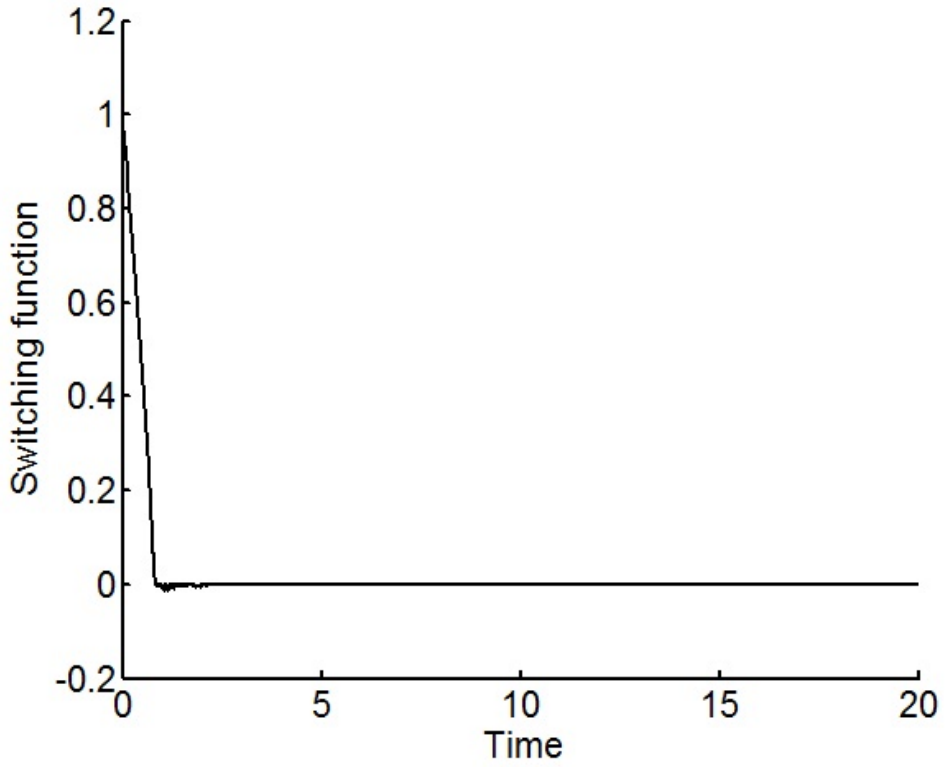

FIGURE 2.7: Time evolution of the switching function (2.8) for the pendulum system (2.10) with $a_1 = 0.5$ under the switched control (2.14) with $m = 1$ and $\rho = 1$

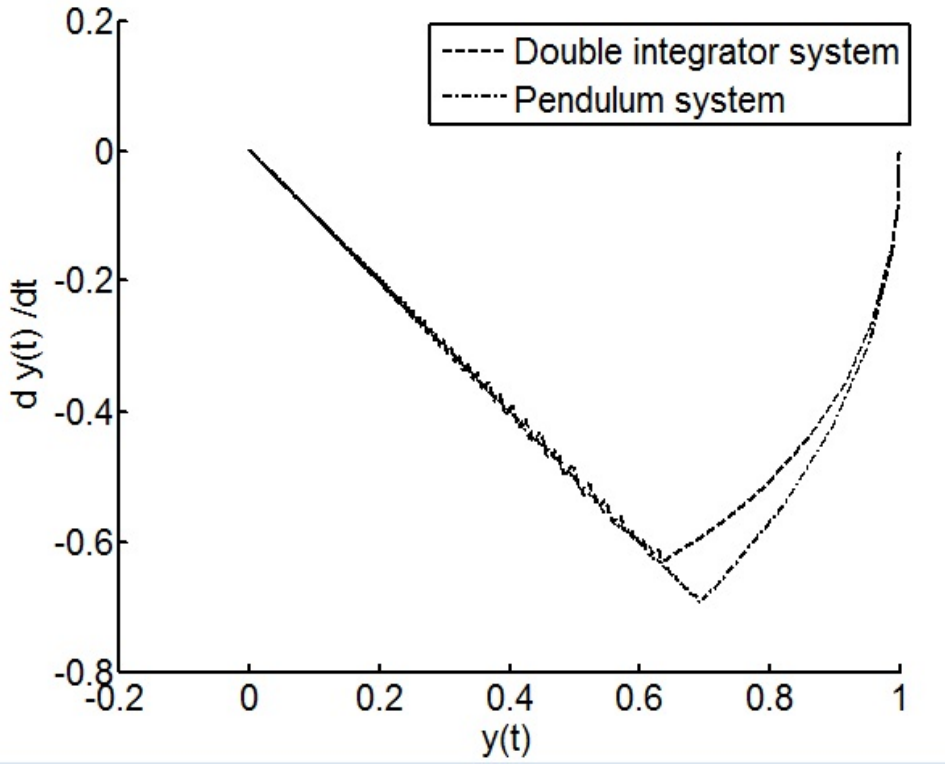

FIGURE 2.8: Phase portrait of the double integrator system (2.1) and the pendulum system (2.10) with a sliding mode

theoretical control action needed to maintain sliding motion. It should be noted that the equivalent control is only valid after the time at which sliding motion takes place. It is not the actual discontinuous control signal applied to the system. The equivalent control action can be regarded as the average injection produced by the applied control signal. The inherent robustness of the closed-loop dynamics resulting from the VSC law is proven by the fact that when the reachability condition (2.19) holds and $s = 0$,

$$\begin{aligned} \dot{s} = & \quad m\frac{dy(t)}{dt} + \frac{d^2y(t)}{dt} \\ = & \quad m\frac{dy(t)}{dt} + \omega(t) + u_{eq}(t) \\ = & \quad 0 \end{aligned} \tag{2.21}$$

Hence, the effects of the uncertainty is effectively cancelled as long as sliding motion holds because the reachability condition (2.19) is satisfied.

. Besides, the concept of the equivalent control has been shown to be useful to investigate the dynamics of the unknown input signals [10, 13, 14, 16].

In applications where the effects of a discontinuous control signal are undesirable, a continuous approximation of the discontinuity is employed [15, 21, 22, 63]. A typical smoothing function for the signum function is expressed as

$$\frac{s}{|s| + \delta} \tag{2.22}$$

where $\delta > 0$ is a designed parameter which determines the steepness of this saturation function. As a result, a continuous approximation of the control law (2.14) is given as

$$u(t) \quad = \quad -m\frac{dy(t)}{dt} - \rho\frac{s}{|s| + \delta} \tag{2.23}$$

Using this smooth control signal with $\delta = 0.01$, ideal sliding motion does not occur but the switching function (2.8) is confined in a vicinity of the switching manifold where $|s| < \delta$, see Fig. 2.9. This motion of the system trajectories within this boundary layer is called a pseudo-sliding mode [10]. In some applications, desirable performances can still be achieved whilst remaining within a certain neighborhood of the sliding manifold [21]. Therefore, maintaining the switching function within a certain boundary layer of the desired manifold

using a smooth control signal has been shown to be good enough to achieve desired system performance [10, 21].

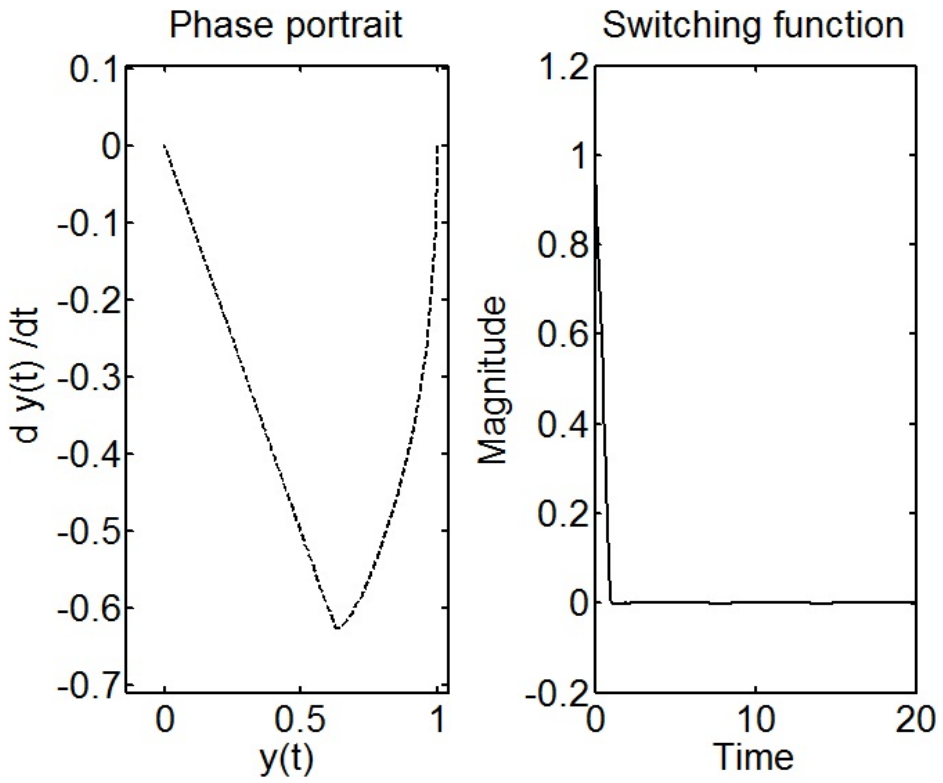

FIGURE 2.9: Pendulum system (2.10) produced by a smooth control (2.23).

Since the continuous control (2.23) does not achieve ideal sliding motion, the effects of matched uncertainty and disturbances cannot be completely rejected. Nevertheless, the closed-loop dynamics still exhibit some level of robustness to parameter and model uncertainty because the smooth control action behaves like a high gain control feedback during pseudo-sliding mode [10, 21].

Of note, the choice of the parameter δ determines both the magnitude of the boundary layer around the sliding manifold $s = 0$ as well as the steepness of the saturation function (2.22). To achieve better performance and robustness, various approaches have been developed to have δ as a function of time or state variables to produce a dynamic boundary layer [15, 22, 63].

Interestingly, (2.22) is similar to saturation functions used to represent T cell activation [1, 29, 71]. For instance, a common one is the Michaelis-Menten function [71–73] given as:

$$V_0 = V_{max} \frac{S}{S + K_m} \tag{2.24}$$

where $0 \leq S$ is the substrate concentration, $V_{max} > 0$ the maximum rate produced at maximal substrate concentration and $K_m > 0$, the Michaelis-Menten constant. As a result, the Michaelis-Menten function (2.24) shares identical properties with (2.23) when $0 \leq s$. Further, the Michaelis-Menten constant defines the steepness of the curvature of the saturation function (2.24). The effects of the Michaelis-Menten function as an candidate control function will be investigated in the next chapters.

2.5 Conclusion

In this chapter, the phase portrait analysis of engineering systems under a variable structure control law was used to present the dynamical behaviour and benefits of variable structure control systems. Similarly, in the following chapter, a phase portrait analysis will be conducted to demonstrate the synergies between the dynamics of the specific T cell response and the ones of engineering systems with a VSC law. Next, the dynamics of the specific T cell response following vigorous infection will be studied from a variable structure control perspective. The framework of sliding mode control presented in this chapter is used to understand the switching mechanism of the specific T cell response. Moreover, this chapter has shown that the reachability condition for a sliding mode defines a dynamical and sufficient condition for any candidate control strategy to enforce desired stability and performance requirements. In the following chapters, the reachability paradigm will be used along with a model of dynamics of the Human immunodeficiency Virus (HIV) infection in vivo to formulate a dynamical condition for immunity. Hence, the purpose of this chapter was to provide the necessary background to understand the subsequent investigation of T cells and virus dynamics using tools from variable structure control and sliding mode control paradigm.

Chapter 3

Synergies Between the Dynamics of the Immune Response of T Cells and the Variable Structure Control Paradigm

3.1 Introduction

In the previous chapter, it has been demonstrated that for a closed-loop system with a variable structure control law, switching between different feedback regimes using information from the states of the system is an approach to satisfy some constraints and performance requirements. Interestingly, experimental studies in immunology reveal that the population dynamics of the specific CD4+ and CD8+ T cell response following vigorous infection are governed by an inherent "immune response program" which changes the population size and dynamic of the response to achieve immunity [32, 38, 39, 43, 44]. Furthermore, experimental observations have shown that the T cell population dynamic resulting from this immune response program exhibits some robustness to variations in some virological, cellular and host factors [2, 39, 44, 45, 74].

Developing mathematical models and techniques to study T cell kinetics is important to investigate the quantitative characteristics and dynamical features of T cell mediated immune responses. In fact, it is crucial to understand the factors determining success or failure

of the specific T cell response in various contexts such as transplantation, autoimmunity, chronic infection and drug treatment [2, 29, 30, 42, 55]. The mathematical models of the dynamics of the immune system can be constructed using a system of Ordinary Differential Equations (ODEs) analogous to the Predator-Prey models from ecology [73]. These models describe the dynamics of some cellular and molecular phenomenon in an immunological scenario of interest. Importantly, mathematical modelling and investigations have provided several insights in immunology [29, 30, 32, 55].

Experimental studies have extensively investigated the kinetics of some antigen-specific CD8+ T cell responses because this immune response has been shown to play a major role in the control of infection [2, 38, 57, 75]. As a result, quantitative data have been published and used to perform model-fitting and parameter estimation [1, 76]. Modelling the specific T cell response involves defining a sensible mathematical relationship between the antigen stimulation and the subsequent antigen-specific T cell population dynamics. Mathematical modelling of the T cell population dynamics has shown that the immune response program of CD8+ T cells can be appropriately modelled using a sigmoidal or a discontinuous function [29, 38, 39]. In effect, candidate immune response functions dictate the dynamical behaviour of the antigen-specific T cells. Importantly, the immune response function influences both transient dynamics and the steady-states of T cell population [43, 51, 55, 74, 76].

Consequently, the specific T cell response to pathogens can be regarded as a closed-loop system because it consists of intrinsic biological feedback mechanisms which allow the immune response to be activated and inhibited to remove the pathogen and maintain a healthy state. Thus, tools from control theory can be used to analyse the performance of these naturally occurring feedback mechanisms to understand dynamical factors underpinning health or disease. The work in [77] has looked at the specific T cell response as a decentralized control system in which the local interaction of different types of cells engenders a population dynamic response. Interestingly, this dynamic response has been shown to contain, a differential sensor, an on/off switch and an integral feedback.

The variable structure control paradigm introduced earlier is utilized in this chapter to demonstrate the synergies between the dynamics of the specific T cell response and the dynamics of engineering systems with a variable structure control law. Though the cellular and molecular feedback mechanisms which take part in the immune response are still the subject of active research, current findings in immunology provide compelling evidence that

the dynamic response of the population of antigen-specific CD4+ and CD8+ T cells, as shown in [1, 39, 44, 45] behaves as a variable structure control system.

As a VSC law, the immune response program is shown to enforce T cell expansion or contraction dynamics for a given period of time according to some inherent immunological law to achieve the control of acute infection. Moreover, this switching mechanism correlates with changes in the metabolic energy regime of the responding T cells [32, 61, 78, 79].

The chapter is structured as follows: firstly, the biology of specific immune response of T cells is reviewed. Secondly, the similarities between the VSC paradigm and the immune response program are highlighted and discussed. Finally, a robustness analysis is conducted to show that the specific T cell response exhibits some inherent robustness properties.

3.2 Review of the specific T cell response

The immune system consists of various cell populations which interact to achieve immunity and maintain health [31]. The population of T cells or T lymphocytes is a type of white blood cells which are produced by the bone marrow and matured in the thymus, a lymphoid organ. The population of T cells consists of billions of clones having a unique T cell receptor (TCR) which characterizes the specificity of the response. The TCR determines the binding affinity of the clone to antigen i.e a complex of peptides bound to molecules of the major histocompatibility complex (MHC). The T cell response is antigen specific because each T cell clone is activated by a particular combination of peptides bound to MHC. A self-antigen is formed by peptides derived from protein within the body whilst a foreign antigen is not. The differentiation between self and foreign antigen by T cells is crucial because improper activation of T cells by self antigen, known as autoimmunity, induces damage to self tissues [31, 80]. Therefore, the dynamic response of T cells following antigen stimulation play an important role in the control of infection and the maintenance of good health [2, 31, 42, 53]. Also T cell can further be classified based on their cell surface molecules or physiology. For instance, CD4+ T cells are regarded as helper T cells because they contribute to the activity of other immune cells. Whilst CD8+ T cells also known as killer T cells aim at destroying foreign and infected tissues. Moreover, the population of T cells can be divided into different subtypes based on their phenotypes [29, 37].

Naive T cells are identified as conventional T cells whose unique antigen specific receptors have never been stimulated by the matching self or foreign epitopes (antigen). The recognition of the threat by the immune system involves identifying the presence of pathogen destroying healthy cells. The presence of the threat usually leads to an increase in the population of damaged cells and the production of antigen specific to the pathogen. In the presence of signals from the innate immune response, immature Antigen Presenting Cells (APCs) residing in the tissues absorb peptides at the site of the infection or inflammation. As a result, APCs undergo maturation and become professional antigen presenting cells which are the only type of cell capable of providing the required signals to activate naive T cells. Naive T cells move towards APCs such as Dendritic cells (DCs) and macrophages, scan them by brief contacts while they are constantly recirculating through the blood stream and through the peripheral lymphoid[29, 40]. Two types of signals are needed from professional APCs so as to activate naive T cells. Those signals are from the recognition of naive T cell cognate antigen presented by professional APCs and from the interaction with the co-stimulatory molecules on the same APCs [40, 81].

The activation of naive T cell stops their recirculation and activated T cells remain in the peripheral lymphoid tissue. The immune response is produced by the maturation of naive T cells, with proliferation and differentiation mostly into effector cells [40, 77]. Cytokine interleukin (IL)-2, produced by activated T cells and by other sources, drives the reproduction of mature T cells [9, 37, 77, 82]. After differentiation of mature T cells, effector T cells are released into the blood stream through the lyphagion and are directed to the site of the infection. Subsequently, T cell-mediated immune response is performed and supported by complementary immune system mechanisms such as B cells action.

From experimental studies on LCMV infection in mice [1, 2], measurements of virus titers and LCMV-specific CD8+ T cells in the spleen at various days post acute infection produce the trajectories displayed in Fig 3.1.

The initial number of activated T cell clones specific to the pathogen increases to a large number to contain the infection. Following the eradication of the pathogen after an acute infection, the population of activated T cells undergo a contraction phase in which activated T cells die. Antigen-specific T cells are cleared from the infection site via apoptosis or due to the effects of regulatory T cells [37, 39, 43, 50, 83]. Although the existence and action of regulatory T cells has been proved and supported by different experimental and

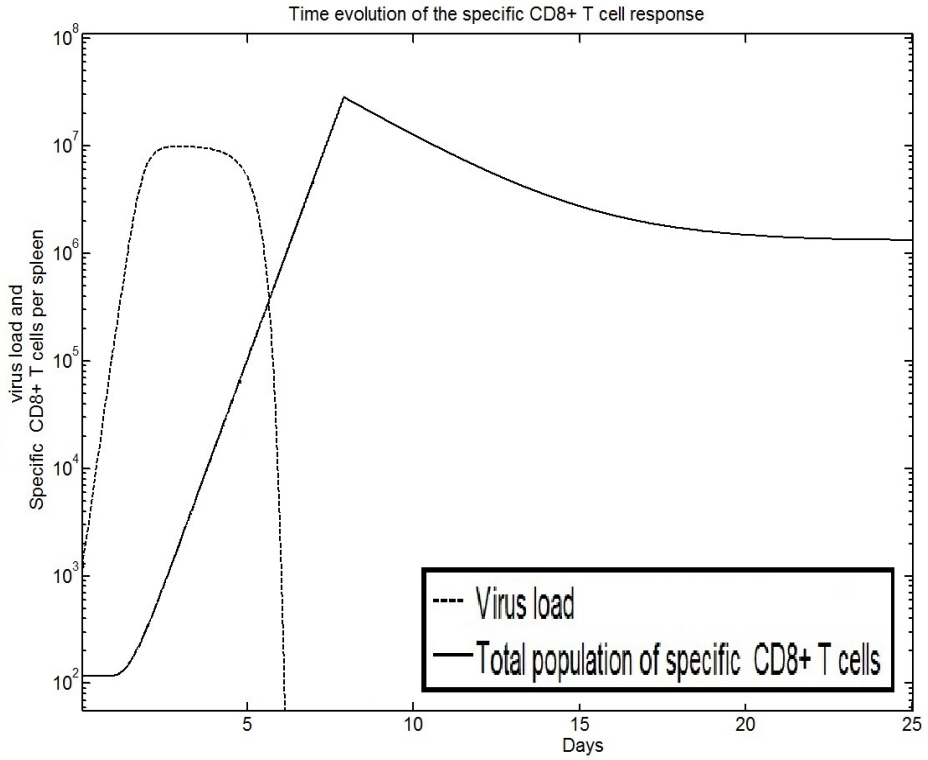

FIGURE 3.1: Time evolution of the population dynamics of specific CD8+ T cells after acute infection from experimental data in [1, 2]

mathematical works, the mechanism by which regulatory T cells exert suppression remains unclear [40, 84–89]. A proven and recognized apoptotic process is Cytokine Deprivation Induced Death (CDID). CDID consists in causing T cell death by the depletion of cytokine. This greatly reduces the growth factor of T cells [37, 90]. Independently of the mechanisms, the contraction phase is needed so that responding T cells do not cause damage to the surviving or surrounding healthy cells as well as to prevent autoimmunity. After the immune response, a small number of activated cells survive the contraction phase and differentiate into memory T cells. Immunological memory is formed from those remaining T cells. Importantly, the response of memory T cells to the same antigen in case of acute infection is better than the ones of naive T cell [2, 29, 74].

From this review of the immunology of the specific T cell response, it can be deduced that suitable regulation of the activation, expansion and reduction of the population size of specific T cell clones is required to satisfy immunological requirements. Similarly, in engineering systems with a variable structure control law, appropriate switching between different feedback structures is necessary to realise the desired outcome [7, 15, 16, 21, 22].

Hence, it can be argued that the switching mechanism of the T cell response is an important feature which underpins the achievement of immunity and the maintenance of good health.

3.3 Synergies between the dynamics of the immune response of T cells and the variable structure control paradigm

In this section, VSC techniques are used to interpret recent experimental and mathematical work related to the dynamics of the antigen-specific T cell response. In [29], the following ODEs have been proposed to model the population dynamics of antigen-specific CD8+ T cells following infection:

$$\frac{dN}{dt} = \sigma + r_N - a_N\mathcal{F}(t)N - d_N N \tag{3.1}$$

$$\frac{dA}{dt} = \mathcal{F}(t)\left(a_N N + a_M M + \rho A\right) - (1-\mathcal{F}(t))(mA) - d_A A \tag{3.2}$$

$$\frac{dM}{dt} = (1-\mathcal{F}(t))mA + r_M M - a_M\mathcal{F}(t)M - d_M M \tag{3.3}$$

The state variables N, A and M represent the time evolution of the population of naive, activated and memory CD8+ T cells responding to a specific antigen following infection. The parameters σ, r_N and d_N denote the production, replication and death rate of naive T cells respectively. Activated T cells proliferate at a rate ρ, die at a rate d_A and differentiate into memory T cells at a rate m. The generated memory T cells replicate at a rate r_M, get activated at a rate a_M and die at a rate d_M. A brief description of the terms of the model eq (3.1)-(3.3) is provided in Table 3.1 and Table 3.2. The likely range of the parameters given in Table 3.2 are obtained from the work in [1, 29, 91].

TABLE 3.1: List of the state variables of the general model of the antigen-specific T cell response eq (3.1)-(3.3)

State variable	Symbol
Number of naive T cells	N
Number of activated effector T cells	A
Number of memory T cells	M

The scenario of a primary specific CD8+T cell response to an acute infection [2, 43–45] is considered. The model (3.1)-(3.3) has been chosen because the studies in [1, 29] have demonstrated that it describes well the immunological phenomenon of interest. The state

TABLE 3.2: List of parameters for the general model of the antigen-specific T cell response eq (3.1)-(3.3)

Description	Symbol	Unit	Nominal Value	Likely Range
Production rate of naive T cells	σ	day^{-1}	0	$0 \leq \sigma$
Replication rate of naive T cells	r_N	day^{-1}	0	$0 \leq r_N$
Activation rate of naive T cells	a_N	day^{-1}	1	$0 < a_N$
Death rate of naive T cells	d_N	day^{-1}	0.001	$0.027 \leq d_N \leq 0.007$
Proliferation rate of activated T cells	ρ	day^{-1}	1.93	$1.4 \leq\leq 3.0$
Death rate of activated T cells	d_A	day^{-1}	1	$0.19 \leq d_A \leq 1$
Production rate of memory T cells	m	day^{-1}	0.05	$0.008 \leq m \leq 0.05$
Replication rate of memory T cells	r_M	day^{-1}	0	$0 \leq r_M$
Activation rate of memory T cells	a_M	day^{-1}	1	$0 < a_M$
Death rate of memory T cells	d_M	day^{-1}	0.01	$0 \leq d_M$
Immune response function	$\mathcal{F}(t))$			$0 \leq \mathcal{F}(t)) \leq 1$

variables, parameters and the complexity of mathematical representation have been designed to capture the impact of various cellular or molecular mechanisms involved in the specific T cell response to foreign pathogen.

The default initial conditions are: $N(0) = 100; A(0) = M(0) = 0$ is chosen to be the default initial conditions as in [1, 29]. The default parameter values, taken from [29], are as follows: $\sigma = r_N = 0$ day^{-1}; $d_N = 0.001$ day^{-1}; $a_N = 1$ day^{-1}; $\rho = 1.93$ day^{-1}; $d_A = 1$ day^{-1}; $m = 0.05$ day^{-1}; $r_M = 0$ day^{-1}; $a_M = 1\text{day}^{-1}$; $d_M = 0.01$ day^{-1}. These initial conditions and biological rates are analogous to the ones used in some previous studies [1, 29].

The immune response program of CD8+ T cells is defined by the function $0 \leq \mathcal{F}(t) \leq 1$. Here, the impact of $\mathcal{F}(t)$ on the population dynamic of responding CD8+ T cells is examined from a control engineering perspective to demonstrate that the immune response program [38] fits the variable structure control paradigm [7, 15, 21, 22, 63].

Now, the dynamical behaviour produced by a fixed structure immune response function with $\mathcal{F}(t) = 0$ and $\mathcal{F}(t) = 1$ is investigated using a phase portrait analysis as in Chapter 2. The phase portrait of the closed-loop dynamics with $\mathcal{F}(t) = 1$ shows that this structure leads to a motion away from the unique equilibrium located at the origin, see Fig 3.2. This motion corresponds to an exponential increase in the population size of activated T cells. As a result, this fixed structure engenders the clonal expansion phase only. The stability analysis of the system reveals that this clonal expansion phase is underpinned by an unstable dynamic because the equilibrium has an unstable pole. This unstable dynamic leading to a rapid increase in the number of activated T cells is desirable to achieve protective immunity quickly [2, 91]. However, a prolonged expansion phase of activated T cells can lead to detrimental effects such as autoimmunity [37, 42, 92]. In contrast, stable dynamics and a reduction of the population of activated T cells are enforced by the fixed structure with $\mathcal{F}(t) = 0$. The phase portrait, see Fig 3.2, shows that the dynamics of the system move towards the origin. Imposing this structure right after the initiation of an infection is undesirable because it prevents clonal expansion to take place. Nevertheless, this structure is useful after the clearance of the infection to enforce the contraction and memory phase of the specific T cell response. From these closed-loop dynamics with a fixed structure immune response program, it is clear that an immune response function with a single structure is not able to provide the required and observed dynamical changes in the population of antigen-specific T cells following infection. In fact, $\mathcal{F}(t)$ must be designed to describe a realistic relationship between the antigen stimulation and the dynamic response of T cells following infection [1, 29, 38, 39].

Interestingly, experimental and mathematical studies [1, 29, 39] have demonstrated that the following discontinuous immune response program can be used to reproduce the dynamics of the specific T cell response

$$\begin{aligned} \mathcal{F}(t) &= 1 \quad \text{if} \quad t_{on} \leq t \leq t_{off} \\ \mathcal{F}(t) &= 0 \qquad \text{otherwise} \end{aligned} \tag{3.4}$$

where experimental records have provided

- t_{on}: the time (in days) at which the number of activated T cells starts to increase to combat the infection

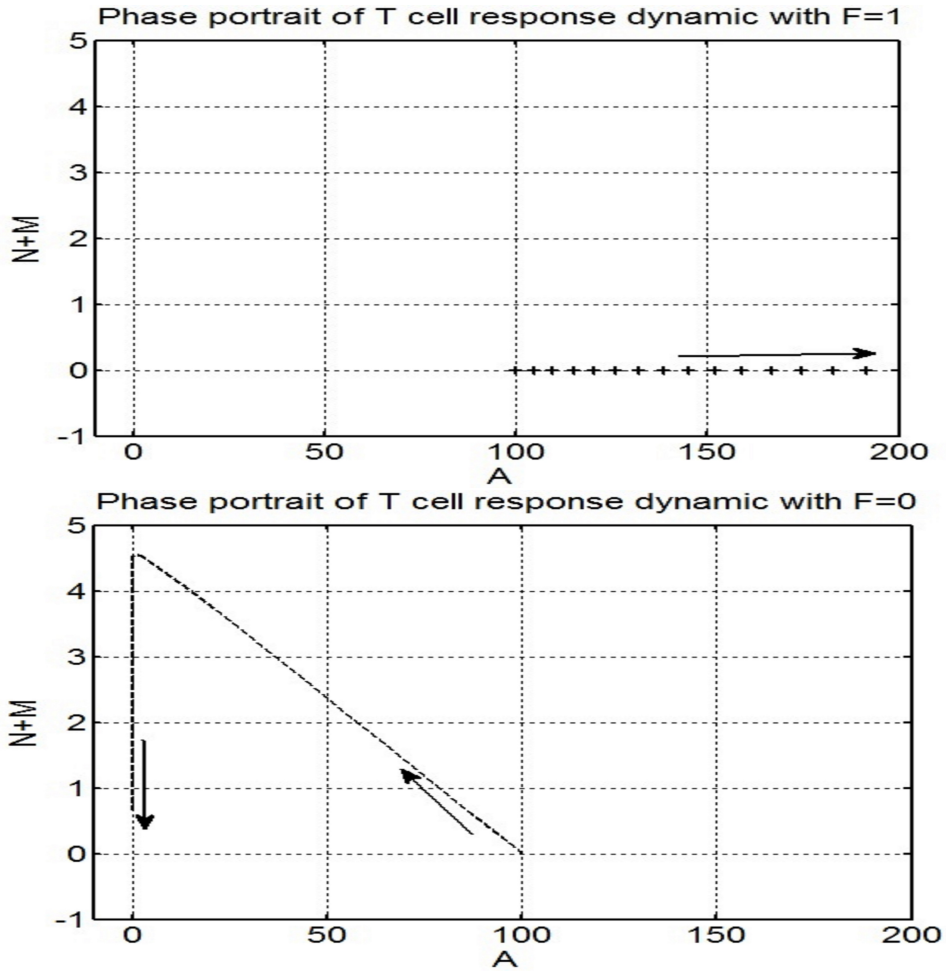

FIGURE 3.2: Phase portrait analysis of the T cell population dynamics of (3.1)-(3.3) with an activation function having a fixed structure. Top: the trajectory of the T cell response generated by $\mathcal{F}(t)) = 1$ is shown. This induces unstable dynamics and a motion away from the origin. The trajectory depicts an exponential and unbounded expansion of activated T cells. Bottom: the trajectory of the T cell response generated by $\mathcal{F}(t)) = 0$ is seen. The trajectory exhibits a stable motion towards the origin. This motion depicts the contraction of the population of activated T cells and the formation of memory T cells.

- t_{off}: the time (in days) at which the decay of the population of activated T cells is enforced after the infection

It is worth to mention that t_{on} and t_{off} are not external inputs. In vivo, these parameters are indeed influenced by the states of the system.. For more details, please refer to [1, 29, 38, 93].

The output dynamics and phase portrait generated by (3.4) are shown in Fig. 3.3. During the expansion phase i.e $\mathcal{F}(t) = 1$, this induces an unstable positive feedback with motion of the trajectories away from the origin. This motion ensures rapid increase in the number of activated T cells as required to respond to infection [2, 43, 48, 94]. Next, when $\mathcal{F}(t) = 0$

is enforced, the immunological control structure switch to a stable negative feedback which forces the decay of the activated T cells and the production of memory T cells is imposed on the system. Individually, each feedback structure is inappropriate to reproduce the T cell response observed post-infection. Therefore, without a suitable switching mechanism between these different immunological feedback structures, the population dynamic of the T cell response is not consistent with experimental data. Hence, the model (3.1)-(3.3) of the T cell response dynamics without switching behaviour is unable to replicate the dynamic behaviour observed in practice [29, 38, 51, 77].

The time-based on/off activation function (3.4) defines a switched control law and enables the system to exhibit appropriate immunological feedback control. T cell population dynamic from the expansion phase to the contraction phase is underpinned by a sharp switching from a positive to a negative feedback. The VSC viewpoint on modelling the dynamics of the immune response of T cells implies that there exists an inherent immunological switching logic associated with $\mathcal{F}(t)$ which governs the response of the T cells. Although early work has argued that changes in the population dynamics of T cells post-infection are orchestrated by an intrinsic time-based autonomous program [1, 29, 38], recent experimental and mathematical publications in immunology suggest that changes in the population dynamics of T cells after infection are the result of interactions between different immunological feedback mechanisms which increase or decrease the population size of responding T cells [2, 38, 93, 94]. The immunological dynamics involved in this inherent switching rule are still the topic of active research [2, 94]. Hence, this suggests that the VSC paradigm is a suitable means to explain the observed antigen-specific T cell response following vigorous infection.

In [1, 29], a candidate Michaelis-Menten function has been utilized to provide a smooth switching process between the activation and the inhibition of the specific T cell response based on the time evolution of the antigen concentration following viral infection. This saturation function is expressed as

$$\mathcal{F}_1(t) = \mathcal{F}(B) = \frac{B}{h+B} \tag{3.5}$$

Where B is the antigen concentration and $h > 0$ is the antigen concentration at which $\mathcal{F}(B)$ is half maximal. Consider the pathogen dynamics given as

$$\frac{dB}{dt} = rB - kBA \tag{3.6}$$

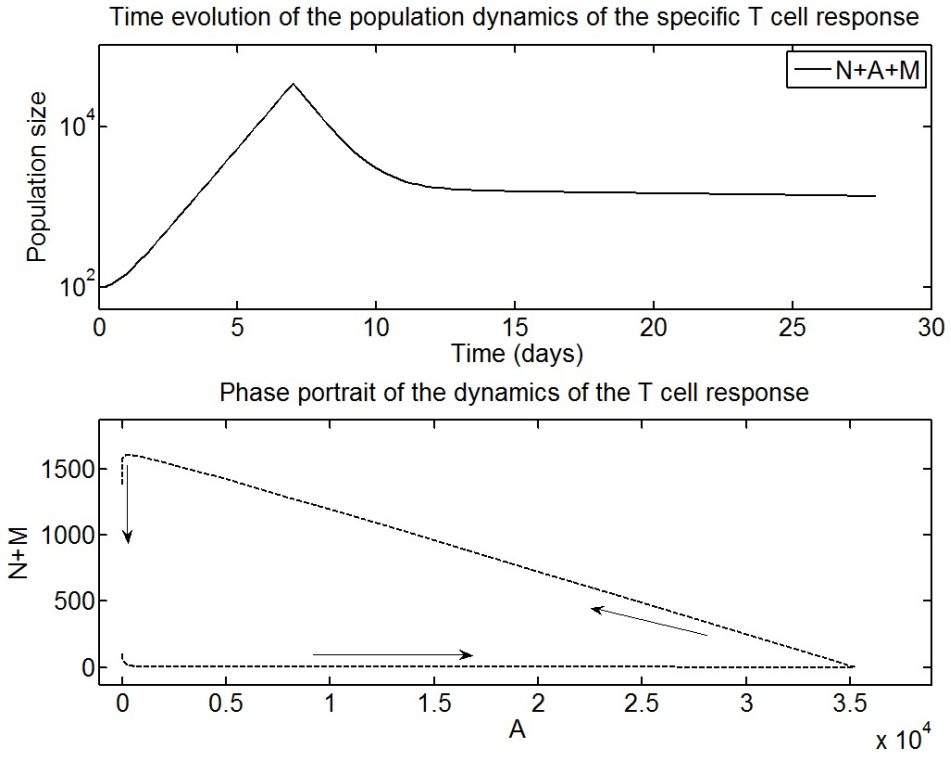

FIGURE 3.3: Population dynamics of the specific T cell response of the model (3.1)-(3.3) with a discontinuous immune response function (3.4).

where r is the replication rate of the pathogen and k is the killing rate by activated CD8+ T cells [91]. Let a closed-loop system formed by (3.1)-(3.3),(3.6) with the immune response function (3.5). let $B(0) = 1000$, $r = 5$ day^{-1} and $k = 310^{-8}$ day^{-1} from [29, 91]. The time evolution of the total antigen-specific T cell population, see Fig 3.5 is consistent with the ones observed in experimental studies [1, 2, 43]. Furthermore, the corresponding phase portrait, see Fig 3.5 depicts a stable dynamics towards the origin after a transient period. Though, the subsystems with $\mathcal{F}_1(t) = 1$ and $\mathcal{F}_1(t) = 0$ independently exhibit unstable and stable dynamics, yet the switching strategy with (3.5) ensures the overall motion is stable and desirable in terms of speed of response. This dynamical behaviour is typical of VSCS [13, 14, 16, 22]. From the viewpoint of variable structure control [7, 13, 14], (3.5) defines a switching logic to enforce the clonal expansion phase and then contraction phase according to the antigen density. In effect, this saturation function induces appropriate variation with time of the population size of antigen-specific T cell in response to infection [1]. Hence, the phase portrait analysis of the specific T cell response presents a strong case for the synergies between the dynamics of the specific T cell response and the ones of engineering systems with a variable structure control law. Indeed, realistic models of the specific T cell response [29, 32, 38, 39] are shown to support the reasoning that the function modelling

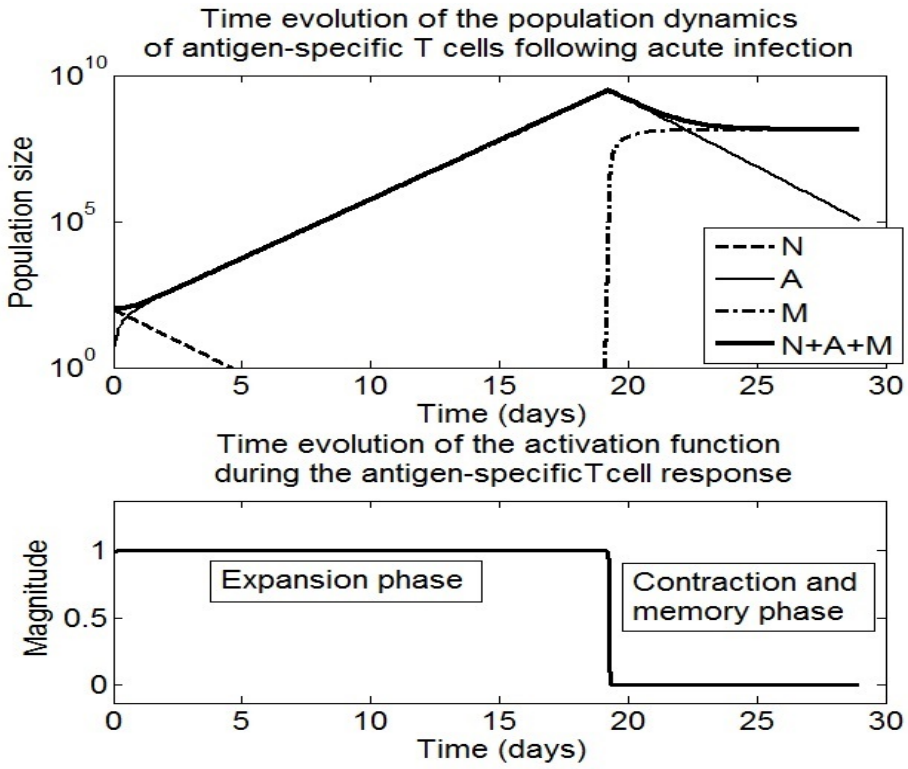

FIGURE 3.4: Simulation of the scenario of CD8+ T cell population dynamics following acute infection. Top: Time evolution of the population dynamics of the antigen-specific T cell response, closed-loop system formed by (3.1)-(3.3),(3.6). Bottom: the time evolution of the antigen-dependent activation function eq (3.5). Following infection, the magnitude of the activation function is at a maximum. This induces the reduction of the state N and an increase of the state A. The state variable N decreases because naive T cells become activated T cells. The state variable A increases due to the expansion of the population of activated T cells. When the magnitude of the immune response function falls to zero, the expansion phase is interrupted. There is production of memory T cells, the state M increases whilst the activated T cells undergo contraction i.e the state A decreases. Consequently, the activation function prescribes the variation over time of the total population of the antigen -specific T cells $(N + A + M)$ following infection.

the immune response program of T cells can be considered as a VSC feedback control. This suggests that the response of the population of antigen-specific T cells observed in experiments [2, 94, 95] is the result of switching between different immunological dynamics.

Different mathematical functions, motivated by different biological assumptions, have been proposed to describe T cell response dynamics following antigen stimulation. The differences in the expression of the immune response function reflect various views on the characteristics of the immune response program. From predator-prey dynamics in the domain of ecology, a mass action kinetic has been assumed and utilized in different studies [54, 55, 96]. Besides, various saturation functions have been formulated from a Michaelis-Menten analysis of the process of T cells binding to APCs [1, 46]. These saturation functions output the maximal T cell proliferation when the antigen stimulation or concentration is high.

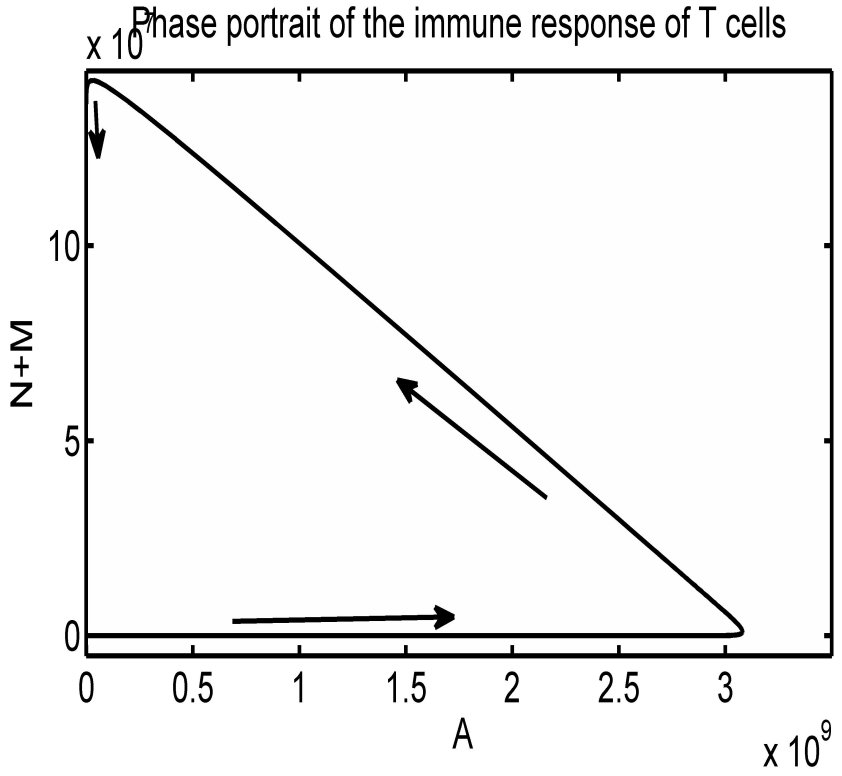

FIGURE 3.5: Phase portrait of the trajectories of the specific T cell response. Closed-loop system formed by (3.1)-(3.3),(3.6) with the sigmoidal antigen-dependent activation function (3.5)

Fundamentally, using sigmoidal or discontinuous candidate immune response program, similar results can be obtained. For instance, the following candidate saturation function has been proposed in [46]:

$$\mathcal{F}_2(t) = \quad \mathcal{F}(B) = \quad \frac{B}{1/K + B + A} \tag{3.7}$$

where K is a Michaelis-Menten like constant reflecting the ability of activated T cells to proliferate. This function incorporates a double saturation mechanism based on the antigen concentration and the population of activated T cells. Interestingly, this candidate function has been shown to generate a net expansion of T cell population when the antigen concentration exceeds a certain threshold.

Apart from these antigen dependent immune response functions, experimental studies on the CD4+ and CD8+ T cell response dynamics following vigorous infection have observed that the clonal expansion continues for few days after the clearance of the infection [2, 39, 97]. Additionally, experimental studies have successfully determined the precise timings and magnitude of the expansion and contraction of the population of specific CD8+ T cells

for different viral or bacterial infection [29, 44, 45, 74]. These findings have motivated the development of antigen-independent immune response program which provide a continuous or a discontinuous switch between the extremum of $\mathcal{F}_1(t)$ post infection [29, 38, 98]. Using these timings provided by experimental data, some models of the antigen-independent response are constructed using a time based switching logic [29, 76, 99].

Nevertheless, the recent experimental studies such as [2, 93, 94, 97, 100] suggest that the type of pathogen strains, the initial infection dose or early curtailment of the infection and antigen presentation induce changes in the duration and magnitude of the clonal expansion. Therefore, it can be argued that the timings and magnitude of the expansion and the contraction phase are produced by cellular and molecular feedback mechanisms [32, 38, 93]. Consequently, current thoughts consider that the immune response program of T cells consists of an antigen-dependent phase followed by an antigen independent phase [38, 47, 93, 97].

From this review of the immune response program, it is proposed that the population dynamic of the specific T cell response following infection incorporates a switching mechanism based on some inherent dynamics to enforce the expansion and the contraction phase at appropriate timings to achieve immunity. Therefore, it can be argued that the dynamical behaviour of the specific T cell response is prescribed by an inherent switched control feedback which aims to combat infection and maintain health. Hence, this work suggests that immunological objectives could be achieved via a VSC mechanism.

3.4 Robustness analysis

In immunology, there is a need to understand the factor sustaining or impairing the specific T cell response [2, 31, 32, 42]. In the context of designing a control strategy for an engineering system, a robustness analysis is conducted to investigate how modelling and parameter uncertainty affect the stability and the performance enforced by the designed control action [10, 67, 101]. Formulating the immune response function as a VSC law is useful to provide a constructive framework to investigate the effects of uncertainty and perturbations on the T cell population dynamics.

Uncertainty associated with the model of the specific T cell response (3.1)-(3.3) can be related to changes in biological rates, neglected immunological dynamics such as the dynamics of APCs and perturbations caused by pathogen. In the following, the term d_u is introduced to represent some biological perturbations in the dynamics of the activated T cells. It is worth to mention that instead of this additive perturbation, parameter and modelling uncertainty can also be considered. The dynamical equation for the population of activated T cells becomes

$$\frac{dA}{dt} = \mathcal{F}(t)\left(a_N N + a_M M + \rho A + mA\right) - (m + d_A)A + d_u \tag{3.8}$$

This is motivated by the fact that the dynamic of the population of activated T cells can be impaired by the effects of pathogen following infection [2, 42, 48, 52, 57, 102]. In this section, a particular type of VSC, the so-called sliding mode control [13–16] is used to analyse the dynamics of the specific T cell response observed experimentally [2, 45, 103].

In Chapter 2, sliding mode control principles have been reviewed using the classical example of the pendulum system [7, 10]. A switched control strategy was formulated to drive and then constrain the states of the pendulum system to lie within a close neighbourhood of a predefined switching function. Furthermore, the choice of the switching function has been shown to dictate the dynamic behaviour of the system. Additionally, the switching function provides a measure of the desired performance of the system. Here, the sliding mode control framework and analytical tools are not used to design and implement a controller but to study the immune response function as a VSC immanent in the dynamics of the specific T cell response.

The following switching function,

$$s_1 = A \tag{3.9}$$

is chosen because the manifold $s_1 = A = 0$ is associated with the absence of an ongoing immune response and a healthy state. Furthermore, $s_1 = 0$ enforces a stable immunological steady-state. The reachability condition to attain and maintain sliding mode on $s_1 = 0$ is given as:

$$\begin{aligned} s_1 \frac{ds_1}{dt} &< 0 \\ A\left(\mathcal{F}(t)\left(a_N N + a_M M + \rho A + mA\right) - (m + d_A)A + d_u\right) &< 0 \end{aligned} \tag{3.10}$$

Note that s_1 is always non-negative because this switching function represents a number of cells. The expression of the reachability condition (3.10) reinforces that the immune response function $\mathcal{F}(t)$ plays a major role in the determination of the dynamical behaviour of the specific T cell response. Considering the values of biological rates estimated in various studies, see Table 3.2 and [1, 29, 91], (3.10) shows that the immune response program is robust to variations in the values of these biological rates due to changes in virus strains and epitopes. In essence, despite the occurrence of biological perturbations following infection, the immune response function must satisfy $s_1 \frac{ds_1}{dt} > 0$ to induce the clonal expansion phase for a certain period of time to clear the infection as well as switch to $s_1 \frac{ds_1}{dt} < 0$ to enforce the contraction and memory phase of the specific T cell response. Consider the time evolution of the reachability condition in Fig 3.6 from the simulation of the specific T cell response in Fig 3.4. Initially, s_1 moves away from the chosen sliding manifold $s_1 = 0$. However, this transient dynamic is necessary from an immunological standpoint because it enforces the rapid proliferation of activated T cells to contain the infection to achieve protective immunity [1, 2]. After the transient phase of the clonal expansion, the manifold $s_1 = 0$ is rendered attractive by the immune response function. As a result, the trajectory of s_1 is driven towards the origin and the contraction and memory phase of the T cell response is induced. Hence, the reachability analysis used here, delivers analytical conditions for the immune response program to prescribe desirable T cell population dynamics.

The simulation of the model for an extended time period shows that the switching function (3.9) exhibits a sequence of oscillations rather than lying on the manifold $s_1 = 0$. These oscillations are caused by frequent rebound of the pathogen. In fact, the considered dynamical equation (3.6) for the pathogen growth dynamic does not produce a steady-state behaviour matching that of acute viral/bacterial infection [2, 44]. However, the transient dynamics generated by the resulting closed-loop system is consistent with the ones of the primary antigen-specific CD8+ T cell response up to day 28 [29].

Thus, the dynamics of the model after day 28, do not allow the reachability condition to remain satisfied. Hence, the reachability analysis is shown to capture the discrepancies between the dynamical behaviour of the model and experimental observations in [1, 2, 29]. The limitation of this model is due to the mathematical relationship between the pathogen dynamic (3.6) and the candidate antigen-dependent immune response function (3.6). On the one hand, the mathematical expression of eq (3.6) has an unstable pole i.e $r > 0$ at the healthy state where $B = 0$. This feature allows the model to reproduce the rapid growth of

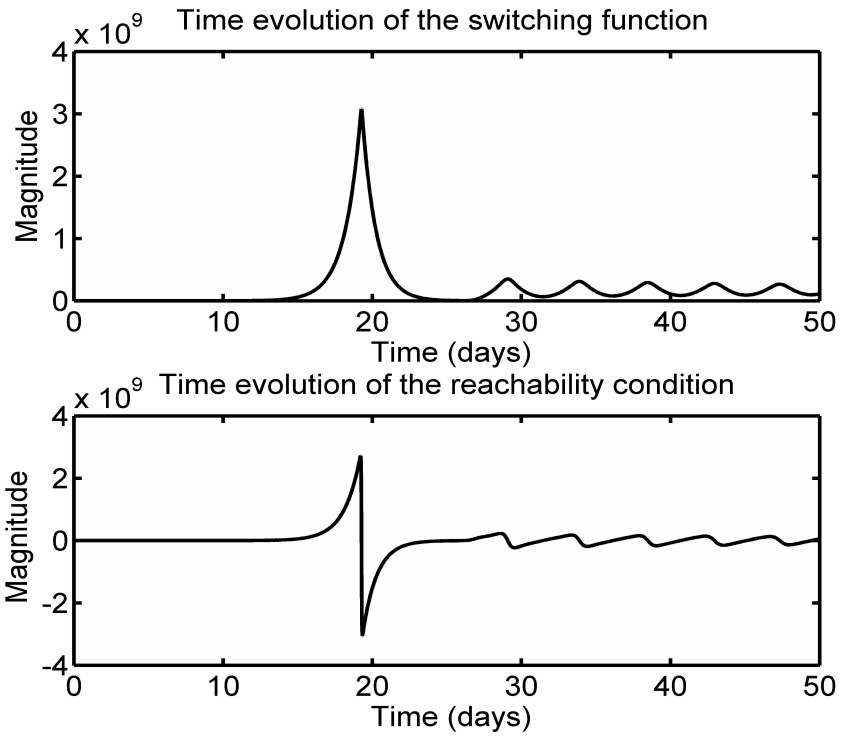

FIGURE 3.6: Time evolution of the sliding surface and reachability condition for the dynamics of the specific T cell response described by the closed-loop system formed by (3.1),(3.3),(3.6) and (3.10) with the antigen-dependent activation function (3.5)

the pathogen in the early days post infection but also prevents the model exhibiting realistic kinetics of pathogen decay and clearance observed after acute infection [2]. On the other hand, the candidate antigen-dependent immune response function (3.6) solely relies on the pathogen dynamics to provide the required switch in the feedback regime governing the population dynamics of T cells. Although this simple expression delivers reasonable results, it is clear that the connection between the antigen stimulation and T cell response dynamics is more sophisticated. Consequently, in other studies it is important to determine the boundaries within the model match experimental observation and to investigate a sensible relationship between the kinetics of the pathogen concentrations and the kinetics of T cell populations.

From this point onwards, the work focuses on the time window from day 0 to day 28 post-infection because these dynamics match the ones observed in experimental studies [2, 29].

The analysis of the simulation of the model eq (3.6)-(3.3) with eq (3.5) reveals that the model appropriately captures the dynamics of the T cell response to acute infection for a given period of time.

After considering the nominal case with $d_u = 0$ in Fig 3.4 and Fig 3.6, the impact of perturbation signals on the population dynamic of the specific T cell response is examined by analysing the dynamics of the system in the sliding mode. Assume that after a time t_s, the sliding mode occurs and $s_1(t) = \frac{ds_1}{dt} = 0$ for all $t > t_{s_1}$. It follows that $\dot{s}_1 = A = 0$ and thus an *equivalent control* action, introduced in Chapter 2 section 4, can be computed as follows:

$$\mathcal{F}(t)_{eq} = -\frac{d_u}{a_n N + a_m M} \tag{3.11}$$

By substituting (3.11) in (3.8), it is seen that the action of the immune response cancels the effects of the disturbance in the sliding mode. This demonstrates that the immune response program effectively possesses some robustness properties.

Furthermore, consider a candidate Lyapanov function for the reduced order dynamics given by $V(N, M)$ where

$$V(N, M) = N + M \tag{3.12}$$

$$\frac{dV(N, M)}{dt} = -(a_n N + a_m M)\mathcal{F}(t)_{eq} - d_N N - d_M M \tag{3.13}$$

This Lyapanov function is positive definite as required [104] because the state variables $N \geq 0$ and $M \geq 0$. From (3.11), it can be deduced that when the perturbation signal is a function of A, the dynamics in the sliding mode are not affected and remain stable. Nevertheless, this type of perturbation can drastically influence the transient dynamics of the immune response when they have a sufficient magnitude to change the sign of $s_1 \frac{ds_1}{dt}$, see (3.10). In practical implementation of sliding mode control, it is well known that though some disturbances are cancelled when sliding mode is reached, they might impair the reaching phase and transient dynamics of the system [10, 13, 16, 17, 22]. In the VSCS example presented in Chapter 2, it has been seen that the designed discontinuous control action provides complete invariance to parameter and modelling uncertainty when sliding mode occurs.

In experimental and mathematical studies of the kinetics of the virus-specific memory CD8+ T cell response following chronic infection, it has been shown that the clonal expansion phase is impaired [2, 48]. In effect, activated memory CD8+ T cells undergo a block in their proliferation and the clonal expansion phase does not last long enough to clear the infection [2]. The simulation experiment conducted in Fig 3.7 shows a perturbation signal

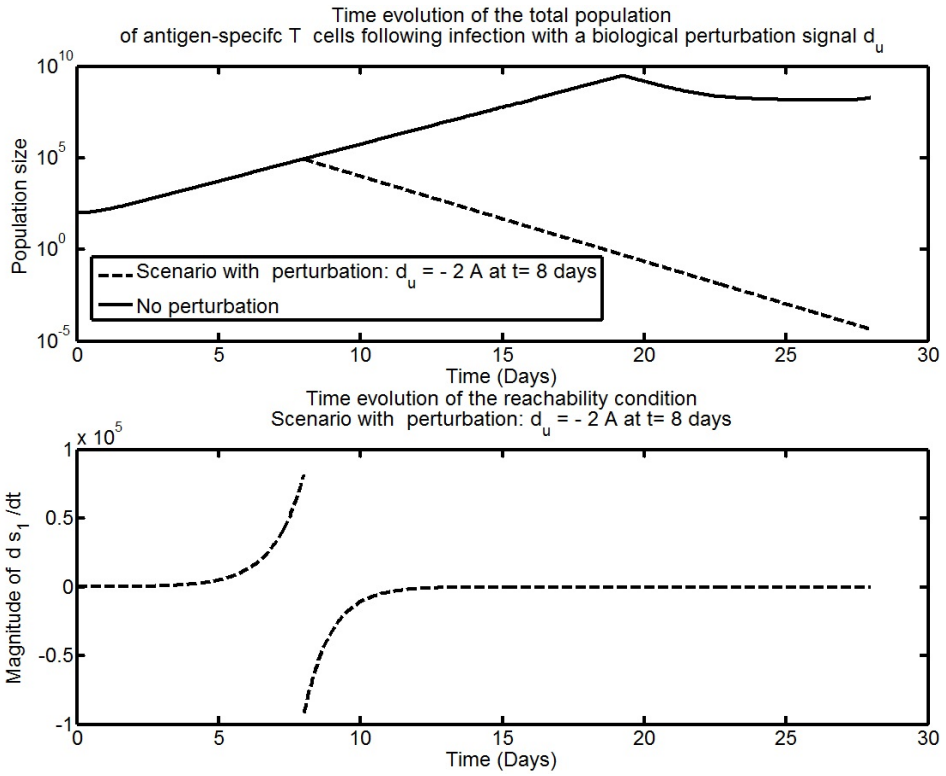

FIGURE 3.7: Time evolution of the reachability condition and total population of antigen-specific T cells in the presence of a strong biological perturbation. $d_u = -2A$ for $t > 8$ and $d_u = 0$ otherwise. Model of the specific T cell response described by the closed-loop system formed by (3.1),(3.3),(3.6) and (3.10) with the antigen-dependent activation function (3.5)

$d_u = -2A$ which occurs during clonal expansion. The resultant population dynamic of the T cell response is consistent with the ones observed in experiments. From the reachability analysis, it is clear that when the disturbance signal occurs, the condition $s_1 \frac{ds_1}{dt}$ to maintain cell proliferation is no more satisfied. This causes an early and undesirable reduction of the population size of activated T cells. From a VSC standpoint, the magnitude of the proliferation of activated memory CD8+ T cells must be boosted to keep $s_1 \frac{ds_1}{dt} > 0$ as long as required to achieve protective immunity despite chronic infection.

Though the disturbance signal $d_u = -2A$ alters the transient dynamics of the T cell response, (3.11) shows that this is effectively a zero perturbation in the sliding mode because $s_1 = A = 0$. The Lyapanov stability analysis from (3.12)-(3.13) confirms that the dynamics in the sliding mode remain stable when $d_u = -2A$. Besides, a disturbance signal which is a time-invariant function or a function independent of the population of activated T cells or a function of the virus dynamic does not vanish in the sliding mode, see (3.11). Of note, this type of perturbations are completely rejected when the immune response function establishes a sliding mode. In Chapter 2, it was demonstrated that when the designed

control action enforces sliding mode, the control action totaly rejects the effects of matched uncertainty such as non-vanishing perturbation signals acting in the input channel.

Although the population dynamic of CD8+ T cells exhibits some inherent robustness properties, some biological phenomena such as unwanted T cell activation have the potential to disturb feedbacks regulating the appropriate dynamic and population size of CD8+ T cells [37, 40, 42, 45]. In fact, inappropriate activation or inhibition of the immune response of T cells can lead to inflammation-induced tissue damaged, persistent infections or autoimmunity [2, 31, 42, 105]. In a VSCS under the effects of disturbance, failure of the reachability condition is synonymous with the inability of the designed control action to enforce a sliding motion in the presence of these disturbances [10]. In other words, the magnitude of the control action is insufficient to cancel the effects of the disturbance. In such cases, a different equilibrium (stable or unstable) is exhibited by the system.

The scenario of an inappropriate CD8+ T cell activation caused by non-specific proliferation signals or bystander effects [9, 37, 40, 52] is simulated in Fig 3.8. This simulation demonstrates that when a potent disturbance signal occurs (in this case an inappropriate activation), the immune response program fails to overcome the effects of the disturbance. Consequently, the reachability condition is no longer satisfied and the sliding motion is lost. Hence, failure of the dynamical conditions provided by the reachability analysis in presence of disturbance is congruent with inappropriate T cell response dynamics.

3.5 Conclusion

In this chapter, experimental and mathematical studies on the specific T cell response dynamics following infection [2, 29, 38, 39, 76] have been revisited from a control engineering standpoint. The immune response program, the function describing the dynamical behaviour of antigen-specific T cells in response to the infection, has been shown to possess characteristics similar to the ones of a variable structure control law. In essence, this function switches between different feedback regimes to enforce the clonal expansion phase followed by the contraction and memory phase of the T cell response to achieve immunological requirements. Furthermore, the robustness properties of the dynamics of the specific T cell response observed in experimental studies have been formally assessed using tools from sliding mode control theory.

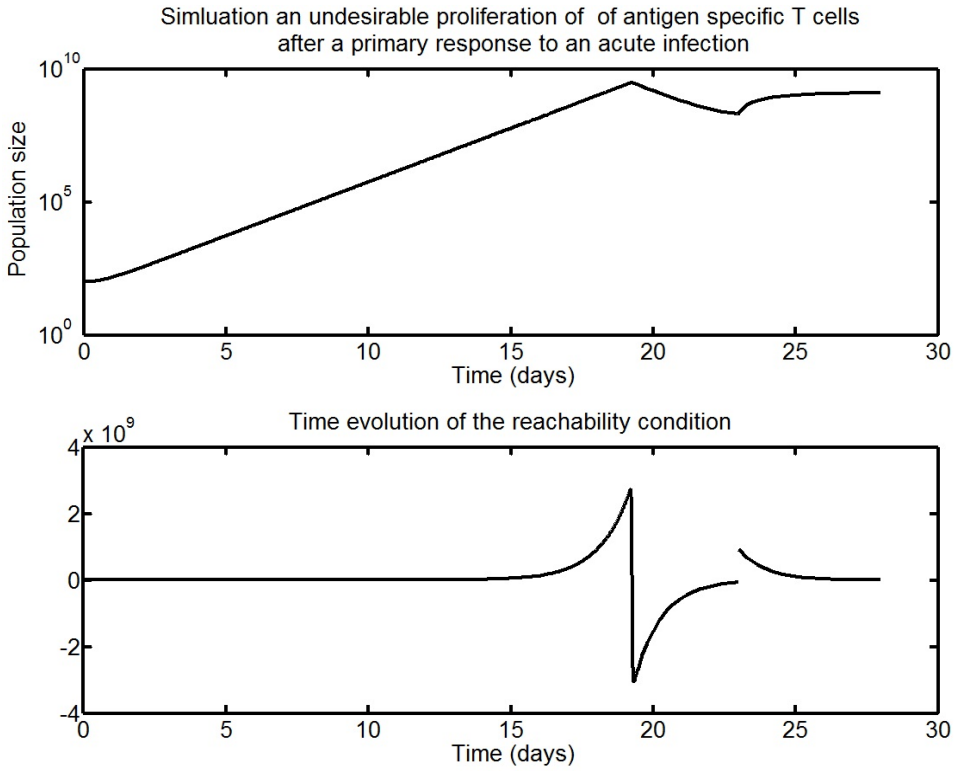

FIGURE 3.8: Time evolution of the reachability condition and total population of antigen-specific T cells following infection with an undesirable proliferation signal d_u at day 23. Model of the specific T cell response described by the closed-loop system formed by (3.1),(3.3),(3.6) and (3.10) with the antigen-dependent activation function (3.5)

Collectively, the results of this chapter motivate the analysis of the immune system as a closed-loop feedback system in which the immune response function changes T cell population dynamics to respond to threat and to maintain health. Importantly, analytical tools from variable structure control are shown to provide sensible means to study the dynamics of proper and improper T cell responses.

Consequently, control engineering techniques are used to examine the dynamics of tolerance and autoimmunity in the next chapter. Furthermore, the dynamics of Human Immunodeficiency Virus infection in vivo are considered and the reachability analysis is used to provide dynamical conditions to enforce the containment of the infection by the HIV-specific CD8+ T cell response and by antiretroviral drugs.

Chapter 4

Self-Tolerance Mechanism of T Cells, a natural VSC

4.1 Introduction

In this chapter, the characteristics of the control mechanism governing the self-tolerance dynamics of T cells are studied using tools from control theory. The novelty of this approach resides in the use of VSC techniques to study tolerance mechanism of the immune system. Candidate immune response functions are analysed as different control strategy to achieve tolerance. Motivated by the synergies between the immune system and VSCS shown in Chapter 3, the sliding mode control paradigm introduced in Chapter 2 is used to design an adaptive sliding mode control modelling immunological feedbacks which suppresses autoimmune responses and achieve a robust tolerance steady-state.

The maintenance of a healthy state by the immune system is underpinned by an appropriate regulation of immune responses to clear infection as well as to prevent damage of self tissues [31, 32]. The notion of self-tolerance of the immune system refers to the ability of the immune system to both prevent and suppress autoimmune responses i.e immune responses targeting self tissues. In effect, the immune system incorporates feedback mechanisms to regulate the dynamics of self-reacting T cells to establish a healthy tolerance state. Consequently, the healthy state enforced by the immune system is maintained despite the presence of self-antigen and self-reacting T cells.

The relation between the density of self-antigen and the inducement of tolerance or autoimmunity influences the dynamics of immune cells and determines the maintenance or loss of a healthy state. Different immune response functions have been proposed in [40, 51, 52] to investigate different ways in which the density of self antigen induces the activation/proliferation of self-reacting T cells. Fundamentally, these candidate immune response functions establish a positive feedback between the density of self antigen and the population dynamics of self-reacting T cells.

When a linear or a Michaelis-Menten immune response function is used, the work in [40, 51] have shown that the concept of the reproductive ratio can be used to determine the maintenance of the tolerance steady-state. In effect, the reproductive ratio in this context highlights a steady-state condition for the stability of the tolerance steady-state. This approach infers that the break down of tolerance state imposed by the immune response function is sensitive to changes in the values of the biological rates of the model. In contrast, when a sigmoidal immune response function is considered, the reproductive ratio cannot be defined and the attainment of the tolerance steady-state depends on the density of self antigen. Hence, the framework of the reproductive ratio is not robust to changes in the mathematical formulation of the immune response function.

The framework of control engineering is considered because the work in Chapter 3 has demonstrated that the specific T cell response to acute infection is effectively a closed-loop dynamical system. Furthermore, the control analysis performed in Chapter 3 has proved that the immune response program, which dictates T cell population dynamics following infection, fits the variable structure control paradigm presented in Chapter 2. In fact, the immune response program operates as a variable structure control law which changes in T cell population dynamics to clear the infection and restore a healthy state. Moreover, it was shown that analytical tools from sliding mode control provide means to examine the conditions for the robustness of the closed-loop dynamics imposed by the immune response function. Motivated by these results, the framework of sliding mode is utilized to formulate a dynamical condition for the immune response function to enforce a robust tolerance steady-state.

Current findings in immunology indicate that self-tolerance is not only due to a weak positive feedback between the density of self antigen and the responding CD4+ or CD8+ T cells [31, 50, 80, 83]. In fact, the population dynamic of regulatory T cells has been shown to be crucial for the maintenance of a robust tolerance state. The action of regulatory T

cells operates a negative feedback suppressing ongoing autoimmune responses [31, 86, 106]. In the mathematical studies in [9, 40, 87, 107] where the population of regulatory T cells is modelled explicitly, the gain of the feedback engendered by regulatory T cells must have a sufficient magnitude to enforce the tolerance steady-state. The similitude between the robustness properties of high gain linear state feedback systems and discontinuous systems have been proven by control theory [10, 21]. Further, it is demonstrated that a discontinuous feedback inhibiting autoimmunity can indeed establish a robust tolerance steady-state.

The organisation of the chapter is as follows. First, the tolerance mechanisms of the immune system are reviewed. Next, a model of the immune system is considered and the impact of some candidate immune response functions on the maintenance of tolerance is analysed. Finally, a sliding mode control analysis is performed to model a robust tolerance mechanism.

4.2 Review of tolerance mechanisms

The seminal paper of Medawar [108] introduced the notion of immune tolerance to self tissues in 1953. This early work shows that there is a central mechanism of tolerance exerted by the thymus. It was first thought that tolerance was established by the elimination of all T cells in the thymus. Subsequent experimental studies [106] clarified that many autoreactive T cells undergo clonal deletion in the thymus due to negative selection. Unexpectedly, it was found that some T cells with a high affinity to self antigen are preferentially selected and survive to form the population of natural regulatory T cells (nTregs). Nonetheless, there are autoreactive T cells which are able to exit the thymus and circulate in the lymphoid and peripheral blood stream.

Furthermore, there exist peripheral tolerance mechanisms which prevent or shut down immunogenic responses against self tissues [31]. The activation and clonal expansion of T cells requires three signals: antigen presentation signal, costimulatory signal and cytokine IL-2 signal. Inappropriate T cell activation signals at the cell surface engender clonal deletion and/or anergy. Interestingly, each of these signals is associated with a certain tolerogenic process [31]. In addition, the combination of these signals at the cell surface obeys a particular decision-making rule to induce antigen-specific T cell responses [37]. In fact, the avidity of the T-cell-receptor (TCR) interaction with cognate antigen must exceeds a certain threshold to activate the T cell [109, 110]. This activation threshold is determined by a certain costimulatory molecule [111] and the avidity is influenced by both

the affinity of the antigen with the TCR and the quantity of available antigen [110]. Hence, different molecular feedback mechanisms allow the immune system to tolerate the presence of mature autoreactive T cells in the peripheral blood and tissues [31, 106].

Besides, recent experimental studies have demonstrated the existence of regulatory T cells and their dominant role in the control of immune responses elicited by self and foreign antigen as well as the maintenance of immunological homeostasis [31, 42, 50, 86, 88, 106]. In addition, to the existing population of natural regulatory T cells, adaptive regulatory T cells are generated from naive CD4+ T cells during inflammation [31, 106]. The activities of both natural and adaptive regulatory T cells provides an active mechanisms to generate robust tolerogenic responses and maintain a robust tolerance steady-state [31, 50, 86]. In the case of autoimmunity, an insufficient number of regulatory T cells or defective regulatory T cells are found at the site of the inflammation or damage [50, 92, 106]. Thus, the state of autoimmunity results from an improper balance between immunigenic and tolerogenic mechanisms. Interestingly, therapeutic strategies have shown that the healthy balance can be restored using cytokine IL-2 to increase the number and/or to enhance the efficiency of regulatory T cells [31, 92].

Collectively, current experimental findings reinforce the notion of tolerance as active mechanisms which dynamically regulate and control immune responses [31, 92]. Fundamentally, the induction and maintenance of tolerance is achieved by the interactions between different types of cells and molecular pathways. Appropriate switching between feedback regimes that trigger or suppress the immune response is accomplished by the immune system to provide required immunological actions to sustain good health [2, 31, 42, 80]. Consequently, there exists strong synergies between the dynamics of the immune system and the dynamics of engineering systems with a switched control law shown in Chapter 2. Inherent immunological switching rules in combination with cellar and molecular feedback mechanisms allow the immune system to change its dynamics (expansion or reduction of some cell population) to achieve immunity and tolerance. It can be argued that experimental results and insights on the mechanisms of tolerance [31, 106] constitute compelling evidence for the notion of the immune system as a robust variable structure control system.

4.3 Analysis of dynamics of self-tolerance

A simple mathematical model as been presented in [51] to study the mechanisms underpinning the dynamics of tolerance and autoimmunity. The dynamical equations are given as:

$$\begin{aligned} \dot{T} &= \lambda - \mu T - \beta TC \\ \dot{D} &= \beta TC - \alpha D \\ \dot{C} &= u - \gamma C \end{aligned} \tag{4.1}$$

The state variables are T, the population of healthy target cells (cells/ml), D the population of damaged target cells (cells/ml) and C, the population of self-reacting T cells (cells/ml) destroying target cells. Note that in the model (4.1), the effects of other molecular or cellular dynamics such as cytokine Il-2, dentritic cells or regulatory T cells are implicit.

Various mathematical models have been proposed to study the dynamics of self-tolerance [9, 40, 51, 82, 107, 112]. The differences in the dynamical equations are due to differences in modelling assumptions and focus of the investigations. A block diagram of the model (4.1) is given in Fig. 4.1.

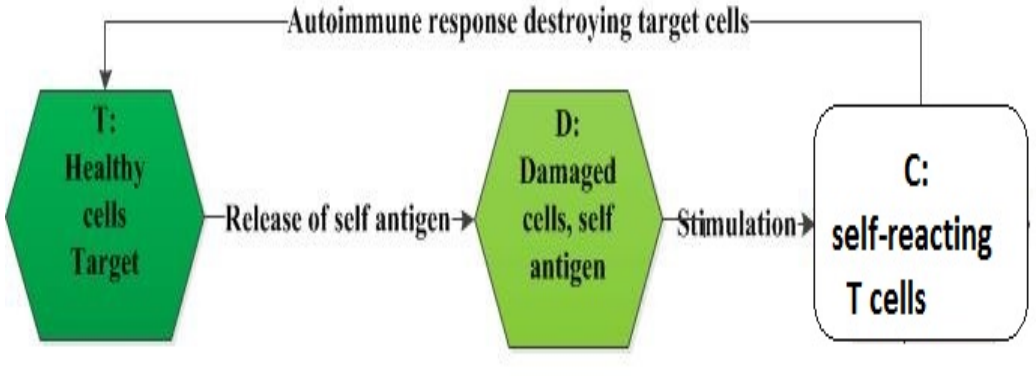

FIGURE 4.1: Model (4.1) of self-tolerance/autoimmunity where the immune response function describes the dynamic response of self-reacting T cells after self-antigen stimulation

The model (4.1) has been chosen due to its simplicity and especially due to the fact that it describes the dynamical interactions between self reactive T cells and the targeted self tissues. This simplicity facilitates the mathematical analysis to study the impact of the immune response function in the context of self-tolerance. Additionally, it was shown in

[51] that this model produces reasonable qualitative behaviour despite the fact that various cell populations such as antigen presenting cells, regulatory T cells and some molecular dynamics are not explicitly represented in the dynamical equations.

Here, the model (4.1) describes the scenario of an autoimmune response of C, a population of self-reacting T cells (CD4+ or CD8+ T cells) towards a target tissue T after simulation by self antigen from damaged target cells D. Consequently, the default initial conditions are chosen to be $T(0) = \frac{\lambda}{\mu}; D(0) = 1; C(0) = 0$ as in [51].

Target cells are produced at a constant rate λ and die at a constant rate μ. Thus, the population growth of healthy cells (T) is assumed to be affine in this model. The parameter β describes the efficacy of the damage process induced by autoreactive T cells. From [51], β also refers the rate at which immune cells find target cells and the rate at which the target cells are successfully attacked by immune cells. The parameters α and γ denotes the death/clearance rate of damaged cells and autoreactive effector T cells respectively. It is assumed that there are constant death rates for each type of cell. Of note, these biological parameters and state variables are non-negative due to their biological meanings.

The default parameter values are taken from [51] and given as: $\lambda = 10$; $\mu = 0.1$; $\beta = 0.5$; $\alpha = 1.1$; $\gamma = 0.1$.

Consider u, an immune response function influencing the dynamic response of the population of self-reacting T cells following self antigen stimulation. A candidate closed-loop dynamics formed by

$$u = F_{PI}(D) \tag{4.2}$$

The personal immune response function approach in [51, 52] effectively assumes that different people have different immune response characteristics. The function u is studied here as an inherent immunological control feedback for the closed-loop model (4.1). The impact of candidate mathematical functions for u to model the establishment of tolerance or autoimmunity will be investigated from a control standpoint.

The general expression of the equilibrium of the system (4.1) is given as;

$$T_{ss} = \frac{\lambda}{\mu + \beta C_{ss}}; \quad D_{ss} = \frac{\beta T_{ss} C_{ss}}{\alpha}; \quad C_{ss} = \frac{u}{\gamma} \tag{4.3}$$

and the Jacobian matrix of the equilibrium (4.3) is given as:

$$J = \begin{pmatrix} -\mu - \beta C_{ss} & 0 & -\beta T_{ss} \\ \beta C_{ss} & -\alpha & \beta T_{ss} \\ 0 & \frac{du}{dD} & -\gamma \end{pmatrix} \tag{4.4}$$

From (4.3), it is clear that the immune response function u determines both the expression and magnitude of the steady-state of the cell population. In experimental studies [31, 80, 113, 114], the population size of target cells and self-reacting effector T cells are sensible indicators to monitor and diagnose autoimmunity. It can be deduced from (4.3) that the immune response function influences the observed immunological steady-states.

The trivial equilibrium

$$T_0 = \frac{\lambda}{\mu}; \quad D_0 = C_0 = 0 \tag{4.5}$$

where $u = 0$, corresponds to a tolerance steady-state because the population of target cells is not affected by autoreactive T cells. From a control perspective, a means to achieve robust tolerance is to ensure that the population dynamics of the system (4.1) attain and remain at this healthy equilibrium irrespective of initial conditions, parameter and model uncertainty. The characteristic equation obtained from the computation of the Jacobian matrix (6.9) at this trivial equilibrium is given as:

$$(s_s + \mu)(s_s + \alpha)(s_s + \gamma) = 0 \tag{4.6}$$

Consequently, the tolerance steady-state (4.5) is stable because the characteristic equation (4.6) has three real and negative poles which are $-\mu, -\alpha$ and $-\gamma$ [51, 69]. Recall that these biological decay rates are positive.

Next, consider the stability and performance of the open-loop system where u is not a function of the states of the system. This open-loop system has only one equilibrium, see (4.3). From the characteristic equation of the open loop system, a root-locus analysis is performed. Changes in the values of u in Fig. 4.2 demonstrate that the immunological steady-state is imposed by the considered open-loop system. Although changes in the magnitude of u affects the amplitudes of the poles, they remain in the left hand side of the complex plane. Nevertheless, different values of u lead to different clinical interpretations of

the exhibited immunological steady-state due to the associated changes in the population size of target cells and self-reacting effector T cells.

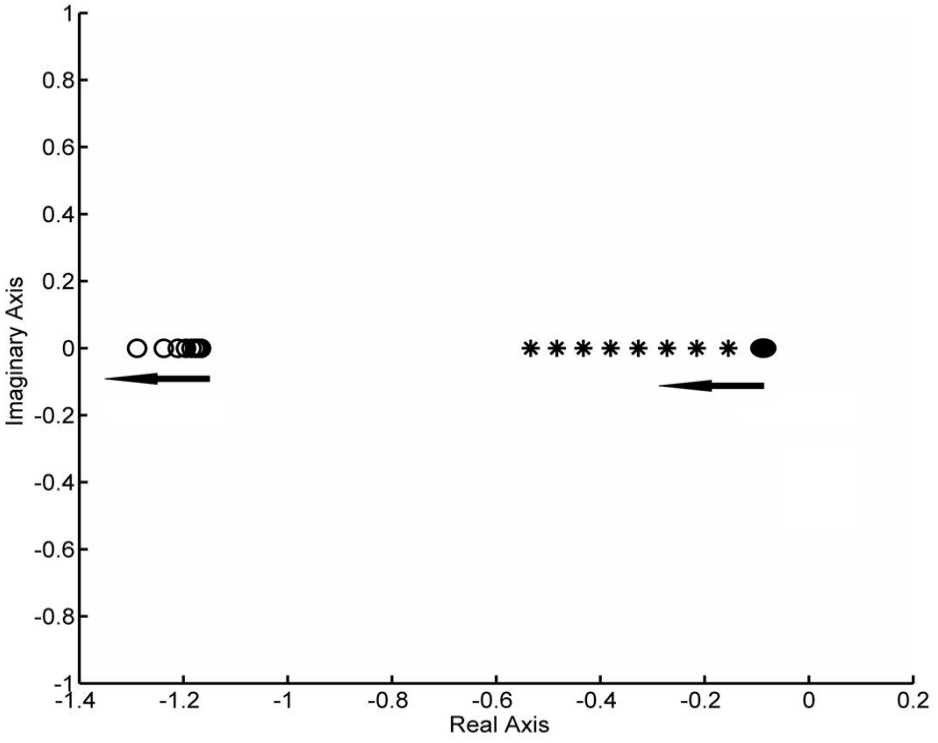

FIGURE 4.2: Variation of the poles with respect to an increase in the value of the open-loop control $0 \leq u \leq 2$ for the system (4.1)

The simulations in Fig. 4.3 and Fig. 4.4 produced using different constant values of u depict a tolerance and an autoimmune disease steady-state respectively. As the value of u increases from zero, the population of self-reacting effector T cells C increases and this leads to the reduction of the population of healthy target cells. Consequently, the dynamics of the system move away from the tolerance steady-state and attains a stable non-trivial autoimmune disease steady-state.

Now, consider the closed-loop dynamics formed by (4.2), an antigen dependent immune response function is considered. The function $F_{PI}(D)$ is effectively an immune response program [1, 32, 38, 80] which defines how the density of self antigen influences the activation/proliferation of self-reacting effector T cells. From a control standpoint, (4.2) represents a state feedback which closes the loop for the system (4.1). Consequently, candidate immune response functions proposed in the literature [46, 51, 52] are examined as candidate feedback regime which determine the dynamics of the immunological response upon antigen stimulation.

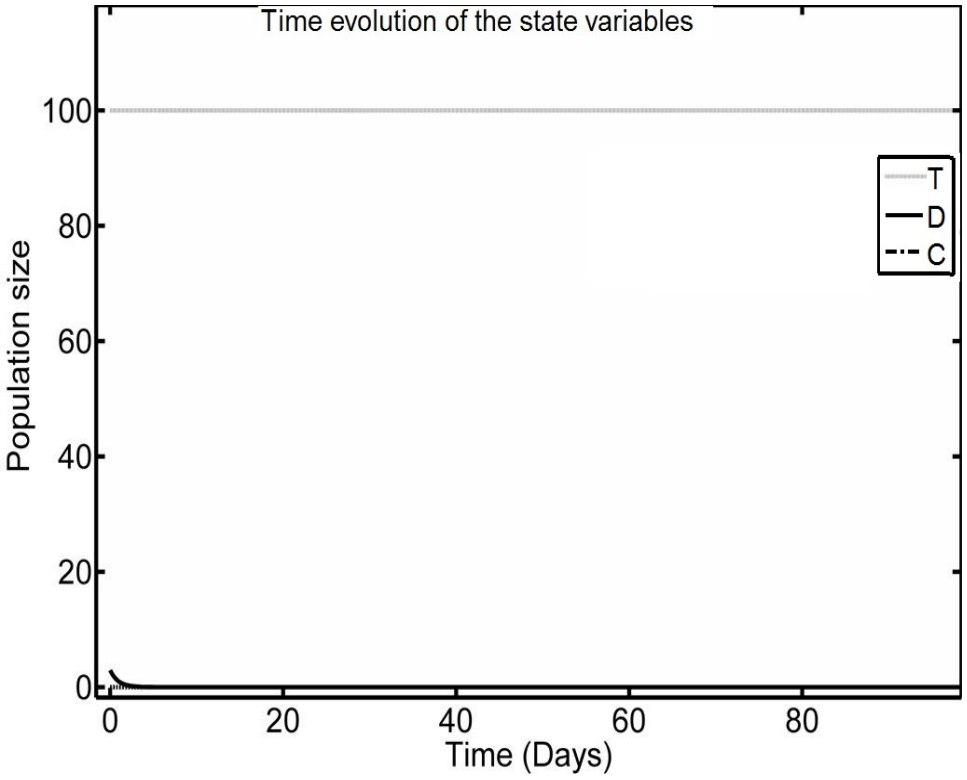

FIGURE 4.3: Simulation of the open-loop system $u = 0$ in system (4.1).

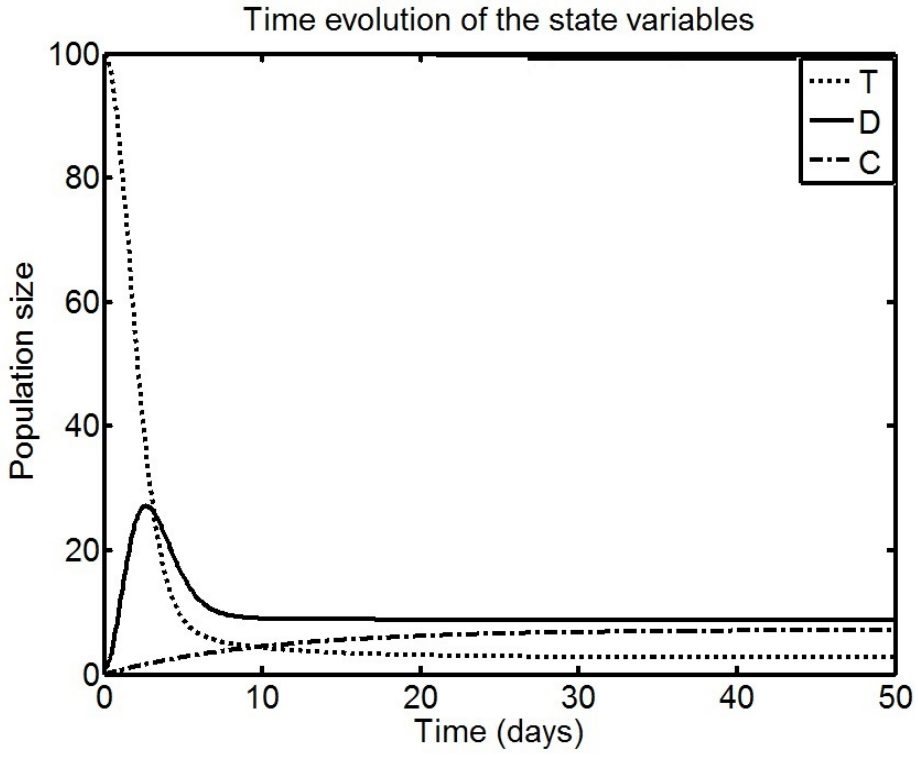

FIGURE 4.4: Autoimmune disease scenario when the open-loop $u = 0.7$ in system (4.1)

A basic approach is to suppose that the proliferation of autoreactive T cells is proportional to the antigen density. This leads to the linear immune response function given as

$$F_{PI1}(D) = kD \tag{4.7}$$

where $k > 0$ is the average magnitude of activation/production of T cells responding to antigen stimulation [51]. This formulation of the immune response function has been used in various studies [40, 51, 54]. The use of (4.7) reduces the complexity of the mathematical model. The closed-loop system with (4.7) has two steady-states: the tolerance steady-state (4.5) and a non-trivial equilibrium located at $T_{L1} = \frac{\alpha\gamma}{\beta k}; D_{L1} = \frac{\lambda}{\alpha} - \frac{\mu\gamma}{\beta k}; C_{L1} = \frac{\lambda k}{\alpha\gamma}$ corresponding to an autoimmune disease state. The relation $\lambda\beta k - \mu\gamma\gamma = 0$ obtained from the characteristic equation at the tolerance equilibrium determines the sign of the poles at the equilibrium. Therefore, the stability of the equilibria is dictated by parameter values. This relation obtained at the steady-state underpins the reults produced by the reproductive ratio $R_0 = \frac{\beta k T_0}{\gamma\alpha}$ in [51].

From a biological perspective, (4.7) implies that self-tolerance is accomplished when the magnitude of the activation rate k is small enough to keep the tolerance equilibrium (4.5) stable despite the density of self antigen. The state of tolerance is lost and an autoimmune disease steady-state is reached when the value of k is large or due to variations in the values of the biological rates. From a control perspective, (4.7) represents a linear state feedback, as such, the dynamics prescribed by (4.7) are sensitive to parameter variations and modelling uncertainty, see simulation results in [51]. Changes in the value of any single parameter or multiple parameters can trigger autoimmunity. Consequently, the use of (4.7) generates some unrealistic insights on the robustness of the tolerance steady-state. For instance, changes in the value of λ, the production rate of target cell can induce autoimmunity and this is not realistic [31, 80].

Alternatively, a number of investigators have assumed a Michaelis-Menten kinetics to formulate the immune response function as follows:

$$F_{PI2}(D) = \frac{mD}{K_m + D} \tag{4.8}$$

where m is the maximum proliferation rate of self-reacting T cells and K_m is the antigen concentration at which the proliferation rate is half maximal [1, 29, 40, 51, 71, 98]. The function (4.8) is a hyperbolic function which is well established in enzyme kinetics within chemistry. Additionally, it has been applied in a diverse range of systems including ecology, the immune response and analysis of epidemics, functional response [71–73]. At low antigen

concentration, when $D \ll K_m$, $F_{PI}(D) = \frac{m}{K_m} D$ so that the rate is directly proportional to the antigen concentration. At high antigen concentration, $F_{PI}(D) = m$ so that the rate is maximal and independent of antigen concentration. When $D = K_M$, then $F_{PI}(K_m) = \frac{m}{2}$ and K_M is equal to the antigen concentration at which the reaction rate is half its maximal value [71–73]. Thus, the Michaelis-Menten function (4.8) is effectively an asymptotic switching curve. The stability and performance characteristics of the closed-loop system with are sensitive to parameter variations [51].

Using the linear approximation (4.7) or the Michaelis-Menten function (4.8), the system (4.1) has a tolerance steady-state (4.7) and a nontrivial equilibrium associated with an autoimmune disease state. When one equilibrium is stable, the other one is unstable. The parameter values of the system determine which one of these equilibria is stable. Importantly, these functions yields poor robustness properties and do not allow a dynamic switch of the immune system between tolerance state and a state of autoimmunity upon self antigen stimulation as observed in experimental studies [31, 80, 113].

Consider the candidate Holling type III personal immune response function from [51] given as

$$F_{PI3}(D) = \frac{mD^2}{D^2 + h^2} \tag{4.9}$$

where m is the maximum proliferation rate of immune cells and h is the antigen concentration at which the proliferation rate is half maximal. This function can also be referred to as a sigmoidal Hill function. The nonlinearity is achieved by increasing the effect of the state D and the variable K_M of the Michaelis-Menten candidate (4.8). (4.9) suggests that the proliferation of rate of activated T cells saturates at high antigen density. The resulting closed-loop system has three equilibria which exist if and only if $\lambda^2\beta^2m^2 - 4\mu\gamma\alpha^2h^2(\mu\gamma + \beta m) > 0$, see analysis in [51]. There is the tolerance steady-state (4.5), an unstable transient equilibrium E_- and a autoimmune disease steady-state E_+ . The poles of the tolerance equilibrium are : $-\mu; -\alpha; -\gamma$. These poles are negative because these parameters are positive biological constants. Therefore, the tolerance steady-state is always stable. It has been proven that whenever E_+ exists it is always stable if $\mu >> \gamma$. E_- is a saddle equilibrium having a two-dimensional stable manifold and a one dimensional unstable manifold. It was shown in Fig. 8 in [51] that E_- depicts a boundary surface between the absorbing domain of E_0 and E_+. When the antigen population is small the stable trivial equilibrium is reached, whereas the stable autoimmune disease equilibrium is experienced when the antigen concentration is large. As a result, the closed-loop system with (4.9) is a bistable system. The initial

conditions influence the dynamic response produced by the sigmoidal immune response function (4.9). Hence, the nonlinear state feedback generated by (4.9) generates a new dynamical behaviour and changes the mathematical structures of the equilibria, leading to a bistable immune system with some robustness properties. It can be deduced that (4.9) acts as a smooth variable structure control for the system (4.1) because it changes the dynamic response and structure of the system based on the antigen density.

In chapter 3, it has been demonstrated that the dynamics of the specific T cell response behaves as a variable structure control system in which the control law is defined by the immune response function. Further, the dynamical behaviour and robustness properties generated by the immune response function were shown to be similar to the ones of engineering systems with a discontinuous control feedback.

Considering the immune response function as a control switch, it can be deduced that there are strong similarities between the dynamics of VSCS shown in Chapter 2 and the closed-loop dynamics produced by biologically-inspired saturation functions [29, 46, 51, 52] for the immune responses. As seen in Chapter 2, the choice of the feedback strategy and its magnitude determines the robustness properties. This contributes to new understanding the nature of feedback mechanisms underlying biological phenomena.

Motivated by the observed activation threshold of the immune response [31, 82, 109, 115] and knowledge of variable structure control, a discontinuous function which models this switching mechanism and yields an improvement in the robustness of the immunological steady-states is proposed. This discontinuous immune response function given as

$$\begin{aligned} F_{PI4}(D) &= \frac{1}{2} m\,(S+1) \\ S &= sign(D-h) = \frac{D-h}{\|D-h\|} \end{aligned} \tag{4.10}$$

where h is an antigen threshold, has been developed from a control engineering perspective. This function reflects an activation/proliferation of antigen-specific T cells which depends on a threshold based on the antigen stimulation (density) as observed in experimental studies [31, 80, 109–111]. An on/off immunological switch is constructed using a sign function based on D. To yield a non-negative output, the sign function is shifted in the positive quadrant. The amplitude of the response m, is the saturation (maximum) proliferation

rate of the attacking autoreactive T cells. It has a step-like behaviour made up of a brutal (sharp) change in its output, the proliferation of autoreactive T cells. The discontinuous behaviour also yields antigen tolerance but implies an instantaneous change of behaviour (activation/inhibition). The behaviour of the discontinuous personal immune response function is the switching logic which changes the mathematical structure of the immune system whilst moving between the healthy and the autoimmune disease state.

The closed-loop system with (4.10) has three equilibrium points: the tolerance equilibrium (4.5) a transient equilibrium and an autoimmune disease equilibrium. The output of (4.10) determines which equilibrium is enforced. Considering the case where $S = -1 => F_{PI}(D) = 0$ which means that the population of antigen is less than the threshold, the tolerance equilibrium point is obtained.. The Jacobian is evaluated at (4.5). The roots of the characteristic equation are : $-\mu; -\alpha; -\gamma$. Since death rates are always positive, the poles are always negative. Therefore, the tolerance steady-state is always stable.

When the concentration of antigen is equal to the antigen threshold that is $S = 0 <=> F_{PI} = m/2$. the immune response is in a transient phase so it produces half the maximum proliferation rate of autoreactive T cells. The transient equilibrium point is:

$$T_1 = \frac{2\lambda\gamma}{\beta m + 2\mu\gamma}; \quad D_1 = \frac{\beta\lambda m}{\alpha(\beta m + 2\mu\gamma)}; \quad C_1 = \frac{m}{2\gamma} \tag{4.11}$$

The Jacobian at this equilibrium point is evaluated. The characteristic equation is a third order polynomial having positive coefficients for all powers of s_S. The Routh-Hurwitz stability criteria are applied and the transient equilibrium (4.11) is unstable. Now, the immunological scenario where $D > h <=> S = 1 <=> F_{PI}(D) = m$. This indicates that the antigen threshold is surpassed and the personal immune response function delivers the maximum proliferation rate. The resultant equilibrium point is expressed as:

$$T_2 = \frac{\lambda}{\mu + \frac{m\beta}{\gamma}}; \quad D_2 = \frac{m\beta\lambda}{m\beta\alpha + \alpha\mu\gamma}; \quad C_2 = \frac{m}{v} \tag{4.12}$$

This non-trivial equilibrium (4.12) is associated with an active autoimmune response and the reduction of the population of target cells. The Jacobian at this equilibrium (4.12)

is evaluated and its eigenvalues are: $-\alpha; -\gamma; -(\mu + \frac{m\beta}{\gamma})$. Since biological parameters are always positive, the eigenvalues are all negative. Therefore, this autoimmune disease steady-state is also stable. Hence, when the concentration of antigen is above the threshold, the immune response is activated and a stable chronic autoimmune disease state is exhibited. The function (4.10) thus provides a discontinuous switch between a stable tolerance steady-state and a stable autoimmune disease steady-state. It should be noted that the stability of these equilibria is insensitive to parameter variations. Importantly, the closed-loop dynamics generated by this discontinuous immune response function exhibit bistability and robustness to parameter uncertainty.

In summary, the nature of the immune response function significantly impacts the stability and robustness properties of the system (4.1) as seen in Table 4.1. The behaviour of the reviewed immune response switching curves upon antigen stimulation is shown in Fig 4.5. In simulations, using the analytical expression of the equilibria, each candidate function can be parameterized to have identical numerical coordinates for a stable non-trivial equilibrium to reach a common autoimmune disease steady-state. The purpose of Fig 4.6 is to highlight that each candidate immune response function engenders a particular transient dynamics. Thus, the nature of $F_{PI}(D)$ influences the stability, performance and robustness of the observed immunological states as well as their corresponding mathematical structures. It can be concluded that the immune response function of the form $F_{PI}(D)$ which models a positive feedback for the proliferation of self-reacting T cells by self antigen must change its structure dynamically to allow the immune system to switch between the tolerance and the autoimmune disease state.

Collectively, the analysis of the impact of the immune response function on the maintenance of self-tolerance [40, 51, 52] reinforces the argument that the immune response function is an immanent VSC feedback which governs the dynamic response of T antigen-specific T cells as well as the establishment of tolerance and autoimmune disease steady-state.

In Chapter 2, it has been seen that analytical tools from sliding mode control theory delivers means to investigate the stability, performance and robustness of VSCS. Further, the work in Chapter 3 proves that the framework of sliding mode control provides sensible insights on the dynamical behaviour and robustness of the specific T cell response following acute infection. Consequently, if the state of tolerance can be associated with an attractive manifold of the state-space, a reachability analysis can be performed to investigate the

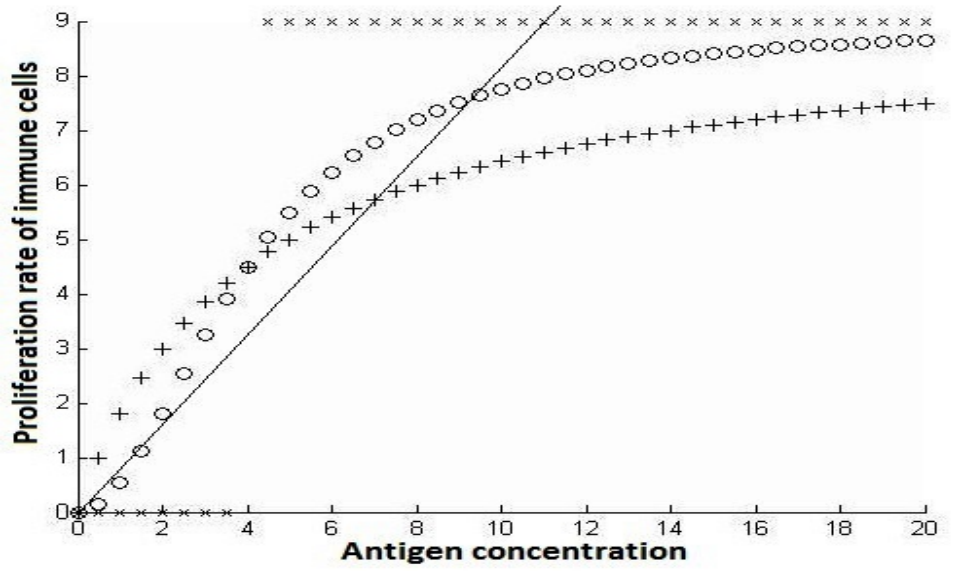

FIGURE 4.5: Different personal immune response curves (4.7)-(4.10): - linear, + Michaelis-Menten, o sigmoidal and x discontinuous.

performance of the immune response function, as an inherent control to achieve robust tolerance.

4.4 Sliding mode control framework

The framework of sliding mode control is considered to investigate the dynamics of tolerance due to the fact that the immune system as demonstrated in the previous sections

TABLE 4.1: Comparison of the mathematical structures and robustness of the immune system due to changes in the personal immune response function.

Personal immune response function	Qualitative behaviour
Proportional to antigen concentration as in equation (4.7), [116]	Stability and performance of the two equilibria are sensitive to parameter values
Michaelis Menten as in (4.8), [51]	Similar to above
Sigmoidal (Holling type III) equation (4.9), [51]	Bistability Saddle equilibrium Robust performance
Discontinuous switch based on antigen population equation (4.10)	Bistability Unstable equilibrium Robust performance

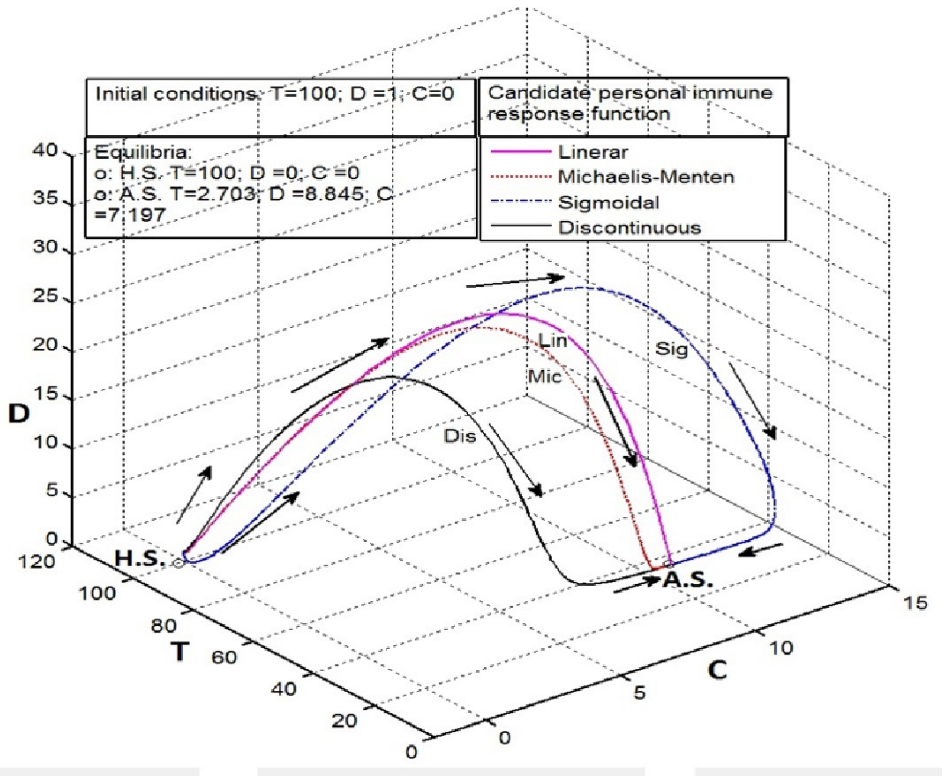

FIGURE 4.6: 3D plot of the dynamical behaviour of the immune system (4.1). Comparison of the transient dynamics resulting from the implementation of the candidate immune response functions (4.7)-(4.10). H.S.: Healthy tolerance steady-state (4.5), A.S.: Autoimmune disease steady-state. T: Target cells, D: damaged cells and C: self-reacting effector T cells.

incorporates an intrinsic VSC feedback, the immune response function which determines immunological responses and outcomes. Further, the reachability paradigm is used as a tool to assess dynamical conditions for the maintenance of tolerance. This adds to the state-of-the-art because when the reproductive ratio can be defined, it only provides a time invariant steady-state condition for the maintenance of tolerance [40, 51]. Furthermore, analytical tools from sliding mode control are utilized to assess the robustness of the immunological dynamics prescribed by the immune response function in the context of tolerance/autoimmunity as performed in chapter 3 in the scenario of infection.

A switching function given as:

$$s = D + C \tag{4.13}$$

has been designed using self antigen and autoreactive T cell dynamics because these dynamics are strongly involved with the dynamic response of the immune system to enforce tolerance homeostasis [31, 80, 109, 113, 117]. Importantly, the manifold $s = 0$ is associated

with the tolerance steady-state (4.5). Consequently, the tolerance state will be exhibited when the states of (4.1) lie on this manifold.

The reachability condition, introduced in Chapter 2, is expressed as:

$$s\dot{s} \quad < \quad 0$$

From (4.1) and (4.13),

$$s\dot{s} \quad < \quad s(\beta TC - \alpha D + u - \gamma C) \tag{4.14}$$

This inequality represents a dynamical condition for the immune response function u to allow the states of the system (4.1) to attain and remain on the manifold $s = 0$ associated with the tolerance steady-state (4.5). Consequently, the reachability condition (4.14) is a means to determine in the maintenance or loss of the tolerance state.

As seen in the previous section, the antigen-dependent immune response functions (4.7)-(4.10) describe a positive feedback mechanism in which the increase of the density of self antigen leads to an activation/proliferation of self-reacting T cells which causes the reduction of the population size of self tissues. Consequently, the output of the candidate immune response functions (4.7)-(4.10) where $u = F_{PI}(D)$ must vanish after self antigen stimulation to allow their respective closed-loop dynamics satisfy (4.14). In effect, when the output $F_{PI}(D) \to 0$ and vanishes because this leads to $C \to 0$ and an exponential decay of the states of the system towards the manifold $s = 0$.

When the reachability condition (4.14) is satisfied, it follows that $s = \dot{s} = 0$. The dynamics of the system under sliding mode are reduced to

$$\dot{T} \quad = \quad \lambda - \mu T \tag{4.15}$$

since $C- > 0$. This dynamical equation for the target cell population has a unique equilibrium $\frac{\lambda}{\mu}$ and a stable pole at $-\mu$. It can be deduced that when immune response function render $s = 0$ attractive and achieves tolerance, the effects of self-reacting T cells on the population dynamic of target cells are cancelled.

In essence, the candidate immune response function (4.7)-(4.10) describe the positive feedback of self antigen stimulation on the activation/proliferation of self-reacting effector T cells. Autoimmunity sets off when the magnitude of this positive feedback is sufficient to fail the reachability condition (4.14) and induces proliferation of autoreactive effector T cells. In immunology, it is well know that the presence of self antigen also triggers cellular and molecular mechanisms such as regulatory T cells and co-stimulatory molecules to suppress autoimmune responses [31, 50, 84, 86, 106, 111]. The action of these mechanisms can be regarded by biologists as regulatory loops that the immune system possesses to maintain robust tolerance homeostasis. Further, in mathematical studies where the dynamics of regulatory T cells explicitly represented [40, 87, 107], they produce a negative feedback to slow down or stop the proliferation of self-reacting T cells.

Current findings in immunology show that the immune system possesses regulatory mechanisms to suppress unwanted immune responses [31, 50, 86]. Physiologically, self-tolerance or autoimmune response inhibition is driven by immunological mechanisms which induce the death of activated autoimmune effector T cells [31, 86, 88]. Based on self antigen stimulation, the dynamics of regulatory T cells and other molecular signals produce a negative feedback to suppress autoimmunity and maintain a robust tolerance equilibrium.

The work in Chapter 2 has shown that when reachability condition for a sliding mode is satisfied, the states of the system are driven to chosen sliding manifold and remain on it. As a result, the closed-loop dynamics prescribed by the chosen sliding manifold are exhibited. In effect, the reachability analysis is used to design a VSC strategy to render the sliding manifold attractive to the states of the system. Motivated by the synergies between the control mechanisms of the immune system and the VSC paradigm shown in the previous sections, sliding mode control techniques are used to design a negative feedback modelling the effects of regulatory loops which inhibit autoimmunity. Since the manifold (4.13) is associated with the tolerance steady-state, a VSC strategy is designed to achieve a sliding monde on this manifold to produce a robust feedback to inhibit autoimmunity. Consider the following discontinuous function which yields autoimmune response inhibition when D and C are present:

$$u_1 = -\rho sgn(s) = -\rho \frac{s}{|s|} = -\rho \frac{D+C}{|D+C|} \tag{4.16}$$

The reachability condition (4.14) becomes:

$$\begin{aligned} s\dot{s} &\leq s(\beta TC - \alpha D - \rho sgn(s) - \gamma C) \\ s\dot{s} &\leq |s|(\beta TC - \alpha D - \gamma C - \rho) < 0 \end{aligned} \tag{4.17}$$

Since $s > 0$, the sign of (4.21) depends only on $\dot{s}$. The reachability condition thus reduces to:

$$\begin{aligned} \beta TC - \alpha D - \gamma C - \rho &< 0 \\ \beta TC - \alpha D - \gamma C &< \rho \end{aligned} \tag{4.18}$$

The amplitude of the controller for which the reachability condition is satisfied is sought. Failure of the reachability condition is a condition for failure of self-tolerance. For a range of initial conditions, a static value of ρ can be chosen to guarantee that the condition (4.18) is met and the sliding surface is reached. From (4.18), it can be noticed that the reachability condition is a function of the state variables and parameter values. The amplitude of ρ required to satisfy this condition will vary during the motion. The adaptation algorithm in [25] has been designed assuming a sliding mode condition which is a time-varying parameter bounded above and below. (4.18) does not directly yield an implementable controller in the case where parameters are uncertain.

It is an open problem to design a dynamic adaptive gain controller which produces the minimum magnitude of the discontinuity under uncertainty before and after ideal sliding motion.

An adaptation scheme is considered to reflect the fact that the regulatory loops of the immune system produces a dynamic response to suppress autoimmunity [31, 80, 86, 88]. The adaptation method considered here is a control gain proportional to the state variables. This tuning of the magnitude of the discontinuity has the benefit of reducing high control activity [10, 15]. Let ρ be a function of the state variables.

$$\rho = \rho_o + \beta_o TC \tag{4.19}$$

where ρ_o is a small constant. This produces the following adaptive sliding mode control

$$u_1 = -(\rho_o + \beta TC)sign(s) \tag{4.20}$$

A block diagram of this self-tolerance mechanism is given in Fig. 4.7.

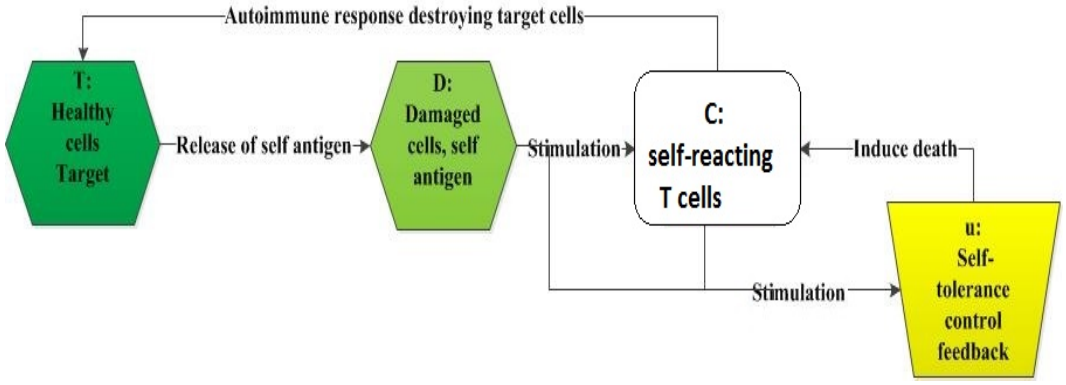

FIGURE 4.7: Model (4.1) of self-tolerance/autoimmunity where the immune response function u (4.20) is an adaptive sliding mode control feedback which imposes a robust state of self-tolerance via inhibition of self-reacting T cells

The ability of this function to enforce the tolerance steady-state and to render the manifold $s = 0$ is proven by substituting (4.20) in the expression of the reachability condition (4.14). This yields

$$\begin{aligned} s\dot{s} &< s(\beta TC - \alpha D - (\rho_o + \beta_o TC)sgn(s) - \gamma C) < 0 \\ -\beta_\delta TC - \alpha D - \gamma C - \rho_o &< 0 \end{aligned} \tag{4.21}$$

since $|s| = sign(s)$ and $s > 0$ and $\beta_\delta = \beta_o - \beta > 0$. As a result, u_1 satisfies the reachability condition. The desired negative feedback control action u_1 ensures that the trajectories of (4.1) reach the manifold $s = 0$ in finite time and remain on it. Consequently, he stable healthy tolerance steady-state (4.5) is enforced.

Consider the nominal values of the parameter of system (4.1) taken from [51]: $\lambda = 10$; $\mu = 0.1$; $\beta = 0.5$; $\alpha = 1.1$; $\gamma = 0.1$; $\beta_o = 1$; $\rho_o = 0.0$.

The purpose of the simulation in Fig. 4.8 is to demonstrate that function (4.20) as a regulatory feedback is capable of forcing the system trajectories to move and remain at the self-tolerance equilibrium (4.5). The negative feedback (4.20) engenders a rapid inducement

of inhibition of autoreactive T cells due to a step-like function. Fig. 4.10 shows that the reachability condition is satisfied during the whole simulation. Therefore, the manifold s is attractive and the states D and C attain $s = 0$ after a fine time and stay on it, see Fig. 4.10. Thus, the dynamical behaviour of the immune system induced by the discontinuous self-tolerance feedback is shown to exhibit a sliding mode which enforce the tolerance state.

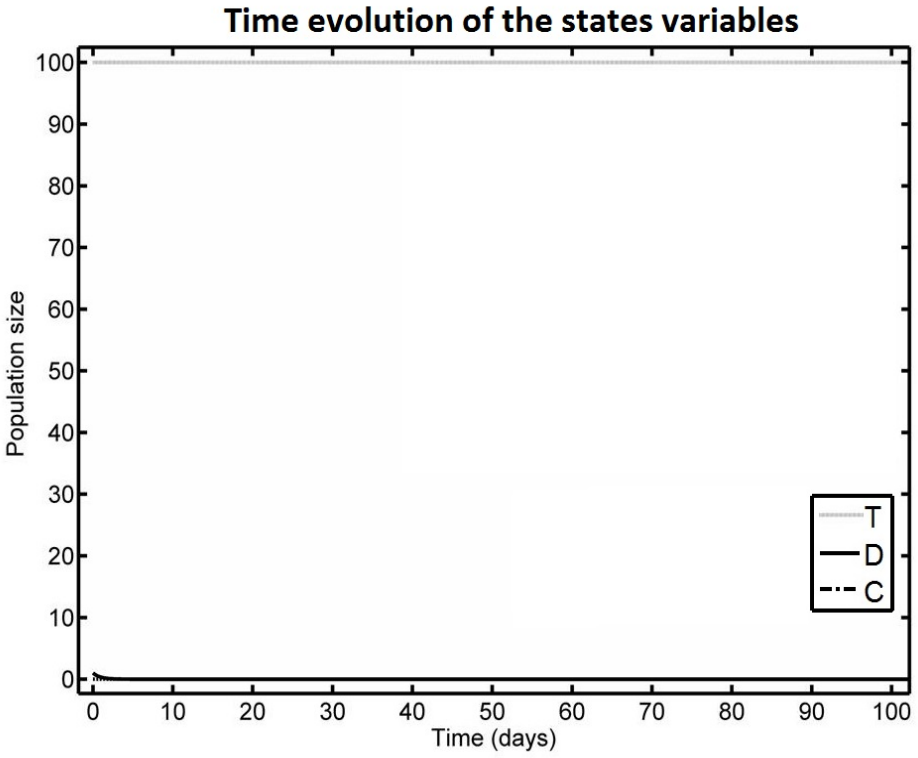

FIGURE 4.8: Immunological dynamics driven to the tolerance steady-state (4.5). Closed-loop system (4.1) with the negative tolerance feedback (4.20) .

When an ideal sliding mode takes place after a time t_s, $s = \dot{s}(t) = 0$ for all $t >= t_s$. The concept of the equivalent control introduced in Chapter 2 is considered. Here, the equivalent control represents the theoretical injection required to maintain sliding motion on (4.13) to exhibit tolerance. From $\dot{s}(t) = 0$, the expression of the equivalent control is given as:

$$u_{eq} = \alpha D + \gamma C - \beta TC \quad (t >= t_s) \tag{4.22}$$

The time evolution of the equivalent control action, see Fig. 4.11 illustrates the variation over time of the magnitude of the suppression signal acting on the population dynamic of autoreactive T cells C due to the intrinsic self-tolerance control feedback (4.20). This

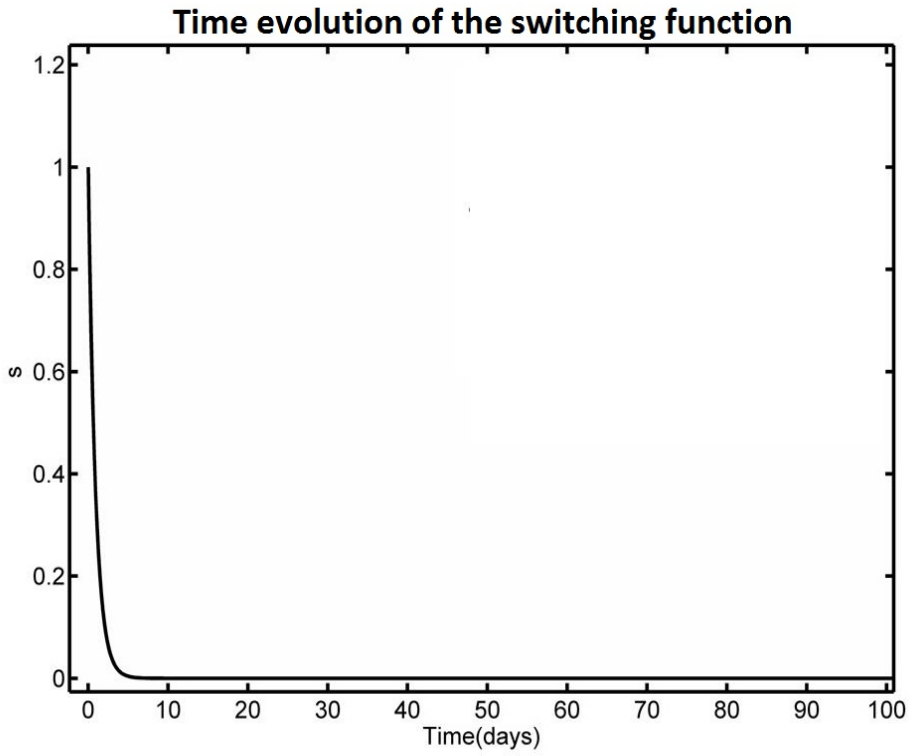

FIGURE 4.9: Time course of the switching function (4.13). Closed-loop system (4.1) with the negative tolerance feedback (4.20).

exemplifies the notion that self-tolerance as an active immunological VSC action to maintain desirable homeostasis and a healthy state [31, 40, 50, 83]. The amplitude of the equivalent control is proportional to the state variables. Considering the trivial equilibrium values of the state variables, it is clear that in the absence of disturbance, the equivalent control action vanishes when the tolerance equilibrium (4.5) is attained. This can occur in sliding mode control and may be expected at nominal conditions [23].

The dynamical behaviour of the immune system with respect to changes in one or more parameter values is analysed. The parameter values used in the mathematical studies of self-tolerance dynamics in [51, 52] are chosen to test the stability and performance of the design control outside of nominal conditions. Changes in parameter values represent changes in the rate of biological processes such as production rates and death rates. The following uncertain parameters are considered: $\lambda = 2$, $\mu = 0.1$, $\beta = 0.45$, $\alpha = 0.145$, $\gamma = 0.01$.

Unfortunately, it has not been possible to obtain experimental data for the model (4.1). As discussed in [82], mathematical models to study self-tolerance dynamics have not yet

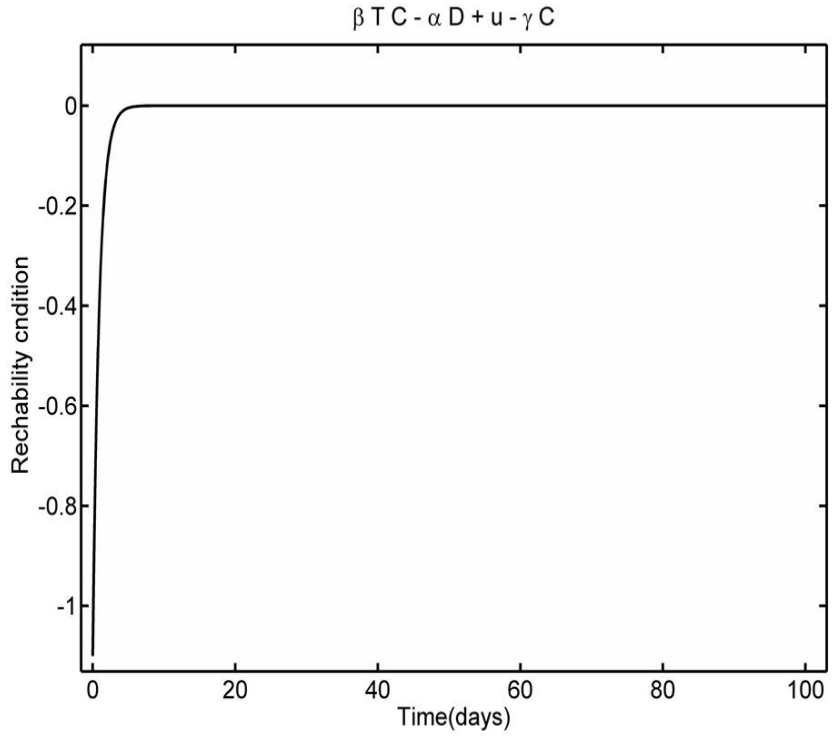

FIGURE 4.10: Time course of the reachability condition (4.21). Closed-loop system (4.1) with the negative tolerance feedback (4.20).

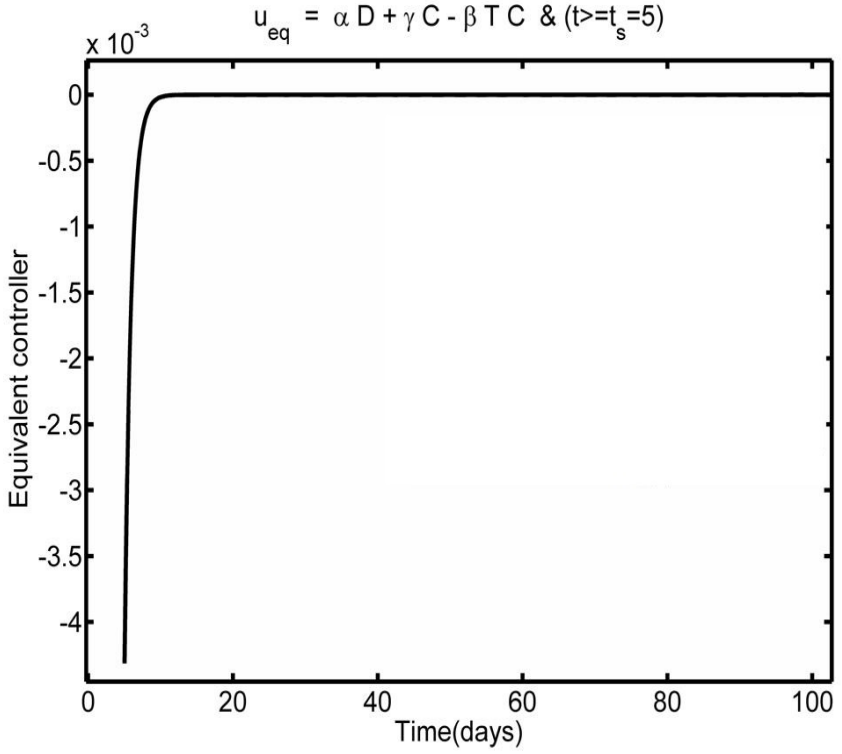

FIGURE 4.11: Time course of u_{eq}, the equivalent control signal (4.22) $t > t_s = 5days$. Closed-loop system (4.1) with the negative tolerance feedback (4.20)

been enriched by kinetics data from mouse or human experiments. In contrast, mathematical investigations have benefited from experimental studies on HIV infection dynamics to deliver sensible immunological insights [30, 35]. This motivates the study of HIV infection dynamics in the next Chapters.

Simulations are conducted in Fig. 4.12 to compare the robust stability and robust performance of (4.20) with the ones generated by a linear feedback $u_2 = kD$. In [51], u_2 has been shown to achieve nominal stability and performance of the tolerance state.

Looking at Fig. 4.12, the immunological rates are different from the ones which have been discussed in the nominal case. Parameter variations in λ and μ affect the steady-state population size of target cells. Although the population of healthy cells has greatly decreased, the dynamical behaviour induced by (4.20) satisfy the reachability condition (4.14) and exhibits a tolerance state. In effect, the concentration of self antigen and autoreactive T cells are driven to zero and the trajectories reach and remain on the sliding manifold (4.13). Unlike u_1, the control u_2 cannot reject the perturbation in parameter values. In fact, u_2 does not satisfy the reachability condition (4.14). This comparison of the immunological behaviours is evidence that (4.20) achieves robust stability and robust performance of the healthy immune system.

The effect of modelling uncertainty in (4.1) is investigated. Changes in the assumed growth function of target cells are considered to reflect different tissue growth dynamics. The linear growth process of target cells in (4.1) is substituted by a logistic and density dependent process as in [51]. The dynamical equation related to the target cells becomes:

$$\dot{T} \quad = \quad \lambda + (pT)(1 - \frac{T}{L}) - \mu T - \beta TC \tag{4.23}$$

Here, target cells can be created both by a constant production rate λ and by the proliferation of existing target cells with p as the maximum proliferation rate. Also, the target cell population saturates at a predefined carrying capacity L.

The expression of the reachability condition in (4.21) prove that the adaptive scheme included in the control (4.20) allows this control feedback to keep the inequality (4.21) true despite the variation of the population size of target cells. As a result, the manifold $s = 0$ remains attractive to the states of the system and self-tolerance is achieved despite changes

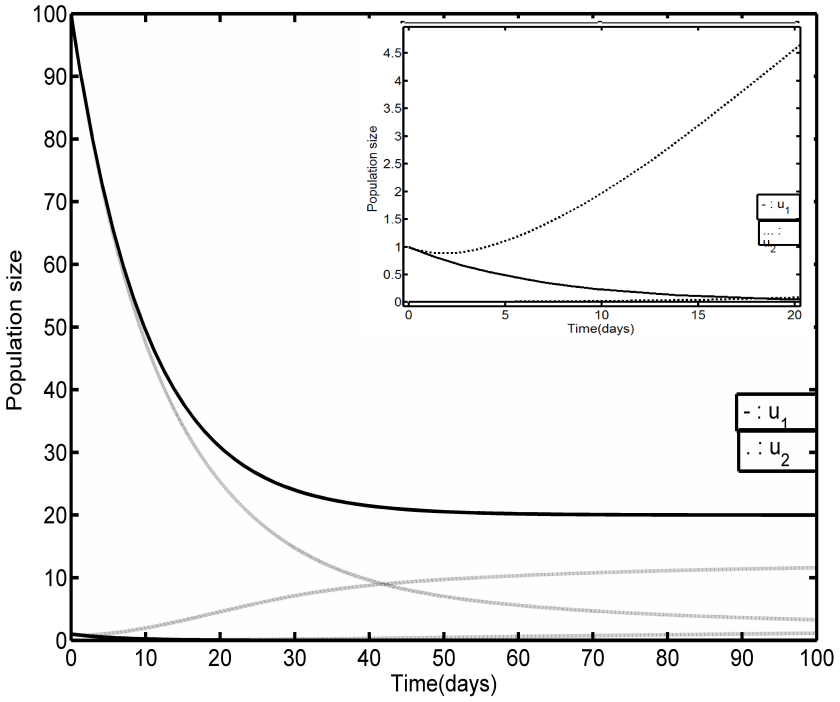

FIGURE 4.12: Comparison of the performance of control laws u_1 in (4.20) and $u_2 = kD$ with parameter disturbance: $\lambda = 2$, $\mu = 0.1$, $\beta = 0.45$, $\alpha = 0.145$, $\gamma = 0.01$ and $k = 0.002$

in the dynamics of target cells. The dynamical behaviour of the system trajectories is similar to that observed in Fig. 4.8. During ideal sliding motion $s = D + C = 0$. Since $D > 0$ and $C > 0$, $D = C = 0$ when sliding mode occurs. Therefore, the term βTC vanishes in (4.23). This means that when the control (4.20) enforces a sliding mode and achieve tolerance, the dynamics of target cells are not impaired by the effects of self-reacting T cells. Hence, the self-tolerance dynamics generated by the control law (4.20) are robust to changes in the dynamics of target cells. This matches with the immunological reality because the tolerance state is exhibited in vivo for various tissues [31, 92].

Together, the results of the conducted robustness analysis demonstrate the synergies between sophisticated immunological control mechanisms and robust engineering control strategies.

4.5 Conclusion

In this chapter, tolerance mechanism have been examined from a control engineering perspective. Analytical and numerical analysis highlight that the characteristics of the immune

response function determine the establishment and maintenance of a robust tolerance state. Furthermore, feedback mechanisms to establish a robust tolerance steady-state are investigated using the framework of sliding mode control introduced in Chapter 2. A manifold associated with the tolerance steady-state has been identified and the conditions for enforcing sliding motion on this manifold are determined. Conditions for the establishment of self-tolerance by the immune response function are found to be consistent with conditions for a sliding mode. Importantly, the reachability condition delivers a nonlinear tool to assess and monitor immunological dynamics. The study of self-tolerance mechanisms of the immune system strengthens the argument that the immune system is naturally a VSCS because the establishment of tolerance is achieved by inherent immunological switching logic and feedback loops.

The advantage of the sliding mode control approach is based on the fact that it binds immunological requirements with the reachability conditions. As seen in this chapter, this provides a means to understand how a given immunological control feedback realise the desired immunological outcome. In the context of HIV infection, it is important to understand how the HIV-specific CD8+ T cell response achieves immunity. Consequently, analytical tools from sliding mode control will be used in the next chapter to investigate the containment of HIV infection in vivo by the HIV-specific T cells response. Finally, in Chapter 6, the availability of patient data from HIV clinical trials motivates a case study in which the reachability paradigm is used to monitor the containment of HIV infection by antiretroviral drugs.

Chapter 5

Evaluation of the Conditions for the containment of HIV infection by the HIV-specific CD8+ T Cell response, a Variable Structure Control Perspective

5.1 Introduction

In this chapter, it is demonstrated that the reachability paradigm introduced in Chapter 2 can be utilized to formulate a dynamical condition for the control of HIV infection by the HIV-specific CD8+ T cell response.

HIV is a persistent infection which mainly targets CD4+ T cells and in most cases leads to Acquired Immune Deficiency Syndrome (AIDS) [30, 37, 118]. Experimental studies have demonstrated that the HIV-specific CD8+ T cell response is a major immunological dynamic opposing the spread of infection in the host [30, 55, 57, 58]. It is of current interest to understand how the HIV-specific CD8+ T cell response contains HIV infection [30, 57, 119]. It is not clear whether immunity is achieved by the cytolytic or the non-cytolytic killing mechanism of HIV-specific CD8+ T cells [55, 56, 75]. This motivates the

use of control theory to formally investigate the control action of the killing mechanism of the HIV-specific CD8+ T cell response.

Mathematical modelling of HIV dynamics in vivo has significantly contributed to the understanding of the HIV pathogenesis along with the design of treatment regimes to boost the immune response and/or to reduce the severity of the infection [30, 53, 60]. Early mathematical models of HIV dynamics in vivo can be found in the seminal papers [60, 120]. A third order model can encompass the observed biological characteristics of the acute phase of HIV infection using the variation over time of the population of healthy CD4+ T cells, the infected population of CD4+ T cells which produce new virion along with the concentration of the HIV-1 free virus [35, 60]. Although this model describes experimental data well, it does not include the dynamics of the HIV-specific CD8+ T cell response explicitly [55, 60].

HIV-specific CD8+ T cells combat HIV by killing HIV infected cells [57, 118, 119]. Early thoughts assumed that HIV-specific CD8+ T cells kill HIV-infected cells whilst they are producing new virion [56, 58, 60, 102] but recent studies proved that HIV-specific CD8+ T cells have a minor impact on the death rate of virus-producing HIV-infected cells [30, 58, 75]. Current findings suggest that HIV-specific CD8+ T cells kill HIV-infected cells via a cytolytic mechanism during the eclipse phase of the infection, before infected cells start producing new virion. Furthermore, the non-cytolytic mechanism of HIV-specific CD8+ T cells has been demonstrated to have an important role on the containment of the infection by preventing the infection of new cells [35, 56, 75]. Consequently, these features have been explicitly incorporated in recent models to improve the realism of the model as well as the understanding of the impact of the HIV-specify CD8+ response on the containment of the infection [56, 58].

The outcome of a viral infection in a host is classically evaluated using the reproductive ratio R_0 which measures the number of new cells that a single infected cell produce at the start of infection when there is no target cell limitation [34, 35]. The reproductive ratio is an algebraic combination of some biological rates which can be retrieved using the constant term of the characteristic equation of the nonlinear dynamical equations of an HIV dynamic model linearized at the infection-free steady-state [35, 56]. Typically, when $R_0 < 1$, the infection-free steady-state is stable and the infection will not spread. Since the parameters

associated with the killing efficacy the HIV-specific CD8+ T cell response are included in the expression of the reproductive ratio, the condition for the containment of the infection depends on the HIV-specific CD8+ T cell killing mechanism to enforce the reproductive ratio to be below unity [35, 56, 121]. Thus, the framework of the reproductive ratio provides a static condition which infers that the condition for the containment of the infection solely depends on the values of some biological rates rather than population dynamics.

However, recent studies argue that the immunological requirements for the containment of the infection rather than being static changes during the course of the infection [34, 102, 119]; the immunological requirements might be weaker before the peak of the virus load due to the small number of viral particles at the site of the infection [34]. The work in [122] suggested that the failure of the HIV-specific CD8+ T cell response to eradicate the infection is explained by a low ratio between the number of effector HIV-specific CD8+ T cells and the population size of the infected cells (target) at the early stage of the infection before the peak of the virus load. The effector/target ratio increases after the peak of the virus load and a greater immunological pressure is exerted on the infection dynamics. Furthermore, experiments have demonstrated that the depletion of virus-specific CD8+ T cells post infection leads to an increase of the virus load [56]. Hence, the framework of the reproductive ratio does not encompass the emerging notion that the condition for the containment of the infection changes during the course of the infection according to changes in biological rates and population dynamics [30, 34, 102, 119].

The dynamic of HIV in vivo is inherently a closed-loop system because natural control strategies such as the non-cytolytic and the cytolytic mechanism of the HIV-specific CD8+ T cell response are intrinsically applied by the immune system to eradicate HIV infection [30, 56, 58]. Therefore, models of HIV dynamics in vivo can be analysed using the tools of control theory to evaluate the performance of the HIV-specific CD8+ T cell response and to develop additional feedback strategies, which in this context amounts to hypothesizing treatment regimes.

Exploring immunological mechanisms from the perspective of control engineering can be found in several papers in the literature relating to both theoretical biology and control

engineering. A significant set of publications focus on enhancing the action of the immune response and antiretroviral drugs to contain the infection.

Optimal control strategies have been investigated to design treatments. In [123], the control analysis has postulated the early start of treatment to improve success. The method proposed in [124] offers some robustness with parameter perturbation. The control and therapy strategy is to have a slow reduction of the drugs dosage during the course of the treatment. This investigation was inspired from an optimal control strategy which developed a minimal cost function for drugs therapy in HIV [125].

Model predictive control techniques have been considered due to problems with safety and difficulty of implementation of the continuous treatment regime resulting from optimal control strategies [126]. In [127], interrupted drug scheduling was investigated. Using this approach, a new optimal control law is computed at each sampling period. This has the benefit of boosting the immune response to provide stability of the immunological state and to exhibit robustness to parameter and model uncertainty [126, 127].

Besides, nonlinear two loop feedback controls law is developed in [128]. An inner controller aims to cancel the effects of the nonlinearity caused by the product of healthy CD4+ cell and virus state variables. Using exact linearization methods and measurement of the virus concentration, this inner controller is a function of time which changes by steps. This control law infers that the HIV-1 dynamics progresses according to a series of switched linear dynamic models. As a result, the control signal of the inner controller is not smooth. The control action of the outer loop feedback is based on the availability of measurement of both virus and CD4+ concentrations. In fact, the outer controller compensate the intrinsic nonlinearity of the model using the product of the virus concentration and the sum of uninfected and infected CD4+ concentrations.

The outer loop with a static gain feedback control law manipulates the inner lop and achieves the tracking of the reference (low level) HIV concentration. The smooth control signal is obtained in the absence of noise in the outputs. As in [129, 130], a discrete time version of the control action is implemented for satisfying practical constraints of measurements. The stability and performance of the control strategy is deteriorated with increase in the interval between blood samples. A trade-off between the design of sophisticated control laws and selection of sampling times is suggested to be investigated.

In [131], a control Lyapanov function approach has been used to design a treatment regime for HIV. Using the basic HIV-1 model and parameter values from [132], the nominal design is performed. The most efficient design is to apply the control strategy into the infected cells dynamic. The performance is influenced by parameter uncertainty and noise in the input channel. In presence of +or - 20% variation, the controller reduces dramatically the virus load but the concentration of uninfected T cells fails to reach its desired healthy equilibrium. It interesting to note that the decrease in the value of the natural decay rates is improves the performance.

In [130], the model developed in [133] has been considered for designing a singularity free nonlinear controller. From knowledge of the dynamics of HIV-1 infection, the model is divided into two subsystems. In the finite region corresponding to the origin, a local non-negativity and singularity free controller is designed using a decoupled Lyapanov function over the origin. In the other region, complement to the origin, the properties of the system are exploited using backstepping techniques and a global controller is constructed. Considering the periodical acquisition of blood samples, the control action trough HAART drugs administration to the patient is fixed during the sampling interval to model medical practice as in [37, 134, 135]. The assumption is that the efficacy of the drugs is constant during the sampling interval.

The antiretroviral therapy is adjusted according to measurement of the viral load obtained from a blood sample at a particular instant. In other words, the control action is changed according to the region in which the system is currently in. Furthermore, the blood sampling period is adjusted with respect to the severity of the infection which is determined by the measured virus concentration. For instance, an aggressive control action is applied in the complement region with a high sampling period because the virus concentration is larger than the predefined threshold. Unlike in [129], the control energy can be significantly reduced when the viral load is close to zero due to the fact that an softer control action is applied in this region. Hence, the nonlinear control law implemented in [130] is a variable structure like control strategy [7].

A theoretical sliding mode controller has been investigated as a candidate treatment strategy in [136]. The nominal design of the controller was performed on a basic HIV-1 model such as the one in [60] with parameters values from [137]. The desired healthy equilibrium is shifted to the origin to ease the construction of the sliding surface. The sliding surface consists of both (uninfected and infected)T cells and virus concentration dynamics. The

control action is bounded in the range $[0; 1]$. This is to reflect the effectiveness of the drugs. For example, when $U = 1$, drugs have 100% efficacy. Right after the sliding surface is reached, the discontinuous control action is deliberately replaced by the equivalent controller. A Lyapanov analysis has been used to prove the stability of the desired virus free equilibrium under the closed-loop control. The simulations have shown robust stability and performance with respect to parameter uncertainty. Although the publication [136] stands as one of the first attempt proposing a discontinuous control as a treatment strategy for HIV-1, the controller design needs to be improved by including constraints related to practical issues such as the availability of clinical data [138].

Evaluating the condition for the containment of the infection by the HIV-specific CD8+ T cell response using a Variable Structure Control (VSC) approach can be motivated from the following observations:

1. Experimental studies in [119] show that the dynamic response of an elite CD8+ t cell response contains HIV infection and reduces HIV load below the limit of detection 50 RNA/ml. It has been shown in Chapter 2 that in a variable structure control system, the control structure changes during the process according to a predefined switching law to achieve desired performance [7, 10, 13, 16, 22]. Further, the work in Chapter 3 has demonstrated that the immune response program of the specific CD8+ T cells [30, 55, 56, 139] is effectively an inherent VSC law which dictates the dynamic of the response according to some immunological law. Besides, the recent study in [139] has demonstrated using a double saturation function is appropriate to model the cytolytic mechanism of CD8+ T cells. The findings of this study reveal that the structure of the killing action changes during the course of a viral infection and saturates according to the population size of target cells and CD8+ T cells. Hence, the cytolytic mechanism of CD8+ T cells can be regarded as an inherent VSC to kill infected cells and achieve immunity.

2. The immune system is a highly robust system, maintaining a steady-state corresponding to health or disease in the presence of perturbations and disturbances. A potent cytolytic CD8+ killing action is most simply represented with a large constant killing rate [35, 56]. Alternatively, a Michaelis-Menten Function with a small Michaelis constant and an appropriate saturation rate can be designed to produce similar effects at steady-state [56]. These functions are effectively high gain negative

feedback where the latter is very similar to the continuous approximations used in the domain of engineering to implement discontinuous control strategies. Control theory has demonstrated the similarities between the robustness properties of high gain linear state feedback systems and discontinuous systems [7, 10, 15, 16, 22]. Further, implementation of discontinuous control strategies in the domain of engineering has been routinely carried out using smooth approximations to the discontinuous function; one example is the so called unit vector control law [10]. Moreover, Chapter 4 shows that there are strong similarities between the two domains and the functions used to provide practical robustness.

3. It has been demonstrated that the function describing the killing mechanism of the HIV-specific CD8+ T cell response and the magnitude of this killing action influence the immunological steady-state and the outcome of the infection [56]. In the domain of sliding mode control, the dynamics will typically attain a desired steady state which is defined by the chosen sliding surface when the so called reachability condition is met [7, 15, 16, 22]. When the reachability condition fails to hold, the system will exhibit different dynamics, usually exhibiting a different equilibrium. If appropriate sliding manifolds can be designed to represent the biological phenomena, a reachability analysis can be used to formally assess the condition for the containment of the infection by the HIV-specific CD8+ T cell response.

Unlike the static condition provided by the reproductive ratio computed at the infection-free steady-state, the novelty and the major contribution of the VSC approach resides in the fact that the reachability analysis provides a dynamical condition for the HIV-specific CD8+ T cell response to reach and maintain the infection-free steady-state. Furthermore, this condition encompasses the nonlinearities of the model and exhibits some robustness properties with respect to parameter and modelling uncertainty. Importantly, the dynamical condition for immunity provided by the VSC analysis can be reproduced by experimental studies such as the one in [34, 35] using estimation of the size of the different population and the biological rates involved in the population of dynamic of infected cells in which the HIV-specific CD8+ T cell response is acting.

This chapter is structured as follows: In section 1, a model of HIV dynamics in vivo in which HIV-infected cells are killed in the eclipse phase is presented. In section 2, the

dynamical condition for immunity using the VSC paradigm is formulated. Next, this condition is tailored to candidate control function modelling the cytolytic killing action of the HIV-specific CD8+ T cell response. Afterwards, the steady-state condition for immunity using the reproductive ratio is computed and analysed in section 3. Finally, in section 4, simulation experiments are conducted to support the analytical analysis and the notion that the dynamical condition for immunity from the reachability analysis is an appropriate tool to monitor the immunological requirements to eradicate the infection.

5.2 Model description

The model studied in [56] is considered for investigating the condition for the containment of the infection by the HIV-specific CD8+ T cell response. The state variables are the population of uninfected CD4+ T cells T, the population of HIV-infected CD4+ T cells in the eclipse phase I, the population of HIV-infected CD4+ T cells which produces new virion P, the dynamics of free virions V (virus load per ml) and the population dynamic of HIV-specific CD8+ T cells E. The dynamical equations are given as:

$$\begin{aligned}
\frac{dT}{dt} &= \lambda - \delta_T T - \beta TV \\
\frac{dI}{dt} &= f\beta TV - \gamma I - \delta_T I + u_C \\
\frac{dP}{dt} &= \gamma I - \delta_P P \\
\frac{dV}{dt} &= pP - \delta_V V \\
\frac{dE}{dt} &= gE - \delta_E E
\end{aligned} \tag{5.1}$$

The immune response function for the proliferation of HIV specific CD8+ T cells follows a Michaelis-Menten process and is expressed as:

$$g = \frac{g_{max} I}{h_g + I + E} \tag{5.2}$$

where h_g has been set to zero [55, 56].

The non-cytolytic killing mechanism of the HIV-specific CD8+ T cells is modelled by the parameter f with range $0 \leq f \leq 1$ [56, 58, 140]. A candidate expression for f is given as:

$$f = \frac{1}{1 + \epsilon E} \tag{5.3}$$

where $0 \leq \epsilon E$, and ϵ represents the efficacy of CD8+ T cells exerting non-cytolytic killing of HIV-infected cells in the eclipse phase.

The cytolytic mechanism of the HIV-specific CD8+ T cell response is encompassed in the parameter u_C where $u_C \leq 0$. A block diagram of this process is given in Fig. 5.1.

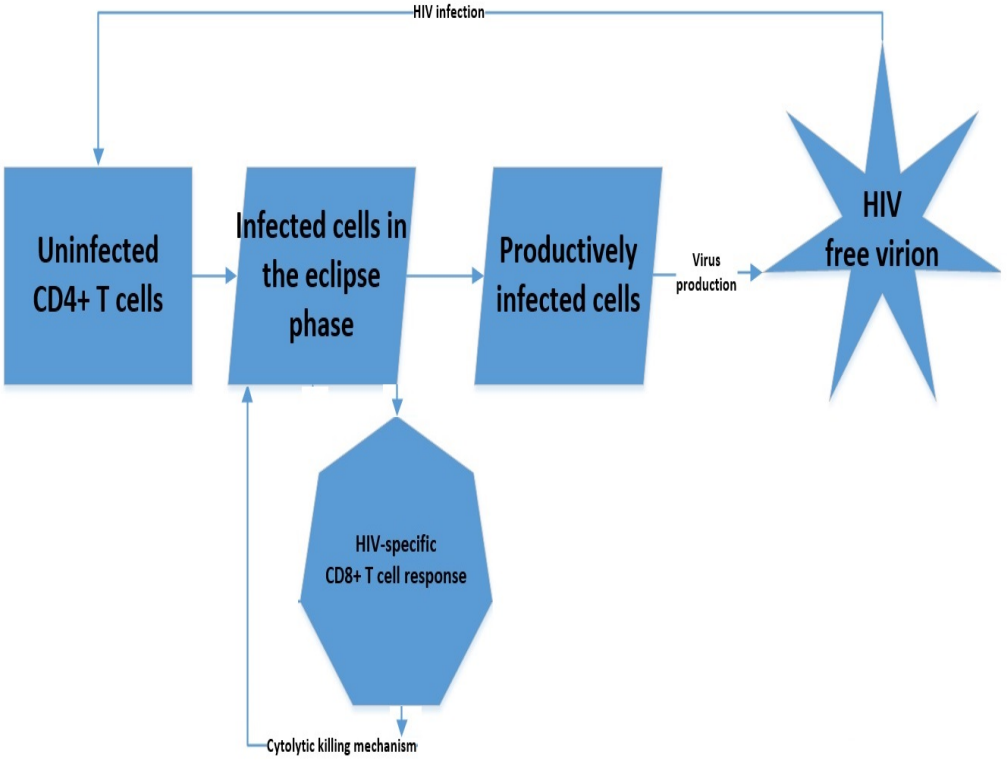

FIGURE 5.1: Model (5.1) of HIV infection dynamics in which infected cells in the eclipse phase are killed by the cytolytic effect of CD8+ T cells

In this chapter, the cytolytic mechanism of HIV-specific CD8+ T cells is treated as an intrinsic immunological control action because it is assumed that HIV-specific CD8+ T cells control/contain HIV infection in vivo via cytolytic mechanism, i.e killing of HIV infected cells in the eclipse phase [55, 56]. The non-cytolytic mechanism is not the focus but constitutes a candidate immunological means to contain the infection in vivo [55, 58, 75].

The infection free steady-state located at the trivial equilibrium of the model (5.1) is given as:

$$T_{s0} = \frac{\lambda}{\delta_T}; \quad I_{s0} = P_{s0} = V_{s0} = E_{s0} = 0 \tag{5.4}$$

Throughout the chapter, the term *condition for immunity* is defined as the condition that the killing mechanism of the CD8+ T cell response needs to satisfy for zeroing the state variable I, the population of HIV-infected CD4+ T cells in the eclipse phase to reach and maintain the infection-free steady-state. Thus, the control objective of u_C is to satisfy the condition for immunity.

5.3 Dynamical condition for immunity using the reachability analysis

As in Chapter 3, the framework of sliding mode control is utilized to investigate the performance of the specific T cell response. Here, a sliding manifold representing the immunological objective of the HIV-specific CD8+ T cell response is defined and a reachability condition is formulated to ensure that immunity is achieved. The sliding surface is given as:

$$s_E(t) = I \tag{5.5}$$

In this sliding mode control approach, the HIV-specific CD8+ T cell response in the ideal case is thought to render the manifold $s_E = 0$ attractive. In the sliding mode,

$$s_E(t) = I = 0 \quad and \quad \frac{ds_E}{dt} = 0 \tag{5.6}$$

defines the dynamical behaviour of the system (5.1). In fact, the sliding surface s_E is selected so that ideal sliding motion yields a stable infection-free steady-state. It should

be mentioned that the sign of $s_E(t)$ is non-negative at all times because it relates to the number of HIV-infected CD4+ T cells in the eclipse phase $I \geq 0$.

The temporal derivative of the sliding surface is:

$$\begin{aligned} \frac{ds_E}{dt} &= \frac{dI}{dt} \\ &= f\beta TV - (\gamma + \delta_T)I + u_C \end{aligned} \tag{5.7}$$

Next, the concept of the equivalent control, introduced in Chapter 2 is considered. The equivalent control u_{Ceq}, the effective control action required to maintain sliding motion on $s_E = 0$, is retrieved from $\frac{ds_E}{dt} = 0$ as follows:

$$u_{Ceq} = -f\beta TV + \gamma I + \delta_T I \tag{5.8}$$

Hence, the equivalent control is meaningful and represents quantities that can be measured or estimated [35, 59, 141].

Here, the reachability condition, introduced in Chapter 2, is given as:

$$\begin{aligned} s_E \frac{ds_E}{dt} &< 0 \\ I\left(f\beta TV - (\gamma + \delta_T)I + u_C\right) &< 0 \\ \left(f\beta TV - (\gamma + \delta_T)I + u_C\right) &< 0 \end{aligned} \tag{5.9}$$

since $0 \leq I$ by definition. This inequality formulates a dynamical condition for the HIV-specific CD8+ T cell response to zero the population dynamic of HIV-infected cells I in the eclipse phase to ensure immunity. This dynamical condition for immunity is the main contribution of this chapter.

This dynamical condition also infers that the negative feedback provided by the HIV-specific CD8+ T cell response should overcome the positive feedback of HIV pathogenesis encompassed by the product βTV. When immunological dynamics satisfy (5.9), $s_E = 0$ is rendered attractive and the population dynamics of the system (5.1) move towards the infection-free steady-state (5.4). Thus, the inequality (5.9) reflects the balance between the progression of the infection and the immunity provided by the HIV-specific CD8+ T cell

response [35, 57, 122]. In fact, the term $f\beta TV$ is a dominant component which sustains HIV pathogenesis. As a result, the condition for immunity is mainly influenced by the infection rate β, the population size of uninfected cells and the virus load. This suggests that the killing mechanism of the HIV-specific CD8+ T cell response might operate as an adaptive control mechanism which aims to provide a sufficient magnitude to achieve and maintain immunity despite fluctuation in the magnitude of the term βTV. This interpretation is consistent with the study conducted in [122] in which the killing action of the HIV-specific CD8+ T cells after vaccination has been demonstrated to be insufficient to prevent viral growth due to a low effector to target cell ratio at the beginning of the infection.

In Chapter 2, it has been shown using the example of the pendulum system that when the system exhibits a sliding mode, the closed-loop dynamics become robust to matched uncertainty and perturbations. Typically, the magnitude of the control action is designed to satisfy the reachability condition despite parameter and modelling uncertainty present in the dynamic where the control action is applied. As a result, the dynamical behaviour of the system prescribed by the choice of the sliding surface is enforced and the dynamics exhibit some invariance properties.

Furthermore, the robustness of the killing mechanism of the virus-specific CD8+ T cell response can be observed in experimental and mathematical studies on acute Lymphocytic Choriomeningitis Virus (LCMV) infection [2, 29, 43, 91]. In these studies, the immunity provided by the virus-specific CD8+ T cell response is robust to various biological factors such as changes in the initial number of responding CD8+ T cells, changes in the rate of clonal expansion, changes in virus strains and in the biological rates associated with the host mice. Additionally, clinical studies have shown a great variety in the population of HIV-infected individuals called elite HIV controllers which are able to maintain the virus load in their body below the limit of detection without receiving any treatment [30, 37, 57, 58]. This suggests that an elite HIV-specific CD8+ T cell response is robust to changes in the biological rates and infection dynamics associated with the difference between patients along with differences in virus strains.

The expression (5.9) provides a means to clarify the effects of uncertainty in the values of biological rates and population dynamic of the system (5.1) on the containment of the infection. In fact, the work in [55, 122, 140] on modelling HIV dynamics in vivo pointed

out that some of the constant parameters in (5.1) represents biological rates which vary according to time or to some population dynamics during the course of the infection. For instance, the infection rate β is influenced by the antibody response to HIV [142]. Also, HIV pathogenesis seems to create a positive feedback which activates uninfected CD4+ T cells and increases their number as a function of the virus load [143]. From (5.9), it is possible to argue that that the condition for immunity is insensitive to changes in the exact mathematical representation of the population of uninfected CD4+ T cells T, the population of infected CD4+ T cells which produces new virion P, the dynamics of free virion V and the population dynamic of HIV-specific CD8+ T cells E. As a result, the condition for immunity (5.9) exhibit some robustness with respect to modelling uncertainty in these dynamics because these uncertainty do not appear in the expression of the reachability condition (5.9). Nevertheless, parameter and modelling uncertainty in the dynamic where the killing action of the HIV-specific CD8+ response is present influence the magnitude of the dynamical threshold and they might cause (5.9) to fail. In essence, the dynamical condition for immunity provided by the reachability analysis holds despite changes in the initial condition of the system. This means that the condition can be used to investigate different infection scenario and vaccination strategies [30, 35, 122].

It should be noted that this condition for immunity is irrespective of a particular candidate control function. In [55, 122], the mathematical representation of the HIV-specific CD8+ T cell response has been shown to influence the immunological requirement to contain the infection. This reachability analysis proves that the dynamical condition for immunity is invariant to the explicit mathematical formulation of the cytolytic or non-cytolytic killing mechanism of the HIV-specific CD8+ T cell response. The inequality (5.9) supports the notion that both cytolytic or non-cytolytic killing mechanism of HIV-specific CD8+ T cells are important to enforce immunity [58, 75, 140]. The expression of a candidate function for the killing mechanism of the HIV-specific CD8+ T cell response rather than affecting the condition for immunity changes the immunological insights retrieved when considering a particular function [55, 56, 122].

Importantly, the dynamical condition for immunity can be examined in experimental studies by estimating the size of the different population and the biological rates involved in the population of dynamic of infected cells in which the killing mechanism HIV-specific CD8

T cells is acting. For instance, the dynamical threshold can be evaluated in the studies in [35, 140] and [122] using the expression of the population dynamic of productively infected cells because in these studies the cytolytic mechanism of the HIV-specific CD8+ T cells acts on this dynamic. As a result, the time evolution of the condition for immunity can be analysed for different combination of parameter values and initial condition. Thus, the condition for immunity provided by the VSC analysis can be used to compare the evolution of the immunological requirement to contain the infection using experimental data from different patients [35, 140].

Hence, this reachability analysis supports the notion that the condition for immunity changes during the course of the infection [30, 34, 122].

5.3.1 Candidate control function modelling the cytolytic killing mechanism

A number of mathematical approach based on different biological assumptions have been proposed to model the HIV-specific CD8+ T cell response [55, 122, 140]. Functional responses inspired from ecology or Michaelis-Menten functions from enzyme-substrate kinetics are often used to model the expansion and cytolytic killing action of the HIV-specific CD8+ T cell response [55, 56, 139]. The mathematical expression of the function describing the killing mechanism and the population dynamic of the HIV-specific CD8+ T cell response are both sensible because they influence the transient dynamics as well as the steady-states of the model along with the corresponding interpretation of the impact of the HIV-specific CD8+ T cell response on the containment of the infection [35, 55, 56, 122, 140].

Typically, functions modelling the cytolytic killing mechanism of CD8+ T cells have the following form:

$$u_C = -\mathcal{K}I \tag{5.10}$$

where CD8+ T cells kill infected cells at a rate $\mathcal{K}$ which encompasses the cytolytic killing process [35, 140]. This immunological control action is effectively an intrinsic negative state

feedback which opposes the infection dynamics in vivo. The simplest approach is

$$\mathcal{K}_1 = k \tag{5.11}$$

where k is a constant killing rate. A candidate linear state feedback is thus formulated as:

$$u_{C1} = -\mathcal{K}_1 I \tag{5.12}$$

The condition for immunity (5.9) associated with (5.12) can be written as:

$$\begin{aligned} f\beta TV - (\gamma + \delta_T)I - kI &< 0 \\ \frac{f\beta TV}{I} - (\gamma + \delta_T) &< k \end{aligned} \tag{5.13}$$

This inequality shows that the killing rate k acting as the gain of the immunological control feedback must be high enough to satisfy these inequalities to render the manifold $s_E = 0$ attractive. This supports the notion that increasing the cytolytic killing rate to a sufficient level is a mean to contain the infection [56, 58]. Thus, a strong cytolytic killing action by HIV-specific CD8+ T cells is analogous to a high gain state feedback [10, 56]. Nevertheless, modelling a potent cytolytic action with a large and fixed value of the killing rate makes the system suffering from the lack of robustness (such as sensitivity to changes in biological rates) of linear state feedback control [10, 21] and the resultant dynamics of the model might not reflect the robustness of the immunity associated elite HIV-specific Cd8+ T cell response [30, 57, 144]. this .

A more realistic assumption is to consider that the cytolytic killing rate of HIV-specific T cells changes during the time course of the infection [122, 140]. Recently, a general functional response of the cytolytic killing mechanism of CD8+ T cells has been formulated [139]. A double-saturation (DS) function with two different saturation constants has been demonstrated to encompass different cytolytic killing processes. Here, the killing rate is dynamical and it is a function of the population of infected cells I and the population of HIV-specific CD8+ T cells E as follows:

$$\mathcal{K}_2 = \frac{k'E}{1 + E/h_E + I/h_I} \tag{5.14}$$

where h_E and h_I are the saturation constant of the population of HIV-specific CD8+ T cells E and the population of infected cells (target) in the eclipse phase I respectively. The parameter k' is a mass action killing rate. As a result, the candidate control action with the DS function is given as:

$$u_{C2} = -\mathcal{K}_2 I = -\frac{k'EI}{1 + E/h_E + I/h_I} \tag{5.15}$$

Tailoring the reachability condition to (5.15), the candidate control action constructed using the general functional response from [139] produces:

$$f\beta TV - (\gamma + \delta_T)I - \frac{k'EI}{1 + E/h_E + I/h_I} < 0 \tag{5.16}$$

This reveals that there exists a dynamical threshold above which the population size of effector HIV-specific CD8+ T cells renders the manifold $s_E = 0$ attractive and forces the decay of the infection. This dynamical condition highlights that changes in the population size of infected cells I and HIV-specific CD8+ T cells induce variation in the magnitude of the killing action and this influences the satisfaction of the condition for immunity. This contributes to the findings in [102] where it has been shown using a bifurcation analysis that the apoptosis of HIV-infected cells and HIV-specific CD8+ T cells affect the immunological steady-state and the severity of the infection.

Further, the value of the saturation constants h_E and h_I plays an important role on the satisfaction of the condition for immunity because the value of these biological rates influences the magnitude of the immunological control action. This result extends the findings in [139] where thef efficacy of the cytolytic killing process has been associated with the value of the saturation constants h_E and h_I of effector CD8+ T cells and target cells respectively.

Hence, the reachability analysis supports the emerging notion that the population size of target cells and virus-specific CD8+ T cells and their corresponding saturation constant determine the ability of the cytolytic killing action of virus-specific CD8+ T cells to "control" the infection and to achieve immunity [56, 91, 122, 139].

In Chapter 2, it has been seen that when a continuous approximation of the discontinuous $sign()$ function is implemented, ideal sliding motion can longer be achieved. Instead, the applied continuous control action keeps the states of the system within a vicinity of the sliding manifold. From the expression (5.15), it is clear that the candidate DS function is not discontinuous. Consequently, it is argued that the cytolytic mechanism of the CD8+ T cell response operates as a nonlinear negative state feedback which forces the population size of infected cells to be confined in a neighbourhood of the ideal sliding manifold $s_E = I = 0$.

Consequently, using the results of Chapter 2 on smoothed variable structure control systems, it can be concluded that the immunological control action of the cytolytic mechanism of the HIV-specific response modelled with the DS function (5.15) rather than zeroing the population of infected cells, forces the population size of infected cells to remain at small steady-state level determined by the magnitude of the cytolytic killing action. Moreover, the DS function, as a nonlinear control feedback, provides some robustness of the immunological dynamics to uncertainty during sliding motion [10, 21, 22, 63].

5.4 Steady-state condition for immunity provided by the reproductive ratio

The reproductive ratio R_0 represents the number of new infected cells that a single infected cell produces in absence of target cell limitation [34, 35, 56]. Here, the concept of the reproductive ratio is reviewed from a control engineering perspective. In the study of virus dynamics, the reproductive ratio is a well-known tool used to evaluate the outcome of infection [34]. The reproductive ratio represents the number of newly infected cells produced by one infected cell during its lifetime, assuming there is no limitation of target cells [34]. The expression of the reproductive ratio derived in [56] using the infection-free steady-sate of model (5.1) is as follows:

$$R_0 = \frac{\lambda}{\delta_T}\frac{\gamma}{\gamma+\delta_I}\frac{1}{\delta_P}\frac{p}{\delta_V}f\beta \tag{5.17}$$

where the first factor is the population size of T at the infection-free steady-state see (5.4). The second factor is the probability that an infected cell becomes a virus-producing cell before it dies. The third factor is the lifetime of a virus-producing cell. The fourth factor is the number of virus particles produced per infected cell, and the last parameter represents the infection rate for a single virus particle in presence of the non-cytolytic effects of HIV-specific CD8+ T cells.

The Jacobian matrix of the system (5.1) at the trivial equilibrium (5.4) is given as:

$$J = \begin{pmatrix} -\delta_T & 0 & 0 & -\frac{\beta\lambda}{\delta_T} & 0 \\ 0 & -\delta_I-\gamma & 0 & \frac{f\beta\lambda}{\delta_T} & 0 \\ 0 & \gamma & -\delta_P & 0 & 0 \\ 0 & 0 & p & -\delta_V & 0 \\ 0 & 0 & 0 & 0 & g-\delta_E \end{pmatrix} \tag{5.18}$$

The characteristic equation can be written as

$$(s-g+\delta_E)(a_4s^4+a_3s^3+a_2s^2+a_1s^1+a_0s^0) \tag{5.19}$$

where the coefficients of the polynomial are as follows:

$$\begin{aligned}
a_4 = & \quad 1 \\
a_3 = & \quad (\delta_T + (\delta_V\delta_T + \delta_T\delta_I + \delta_T\delta_P + \delta_T\gamma)/\delta_T) \\
a_2 = & \quad (\delta_V\delta_T + \delta_T\delta_I + \delta_T\delta_P + \delta_T\gamma + (\delta_V\delta_T\delta_I \\
& \quad +\delta_V\delta_T\delta_P + \delta_T\delta_I\delta_P + \delta_V\delta_T\gamma + \delta_T\delta_P\gamma)/\delta_T) \\
a_1 = & \quad (\delta_V\delta_T\delta_I\delta_P - f\beta\gamma\lambda p + \delta_V\delta_T\delta_P\gamma)/\delta_T \\
& \quad +\delta_V\delta_T\delta_I + \delta_V\delta_T\delta_P \\
& \quad +\delta_T\delta_I\delta_P + \delta_V\delta_T\gamma + \delta_T\delta_P\gamma \\
a_0 = & \quad -f\beta\gamma\lambda p + \delta_T\delta_I\delta_P\delta_V + \delta_T\gamma\delta_P\delta_V
\end{aligned} \tag{5.20}$$

The expression of the reproductive ratio can be computed using $a_0 = 0$ as in [40, 51]. From $a_0 = 0$, the ratio can be formulated:

$$\begin{aligned}
-f\beta\gamma\lambda p + \delta_T\delta_I\delta_P\delta_V + \delta_T\gamma\delta_P\delta_V &= 0 \\
R_0 &= \frac{f\beta\gamma\lambda p}{\delta_T(\gamma+\delta_I)\delta_P\delta_V}
\end{aligned} \tag{5.21}$$

Hence, the expression of the reproductive ratio is retrieved using the stability analysis of the system (5.1) linearised at the infection-free steady-state (5.4). It is clear that the value of R_0 above or below unity influences the sign of a_0. When $R_0 < 1$, $a_0 > 0$ and the characteristic polynomial of fourth order has no sign changes. Using Descartes rule of sign as in [40, 145], it is possible to deduce that the infection-free steady-state is stable. Whilst $R_0 > 1$ implies $a_0 < 0$ and the fourth order characteristic polynomial has a positive pole. As a result, the infection-free steady state is unstable. Thus, the behaviour of R_0 influences the stability of the infection free steady state of the system along with the outcome of the infection.

This well know feature of R_0 [56, 60] has been revisited to evidence that the condition for the stability of the infection-free steady-state i.e the outcome of the infection using the reproductive ratio (**??**) is a steady-state argument. Indeed, the poles of the system (5.1) change during the time evolution of the state variables i.e the time course of the infection. As a result, the value of R_0 is inappropriate to determine the outcome of the infection when the system is not at steady-state. Hence, the reproductive ratio has limitations as a means to monitor dynamically the containment of the infection by the HIV-specific CD8+ T cell

response.

Experimental studies [34, 35] have observed that the value of R_0 is influenced by the HIV-specific CD8+ T cell response. Here, the cytolytic mechanism of the HIV-specific CD8+ T cells is encompassed in δI, the death rate of infected cells in the eclipse phase [56]. As a result, $\delta_I = \delta_T + \mathcal{K}$ because it is assumed that the death rate of infected cells in the eclipse phase is equal to the one of uninfected cells in absence of the cytolytic killing action of HIV-specific CD8+ T cells [55, 56].

Thus, the expression of the reproductive ratio can be rewritten as:

$$R_0 = \frac{\lambda\gamma p f \beta}{\delta_T \delta_P \delta_V (\gamma + (\delta_T + \mathcal{K}))} \tag{5.22}$$

The expression of the reproductive ratio in (5.22) shows that both the non-cytolytic mechanism and the cytolytic mechanism of the HIV-specific CD8+ T cell response affect the value of R_0 and the outcome of the infection [56]. As per experimental data, the reproductive ratio decreases in the presence of the HIV-specific CD8+ T cell response [34, 35, 56].

Using the framework of the reproductive ratio, the cytolytic killing rate of HIV-specific CD8+ T cells should force and maintain the reproductive ratio (5.22) below unity to eradicate the infection [34, 35, 56]. Mathematically, this is formulated as:

$$\begin{aligned} R_0 &< 1 \\ \mathcal{K} &> \frac{f\beta\lambda\gamma p - \delta_T\gamma\delta_P\delta_V}{\delta_V\delta_T\delta_P} - \delta_T \end{aligned} \tag{5.23}$$

The inequality (5.23) is effectively a steady-state condition for the infection-free steady-state to have negative poles and to be stable. Therefore, the gain of the state feedback control (5.10) should exceed a critical threshold value determined by the values of the biological rates present in the right hand side of the inequality (5.23). In other words, a sufficient cytolytic killing rate is needed to eradicate the infection. Further, (5.23) implies that stability of the infection-free steady-sate i.e the eradication of the infection is sensitive to changes in the values of the biological rates involved in the expression of the reproductive ratio. This implies that the cytolytic mechanism of the HIV-specific CD8+ T cells is not

TABLE 5.1: Values of biological rates

Parameter	Value
λ	$210^5(\frac{cells}{day})$
δ_T	$0.1(day^{-1})$
β	$310^{-8}(day^{-1})$
f	$1(day^{-1})$
γ	$1(day^{-1})$
δ_I	$0.1(day^{-1})$
δ_P	$1(day^{-1})$
ρ	$2300(day^{-1})$
δ_V	$23(day^{-1})$
g	$1.5(day^{-1})$
h_g	$0cells$
δ_E	$0.5(day^{-1})$

robust to uncertainty and perturbations in these biological rates because changes in these biological rates affect the required killing rate [35, 56, 140]. This implies a lack of robustness of the HIV-specific CD8+ T cell response which might not be realistic [57, 144].

5.5 Simulation experiments

Immunological experiments are simulated to show that the dynamical condition for immunity (5.9) provided by the reachability analysis appropriately tracks the immunological requirements for immunity during the course of the infection and is superior to the steady-state condition (5.23) formulated using the reproductive ratio (5.22). In the simulations, the initial condition depicts a scenario where the population of uninfected CD4+ T cells is at steady-state $T(0) = \frac{\lambda}{d_1}$, the infection is assumed to be induced by a single virion $I(0) = P(0) = 0; V(0) = 1$ and precursor HIV-specific CD8+ T cells $E(0) = 1$. The parameter values shown in Table 5.1 are taken from [56].

The population dynamics of the system (5.1) in the absence of a killing action from HIV specific CD8+ T cell response i.e $g = 0$ and $u_C = 0$ are displayed in Fig. 5.2. This simulation models experimental studies in which CD8+ T cells are depleted in order to assess their impact of HIV load in vivo [57, 146, 147]. From a control engineering standpoint, this simulation experiment is regarded as an analysis of the open loop dynamics of the system. The open-loop dynamics in Fig. 5.2 are consistent with the experimental findings

in [146, 147] because they show a large viral load steady-state along with the reduction of the population of target CD4+ T cells when HIV-specific CD8+ T cells are absent.

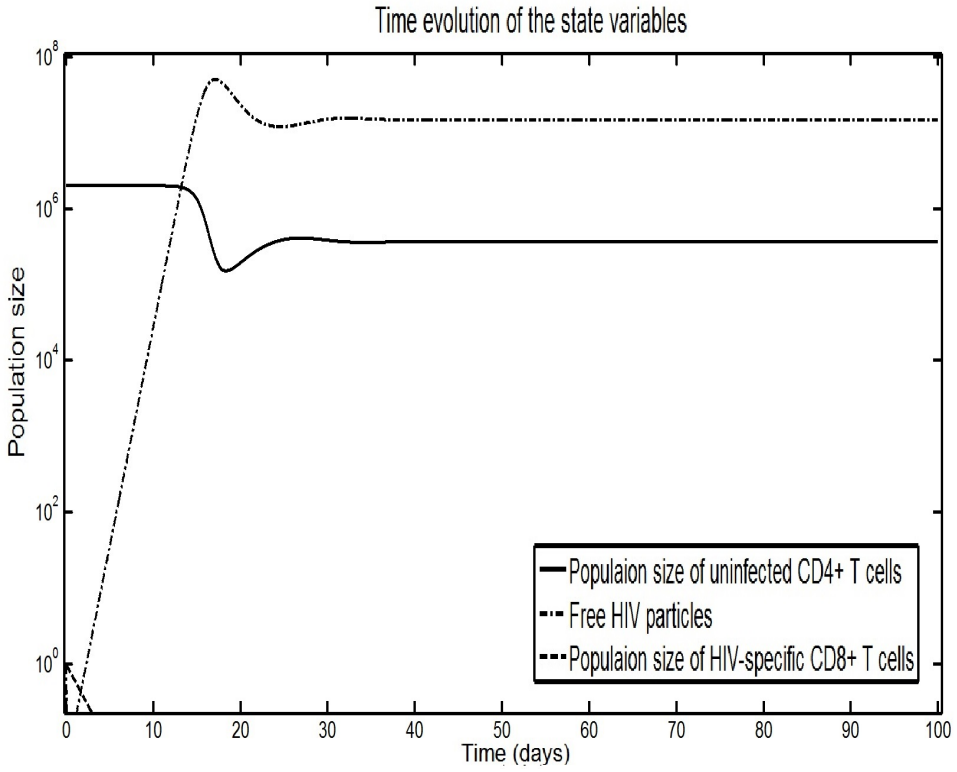

FIGURE 5.2: Open-loop system (5.1). Simulation of HIV infection in the absence of a killing action from the HIV-specific CD8+ T cell response. $T(0) = 2.10^6$; $I(0) = P(0) = 0$; $V(0) = E(0) = 1$. $f = 1; \mathcal{K} = g_{max} = 0$.

Using the biological rates given in Table 5.1, the reproductive ratio (5.22) is $R_0 = 5.45$ and the numerical value of this steady-state condition for immunity using the reproductive ratio is given as:

$$\mathcal{K} > \quad 4.9 \tag{5.24}$$

This inequality is effectively a threshold that the cytolytic killing rate must exceed to produce negative poles to render the infection-free steady-state stable, see characteristic equation (5.19)-(5.20). Since $u_C = 0$, $\mathcal{K} = 0$ for the open-loop dynamics. As a result, (5.24) is not satisfied and the dynamics will not reach the infection-free steady-state. As in [56], the reproductive ratio indicates that the infection will spread.

The purpose of Fig. 5.3 is to show the time evolution of the dynamical condition for immunity when there is no HIV-specific CD8+ T cell response. This is regarded as the condition

for immunity of the open-loop dynamic where there is no control action. Although the steady-state condition for immunity (5.24) using R_0 has a static value, the reachability analysis through Fig. 5.3 demonstrates that the condition for immunity changes during the time evolution of the infection. Concurrently, the magnitude of the sliding surface changes during the infection, see Fig. 5.4. Since the reachability condition is not met, the manifold of interest $s_E = 0$ is not reached and s_E attains a non-trivial steady-state value associated with the HIV infection steady-state.

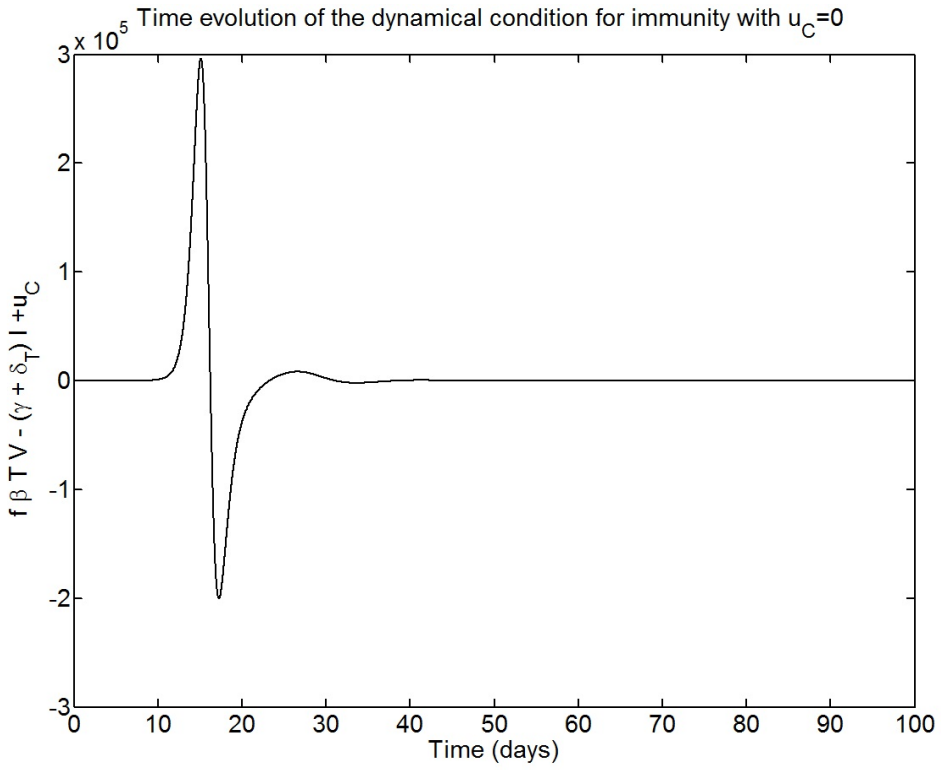

FIGURE 5.3: Time evolution of the dynamical condition for immunity (5.9) in absence of the HIV-specific CD8+ T cell response $u_C = 0$.

From a VSC stand-point, the following dynamical insights can be formulated. Firstly, it is worth to note that the positive peak of the condition for immunity, see Fig. 5.3 is associated with the peak of the virus load, see Fig. 5.2. From Fig. 5.3 and Fig. 5.4 It can be noticed that at the early days following infection (before the peak in viral load) the magnitude of the immunological action required to achieve immunity is smaller. Thus, the VSC analysis reinforces the notion that early therapeutic interventions are desirable [30, 34]. Secondly, the transient negative phase of the dynamical condition for immunity, see Fig. 5.3 shows that the saturation effects caused by the limitation of target cells whilst reducing the viral load satisfy the condition for immunity.

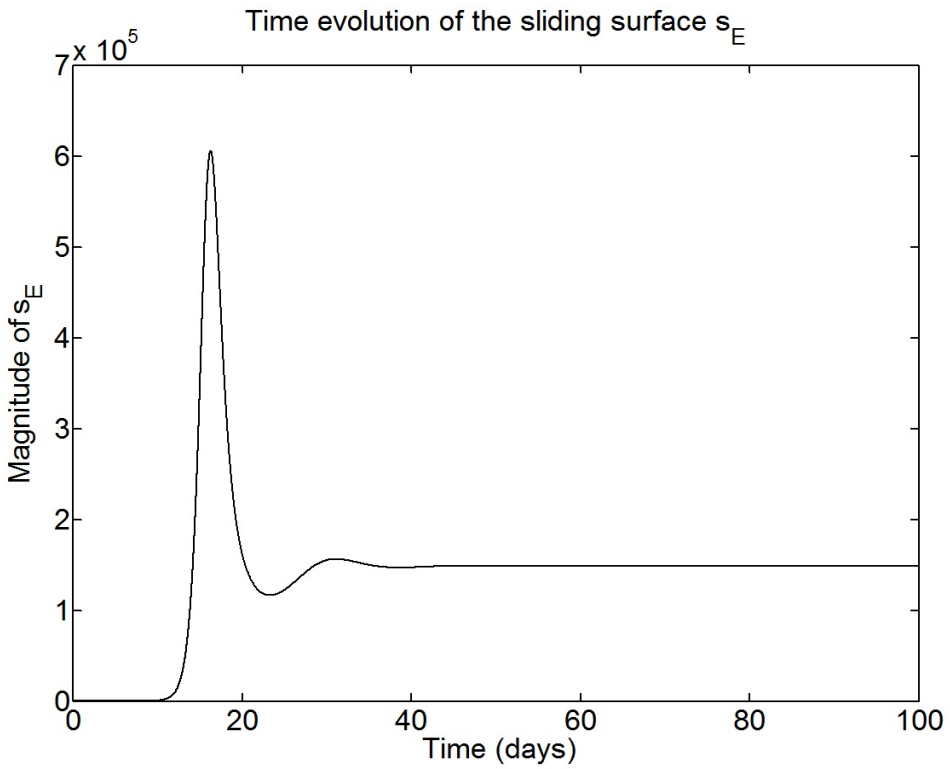

FIGURE 5.4: Time evolution of the sliding surface (5.5) with $u_C = 0$.

It can be concluded that the analysis of the open-loop dynamics show that the framework of sliding mode control is a superior tool to examine the infection dynamics as compared to the reproductive ratio because the formulated condition for immunity determines the outcome of the infection as well as highlights time varying immunological requirements to achieve immunity. This is a contribution from the VSC analysis in this HIV study.

5.5.1 Constant cytolytic killing action

Consider the closed-loop system formed by candidate control function u_{C1} (5.12) with a fixed killing rate $k = 10day^{-1}$.

The value of R_0 with this candidate control action is $R_0 = 0.5$. Note that k has been chosen to satisfy the steady-state condition (5.24) provided by the reproductive ratio. Consequently, the infection-free steady-state (5.4) is stable and the infection does not spread. This result is congruent with the numerical analysis in [56] where it was shown that increasing the killing rate of CD8+ T cells above the value $\mathcal{K} = 5day^{-1}$ produces a reproductive ratio below unity and leads to the eradication of the infection.

Similarly, the time evolution of the dynamical threshold Fig. 5.5 is always negative and this predicts the decay of the infection because the condition for immunity (5.9) is satisfied. In effect, the population of infected cells in the eclipse phase I will keep on decreasing and this leads to a continuous reduction of the virus load.

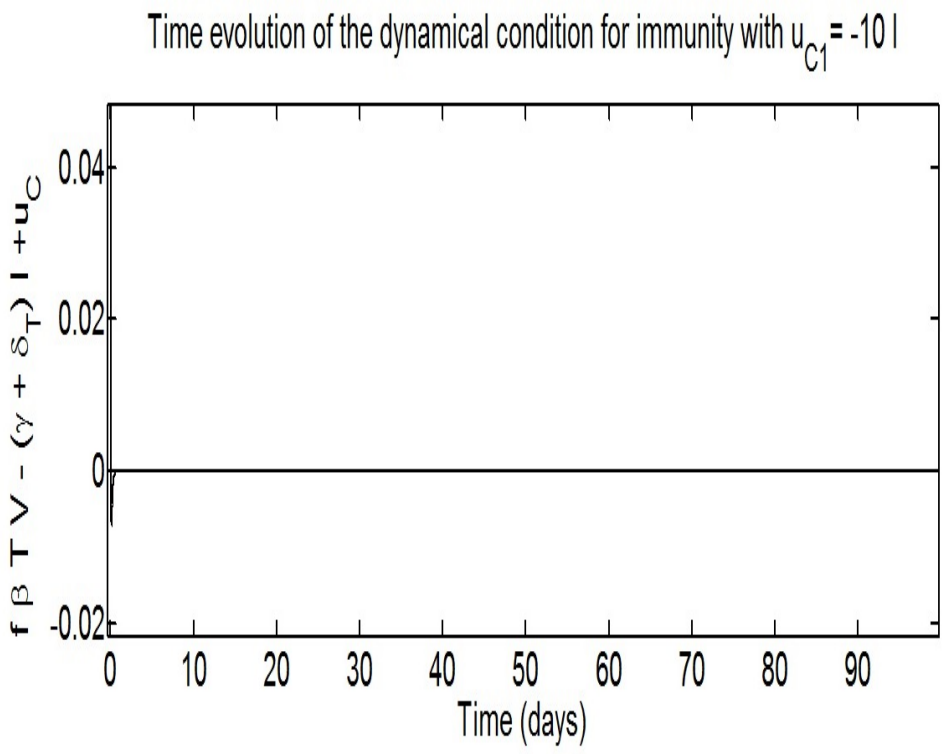

FIGURE 5.5: Time evolution of the dynamical condition for immunity (5.13) with the cytolytic killing mechanism of the HIV-specific CD8+ T cell response $u_{C1} = -10I$.

The time evolution of the sliding surface Fig. 5.6 shows that the large killing rate of the candidate cytolytic killing mechanism u_{C1} produces negative feedback, see Fig. 5.7, of sufficient magnitude to force the switching function s_E to decay exponentially towards the desired manifold $s_E = 0$. As a result, the immunological objective is met and the trajectories of the system move towards the infection-free steady-state.

It is worth to mention that the fast transient observed in Fig. 5.5- 5.7 is due to the fact that a large and constant magnitude of ($k = 10$ day^{-1}) of cytolytic killing action has been utilized in the simulation. These figures represent a proof-of-concept to support the notion that a potent killing action from HIV-specific CD8+ T cells is adequate to enforce a sliding mode on $s_E = I = 0$, to contain HIV infection, and maintain an infection-free steady-state. However, this high and constant cytolytic killing action might not be realized by CD8+ T cells in vivo.

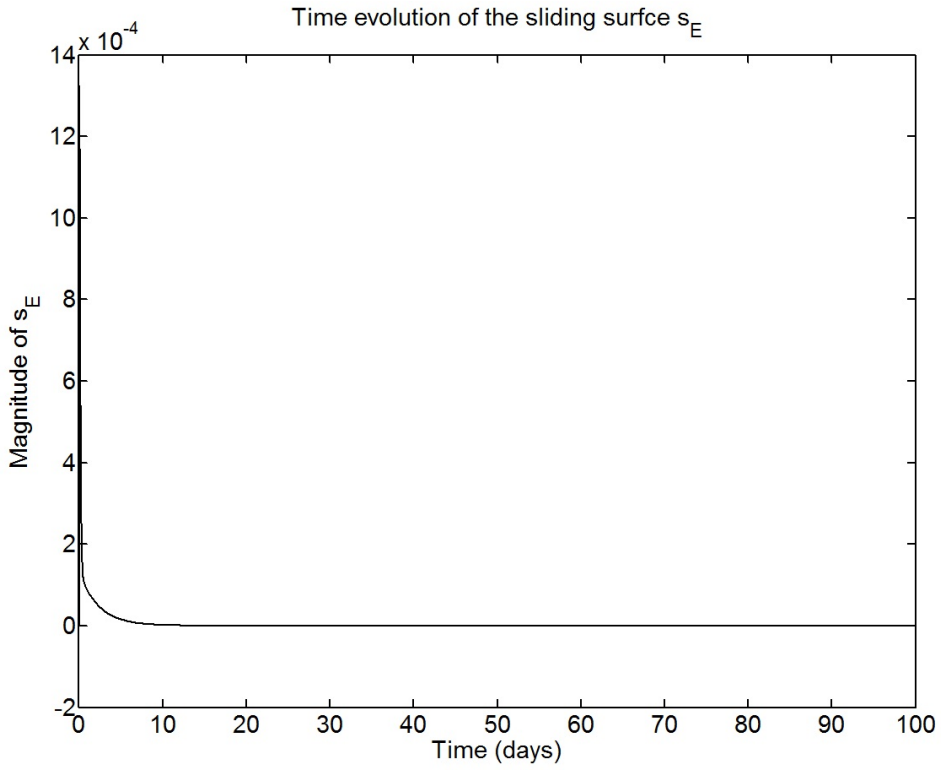

FIGURE 5.6: Time evolution of the sliding manifold (5.5) with $u_{C1} = -10I$

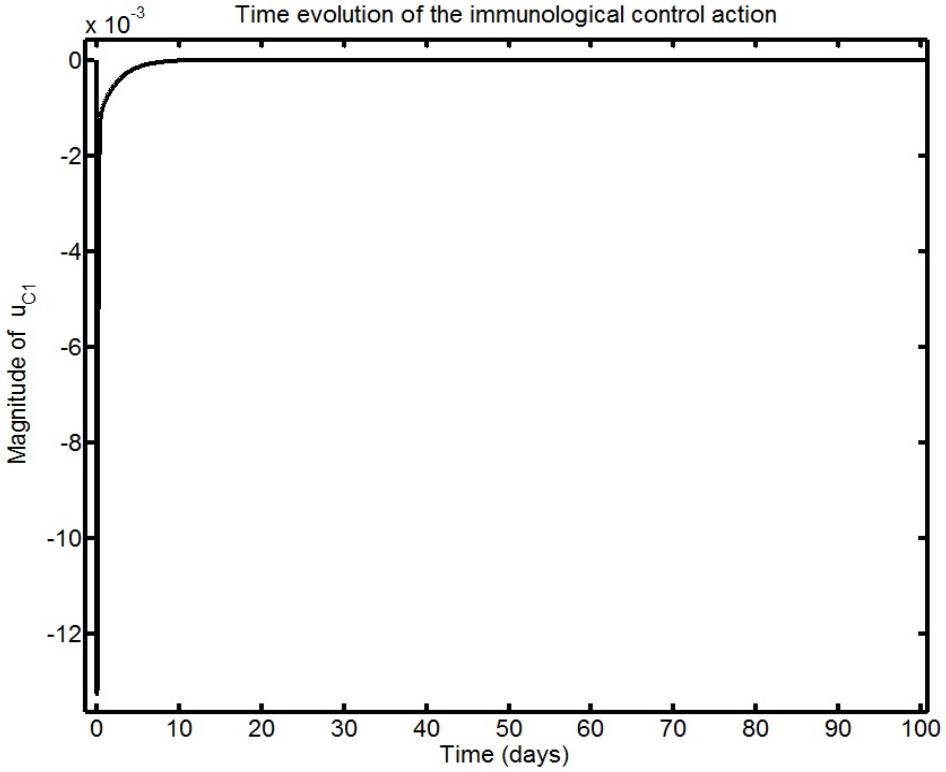

FIGURE 5.7: Time evolution of the control action (5.12) with $u_{C1} = -10I$

It can be deduced that the framework of sliding mode control applied to HIV dynamics in vivo delivers suitable tools to evaluate the outcome of the infection.

5.5.2 Dynamical cytolytic killing action

Consider the closed-loop system where (5.15) is the control. The general functional response from [139] is selected to investigate the containment of the infection because it is a sensible model of the cytolytic killing mechanism. In [56], the specific case of a monogamous killing process derived from (5.15) was considered to study the impact of the cytolytic killing of HIV-infected cells in the eclipse phase. This monogamous killing process describes a cytolytic mechanism where a single effector CD8+ T cell kills target cells. Mathematically, this monogamous killing process is expressed as:

$$u_{C3} = -\frac{k_{max}EI}{h_k+E+I} \tag{5.25}$$

with $k' = \frac{k_{max}}{h_k}$ and $h_k = h_E = h_I$. The maximum killing rate is k_{max} and the parameter h_k which is effectively a Michaelis-Menten constant defines the immune responsiveness [56, 139]. The resultant monogamous killing mechanism (5.25) u_{C3} with the maximum killing rate $k_{max} = 50$ day^{-1} and the saturation constant $h_k = 1$ as in [56].

The expression (5.25) is chosen to conduct the following analysis to build on the findings in [56]. Using numerical analysis, it has been shown in [56] that (5.25) influences the steady-state level of the virus load. It was found that reducing h_k increases the efficacy of the killing process and leads to a reduction in the steady-state value of virus load. Consequently, the findings in [56] motivates a control engineering approach to provide an analytical framework to formally assess (5.25) as a control mechanism to eradicate HIV infection in vivo. Moreover, (5.25) was selected to demonstrate the benefits of the dynamical condition for immunity over the reproductive ratio.

From [56], the reproductive ratio written as a function of the candidate control action (5.25) is as follows:

$$R_0 = \frac{\lambda\gamma p f \beta}{\delta_T\delta_P\delta_V(\gamma + (\delta_T + \frac{k_{max}E}{h_k+I+E}))} \tag{5.26}$$

Here, the value of R_0 changes over time due to changes in the killing rate of u_{C3} during the course of the infection.

The purpose of Fig. 5.8 is to display the time evolution of the biological population dynamics of the closed-loop system (5.1) with the considered monogamous cytolytic killing action. The transient dynamic and the steady-state of the dynamic of free-virion is reduced by the cytolytic killing of HIV-infected cells I by the HIV-specific CD8+ response.

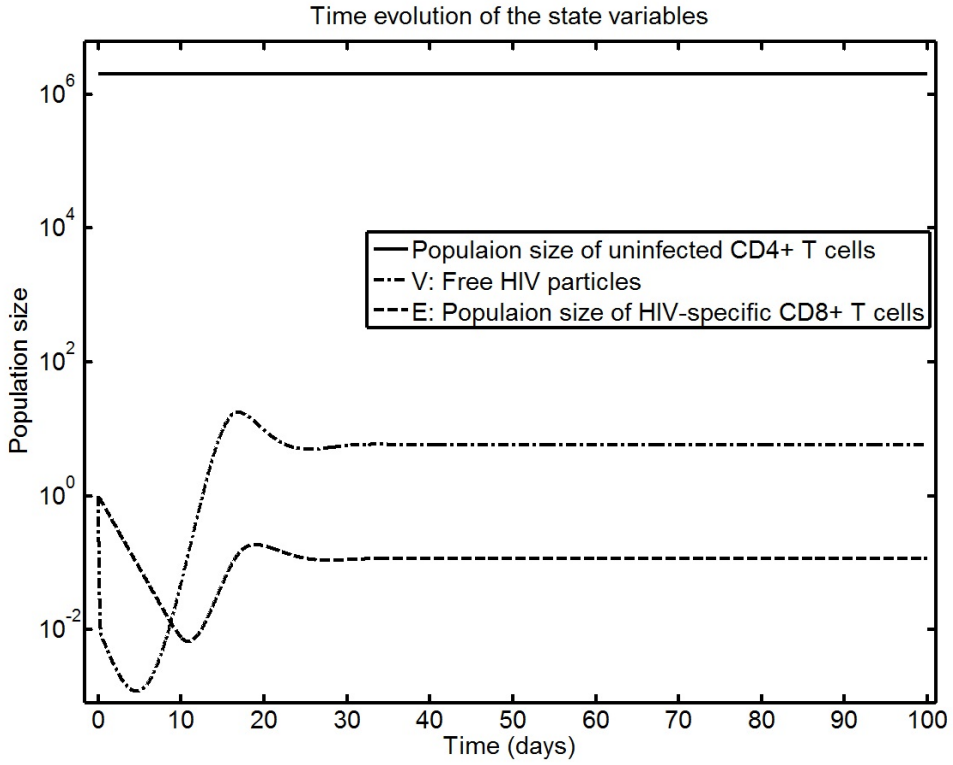

FIGURE 5.8: Closed-loop dynamics (5.1). Simulation of HIV infection with a potent HIV-specific CD8+ response with u_{C1}. $T(0) = 2.10^6$; $I(0) = P(0) = 0$; $V(0) = E(0) = 1$. $f = 1$; $h_k = 1$

From Fig. 5.9 which illustrates the control effort of the monogamous killing cytolytic killing action during the time evolution of the infection, it can be seen that the control effort is in the neighbourhood of the critical threshold (5.24) computed using the reproductive ratio.

Fig. 5.10 reveals that the value of reproductive ratio changes during the time course of the infection. As per the numerical analysis in [56], R_0 approaches unity at steady-state when the control action (5.25) is applied. Importantly, the value of the reproductive ratio during the transient dynamics of the system is misleading to assess the outcome of the infection because the value of R_0 fluctuates above and below unity during the transient phase. $R_0 < 1$ wrongly suggests the eradication of the infection from day 0 to day 10 and from day 18 to day 22, see Fig. 5.10. This is due to the fact that the poles of the system (5.1) vary during the infection before the population dynamics reach a steady-state. This shows the limitation of the reproductive ratio to reflect appropriately the condition for

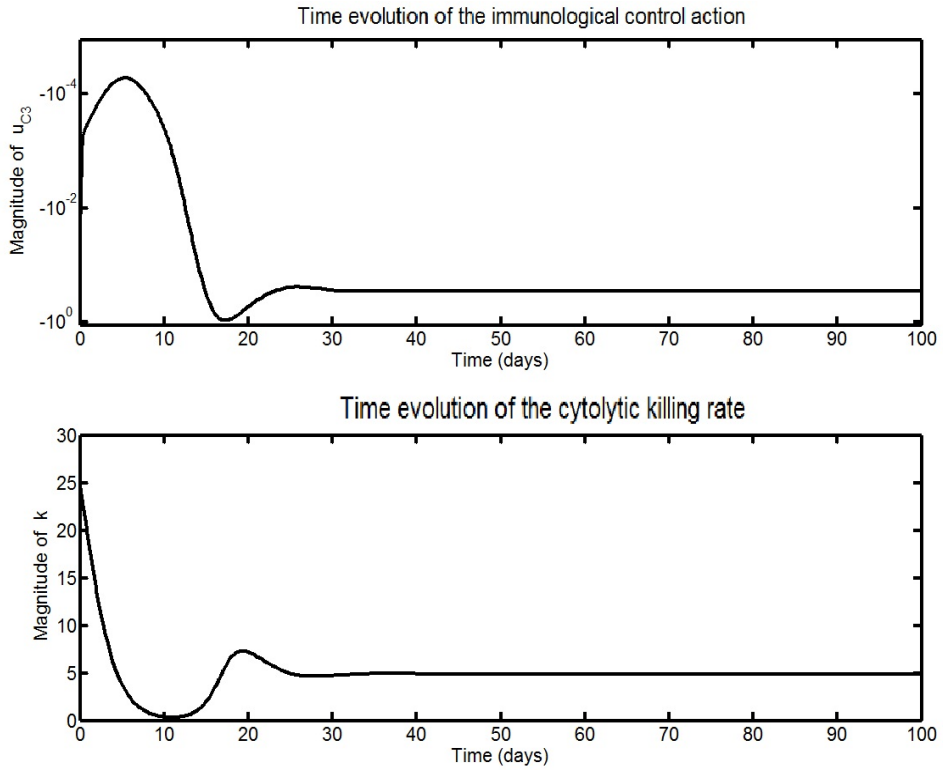

FIGURE 5.9: Time evolution of the control action (5.25) with u_{C3} $h_k = 1$

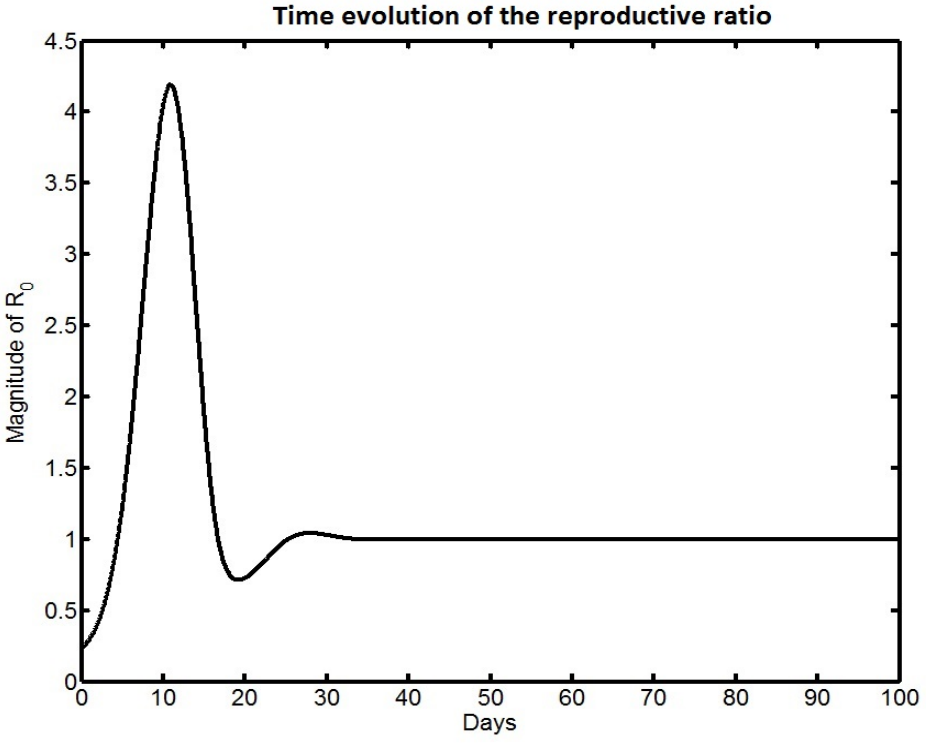

FIGURE 5.10: Time evolution of the reproductive ratio using u_{C3} (5.25) with $h_l = 1$.

immunity when the system is not at steady-state.

The time evolution of the reachability condition displayed in Fig. 5.11 reveals that the condition for immunity is not met at the beginning of the infection in contrast with the prediction of the reproductive ratio. Although, the considered control action u_{C3} reduces significantly the dynamical threshold for immunity but it does satisfy the dynamical condition for immunity (5.16) the manifold of interest $s_E = 0$ is not reached (see Fig. 5.12). Nevertheless, it should be noted that the candidate monogamous cytolytic killing action u_{C3} contains the infection to a low level steady-state close to the infection-free steady-state by keeping the sliding surface close to the desired manifold after a transient period (see Fig. 5.12). Therefore, VSC analysis allows the monitoring of the condition for immunity and the impact of the killing action of the HIV-specific CD8+ T cells during the infection.

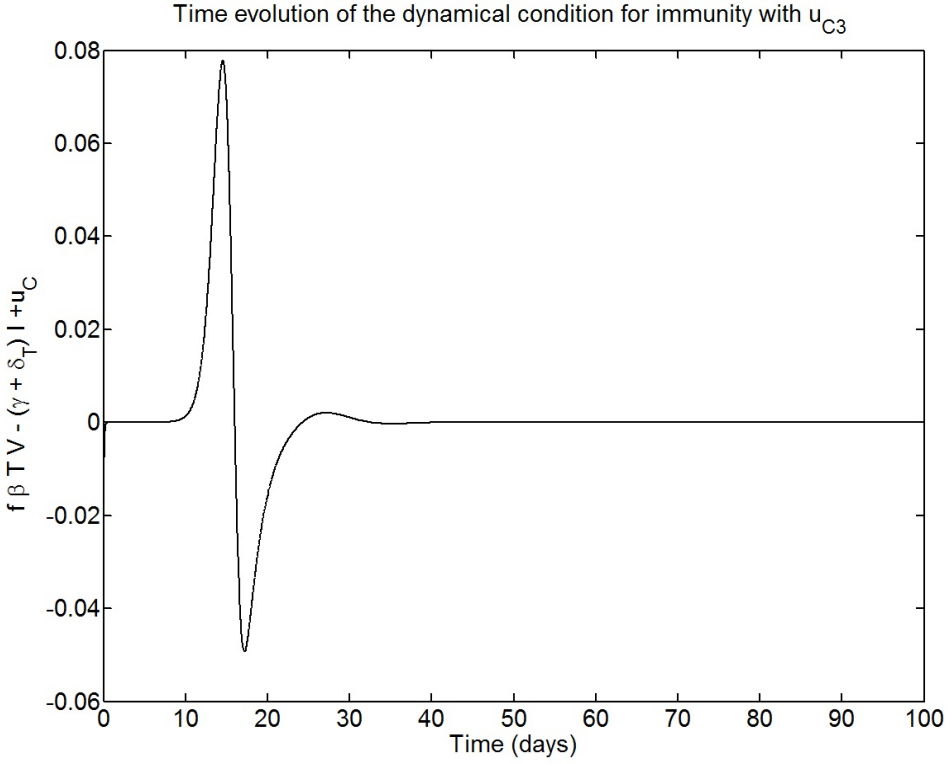

FIGURE 5.11: Time evolution of the dynamical condition for immunity (5.16) with the cytolytic killing mechanism of the HIV-specific CD8+ T cell response u_{C3} (5.25)

In [56], it has been shown using a numerical analysis that the value of h_k affects the steady-state population size of infected cells I and the steady-state level of the virus load. Using the sliding mode framework, changes in the saturation constant h_k influence the magnitude of the control effort (killing action) u_{C3} as well as distance between the manifold of interest $s_E = 0$ and the value of s_E generated by u_{C3} with a particular value of h_k. The reachability condition is not satisfied when h_k is large. This reinforces the notion that the saturation constant plays an important role to achieve immunity [56, 139]. Thus, failure

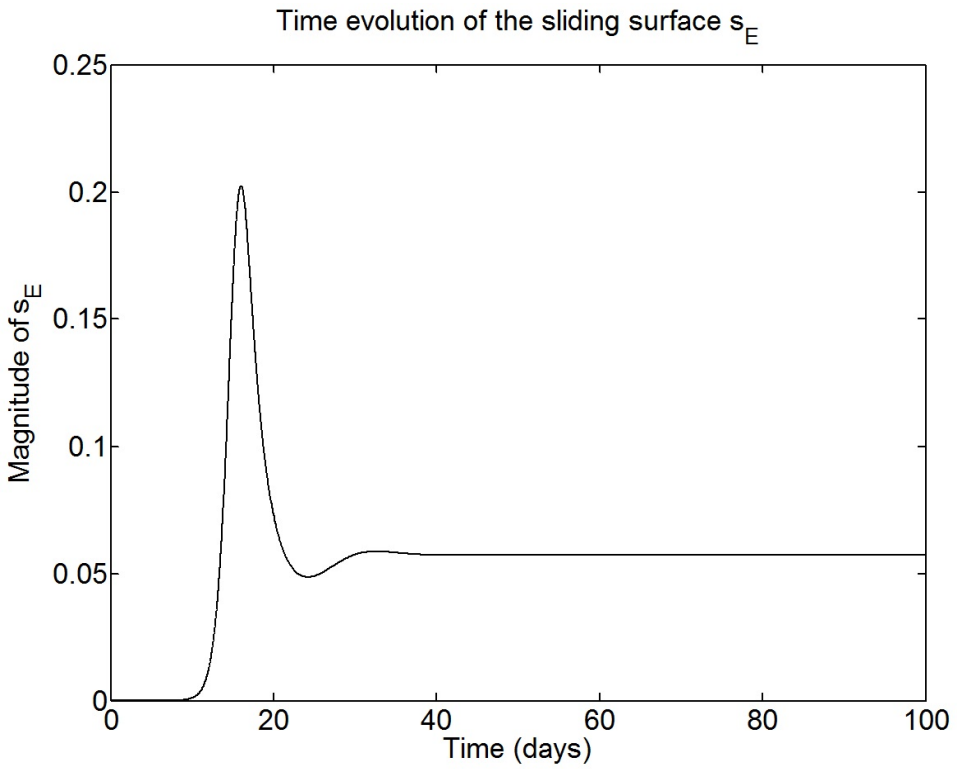

FIGURE 5.12: Time evolution of the sliding surface (5.5) with u_{C3} (5.25).

of the reachability condition explains why this cytolytic killing mechanism fails to zero the population dynamic of infected cells I and to eradicate the infection.

Although the manifold of interest $s_E = 0$ is not attained using the cytolytic killing function u_{C3}, this candidate control action keeps the sliding surface in the neighborhood of the desired sliding manifold and contains the infection within a region close to the infection-free steady-state (see Fig. 5.12 and Fig. 5.8). In effect, the virus load is below the limit of detection which is 50 RNA copies per ml from [56, 148] and the population of uninfected CD4+ T cells is near its infection-free equilibrium. Therefore, from a clinical perspective, this candidate cytolytic killing mechanism produces a desirable outcome.

Thus, the cytolytic control functions which maintain the sliding surface in the vicinity of the sliding manifold $s_E = 0$ can be classified as elite HIV-specific CD8+ response when the control action forces the virus load to remain below the limit of detection [30, 36, 56, 58]. Consequently, the condition for immunity can be relaxed to force the infection dynamics to remain within a boundary region associated with the virus limit of detection and other clinical requirements. Mathematically, this means that the condition for immunity is reduced to $s_E < \delta$ where δ is an upper bound associated with desirable clinical outcome.

These results supports the notion that immunological requirements for the eradication of HIV infection changes during the time course of the infection and the ability of the HIV-specific cytolytic mechanism to induce immunity is influenced by the population size of infected cells and effector Cd8+ cells and their corresponding saturation constant.

Importantly, these findings cannot be retrieved using the reproductive ratio because R_0 suggests just that the infection will decay but does not articulate the decay of the infection in finite time neither a decay to zero.

5.6 Conclusion

In this chapter, tools from VSC theory have been used to articulate a dynamical condition for the cytolytic killing mechanism of the HIV-specific CD8+ T cell response to zero the population of infected cells I. This dynamical condition has been demonstrated to monitor the immunological requirements for immunity during the time evolution of the infection appropriately. Failure of the candidate HIV-specific CD8+ response to satisfy the dynamical condition for immunity is consistent with failure of the CD8+ T cell response to reach and maintain the infection free steady-state. Additionally, the dynamical condition for immunity as compared to the steady-state conation provided by the reproductive ratio describes the immunological requirements for immunity during the course of the infection well.

In the next chapter, the approach developed in this chapter will be applied to investigate the effects of antiretroviral drugs to achieve the containment of HIV infection in vivo. In effect, it has been proven in this chapter that HIV infection dynamics in vivo are effectively a closed-loop system with the HIV-specific immune response as an intrinsic control feedback. As a result, the uptake of antiretroviral drugs represents an outer control feedback to contribute to the containment of the infection.

Chapter 6

Case Study: Prediction of the Containment of HIV Infection by Antiretroviral Therapy - a Variable Structure Control Approach

6.1 Introduction

A case study is conducted in this chapter to demonstrate that the reachability paradigm from Variable Structure Control (VSC) theory presented in Chapter 2 is a suitable framework to monitor and predict the progression of the HIV infection following initiation of antiretroviral therapy.

In the previous chapter, it has been demonstrated that HIV infection dynamics in vivo represent a closed-loop system in which the effects of the HIV-specific CD8+ T cell response operates as a VSC feedback to contain the infection. In the majority of patients infected with HIV this inherent control mechanism fails to clear the infection and recover a healthy state [30, 37, 149].

Antiretroviral therapy (ART) seeks to perturb the pathogenesis of the virus to allow infected individuals to stop exhibiting HIV related symptoms and to recover a certain level of immunity so that the quality of their lives can be improved [149]. Thus, ART can be viewed

as an outer-loop control strategy applied to enforce recovery. Using current experimental facilities, the standard clinical data for diagnosis and monitoring HIV infection in patients are the total number of CD4+ T cells measured by flow cytometry and HIV viral load measured by Polymerase Chain Reaction (PCR) [148–151]. ART attempts to reduce HIV load and this usually leads to recovery to a suitable level of CD4+ T cell count (> 200 cell/mm^3) in the peripheral blood [30, 150, 152]. However, this desirable outcome is not always achieved and the design of appropriate ART, the prediction of outcomes using clinical data and the assessment of virologic failure are the subject of active experimental and mathematical research [59, 153].

To allow mathematical models of HIV dynamics to be used as a tool for personalized clinical diagnosis and ART, it is crucial to estimate all the biological rates of the chosen model for each patients [59, 152, 154]. This can be a challenging problem using standard clinical data [59, 138, 154]. Further, current experimental facilities do not allow direct measurement of some pertinent state variables, such as the population dynamic of HIV-specific CD8+ T cells or infected CD4+ T cells in the eclipse phase [30, 55, 148]. Due to these practical limitations, the HIV model utilized in Chapter 5 is not selected to conduct the following investigations.

A third order Ordinary Differential Equation (ODE) model has been shown to encompass the observed biological characteristics of the acute phase of HIV infection using the variation over time of the population of healthy CD4+ T cells, the infected population of CD4+ T cells which produce new virions along with the concentration of the HIV-1 free virus [60]. Using techniques from engineering, the authors in [137, 141] have proved that the parameters of this model can be estimated from standard clinical data. This method is based on the computation of higher-order derivatives of the output measurements to formulate a set of identification equations and the solution of this system of equations allows the computation of the biological rates of the HIV model. Subsequently, a multiple time point (MTP) estimation algorithm using values at different time instants to reduce the need for higher-order derivatives of the output measurements has been used to formulate the identification equations [59].

Statistical estimation methods such as the simplex method [35], the differential evolution method [59] and the Monte-Carlo approach [148, 155] have been implemented to estimate HIV parameters in patients following the initiation of antiretroviral treatment. More recent contributions in this area can be found in [154, 156]. Together, this literature demonstrates

that the third order model of HIV infection correlates well with clinical data obtained from patients undergoing antiretroviral treatment [59, 148, 154] and that HIV dynamic parameters estimated a few weeks after initiation of ART can be used to investigate the impact of ART on the progression of HIV infection for individual patients [152, 153, 155].

In the literature [59, 60, 153], the impact of antiretroviral drugs on the progression of HIV infection has been investigated using the concept of the reproductive ratio R_0 presented in Chapter 5. In fact, using the values of the parameter estimated for the basic HIV model, the reproductive ratio is calculated to determine the progression of the infection [35, 59, 60]. For the basic third order ODE HIV model, the expression for R_0 is a function of the model parameters and not the states and thus a time-invariant condition for the containment of the infection is formulated. The work in Chapter 5 along with other studies [30, 34, 57, 102] argue that the condition for the containment of the infection rather than being static changes during the course of the infection. Furthermore, the work in [153] has shown that the value of the reproductive ratio estimated at different weeks after the start of ART can switch from $R_0 < 1$ to $R_0 > 1$ in the later weeks due to the appearance of drug resistance.

The purpose of this case study is to utilize the analytical tools from sliding mode control as alternative means to investigate the dynamics of HIV infection following antiretroviral therapy.

From the classical example of a pendulum system with a sliding mode, shown in Chapter 2, it is worthy to note that a manifold of the state space can be formulated to encompass the control objectives imposed on a system. Furthermore, the reachability analysis provides means to investigate how a given control input can satisfy the reachability condition so that the desired control objectives are met. Thus, by binding the desired dynamical behaviour with the attainment of a sliding mode, this VSC approach delivers tools to monitor the closed-loop dynamics and assess the performance of the considered control input.

Additionally, a sliding mode control approach has been used in Chapter 5 to formulate a dynamical condition for the containment of HIV infection by the HIV-specific CD8+ T cell response. The result in Chapter 5 shows that the dynamical condition for immunity provided by the reachability analysis appropriately monitors the progression of the infection. As compared to the reproductive ratio, the VSC approach provides additional insights on

HIV infection dynamics. These findings provides a strong motivation to conduct this case study.

The chapter is organized as follows: Firstly, the HIV model and the reproductive ratio are outlined. In Section 6.3 a dynamical condition for the containment of HIV infection by antiretroviral therapy is formulated using the reachability paradigm from variable structure control. The clinical data sets used for the study and the method used to estimate the parameters of the model are described and evaluated in Section 6.4. Section 6.5 presents the results of the simulation experiments conducted to show that the proposed dynamical condition for immunity is a reliable tool for early diagnosis of the outcome of antiretroviral therapy on HIV infection.

6.2 System model

The dynamical equations of HIV infection for patients being treated with antiretroviral therapy can be written as:

$$\begin{aligned} \frac{dT}{dt} &= \lambda - \delta_T T - \beta_0 TV + u_1(t) \\ \frac{dP}{dt} &= \beta_0 TV - \mu_1 P - u_1(t) \\ \frac{dV}{dt} &= k_0 P - \mu_2 V - u_2(t) \end{aligned} \tag{6.1}$$

with $\delta_T < \mu_1$ [59, 60, 96]. The state variables are the number in $cell/mm^3$ of uninfected target CD4+ T cells (T), the number in $cell/mm^3$ of HIV-infected CD4+ T cells producing new virions (P) and the concentration in $RNA\ copies/ml$ of HIV-1 free virions (V). Fig. 6.1 is provided to improve the understanding of the dynamical system (6.1).

.

Uninfected CD4+ T cells are produced by the thymus at a rate λ (in $cell/day$) and die at a rate δ_T (in day^{-1}). HIV infects healthy CD4+ T cells at a rate β_0 (in $\mu lvirion/day$ $x10^{-3}$). HIV-infected CD4+ T cells produce new virions at a rate k_0 (in $virion/day$) and die at a rate μ_1 (in day^{-1}). HIV free virions are cleared at a rate μ_2 (in day^{-1}) in the peripheral blood. As in [59, 60, 148], these six biological rates are non-negative and assumed to be constant for a given patient. The functions $u_1(t)$ and $u_2(t)$ represent the action of reverse-transcriptase (RT) and protease inhibitor (PT) drugs respectively. The effect of

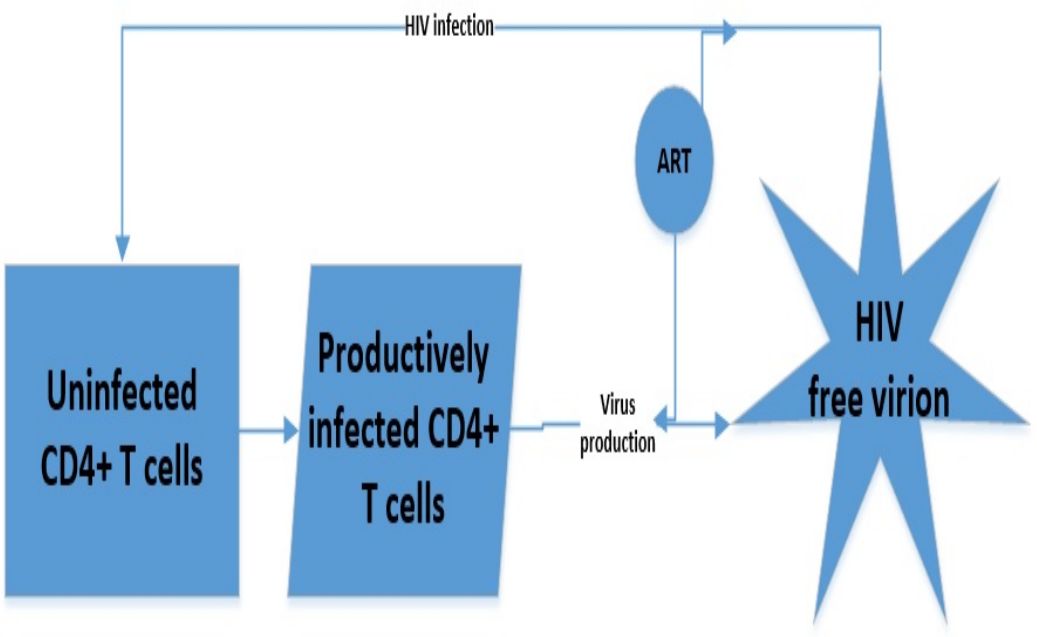

FIGURE 6.1: Model (6.1) of HIV infection dynamics following antiretroviral therapy (ART)

antiretroviral drugs on HIV infection dynamics can be modelled as follows:

$$u_1 = \eta_1 \beta_0 TV \tag{6.2}$$

$$u_2 = \eta_2 k_0 P \tag{6.3}$$

where $0 \leq \eta_1 < 1$ and $0 \leq \eta_2 < 1$ are constants related to the efficiency of the deployed RT and PT drugs, assuming that 100 percent drug efficacy cannot be achieved [60, 157]. The action of antiretroviral therapy will be considered from the perspective of control engineering and regarded as a control action which seeks to enforce the containment of the HIV infection. In practice, antiretroviral therapy is declared efficient when it reduces and maintains the HIV viral load in the peripheral blood stream below the threshold of 50 HIV RNA copies/ml [157]. The available output measurements of (6.1) are assumed to be

$$y_1(t) = T(t) + P(t); \quad y_2(t) = V(t) \tag{6.4}$$

where $y_1(t)$ is the total number in $cell/mm^3$ of CD4+ T cells in blood samples collected from patients [150, 152, 154]. This choice is motivated by the information available in the clinical data sets used for later validation of the proposed methodology.

The clinical trial data available relates to the period following the initiation of antiretroviral therapy and thus it is not possible to estimate the values of β_0 and k_0 [148, 150, 154]. Thus $\beta_0(1-\eta_1)$ and $k_0(1-\eta_2)$ i.e the resultant effects in vivo of the uptake of RT and PT drugs respectively will be considered and in the model (6.1), the following substitutions are made

$$\beta = (1-\eta_1)\beta_0 \tag{6.5}$$

$$k = (1-\eta_2)k_0 \tag{6.6}$$

to yield the closed-loop representation

$$\begin{aligned} \frac{dT}{dt} &= \lambda - \delta_T T - \beta TV \\ \frac{dP}{dt} &= \beta TV - \mu_1 P \\ \frac{dV}{dt} &= kP - \mu_2 V \end{aligned} \tag{6.7}$$

This parametrization of the effects of antiretroviral drugs is as used in previous studies [59, 148, 157]. The model (6.7) has two equilibrium points. There is a trivial equilibrium corresponding to an infection-free steady-state at

$$T_{s0} = \frac{\lambda}{\delta_T}; \quad P_{s0} = V_{s0} = 0 \tag{6.8}$$

The Jacobian of the system (6.7) linearised at the infection-free steady-state (6.8) is given by

$$J = \begin{pmatrix} -\delta_T & 0 & -\frac{\beta\lambda}{\delta_T} \\ 0 & -\mu_1 & \frac{\beta\lambda}{\delta_T} \\ 0 & k & -\mu_2 \end{pmatrix} \tag{6.9}$$

The characteristic equation of (6.9) is

$$\frac{1}{\delta_T}(s+\delta_T)(a_2 s^2 + a_1 s + a_0) = 0 \tag{6.10}$$

where the coefficients of the polynomial are given by:

$$\begin{aligned} a_2 &= \delta_T \\ a_1 &= \delta_T\mu_1 + \delta_T\mu_2 \\ a_0 &= -\lambda\beta k + \delta_T\mu_1\mu_2 \end{aligned} \tag{6.11}$$

Using Descartes' rule of sign as in [40, 145], the stability of the infection-free steady-state is assessed by counting the number of sign changes in the characteristic polynomial in (6.10). Since the biological rates of the model (6.7) are all positive, the coefficients $a_2 > 0$ and $a_1 > 0$. It remains to investigate the sign of the coefficient a_0 in (6.11).

As in Chapter 5 section 3, the reproductive ratio can be utilized to assess the stability of the infection-free steady-state. For the system (6.7), the reproductive ratio is given as:

$$R_0 = \frac{\lambda}{\delta_T}\frac{1}{\mu_1}\frac{k}{\mu_2}\beta \tag{6.12}$$

The first factor is T_{s0}, the population size of uninfected CD4+ T cells T at the infection-free steady-state, see (6.8). The second factor is the lifetime of a virus-producing cell. The third factor is the number of virus particles produced per infected cell and the final parameter represents the infection rate for a single virus particle. Whether the value of R_0 is above or below unity influences the sign of a_0 and thus determines the stability of the infection free steady-state. When $R_0 < 1$, $a_0 > 0$ and the quadratic polynomial has no sign change. Using Descartes' rule of signs [145], this implies that the roots of the quadratic polynomial are negative. As a result, the HIV model (6.7) linearised at the infection-free steady-state (6.8) has negative poles. Thus, the infection free-steady state is stable when $R_0 < 1$. In contrast, $R_0 > 1$ implies $a_0 < 0$. Consequently, there exists a sign change in the second order polynomial in (6.10) which indicates a positive pole. As a result, the infection-free steady state (6.8) is unstable when $R_0 > 1$. Mathematical investigations in [116] have proved that if $R_0 \leq 1$, the infection free steady-state is globally asymptotically stable (GAS).

The expression for the non-trivial equilibrium is given by:

$$T_{s1} = \frac{\mu_1\mu_2}{\beta k}; \quad P_{s1} = \frac{\lambda}{\mu_1} - \frac{\delta_T\mu_2}{\beta k}; \quad V_{s1} = \frac{\lambda k}{\mu_1\mu_2} - \frac{\beta}{\delta_T} \tag{6.13}$$

From the results in [35, 116], the non-trivial equilibrium (6.13) is stable when $R_0 > 1$.

This non-trivial equilibrium can represent either an undesirable steady-state corresponding to chronic infection or a desirable steady-state depending on the parameter values [30, 35, 60, 152]. Since the surrogate markers of the progression of HIV infection in clinical diagnosis are the measurements of the total number of CD4+ T cells $(T + P)$ and HIV load in the peripheral blood stream, a chronic infection steady-state is characterized by a

low number of CD4+ T cells and a large HIV viral load in the peripheral blood samples. A corresponding steady-state of asymptomatic infection which can be enforced as a result of efficient antiretroviral treatment is usually associated with a high number of CD4+ T cells and HIV load below the limit of detection of $50 HIV\ RNA\ copies/ml$ [150, 152]. The state space of the HIV model (6.7) can be partitioned into two regions. In one region, HIV is harmful for the infected individual and the corresponding immunological dynamics and steady-states in this region are undesirable. In the other region, HIV infection is asymptomatic and the related immunological dynamics and steady-state in this region are desirable from a clinical perspective. It is thus of interest to develop mathematical tools to define the boundaries of these regions as well as to predict the location of the steady-state enforced by antiretroviral therapy to inform clinical diagnosis.

6.2.1 The reproductive ratio, a steady-state condition for the success of antiretroviral therapy

Using the framework of the reproductive ratio, antiretroviral therapy must force and maintain R_0 below unity following initiation of treatment to prevent the spread of HIV infection [30, 116, 155, 158]. The effectiveness of antiretroviral therapy is encompassed in the product $k\beta$ because the HIV model (6.7) does not allow decoupling of the effects of RT and PT drugs [155]. Thus, the condition for antiretroviral drugs to eradicate HIV infection derived from the reproductive ratio is given by

$$\begin{aligned} R_0 &< 1 \\ k\beta &< \tfrac{1}{T_{s0}}\mu_1\mu_2 \\ (1-\eta_2)(1-\eta_1) &< \tfrac{1}{T_{s0}}\tfrac{\mu_1\mu_2}{\beta_0 k_0} \end{aligned} \tag{6.14}$$

where $T_{s0} = \frac{\lambda}{\delta_T}$. This inequality is a steady-state condition for the infection-free steady-state to have negative poles and hence to exhibit stable behaviour. The inequality (6.14) implies that antiretroviral drugs achieve eradication of HIV infection when the effective control action exceeds a critical threshold value determined by the biological rates.

As discussed in Chapter 5, the framework of the reproductive ratio has some limitations, When (6.14) is not satisfied, the generated value of R_0 alone cannot be used to predict whether the non-trivial equilibrium (6.13) is located in a state space region associated with a chronic infection state or an asymptomatic state. In effect, the value of R_0 alone does not

provide information on the magnitude of the CD4+ T cell population and HIV viral load at the nontrivial equilibrium. As will be demonstrated later in this chapter, there are also cases where the prediction from R_0 alone is seen to contradict the clinical outcome [155]. The reproductive ratio paradigm is thus seen to have limitations as a means to monitor and predict the containment of HIV infection following drug treatment.

6.3 A reachability condition to monitor the containment of HIV infection

In the context of HIV infection dynamics in vivo, the work in Chapter 5 has demonstrated that these dynamics form a closed-loop system in which the specific immune response of CD8+ T cells against HIV is an intrinsic VSC feedback applied by the immune system to contain the infection. Furthermore, it has been shown that the reachability paradigm introduced in Chapter 2 can be used to formulate a dynamical condition for the containment of HIV infection in vivo. Importantly, this approach provides a nonlinear means to determine and monitor the progression of the infection.

In this section, the approach used in Chapter 5, is considered to investigate dynamical requirements for the containment of HIV infection in vivo following the initiation of antiretroviral therapy.

It will be seen that the variable structure control paradigm will be particularly useful in explaining dynamic behaviour which occurs within a boundary layer of the infection free steady-state. Currently measured data and analytical analysis has produced conflicting conclusions in such cases [30].

The formulation of a reachability condition to monitor the containment of HIV infection involves defining an appropriate switching function to describe the desired clinical outcome of the treatment. A candidate switching manifold is chosen to be compliant with the objective of antiretroviral therapy to reduce and maintain the HIV viral load below the limit of detection. The hypothesis is that in the ideal case, the uptake of antiretroviral drugs, as a control mechanism, has to force the HIV infection dynamics to attain and remain on the infection-free steady-state (6.8).

A valid candidate switching function is

$$s_E(t) \quad = \quad P(t) \tag{6.15}$$

because the manifold $s_E(t) = P(t) = 0$ in which the population dynamic of productively infected CD4+ T cells vanishes has been observed to be a naturally occurring attractive manifold in the state-space of (6.7) when the trajectories exhibit a stable motion towards the infection free steady-state (6.8). The reachability condition for exhibiting a sliding mode is expressed as

$$s_E \frac{ds_E}{dt} \quad < 0 \tag{6.16}$$

$$s_E \left(\beta TV - \mu_1 P\right) \quad < 0 \tag{6.17}$$

$$\left(\beta TV - \mu_1 P\right) \quad < 0$$

This inequality is fundamentally a dynamical condition for the manifold $s_E(t) = 0$ to be attractive. In the present context, enforcing a sliding motion on $s_E(t) = 0$ is synonymous with achieving the containment of HIV infection. In order to ensure (6.16) attains and remains at a negative value, the therapeutic control u_1 associated with the effects of antiretroviral drug therapy must have a sufficiently large magnitude to overcome the positive feedback $\beta_0 TV$ associated with the HIV pathogenesis. The reachability condition (6.16) thus represents a dynamical condition for antiretroviral drugs to force the dynamics to lie within a neighbourhood of the manifold $s_E(t) = 0$. The inequality (6.16) represents a dynamical condition for antiretroviral drug therapy to contain HIV infection. It should be noted that assessing the sign of $\frac{ds_E}{dt}$ is sufficient to determine whether the reachability condition is satisfied due to the fact that $s_E(t) = P(t) \geq 0$ because it represents the number of infected CD4+ T cells producing new virions. The reachability condition (6.16) can be written as:

$$\beta TV - \mu_1 P \quad < 0 \tag{6.18}$$

It is interesting to note that the expression (6.17) can be written in terms of the output dynamics and their derivatives to allow direct monitoring of the condition for immunity

using the measured state variables if desired:

$$\frac{ds_E}{dt} = \beta y_1 y_2 - \left(\frac{\beta y_2 + \mu_1}{k}\right)(\dot{y_2} + \mu_2 y_2) < 0 \tag{6.19}$$

This expression for the reachability condition, which is a function of both η_1 and η_2 demonstrates that RT and PT drugs work synergistically to achieve the containment of HIV infection.

6.4 Parameter identification

It is clear that whether seeking to monitor the clinical outcome of antiretroviral drug therapy in the treatment of HIV using the reproductive ratio or the proposed reachability condition, it is first necessary to determine patient dependent parameter estimates based upon available clinical measurements.

6.4.1 The clinical data sets

Two clinical trials have been considered to evaluate the use of the reachability condition (6.18) as a tool to monitor the containment of HIV infection following antiretroviral therapy. From the theoretical point of view, it is desirable to have a large number of data points at equally spaced intervals. However, practical constraints related to the collection and analysis of blood samples from HIV infected individuals influence the timings and number of the measured data [138, 148, 159]. The selected data sets are chosen to test the practicality of the approach.

The first data set relates to the EDV05 clinical trial conducted at the Centre Hospitalier Universitaire (CHU) de Nantes, France [148, 152, 157]. In this study, measurements of the total number of CD4+ T cells and HIV viral load in the peripheral blood stream were collected following the initiation of Highly Active Antiretroviral Therapy (HAART). The facilities used in that study allowed HIV viral load to be measured up to the limit of $1.6 log_{10}(RNAcopies/ml)$ i.e $50(RNAcopies/ml)$. As in [148, 152], the data collected in the first 21 days are used to compute estimates of the biological rates. This information is then used to predict the outcome of the full treatment regime. The data measured following the initial period of 21 days are used to validate the resulting theoretical predictions of the

efficacy of the treatment. The EDV05 trial has been considered because model parameters have been estimated by other studies for this patient data [148, 152, 155, 160]. This is useful to compare the results of the parameter estimation approach adopted in this work as well as to test the formulated dynamical condition for immunity (6.18). In this chapter, the syntax pt_i is used to refer to the patients involved in the EDV05 trial where i denotes a specific patient number. Note that the results of pt_{10} are discarded because there is no clinical data available from the final follow-up visit in the clinical trial. Thus, the efficiency of the treatment cannot be validated.

The longitudinal data recorded by the AIDS Clinical Trials Group (ACTG 315) [150, 159] are also chosen to verify the performance of the proposed reachability condition for cases of success and failure of HAART. Here, the syntax pa_i is used to refer to the patients involved in this study. For this trial, data points in the interval $[0, 30]$ days are used to compute the estimates of the biological rates. The limit of detection of HIV free virion in this trial is $2log_{10}(RNAcopies/ml)$ i.e $100(RNAcopies/ml)$. Data below this limit were tabulated as $1.699log_{10}(RNAcopies/ml)$. As in [161], data below the limit of detection are not used to estimate the biological rates. As discussed in [138], the selection of a patient data along with segmentation of the data period into data used for parameter estimation and data used for the validation of prediction is driven by the availability of sufficient data points to perform the parameter estimation. The rate at which patient data is sampled differs from study to study and is not constant across a given study. This realistic scenario of data availability will be seen not to affect the predictions. Patient data which do not have data points covering a six month period ($\geq$ 160 days) are discarded due to the fact that no information is available to confirm the predictions and to assess the long term efficacy of the antiretroviral therapy.

6.4.2 Parameter identification procedure

Previous mathematical analysis [59, 137, 152] has proved the algebraic and practical identifiability of the parameter set $\lambda, \delta_T, \beta, \mu_1, k, \mu_2$ of the model (6.7) using the output measurements (6.4).

In [59], it was shown that the multi-point identification method provides some advantage over the higher order identification method used in [137, 141, 162] because it allows the

computation of the estimates using a finite set of output data points instead of computing the higher order derivatives of the output measurements.

Here, the multi-point identification method described in [59] is applied to identify the six biological parameters $\lambda, \delta_T, \beta, \mu_1, k, \mu_2$ of the model (6.7) using measurements taken at irregular intervals within a set period following initiation of antiretroviral treatment for patients across the two data sets. A pseudo code is provided in the appendix A.

For each patient, shape-preserving piecewise cubic interpolation is used to generate a continuous stream of data points within the range of the discrete set of measured clinical data considered for the computation of the estimates of the biological rates. Next, the least-squares polynomial that are the best fit for $y_1(t)$ and $y_2(t)$ are computed to evaluate the time derivatives of the measurements at different time points as in [154]. The degree of the least-squares polynomial for each patient is selected to improve the quality of the fit. Subsequently, the following multi-point identification process is carried out. Consider y_2 and its time derivative up to the third order

$$\begin{aligned} y_2^{(3)} &= \left(y_2^{-1}\dot{y}_2 - \delta_T - \beta y_2\right)\left(\ddot{y}_2 + (\mu_1+\mu_2)\dot{y}_2 + \mu_1\mu_2 y_2\right) \\ &\quad + \lambda k\beta y_2 - \mu_1\mu_2\dot{y}_2 - (\mu_1+\mu_2)\ddot{y}_2 \end{aligned} \tag{6.20}$$

The identification coefficient θ_1 is defined as:

$$\theta_1 = (\beta, \delta, \rho, \nu, \eta) \tag{6.21}$$

where

$$\beta = \beta; \delta = \mu_1; \rho = \delta_T; \nu = \mu_1\mu_2; \mu = \mu_1 + \mu_2; \eta = \lambda k\beta \tag{6.22}$$

This implies that four of the six parameters of the model (6.7) can be identified using measurement of y_2 and corresponding derivatives. The values of the parameters λ and k are indistinguishable and only their product λk can be estimated. Consider the right hand side of (6.20):

$$\begin{aligned} f(t, \theta_1, y_2, \dot{y}_2, \ddot{y}_2, y_2^{(3)}) &= \left(y_2^{-1}\dot{y}_2 - \delta_T - \beta y_2\right)\left[\ddot{y}_2 + \mu\dot{y}_2 + v y_2\right] \\ &\quad + \eta y_2 - \nu\dot{y}_2 - \mu\ddot{y}_2 \end{aligned} \tag{6.23}$$

Assume that the quantities $(y_2, \dot{y}_2, \ddot{y}_2, y_2^{(3)})$ are either available from direct measurement or can be constructed from measurements at five different time points. Denote the values of $(y_2, \dot{y}_2, \ddot{y}_2, y_2^{(3)})$ at $t = t_i$ as $(y_2(i), \dot{y}_2(i), \ddot{y}_2(i), y_2^{(3)}(i))$ and

$$f_i \quad = \quad f\left(t(i), \theta_i, y_2(i), \dot{y}_2(i), \ddot{y}_2(i), y_2^{(3)}(i)\right)$$

for $i = 1, ..., 5$. Using these measurements, a system of five equations and five unknowns can be constructed:

$$\varphi_1 \quad = \quad \left(y_2^{(3)}(i) - f_i\right) = 0 \tag{6.24}$$

If

$$det\left(\frac{\delta\varphi_1}{\delta\theta_1}\right) \quad \neq \quad 0 \tag{6.25}$$

then by the implicit function theorem, the system of equations (6.24) has a unique solution for θ_1. This solution provides an estimate of the biological rates δ_T, β, μ_1 and μ_2. However, λ and k cannot be identified using measurement of y_2 alone.

To recover the remaining parameters, the first derivative of y_1 is written in terms of the output dynamics as follows:

$$\dot{y}_1 \quad = \quad \lambda - \delta_T y_1 - \delta_P P \tag{6.26}$$

where $\mu_1 = \delta_T + \delta_P$. Using the expression for $\dot{y}_2$, the state variable P can be written in terms of the output dynamics y_2 and its first derivative as

$$P \quad = \quad \frac{1}{k}\left(\dot{y}_2 + \mu_2 y_2\right) \tag{6.27}$$

Substitute (6.27) into (6.26) to obtain

$$\dot{y}_1 \quad = \quad \lambda - \delta_T y_1 - \frac{\delta_P}{k}\left(\dot{y}_2 + \mu_2 y_2\right) \tag{6.28}$$

Define the identification coefficient θ_2 as:

$$\theta_2 \quad = \quad (\lambda, \delta_T, \xi, \sigma)$$

where $\xi = \frac{\delta_P}{k}$ and $\sigma = \frac{\mu_2 \delta_P}{k}$. Let the identification function be

$$g(t, y_1, \dot{y}_2, y_2) = \lambda - \delta_T y_1 - \xi \dot{y}_2 - \sigma y_2 \tag{6.29}$$

The multi-point identification process [59] is performed to estimate θ_2. Here, the values of $(\dot{y}_1, y_1, \dot{y}_2, y_2))$ are needed at four different time points to construct a system of four equations and four unknowns to estimate θ_2. Consequently, the identification equation is given by

$$\varphi_2 = (\dot{y}_1(j) - g_j) = 0 \tag{6.30}$$

where $\dot{y}_1(j)$ and g_j denote the values of $\dot{y}_1$ and $g(t, y_1, \dot{y}_2, y_2)$ at four time points for $j = 1, ..., 4$. Proceeding as before, estimates of the biological rates λ,δ_T and μ_2 can be computed. Nevertheless, μ_1 and k cannot be identified using (6.30) only.

It is worth to mention that the computation of the derivatives of the output measurements y_1 and y_2 is delicate process because it plays a major role in the parameter estimation procedure. This difficulty is partially due to the fact that the clinical data are sparse. Different methods have been proposed to estimation of the time derivatives of the clinical data such as in [59, 137, 152, 154] or to avoid this step using alternative methods such as in [156, 161]. Here, the time derivatives of the output measurements are obtained using the least-squares polynomial method, see appendix A for more details.

Combining θ_1 and θ_2 from (6.24) and (6.30) respectively, it is possible to construct estimates of the six biological rates in the model (6.7). In the presented results, λ, δ_T and μ_2 are taken from θ_2, β and $\mu_1 = -\frac{-\nu - \nu^2 + 4\mu^{\frac{1}{2}}}{2}$ are taken from θ_1 and $k = \frac{\eta}{\lambda\beta}$.

The estimation process is conducted for each patient and resulting numerical solutions of the model (6.7) are obtained using the Runge-Kutta method [154]. To estimate the quality of the fits, error vectors are constructed where the error at each data point is given by

$$e_{y1}(t_i) = y_1(t_i) - \hat{y}_1(t_i) \tag{6.31}$$

$$e_{y2}(t_i) = y_2(t_i) - \hat{y}_2(t_i) \tag{6.32}$$

for $i = 1, ..., n$ where i is the time point of the corresponding measurement and n is the number of measurements collected within a set period. $\hat{y}_1(t_i)$ and $\hat{y}_2(t_i)$ are the estimated values of the total number of CD4+ T cells and HIV viral load produced from the numerical

model which uses the estimated parameters. The relative accuracy of the output dynamics produced using the estimated biological rates is evaluated from

$$a_{y1} = 100 \sum_{i=1}^{n} \frac{e_{y1}^2(t_i)}{y_1(t_i)^2} \tag{6.33}$$

$$a_{y2} = 100 \sum_{i=1}^{n} \frac{e_{y2}^2(t_i)}{y_2(t_i)^2} \tag{6.34}$$

for $i = 1, ..., n$.

6.4.3 Parameter estimation results

In the results presented, a set of patients from each clinical trial has been randomly picked. Note that the values of the estimated biological rates presented in the following tables are rounded. The values of the parameters with the accuracy required to reproduce all of the results can be found in the appendix B. The tabulated biological rates may not identically reproduce the results presented for the reproductive ratio as the values of the estimates produced by the identification algorithm are used to compute R_0, a_{y1}, a_{y2}. As will be seen in the results presented, the dynamics exhibit good robustness to such changes in the parameter values.

Previous work in the literature has estimated parameter values for the dynamics of HIV infection in the course of antiretroviral drug treatment [59, 152]. Here biological rates estimated using the Monte Carlo approach from [148, 152] are used to benchmark the results presented in this chapter. For both estimation approaches, the initial conditions are selected such that $T(0) + P(0) = y_1(0)$ and $V(0) = y_2(0)$ where the values of $y_1(0)$ and $y_2(0)$, see (6.4), are taken from the clinical data set relating to the EDV05 trial as published in [152]. It is important to note that for both approaches all the parameter estimates are generated only using data obtained during the initial 30 days of the period of the trial. Motivation for this study is to be able to obtain patient specific data that can be used to predict the likely outcome of the current drug treatment. If the eventual outcome is likely to be unsuccessful, modification of the antiretroviral drug treatment can take place based on the patient specific parameter estimates. In this work, the measured data obtained across the remainder of the trial will be used to validate the parameter estimates as will the known clinical outcome.

TABLE 6.1: Estimates of the biological rates taken from [148, 152]. Common parameters:$\delta_T = 0.01 day^{-1}$, $\mu_1 = 0.05 day^{-1}$ and $\mu_2 = 0.28 day^{-1}$

Results	$T(0)+P(0)$	$V(0)$	λ	β	k	R_0	a_{y1}	a_{y2}
pt_1	200+176	10^6	8.13	1.94e-07	0.04	4.50e-04	4.28	9.25
pt_2	138+92	$10^{5.4}$	9.53	3.27e-07	0.21	0.0047	14.76	8.81
pt_3	110+75	$10^{4.54}$	1.77	8.24e-07	0.41	0.0043	13.36	2.44
pt_4	120+85	$10^{5.3}$	5.45	7.10e-08	293.00	0.809	7.06	22.90
pt_5	200+183	$10^{4.82}$	6.76	3.94e-07	0.004	7.6098e-05	2.75	5.51
pt_6	205+200	$10^{4.972}$	6.94	1.21e-07	46.80	0.2807	7.40	21.76
pt_7	5+4	$10^{5.07}$	3.01	2.43e-06	0.008	4.17e-04	147.01	85.19
pt_8	80+42	$10^{5.3}$	6.41	8.15e-07	0.002	7.46e-05	5.31	5.92
pt_9	68+50	$10^{5.21}$	5.36	7.23e-07	0.003	8.30e-05	11.13	3.95
pt_{11}	10+13	$10^{6.02}$	2.08	1.79e-07	0.012	3.19e-05	11.90	12.31
pt_{12}	200+105	$10^{5.7}$	7.66	2.56e-07	0.002	2.80e-05	4.71	12.56

Table 6.1 reports the results of the Monte Carlo approach from [148, 152]. Table 6.2 shows the results obtained for the procedure described in this chapter. A major difference between the two estimation methods is that the algorithm chosen in [148, 152] uses the same values of the decay parameter δ_T, μ_1 and μ_2 for all patients. Nevertheless, as argued in [154], it is preferable to estimate all parameters to improve personalized treatment and clinical decisions. For example, when comparing the values of the reproductive ratio R_0 presented in Table 6.1 with the corresponding values in Table 6.2 it is clear that the parameter values generated from the methodology presented in this chapter generate more realistic values.

Biological rates estimated using the procedure presented in this chapter and patient data from the ACTG 315 trial are shown in Table 6.3.

TABLE 6.2: Estimates of the biological rates produced by the identification method presented in this chapter. Initial conditions are identical to those in Table 6.1

Results	λ	δ_T	β	μ_1	k	μ_2	R_0	a_{y1}	a_{y2}
pt_1	427.15	0.98	4.09e-04	1.002	1.65	0.39	0.73	3.10	13.74
pt_2	525.63	1.13	1.14e-05	3.07	530.50	0.94	0.95	6.44	25.51
pt_3	137.97	0.70	0.0028	0.90	0.75	0.49	0.92	20.56	7.56
pt_4	91.34	0.21	8.44e-05	0.37	3.50	0.46	0.72	7.97	38.6
pt_5	511.21	1.16	0.0014	1.23	0.106	0.48	0.107	0.78	6.25
pt_6	447.26	0.87	3.83e-04	1.08	0.98	0.20	0.87	3.25	22.72
pt_7	48.54	0.88	1.05e-04	1.09	237.41	1.98	0.63	21.23	84.15
pt_8	77.45	0.30	2.39e0-5	0.67	72.35	0.66	1.002	0.91	0.10
pt_9	255.40	0.83	2.45e-04	1.48	4.66	0.50	0.46	9.50	0.08
pt_{11}	20.23	0.24	2.11e-05	1.59	717.20	0.76	1.008	5.67	0.1
pt_{12}	216.15	0.47	5.53e-04	0.53	0.57	0.87	0.30	0.54	0.01

TABLE 6.3: Estimates of the biological rates produced by the identification method presented in this chapter.

Results	λ	δ_T	β	μ_1	k	μ_2	R_0	a_{y1}	a_{y2}
pa_3	19.44	0.05	1.83e-04	0.39	24.61	0.33	11.50	1.50	1.16
pa_8	72.46	0.18	7.39e-04	1.05	2.49	0.38	4.95	2.10	0.07
pa_{10}	117.28	0.15	4.15e-05	0.53	16.93	0.35	2.85	21.24	0.21
pa_{13}	46.06	0.19	3.82e-04	0.65	0.03	0.27	0.01	1.92	2.17
pa_{24}	118.39	0.34	4.84e-05	0.45	9.10	0.37	0.89	0.75	0.38
pa_{34}	169.72	0.44	1.30e-04	0.46	4.67	0.49	1.01	3.90	3.44
pa_{38}	137.66	0.49	1.76e-04	0.58	3.54	0.28	1.03	5.64	23.12
pt_{43}	234.49	0.64	2.93e-04	0.73	0.45	0.19	0.33	0.86	10.98

The estimated parameter values obtained by the proposed method and presented in Tables 6.2 and 6.3 of the six biological rates of the basic HIV model (6.7) using patient data from the first period of both clinical trials are reasonable and close to the ones published in other studies [59, 154, 155, 161].

Fig. 6.2-6.5 are displayed as examples to show that the output dynamics produced by the estimated biological rates are realistic. In all figures, the parameter estimates have been obtained from clinical measurements obtained in the early phase of the trial and later measurements are presented to validate the output response predicted from the model.

Fig. 6.2-6.3 illustrate cases in which the uptake of antiretroviral drugs enforces the containment of HIV load to a small level along with the recovery to a desirable CD4+ T cell count. Fig. 6.4 relates to cases of immunological failure characterized by a desirable low steady-state HIV load and poor recovery of CD4+ T cell count. Fig. 6.5 depicts a case in which antiretroviral therapy fails. The figures reinforce that the estimation method used in this work produces responses similar to the ones generated by other studies [30, 148, 153, 154, 161] and the responses align well with subsequent measurements obtained later in the drug trial and not used within the parameter estimation procedure.

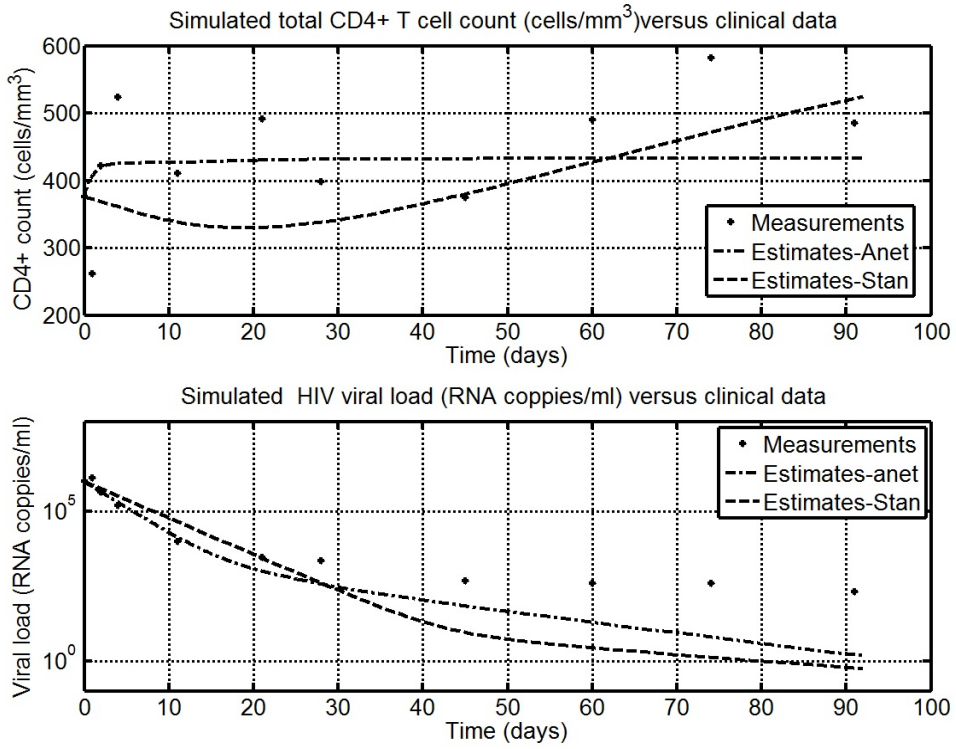

FIGURE 6.2: Comparison of the time evolution of measured CD4+ T cell count and HIV load versus its estimates for pt_1 using the HIV model (6.7).

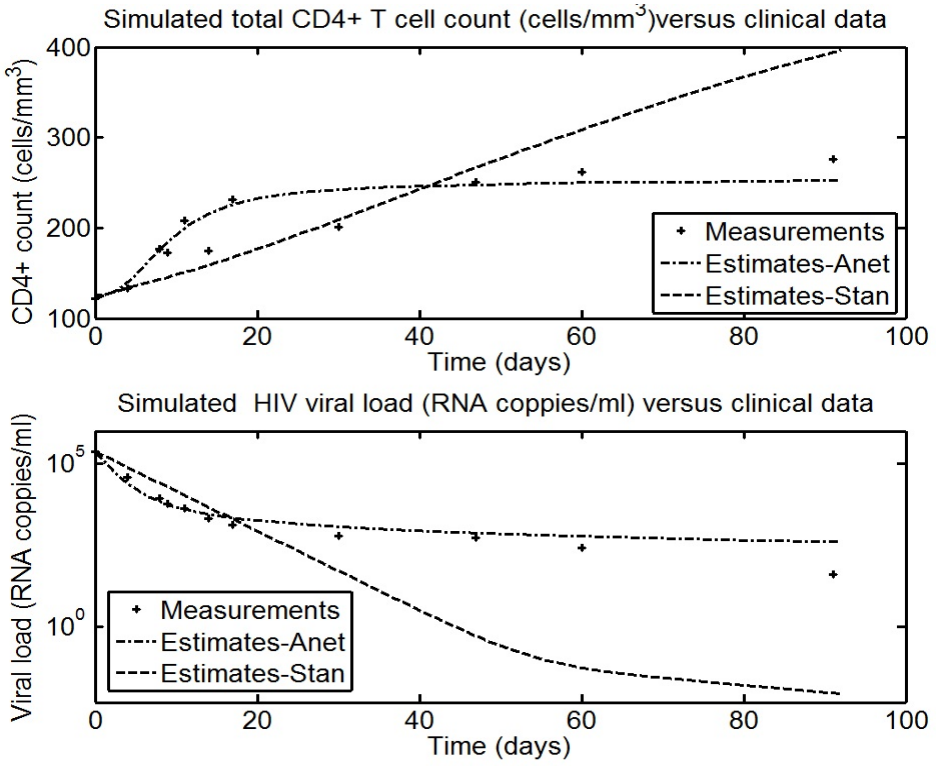

FIGURE 6.3: Comparison of the time evolution of measured CD4+ T cell count and HIV load versus its estimates for pt_8 using the HIV model (6.7).

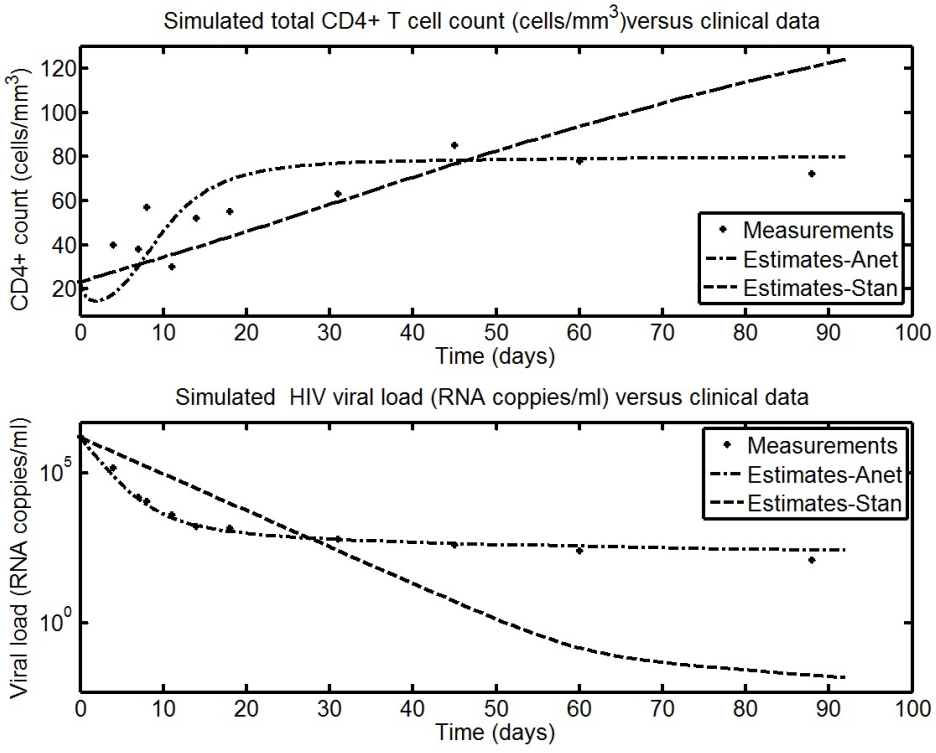

FIGURE 6.4: Comparison of the time evolution of measured CD4+ T cell count and HIV load versus its estimates for pt_{11} using the HIV model (6.7).

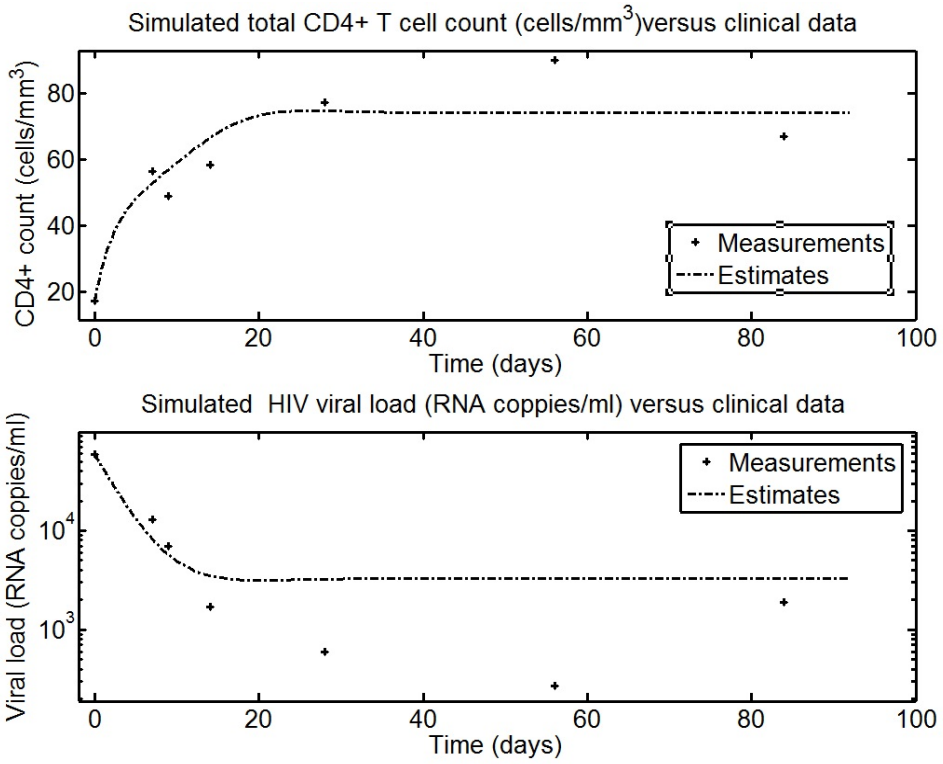

FIGURE 6.5: Comparison of the time evolution of measured CD4+ T cell count and HIV load versus its estimates for pa_3 using the HIV model (6.7).

The data used to estimate the parameters can be expected to incorporate measurement error and it is important to consider the likely effect of such errors on the computed parameter estimates. A comprehensive review of the practical issues relating to the estimation of the parameters of the dynamics of HIV can be found in [138]. Results from both structural and statistical analysis have shown that it is sensible to estimate the parameters using measurements in the early weeks following the initiation of antiretroviral therapy because the transient phase after the initiation of treatment contains more dynamic information [137, 138, 163]. This supports selecting measurements in the first month following initiation of treatment as adopted in this study. A statistical noise model for HIV standard clinical data has recently been determined in [161]. The local polynomial regression technique used in [154] was used to smooth the longitudinal data and to estimate the measurement noise. After conducting normality tests with the Chi-square and Lilliefors tests, the authors concluded that a multiplicative zero mean Gaussian noise affects both measurements of CD4+ T cell count and HIV load. Further, similar noise parameters i.e sample mean and standard deviation have been found for two patient data. Interestingly, an earlier study on noise characteristics based on visual observations of the noise on the viral load data also suggested that the noise might follow a Gaussian distribution [163]. Simulation studies

in a number of publications have incorporated a zero mean Gaussian noise with different levels of standard deviation to the numerical solutions of the basic HIV model to test the practical identifiability of the biological rates [59, 154, 156, 164]. Collectively, these simulation results provide evidence that reasonable parameter estimates can be obtained in the presence of noise in the measured data. Furthermore, the estimated biological rates from patient datasets has been shown to produce viral load dynamics which closely match the trajectory of observed data [148, 154, 161, 163].

To determine the robustness of the biological rates determined in this study to measurement noise, the established noise model from [161] was added to the patient data and a second set of parameter estimates was computed. The responses of the HIV model with parameter estimates generated in the presence of additional noise are compared with the results obtained with parameter estimates obtained without additional noise for pt_1 and pa_3 in Fig. 6.6 and Fig. 6.7. respectively. This reinforces that the output dynamics generated by the estimated biological rates are not dramatically affected by noise and the traces are visually indistinguishable. Hence, the infection dynamics following antiretroviral treatment are shown to exhibit some robustness with respect to measurement noise.

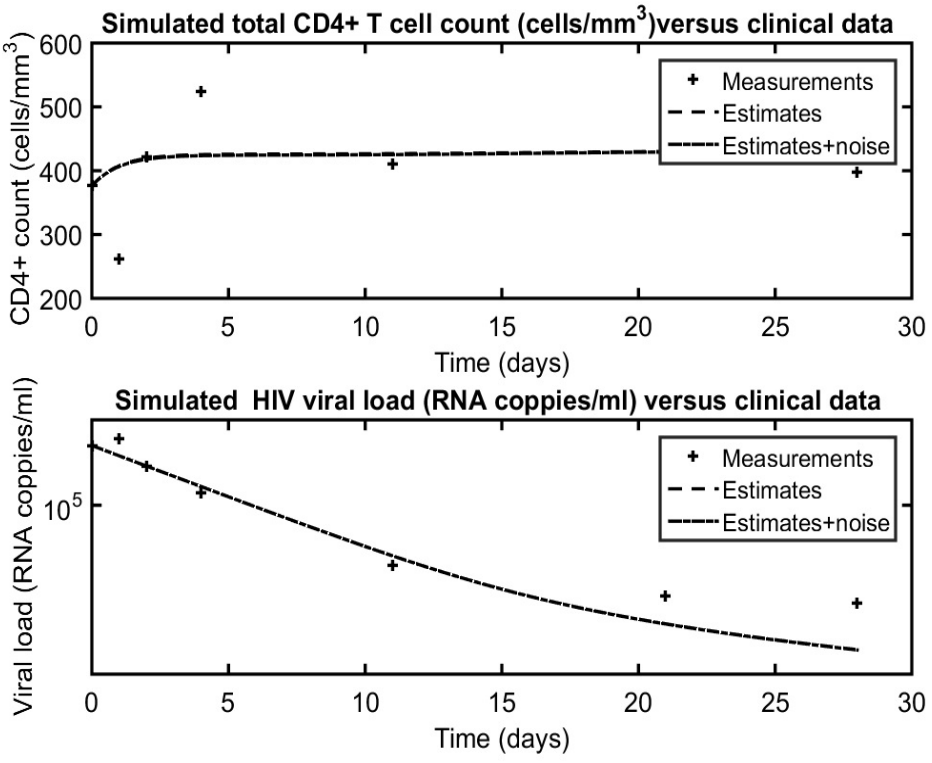

FIGURE 6.6: Comparison of the time evolution of measured CD4+ T cell count and HIV load for pt_1. Original data and the responses generated with parameters estimated in the presence of additional noise and without additional noise are presented. HIV model (6.7).

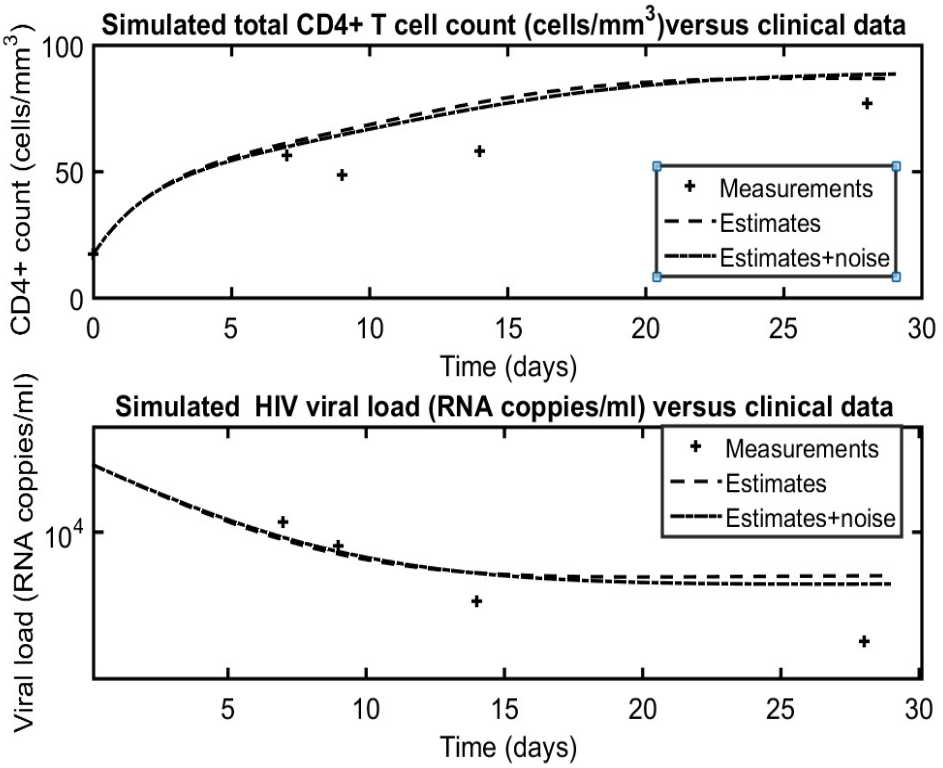

FIGURE 6.7: Comparison of the time evolution of measured CD4+ T cell count and HIV load for pa_3. Original data and the responses generated with parameters estimated in the presence of additional noise and without additional noise are presented. HIV model (6.7).

6.5 Prediction of the outcome of antiretroviral treatment

For each patient listed in Table 6.2 and 6.3, the proposed reachability analysis for the containment of HIV infection is evaluated to predict the outcome of HAART. Note that these predictions are based only on measured data obtained in the first 30 days following treatment. The predictions are then compared with clinical outcomes determined from examining the CD4+ T cell count and HIV viral load at the conclusion of the clinical trial. The findings show that the time evolution of the reachability condition (6.18) and the switching function (6.15) exhibit a particular dynamical behaviour characterizing desirable and undesirable outcomes. This underpins the discrimination of outcomes.

The predictions from the reachability analysis and indeed the reproductive ratio are congruent with clinical outcomes for all patients except pt_7 and pa_{24}. For patient pt_7 and pa_{24}, the reachability analysis suggests that HIV infection will be contained. This prediction fails for pa_{24} because, despite the fact that HIV load fell below $100(RNAcopies/ml)$ within 56 days following the initiation of treatment, a significant viral rebound i.e $y_2(175) = 670.03$ was measured at the final visit of the trial, see Fig. 6.8. Similarly, the data for pt_7 in [152]

shows a large viral rebound i.e $y_2(29) = 2.53$ to $y_2(149) = 5.41 log_{10}(RNA\ copies/ml)$ and the HIV viral load at the final clinic visit is $y_2(212) = 2.58 log_{10}(RNA\ copies/ml)$. These results may correspond to cases where model predictions fail due to the appearance of drug resistance or viral rebound [153]. The results are now explored in situations corresponding to effective treatment, marginal cases and cases where treatment fails.

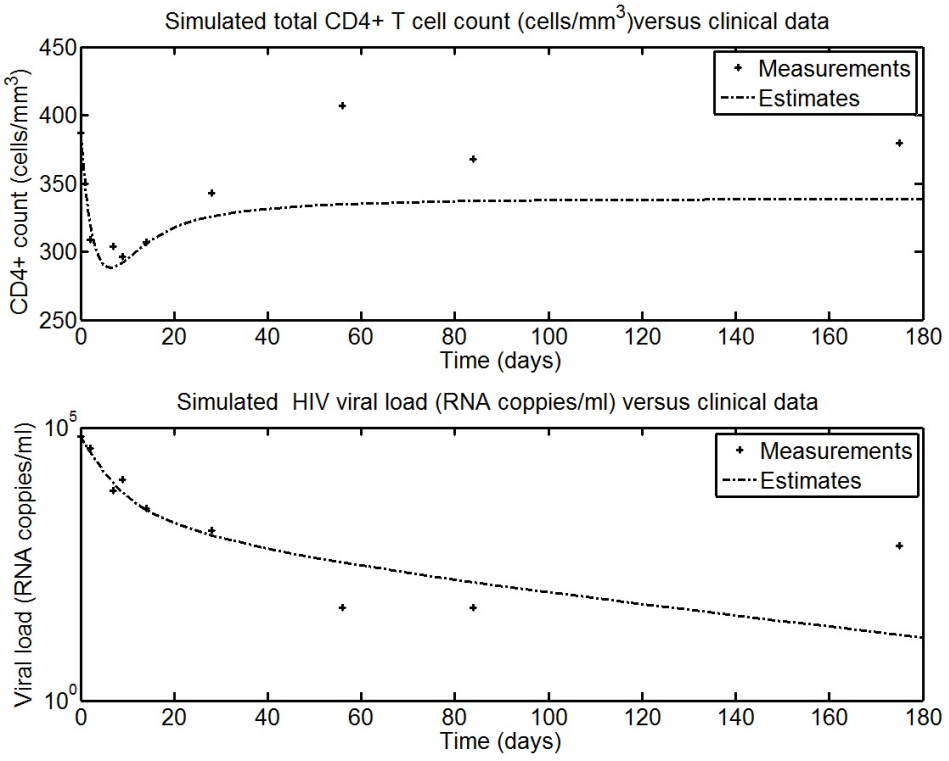

FIGURE 6.8: Comparison of the time evolution of measured CD4+ T cell count and HIV load versus its estimates for pa_{24} using the HIV model (6.7).

6.5.1 Effective treatment

The following results are associated with patients where antiretroviral drugs reduce and then maintain HIV load in the peripheral blood below the limit of $100(RNA\ copies/ml)$ i.e $2log_{10}(RNA\ copies/ml)$ within six months. These cases relate to patients pt_1, pt_2, pt_3, pt_4, pt_5, pt_6, pt_9, pt_{12}, pa_{13}, pa_{38}, and pa_{43}. For these patients, the reproductive ratio is below unity, see Table 6.2 and 6.3 and the existing methods successfully predict that antiretroviral treatment will be able to eradicate the infection. The time evolution of the reachability condition, see Fig. 6.9-6.10 for pt_1 and pa_{13} respectively, are representative of the dynamical behaviour of the reachability condition in the other patients in this category. Antiretroviral drugs in these patients are able to render and maintain the reachability condition negative

some 5 days after the initiation of treatment. As a result, the magnitude of the switching function (6.15) is driven to zero and the dynamics of the system (6.7) are forced to move and remain at the infection-free steady-state (6.8) such as in Fig. 6.2 for pt_1. Thus, the reachability analysis predicts that antiretroviral drugs are successful in eradicating the virus in these patients. Importantly, it should be noted that there is no oscillation in the magnitude of the reachability condition in the first weeks and the term βTV keeps on decreasing before and after the reachability condition is satisfied.

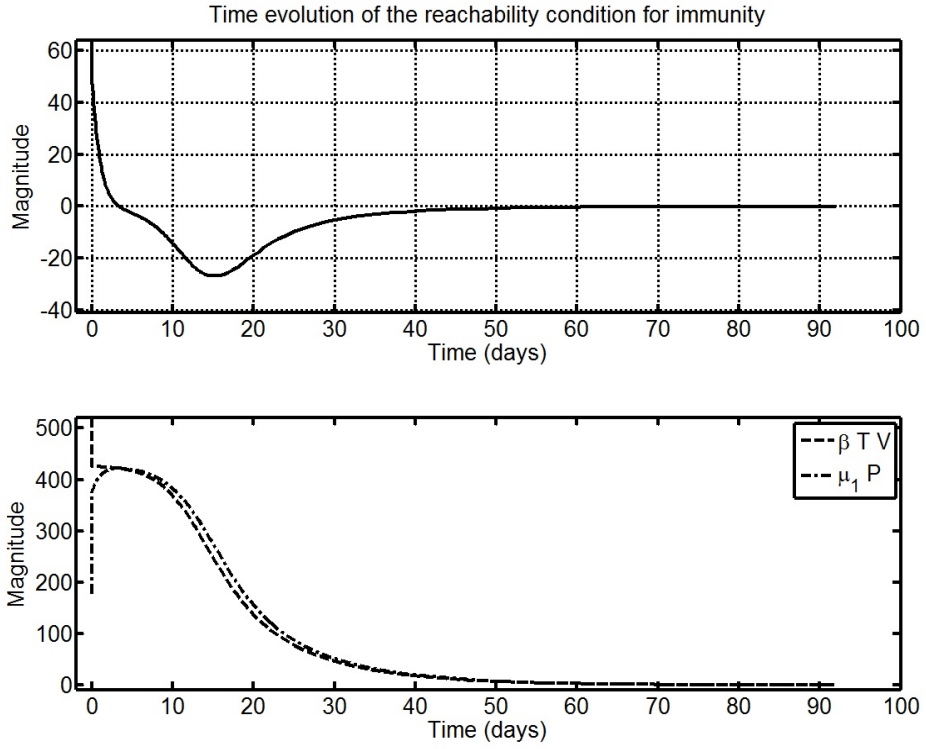

FIGURE 6.9: Time evolution of the dynamical condition for immunity (6.18) using simulation results for pt_1

6.5.2 New insight into marginal cases

Using the values of the biological rates estimated in [148, 152], patients pt_1, pt_2, pt_3, pt_4, pt_5, pt_6, pt_8, pt_9, pt_{11} and pt_{12} have a reproductive ratio below unity, see Table 6.1. The reachability analysis indicates that HIV dynamics engendered by these estimates reach and remain at the infection free steady-state for all these patients. Nevertheless, the multi-point estimation method used here combined with the reachability analysis reveals insight into marginal cases in which the HIV viral load is not completely eradicated by HAART and remains at an undetectable level in the steady-state. From a clinical point of view,

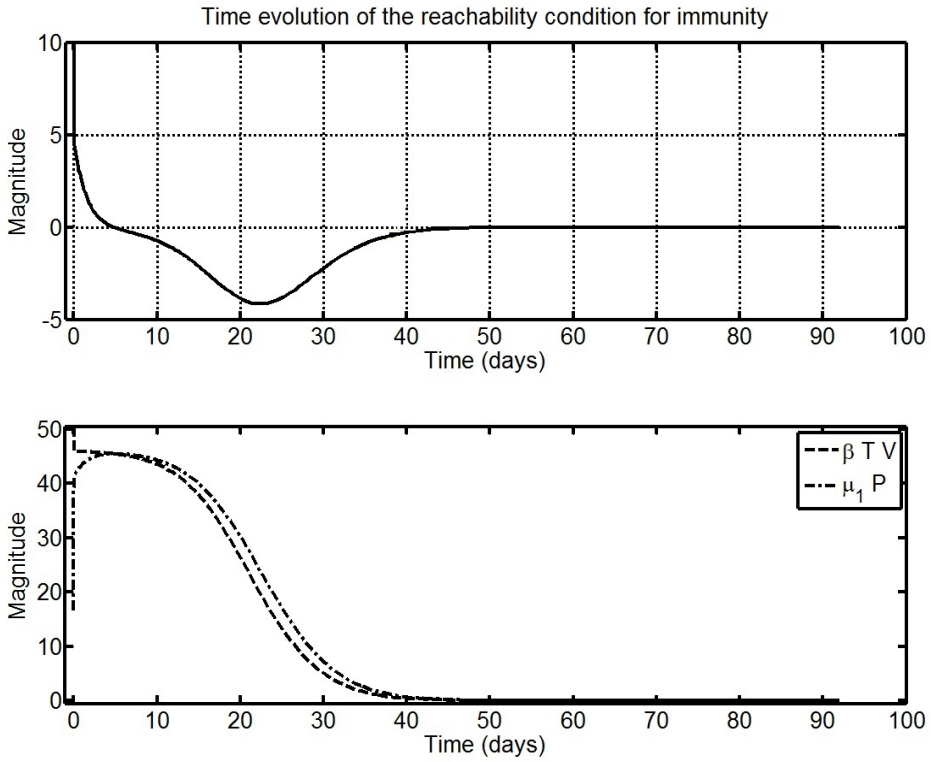

FIGURE 6.10: Time evolution of the dynamical condition for immunity (6.18) using simulation results for pa_{13}

treatment of patient pt_8 is efficient because the antiretroviral drugs reduce and maintain the HIV viral load below the limit of detection of $50 RNA\ copies/ml$ i.e $1.699 log_{10}(RNA\ copies/ml)$ within six months. Nevertheless, the value of the reproductive ratio is above unity in this case, see Table 6.2. Although antiretroviral drugs are classified as efficient, the value of the reproductive ratio infers that the infection may not be eradicated. The existing prediction methodology using R_0 appears to contradict the clinical outcome. In contrast, this prediction is not supported by the reachability analysis because though the time evolution of the reachability condition in Fig. 6.11 shows that antiretroviral drugs are able to maintain the reachability condition negative i.e $\beta TV - \mu_1 < 0$, the switching function $s_E(t)$ does not reach the manifold of interest. Nevertheless, it should be noted that $s_E(t)$ reaches a steady-state value which is close to the desired sliding manifold $s_E(t) = 0$. Similar results are obtained for patient pa_{34} where it is seen from Fig. 6.12 that the reachability analysis predicts the patient will have an asymptomatic status despite the fact that the detection limit of HIV load was $100 RNA\ copies/ml$.

Unlike the measured HIV load data of pt_8, measurements of HIV load for pt_{11} remain above the limit $2 log_{10}(RNA\ copies/ml)$. However, the last measurement $2.02 log_{10}(RNA\ copies/ml)$ is very close to this threshold, see data in [152]. Here again, although the $R_0 > 1$

for pt_{11}, clinicians found this patient asymptomatic because the HIV load is relatively low. The reachability analysis conducted using the biological rates estimated here indicates that $s_E(t)$ for pt_{11} attains a steady-state value close to the desired sliding manifold $s_E(t) = 0$, see Fig. 6.13. Further, the estimated steady-state of the HIV viral load is located in a region where i.e $V_{s1} < 2log_{10}(RNA\ copies/ml)$. Further insight can be gained from

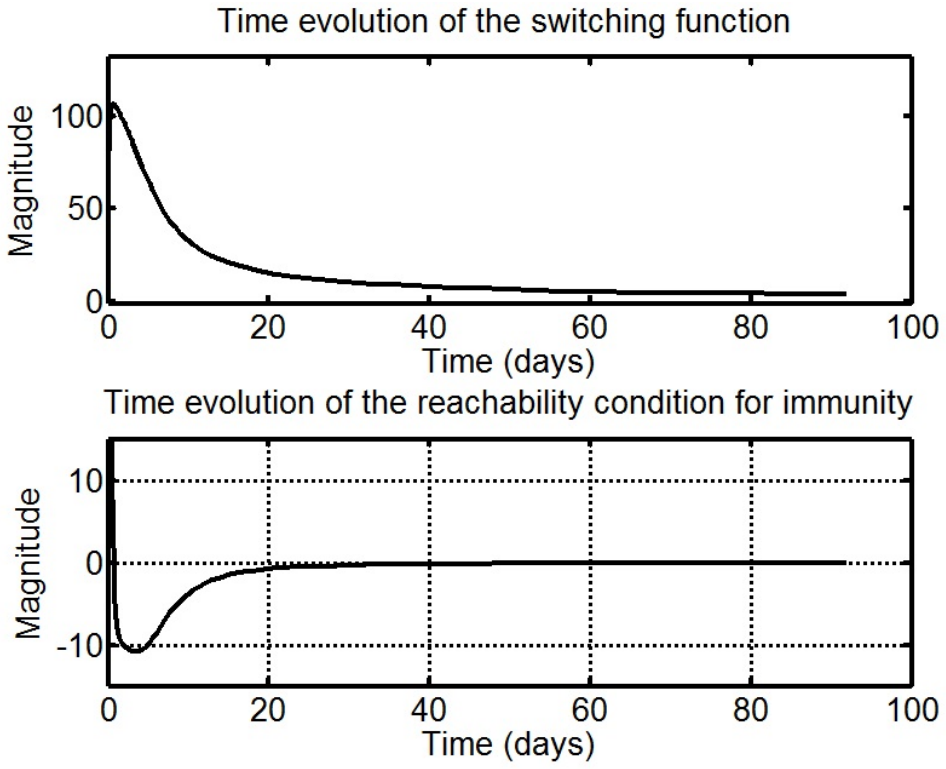

FIGURE 6.11: Time evolution of the switching function (6.15) and dynamical condition for immunity (6.18) for pt_8

the phase portrait of the sliding surface. Fig. 6.14-6.15 reveal that the trajectories move towards an equilibrium point close to the origin. This suggests that the infection dynamics move and remain at a clinically desirable steady-state located close to the infection free steady-state for both pt_8 and pt_{11}. It can be thus deduced that the limit of detection of the HIV viral load in the peripheral blood can be associated with a boundary layer in which the steady-state of HIV viral load is desirable.

In the field of control systems, the concept of boundary layer control is well established [10, 15, 21, 22] and it is acceptable to have a control action which forces the sliding surface to remain within a region close to zero. It is well known that the assumed dynamics of the switching behaviour in the control strategy directly impact on the characteristics of the boundary layer. In Chapter 2, it has been demonstrated that a smooth switch control law

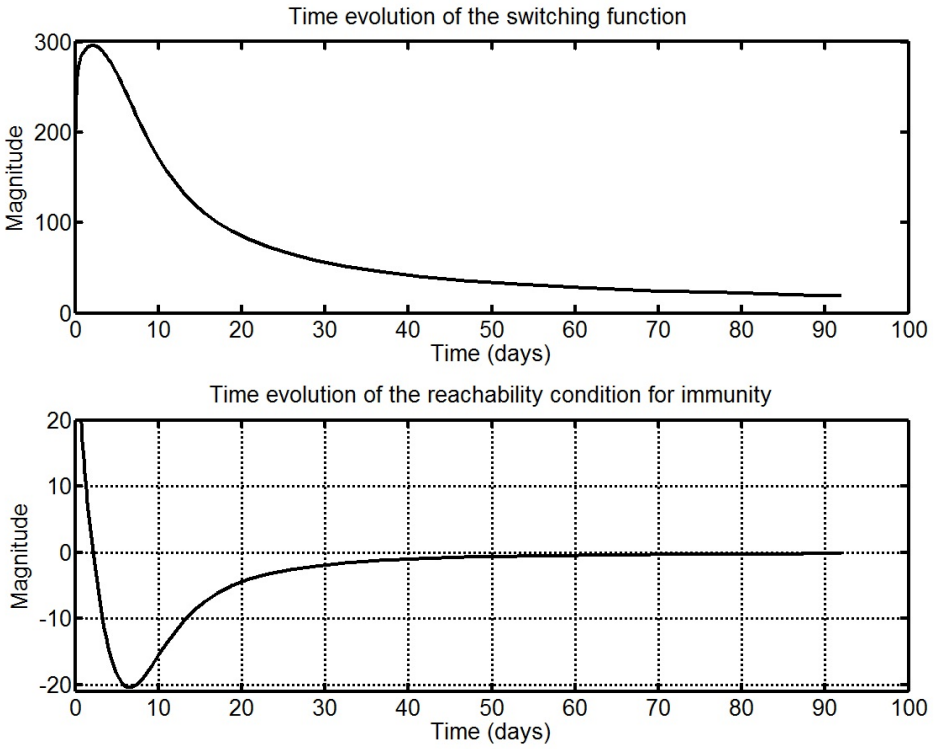

FIGURE 6.12: Time evolution of the switching function (6.15) and dynamical condition for immunity (6.18) for pa_{34}

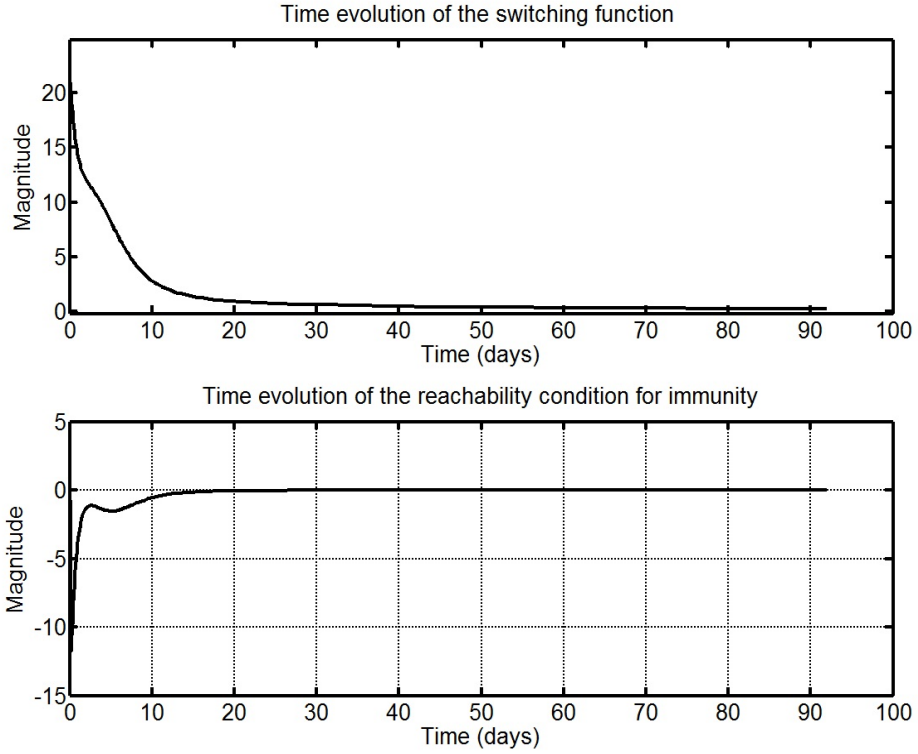

FIGURE 6.13: Time evolution of the switching function (6.15) and dynamical condition for immunity (6.18) for pt_{11}

can be used to generate a boundary layer control action which achieves desirable performance despite the fact that ideal sliding motion is not exhibited. Further, the investigations on the HIV-specific CD8+ T cell response in Chapter 5, have shown that although a potent killing efficacy is not able to enforce ideal sliding motion, an asymptomatic steady-state can be exhibited. Consequently, the concept of boundary layer control explains the difference between the clinical observation and the outcome inferred from the reproductive ratio for these patients. The origin is not attained but the outcome is sufficiently close to the desired outcome and within the limits of accuracy of the measurement approach to be clinically satisfactory.

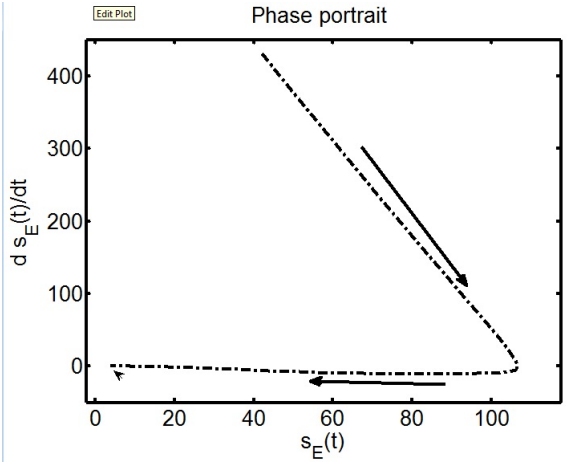

FIGURE 6.14: Phase portrait of the sliding surface (6.15) for pt_8

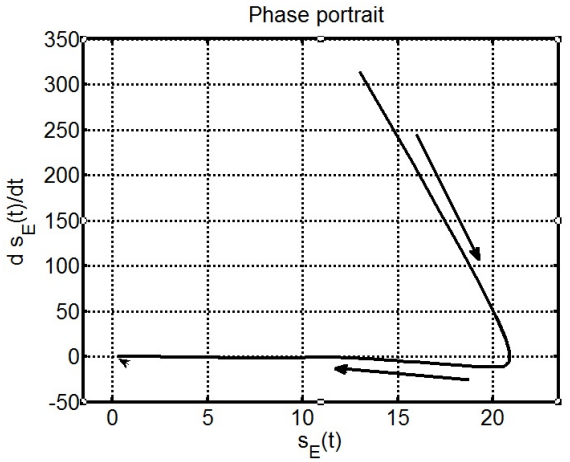

FIGURE 6.15: Phase portrait of the sliding surface (6.15) for pt_{11}

6.5.3 Failure cases

The following results relate to patients pa_3, pa_8 and pa_{10} for whom antiretroviral drugs are unable to reduce and maintain the HIV viral load below $100 RNA\ copies/ml$ i.e $2log_{10}(RNA\ copies/ml)$ within six months. In all cases of failure of antiretroviral treatment, the estimated biological rates predict a steady-state viral load V_{s1}, see (6.13), which exceeds that limit significantly. Furthermore, the reproductive ratio (6.12) is above unity in all failure cases, see table 6.3. Therefore, the value of the reproductive ratio suggests that antiretroviral drugs are not able to render the infection-free steady-state (6.8) attractive and to eradicate the virus. To investigate the performance of antiretroviral drugs in these patients, the reachability analysis is performed. From Fig. 6.16, it can be deduced that the effects of antiretroviral drugs for pa_3 are not sufficient to zero the switching function (6.15). In fact, $s_E(t)$ does not vanish because the magnitude of the reachability condition (6.18) becomes negative for only a very short period of time and then becomes positive. Importantly, this dynamical behaviour of the reachability condition in Fig. 6.17 for pa_3 is the same in all cases where antiretroviral drugs are inefficient, see Fig. 6.18. The oscillatory

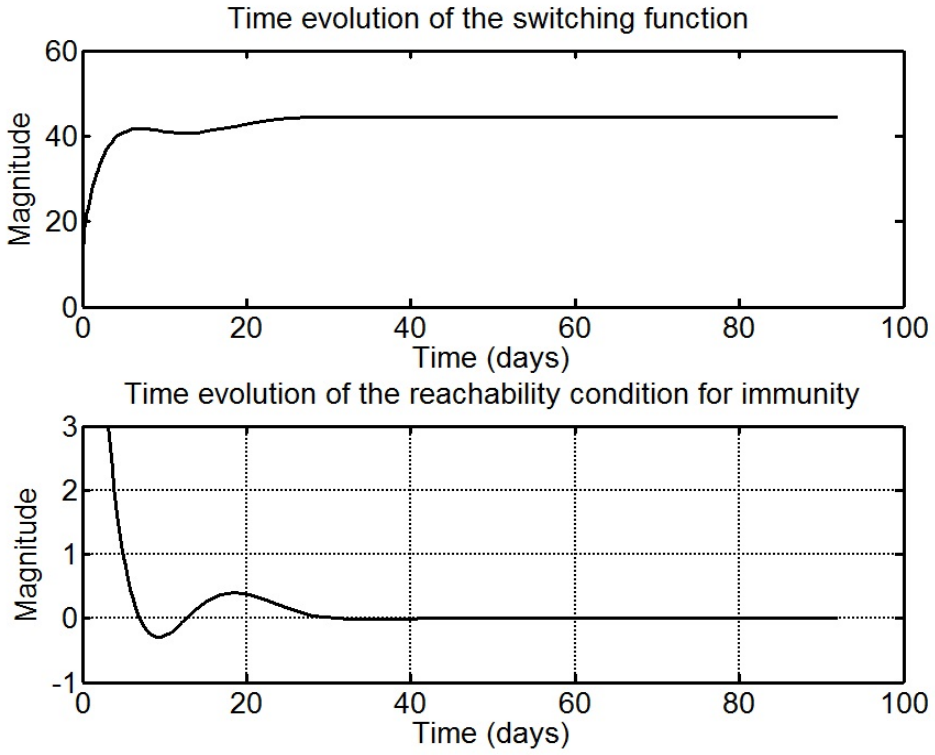

FIGURE 6.16: Time evolution of the switching function (6.15) along with the dynamical condition for immunity (6.18) for pa_3

behaviour observed in the reachability condition reflects the fact that antiretroviral drugs in

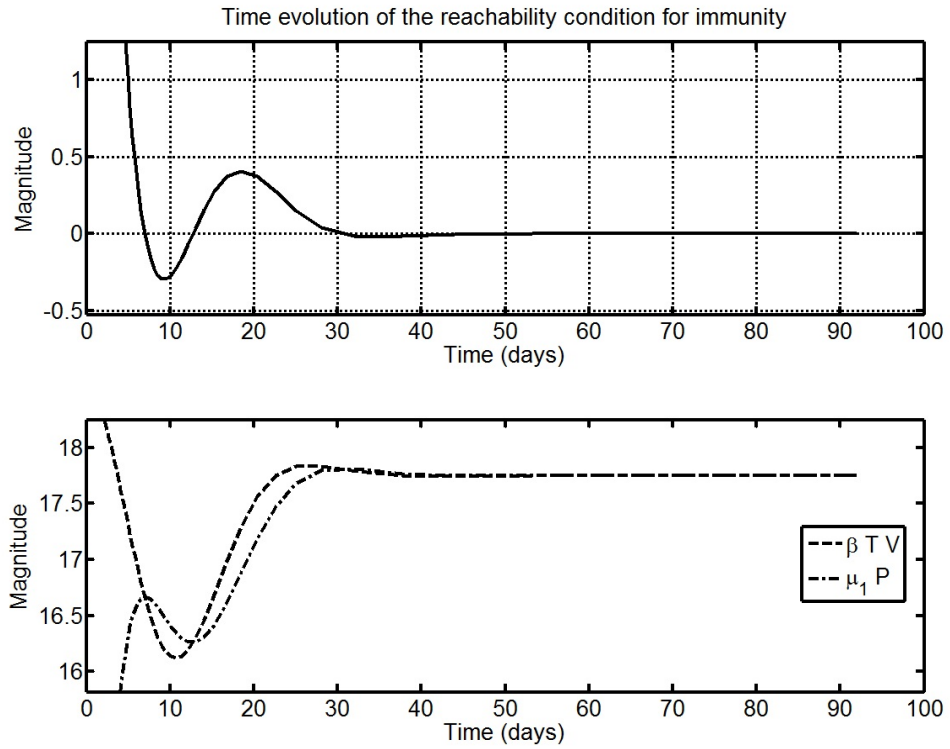

FIGURE 6.17: Time evolution of the dynamical condition for immunity (6.18) using simulation results for pa_3

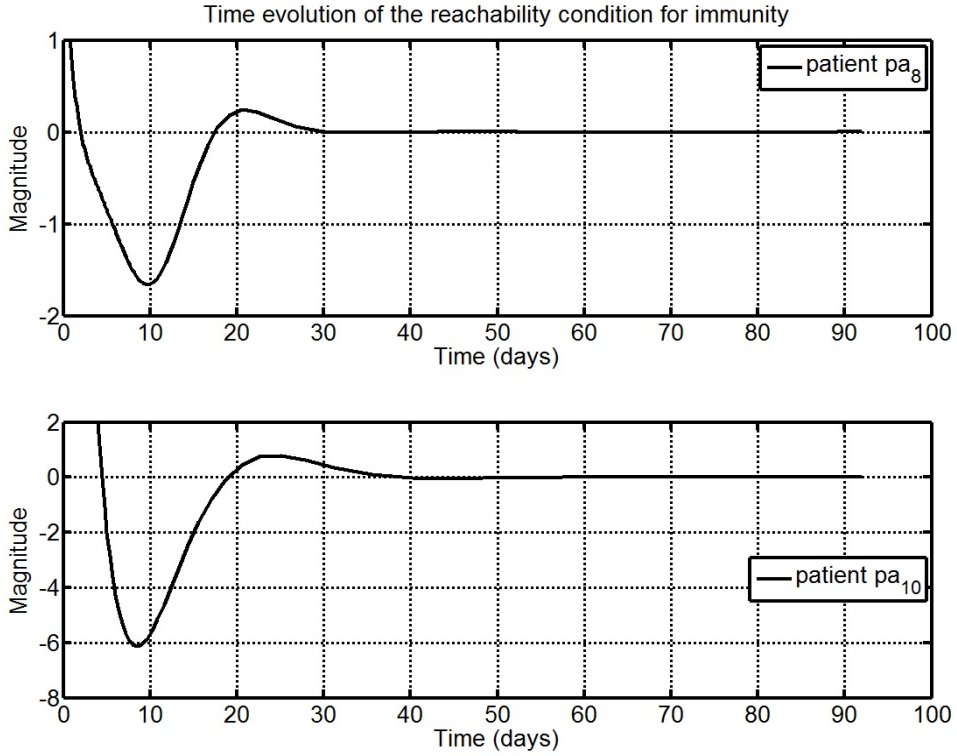

FIGURE 6.18: Time evolution of the dynamical condition for immunity (6.18) using simulation results for pa_8 and pa_{10}

these patients are not able to maintain the reachability condition at the required negative level following the initiation of treatment. Fig. 6.17 shows that the effects of antiretroviral drugs cannot satisfy $\beta TV < \mu_1 P$ for a prolonged period following the initiation of treatment. As a result, the time evolution of the reachability condition predicts that the antiretroviral drugs in these patients are unable to enforce the infection-free steady-state i.e to eradicate the virus. Moreover, the phase portrait of the sliding surface, see Fig. 6.19, for these failure cases demonstrates that the HIV infection dynamics do not reach the infection free steady-state located at the origin but attain a chronic HIV infection steady-state. For instance, the phase portrait of pa_3 shows dynamics moving away from the origin to reach a chronic infection steady-state whilst the dynamics of pa_{10} move towards the origin but stop at a chronic infection steady-state. Importantly, the comparative analysis of the phase portrait of the sliding surface for different patients reinforces the fact that the transient dynamics induced by the antiretroviral treatment are diverse in failure cases. This motivates the design of personalized antiretroviral treatment regimes to improve efficacy and demonstrates that the reachability analysis presented in this chapter may be helpful in developing appropriate treatments.

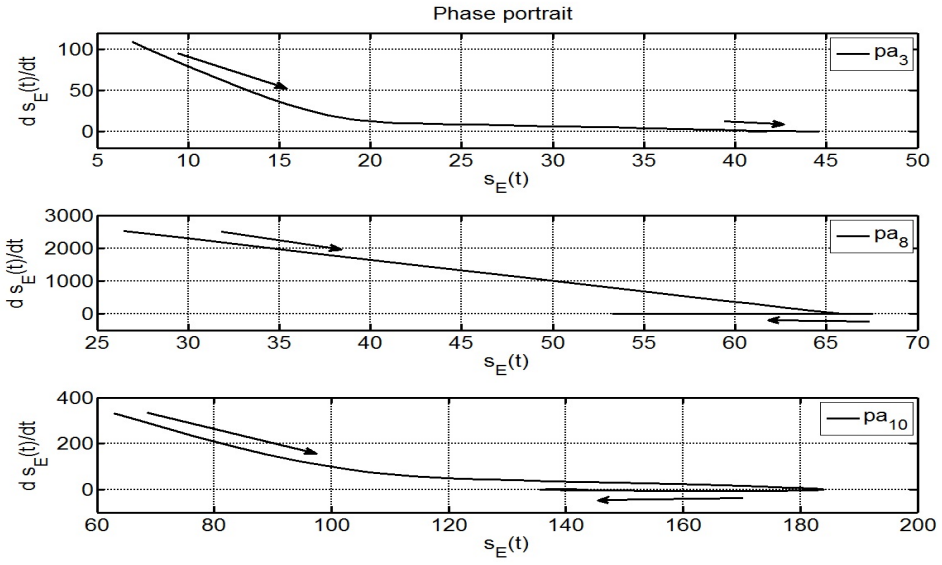

FIGURE 6.19: Phase portrait of the sliding surface (6.15) for pa_3, pa_8 and pa_{10}

6.6 Conclusion

In this chapter, the dynamics of HIV infection following initiation of antiretroviral therapy has been considered as a case study to demonstrate that the framework of the VSC paradigm

finds applications in immunology. Here, tools from sliding mode control paradigm have been utilized to assess the performance of antiretroviral drugs for HIV infection. From the results in Chapter 5, HIV infection dynamics can be regarded as a closed-loop system with the HIV-specific immune response as an inherent VSC feedback.

Motivated by these findings, the effects of antiretroviral drugs have been treated as an outer-loop control input to contain the infection in vivo. The basic model of HIV infection dynamics from [30, 60] has been chosen for this case study because its parameters have been estimated using measurement of CD4 T cell count and HIV load collected during clinical trials. Following the approach developed in Chapter 5, a manifold associated with the infection-free steady-state has been identified. The reachability analysis introduced in Chapter 2, has been used to formulate a dynamical condition for antiretroviral drugs to render this manifold attractive in order to enforce the containment of the infection in vivo. Using two HIV clinical data sets, predictions of the outcome of treatment for a set of patients have been made using the established reproductive ratio and the proposed dynamical condition. The results show that the reachability paradigm is superior to the reproductive ratio because the reachability condition highlights specific dynamical characteristics corresponding to healthy, unhealthy and marginal outcomes.

Hence, the case study conducted in this chapter demonstrates that the framework of VSC delivers additional insights on immunological dynamics. Consequently, this chapter motivates the use of the VSC paradigm to study the dynamics of the immune system in health and disease. The main conclusions and future work are articulated in the next chapter.

Chapter 7

Conclusions and Future work

7.1 Conclusions

In this thesis, the dynamics of the immune system have been analysed using the variable structure control paradigm. The novelty of the approach resides in the fact that the dynamics of the immune system in health and disease are examined as a closed-loop system in which the dynamic response of T cells operates as a control. Collectively, the findings provide clear evidence to support the argument that the dynamic response of T cells operates as a variable structure control to achieve immunity and self-tolerance. This means that the immune system switches between different feedback regimes to establish and maintain a robust, healthy state. Importantly, this thesis contributes to knowledge in mathematical immunology because it demonstrates that the framework of VSC is adequate to deliver insights on the robustness of immunological dynamics. It has been proven that the reachability paradigm from sliding mode control is a novel and efficient means to assess the performance of the specific T cell response and candidate therapies.

The specific contribution is summarized as follows:

- Synergies between the dynamics of VSCS and the population dynamics of the antigen-specific T cell response are demonstrated using a phase portrait analysis. This analysis indicates that the immune response program which describes the dynamic response of T cells following infection is, in essence, a variable structure control strategy to prescribe the required changes in T cells population size to achieve the clearance of the pathogen and the maintenance of a healthy state. From a VSC point of view,

the dynamical behaviour of the population of the specific CD8+ T cell response observed after acute or chronic infection is an output of a sophisticated switch between immunological feedback which promotes or inhibits the immune response. This switching mechanism seems to be based on the dynamical effects of the interaction of different molecular and cellular activities following antigen stimulation. Thus, the immune response program is a switched control feedback strategy which highlights the changes in the feedback regimes underpinning the specific T cell response.

- A reachability analysis has been conducted using a manifold associated with a healthy steady-state to highlight switching conditions to enforce robust expansion and contraction dynamics. This has been shown to be useful to assess the impact of uncertainty and perturbations on the T cell response dynamics. These conditions have been used to explain the robustness of the T cell response dynamics during acute infection, as well as why the T cell response dynamics are impaired during chronic infection. The analysis of the specific immune response of T cells using a VSC approach opens a new framework to evaluate immunological dynamics, and might assist the design of treatment regimes to yield robust immune response dynamics.

- Candidate immune response functions have been analysed as candidate immunological feedback regime for self-tolerance. A threshold immune response function based on the concentration of self-antigen has been constructed to model a threshold based activation/proliferation of self-reacting effector T cells. Besides, an adaptive sliding mode control has been designed to model the suppression of self-reacting T cells by the immune system. The control analysis conducted shows that the nature and shape of candidate immune response function determines the dynamic response of the immune system and the stability of the tolerance steady-state. Additionally, a reachability analysis was conducted using a manifold associated with the tolerance steady-state. This reachability analysis shows how the dynamic response of the immune system can enforce a robust state of tolerance.

- The reachability paradigm has been utilized to analyse the control attributes of the cytolytic killing mechanism of HIV-specific CD8+ T cell response on the containment of HIV infection dynamics in vivo. Using a manifold associated with the infection-free steady-state, the reachability analysis delivers a dynamical condition for immunity which is used to monitor the control performance of the HIV-specific CD8+ T cell response during the course of the infection. The results indicate that the cytolytic

killing mechanism modelled with a double saturation function operates a continuous variable structure control law which yields a boundary layer control of the infection dynamics in vivo. The dynamical condition for immunity also supports the emerging notion that the immunological requirements for the containment of HIV infection changes during the course of the infection.

- The VSC approach has been demonstrated to be a novel means for the evaluation of the impact of antiretroviral therapy on HIV infection dynamics in vivo. A VSC approach has been used to deliver a dynamical condition for the containment of HIV infection in vivo by antiretroviral therapy. The basic model of HIV infection dynamics from [59] has been selected and clinical data from HIV-infected patients has been used to parameterize this model. Unlike the condition from the reproductive ratio, the reachability condition delivers a time varying condition for the infection dynamics to reach and remain at the HIV infection-free steady-state. The findings show that methodology captures the dynamical characteristics of eventual successful, failed and marginal outcomes. Hence, the reachability paradigm from VSC theory is a suitable framework to monitor and predict the progression of the Human Immunodeficiency Virus (HIV) infection after initiation of antiretroviral therapy.

Together, the findings of the different chapters demonstrate that variable structure control theory finds application in modelling and simulation in immunology. Importantly, the approach developed in the thesis makes use of the reachability paradigm to deliver sensible insights on the robustness of immunological dynamics. This doctoral research encourages the use of techniques from variable structure control theory to investigate the dynamics of biological systems with uncertainty.

The work on this thesis was limited by several factors. The approach relies on the fact that a sensible mathematical model of the given phenomenon is available for analysis. Furthermore, the availability of clinical data and reliable parameter estimates affect the scope of the mathematical analysis. Thus, it is recommended to have a good understanding of the biology represented by the mathematical model. A close collaboration between experimental and mathematical studies is highly desirable.

7.2 Future work

The findings of this thesis motivate the use of the variable structure control paradigm to improve understanding of the dynamics of the immune system as well as to design efficient therapeutic strategies.

Future work suggestions from headline finds are as follows:

- In [2, 74, 94], it was shown that the expansion, contraction and memory phase of the specific CD8+ T cell response exhibits different magnitude and kinetics following re-infection with the same antigen. In this thesis, the dynamics of the antigen-specific CD8+ T cell response to acute infection has been considered to show that the immune response program is, in essence, a VSC law governing the population dynamics of the response. Motivated by the work of this thesis, it will be interesting to use these experimental data to construct a mathematical model and to apply a VSC approach to investigate what are the advantages and disadvantages related to changes in the kinetics of CD8+ T cell expansion, contraction and memory following re-infections with respect to the establishment of protective immunity. Since the immune response program is treated as an inherent VSC control, the basic idea is to understand the impact of consecutive infection on the parameters, switching behaviour and performance of this immunological control mechanism. The findings from this research yield the potential to inform the design and scheduling of vaccines to achieve better outcomes.

- The variable structure control paradigm supports results on the design of successful vaccines for chronic infections. To confirm this point, consider the experimental studies in [2] in which the dynamic response of memory CD8+ T cells specific to LCMV is impaired following infection with a high viral load. The experiments in [2] have revealed that activated LCMV-specific memory CD8+ T cells experience a block in sustaining cell proliferation during this chronic infection. Further, it was found that an immunological mechanism defined as CD4+ T cell help is a candidate means of therapeutic intervention. Interestingly, in this context, using an appropriate model of the specific CD8+ T cell response along with the variable structure control paradigm, a reachability condition can be formulated to define a dynamical condition required to maintain the expansion of activated LCMV-specific memory CD8+ T cells following chronic infection. Moreover, this reachability condition together with the

expression for the equivalent control can be used to quantify the level of CD4+ T cell help required to sustain the proliferation dynamic of memory CD8+ T cells in order to enforce immunity.

- Immunological failure is characterized by a level of CD4+ T cells below 200/mm^3 during six months of efficient antiretroviral treatment. The biological mechanisms inducing immunological failure are not fully understood. Different mathematical functions supporting different biological assumptions have been investigated in the literature [152, 155, 160]. Using measurements of the total number of CD4+ T cells and HIV viral load collected from patients in the first month initiation of an efficient antiretroviral therapy, the authors in [152, 155, 160] have identified candidate time invariant parameters to predict immunological failure. To build on this work, it is assumed that immunological failure is caused by an unknown input i.e unknown biological dynamics affecting the population dynamics of CD4+ T cells. Using standard HIV clinical data along with the basic model of HIV dynamics in [152], a sliding mode observer can be constructed. The idea is to use the equivalent control to reconstruct the dynamic associated with immunological failure. The objective is to elucidate the characteristics of immunological failure. The findings could be combined with the results from this thesis to improve early diagnosis and monitoring of antiretroviral therapy.

- In [58, 75], it has been pointed that the non-cytolytic mechanism of the HIV-specific CD8+ T cell response is also an adequate means to contain HIV infection in vivo. Of note, the parameter representing the non-cytolytic mechanism is present in the expression of the dynamical condition for immunity and represents a candidate control action to satisfy the dynamical condition for immunity and contain the infection in vivo. Using the approach developed in this thesis and the data from [75], it could be possible to assess the time evolution of the dynamical condition for immunity for different killing mechanism of the HIV-specific CD8+ T cell response. The impact of the non-cytolytic and the cytolytic mechanism as two inherent control feedback of the HIV-specific CD8+ T cell response can be analysed using the framework of sliding mode control. The dynamic advantages of each mechanism alone and the complementarity of these mechanisms will be investigated to elucidate ways in which CD8+ T cells contain HIV infection in vivo. The findings could be useful to inform robust control mechanisms in the domain of engineering.

- The paper [36] has investigated the control of HIV infection mainly using bifurcation techniques. It was shown that the cytolytic killing rate of the HIV-specific CD8+ T cell response and the size of the latent cell reservoir influence the progression of the infection after cessation of antiretroviral therapy. This thesis has demonstrated that the HIV-specific CD8+ T cell response and the effects of antiretroviral drugs in vivo can be analysed as control inputs which aim to enforce a stable and asymptomatic steady-state. Motivated by the findings of this thesis, it will be interesting to write the analytical expression of a manifold associated with the post-treatment control of HIV infection. The objective is to use this manifold to conduct a reachability analysis. In essence, this will yield a dynamical condition for the killing efficacy of HIV-specific CD8+ T cells and antiretroviral drugs to control HIV infection in vivo. It is of great importance to understand how early uptake of antiretroviral drugs can help the HIV-specific CD8+ T cell response to establish an asymptomatic state and maintain this state even after the interruption of antiretroviral therapy [30, 36]. Hence, the VSC approach used in this thesis has great potential to improve understanding of functional cure of HIV.

Appendix A

Pseudo-code of the Multi-Point Identification Method

Pseudo-code

-Get experimental data -Get time data sp3=[0 4 8 9 11 14 17 30 47 60 91];

-Get Cd4+ count Tvl= [122 133 177 172 208 174 231 201 251 262 276];

get virus load Vvl=[5.38 4.57 3.93 3.76 3.64 3.31 3.12 2.78 2.74 2.42 1.6]; -Convert virus log from the log scale to the decimal scale

$Vlg = 10.^(Vvl)$;

- get initial condition x01=[80;42;Vlg(1)];

- safe copy of measurements Tvla=Tvl; Vlga=Vlg;

- Apply a scaling factor

mxV=max(Vlg(1:6));

mxT=max(Tvl(1:6));

- Get data points of the first 21 days Vlg=Vlg(1:6)./mxV;

Tvl=Tvl(1:6)./mxT;

– copy time points sp=sp3; - t=[0:0.00001:21]; - Get multiple data points

Vm=interp1(sp(1:6),Vlg(1:6),t,'pchip','extrap'); -

Tm=interp1(sp(1:6),Tvl(1:6),t,'pchip','extrap');

-Compute polynomial polynomial -get some value for py (order of the polynomial) n2=0;

polypatienty2=polyfit(t,Vm,py);- - grid - -

-differentiate the polynomials

dp2=polyder(polypatienty2); d2p2=polyder(dp2); d3p2=polyder(d2p2);

-

-choose a set of 5 distinct time points within 0 21 - lpb lower bound, upb uppper bound

spd=linspace(lpb,upb,5); -

- get the values to compute the identification system

y2patientest=[polyval(polypatienty2,spd)]'; y2dotdata=[polyval(dp2,spd)]'; y2dbdotdata=[polyval(d
y2tdotdata=[polyval(d3p2,spd)]';

- compute identification equation

syms B R V M E real ;

$fom = ((y2patientest.^(-1)).*y2dotdata - R - B.*y2patientest).*(y2dbdotdata + M.*y2dotdata + V.*y2patientest) + E.*y2patientest - V.*y2dotdata - M.*y2dbdotdata;$

-solve identification matrix for virus load

rest3=vpasolve(eqest2);

Check for unique solution rb=rest3.B; if (length((rb)) ==1) - - Check the sign of biological rates

$if((rest3.B(1)) > 0 AND AND (rest3.R(1)) > 0 AND AND (rest3.E(1)) > 0 AND AND (rest3.V(1))$
$0 AND AND (rest3.M(1)) > 0$)

pdest=(rest3.R(1));

$mu1t = -(0.*(-rest3.V(1) - ((rest3.V(1).^2) + 4.*rest3.M(1)).^(0.5)));$

-Computation of estimates from virus load and CD4+ measurements

- Get polynomial -px polynomial order polypatienty1=polyfit(t,Tm,+px); polypatienty2=polyfit(t,Vm

-differentiate the polynomials

dp1=polyder(polypatienty1); dp2=polyder(polypatienty2); d2p2=polyd

- get time points

spds=linspace(lpbs,upbs,4); - - Get vakues

y1patientest=[polyval(polypatienty1,spds)]'; y1dotdata=[polyval(dp1,spds)]';

y2patientest=[polyval(polypatienty2,spds)]'; y2dotdata=[polyval(dp2,spds)]';

- Compute identification equation [m,n]=size(sp3(1:4)); omega=[ones(n,1) y1patientest y2dotdata y2patientest];

- rom1=rank(omega) syms TH1 TH2 TH3 TH4 om =[TH1; TH2 ;TH3 ;TH4];

eqest=omega*om;

dom1=[diff(eqest(1),TH1) diff(eqest(1),TH2) diff(eqest(1),TH3) diff(eqest(1),TH4);diff(eqest(2),TH1) diff(eqest(2),TH2) diff(eqest(2),TH3) diff(eqest(2),TH4);diff(eqest(3),TH1) diff(eqest(3),TH2) diff(eqest(3),TH3) diff(eqest(3),TH4);diff(eqest(4),TH1) diff(eqest(4),TH2) diff(eqest(4),TH3) diff(eqest(4),TH4)];

detom1=det(dom1);

if (detom1 = 0)

eqests=y1dotdata -omega*om;

- Solve identification equation (25) rest=vpasolve(eqests);

Check for unpique solution if (length((rest.TH1)) ==1)

if (rest.TH1(1) ¿0)

- Get estimates

pses=double(rest.TH1);

pdes=(-rest.TH2);

pmu2es=(rest.TH4/rest.TH3);

Besg=(rest3.B(1)); pdesg=(rest3.R(1));

$mu1 = -(0.*(-rest3.V(1) - ((rest3.V(1).^2) + 4.*rest3.M(1)).^(0.5)))$; $mu2g = (0.*(-rest3.V(1) + ((rest3.V(1).^2) + 4.*rest3.M(1)).^(0.5)))$;

pdesa=(pdes+pdesg)/2;

K= ((rest3.E)./(rest3.B.*pses));

mu2=(mu2g+pmu2es)/2;

- -get virus steady-state level

ssVn= (pses*K)/(mu1*pmu2es) - (pdes/Besg);

-Filter for realistic parameter values

- check the sign of the biological rates

$if(rest.TH1(1) > 0ANDANDrest.TH2(1) < 0ANDANDrest.TH3(1) < 0ANDANDrest.TH4(1)$ 0)

if (mu1t ¿ pdes)

if (ssVn ¡= (100/mxV)) - -

if (mxT*(pses/pdes) ¿=200)

if (mu1t¡=3.5) if (pmu2es¡=6) if (pdes¡2)

- pses=double(pses);

pdesg=double(pdesg);

mu2g=double(mu2g); Besg=double(Besg); K=double(K); mu1=double(mu1); pmu2es=double(pmu2
pdes=double(pdes);

- Validation check of the output dynamics

- estimation time window tspana=[0 21];

- solve the model with the estimates

odehiv=@(t,x)hivode3(t,x,pses*mxT,pdes,pmu2es, Besg/mxV,K*mxV/mxT,mu1);

[t5,x7]=ode23s(odehiv,tspana,x01);

-Check for positivity of the state variables

-Check for fitness with experimental data

y1sim=x7(:,1)+x7(:,2); y2sim=x7(:,3);

dpl=sum(sum(sp3¡=max(tspana)));

y1s=zeros(1,dpl)

for idp=2:dpl y1s(idp)=y1sim(sum(t5¡=sp3(idp))); end y1s(1)=y1sim(1);

y2s=zeros(1,dpl)

for idp=2:dpl y2s(idp)=y2sim(sum(t5¡=sp3(idp))); end y2s(1)=y2sim(1);

-Compute the error ey1= mxT.*[Tvla(1:dpl)-y1s]';

ey2= mxV.*[Vlga(1:dpl)-y2s]';

Check the fit

$dey1h = 100 * (sum(ey1.^2)/sum((mxT. * Tvla(1 : dpl)').^2))$

$dey2h = 100 * (sum(ey2.^2)/sum((mxV. * Vlga(1 : dpl)').^2))$

-Filter for better fitting

if (((dey2h+dey1h)¡= (dey2i + dey1i)))

dey2i=dey2h

dey1i=dey1h - - Save the results

-save settings spd=spd

spds=spds

px1=px

px2=px py=py

q=q

ddetom1=(detom1)

mxTi=mxT mxVi=mxV

dey1h=dey1h

dey2h=dey2h

ser=dey2h+dey1h

- Save estimates

pses=(rest.TH1)

pdes=(-rest.TH2)

Besg=(rest3.B(1))

$mu1 = -double(0.* (-rest3.V(1) - ((rest3.V(1).^2) + 4.* rest3.M(1)).^(0.5)))$

K= ((rest3.E)./(rest3.B.*pses))

pmu2es=(rest.TH4/rest.TH3)

psesm=(rest.TH1)*mxT Besgm=(rest3.B(1))/mxV Km=K*mxV/mxT

$Reproductive_ration = double((pses * Besg * K)/(pdes * mu1 * pmu2es))$

- - ssVn=ssVn

ssVm= (pses*mxT*K*mxV/mxT)/(mu1*pmu2es) - (pdes/(Besg/mxV)); ssVm=double(ssVm)

ET=mxT*(pses/pdes)

-End ifs -End loops

-End

Appendix B

Estimates of HIV Dynamics Parameters following Antiretroviral Therapy

Pseudo code of the multi-point method

Parameter estimation results

The following are the results of the parameter estimation procedure described in Chapter 5. The computational process has produced these estimates with a high precision. It is shown in the next section that such high precision is not compulsory and biologically relevant.

Patient pt_1

$\lambda = 427.1534026447107000$ $\delta_T = 0.9876391196788116$ $\beta = 0.0004093987658605$ $\mu_1 = 1.0026999999999999$ $k = 1.6594605365105060$ $\mu_2 = 0.3979593353698864$

Patient pt_2

$\lambda = 525.6326523532495700$ $\delta_T = 1.1393025728584869$ $\beta = 0.0000114292728371$ $\mu_1 = 3.0764000000000000$ $k = 530.5060041665457200$ $\mu_2 = 0.9490449503506817$

Patient pt_3

$\lambda = 137.9741119638239900$ $\delta_T = 0.7038155848335397$ $\beta = 0.0002826190338890$ $\mu_1 = 0.9031000000000000$ $k = 7.5114253152300359$ $\mu_2 = 0.4962904358494573$

Patient pt_4

$\lambda = 61.1615973565333850$ $\delta_T = 0.2155640611980289$ $\beta = 0.0000844969285702$ $\mu_1 = 0.37460000000000$ $k = 5.2335290818264886$ $\mu_2 = 0.4525321093719749$

Patient pt_5

$\lambda = 511.2167264389443600$ $\delta_T = 1.1618006804012180$ $\beta = 0.0013574984809959$ $\mu_1 = 1.2355000000000000$ $k = 0.1063031494385558$ $\mu_2 = 0.4802282398429222$

Patient pt_6 $\lambda = 447.2664063299146200$ $\delta_T = 0.8700912309267833$ $\beta = 0.0003833533433395$ $\mu_1 = 1.0826000000000000$ $k = 0.9867397078338738$ $\mu_2 = 0.2044200509728017$

Patient pt_7 $\lambda = 48.5473106245905160$ $\delta_T = 0.8822498032971305$ $\beta = 0.0001059037437115$ $\mu_1 = 1.0950000000000000$ $k = 237.4106883197578400$ $\mu_2 = 1.9837037442920844$

Patient pt_8 $\lambda = 32.0253577139126050$ $\delta_T = 0.1226941299773771$ $\beta = 0.0000224738651096$ $\mu_1 = 0.6715000000000000$ $k = 163.5680183774189200$ $\mu_2 = 1.4160782657508266$

Patient pt_9 $\lambda = 255.4070488046519600$ $\delta_T = 0.8378135735937042$ $\beta = 0.0002456884900764$ $\mu_1 = 1.4867999999999999$ $k = 4.6674823943125769$ $\mu_2 = 0.5083553798664283$

Patient pt_11 $\lambda = 20.2317632084434820$ $\delta_T = 0.2487626750256210$ $\beta = 0.0000211458811785$ $\mu_1 = 1.5947000000000000$ $k = 717.2060327118180100$ $\mu_2 = 0.7670342435229737$

Patient pt_12 $\lambda = 216.1561150733994300$ $\delta_T = 0.4764870265142694$ $\beta = 0.0005537155404234$ $\mu_1 = 0.5379000000000000$ $k = 0.5742665980752227$ $\mu_2 = 0.8759987609017709$

Patient pa_3 $\lambda = 19.4408623647801560$ $\delta_T = 0.0568538325062474$ $\beta = 0.0001830425581339$ $\mu_1 = 0.3996000000000000$ $k = 24.6106645104727730$ $\mu_2 = 0.3349133769729255$

Patient pa_8 $\lambda = 72.4635991045300470$ $\delta_T = 0.1841155797175370$ $\beta = 0.0007394551099452$ $\mu_1 = 1.0537000000000001$ $k = 6.9008108987446164$ $\mu_2 = 0.3845808819584701$

Patient pa_10 $\lambda = 117.2810831471476300$ $\delta_T = 0.1525813697842263$ $\beta = 0.0000415717722124$ $\mu_1 = 0.5315000000000000$ $k = 16.9338333596265510$ $\mu_2 = 0.3564434330432689$

Patient pa_13 $\lambda = 43.2603737796453630$ $\delta_T = 0.1980028036690134$ $\beta = 0.0014961695065872$ $\mu_1 = 0.6526000000000000$ $k = 0.0087237030026186$ $\mu_2 = 0.2784742989866295$

Patient pa_24 $\lambda = 118.3944765066074500$ $\delta_T = 0.3494973739820475$ $\beta = 0.0000484570236368$
$\mu_1 = 0.4511000000000000$ $k = 9.1057495433492903$ $\mu_2 = 0.3718590222853928$

Patient pa_34 $\lambda = 169.7212477179362800$ $\delta_T = 0.4489658853123205$ $\beta = 0.0001301732247592$
$\mu_1 = 0.4607000000000000$ $k = 4.6706068433784020$ $\mu_2 = 0.4924810339778832$

Patient pa_38 $\lambda = 137.6607843710946200$ $\delta_T = 0.4911172096189913$ $\beta = 0.0001765832669711$
$\mu_1 = 0.5892000000000000$ $k = 3.5485606943201660$ $\mu_2 = 0.2886473516225888$

Patient pa_43 $\lambda = 234.4995186440960100$ $\delta_T = 0.6425517170861793$ $\beta = 0.0002931044629164$
$\mu_1 = 0.7370000000000000$ $k = 0.4583934984202140$ $\mu_2 = 0.1987462564206444$

Robustness to precision

The 16 digit precision for the estimates was obtained because the identification procedure computed in Matlab used a 16 digit precision. The estimated biological rates are float numbers because the unique solutions of the system of equations (6.19) and (6.25) used to compute the estimates are produced with a 16 digit precision. As mentioned in the paper, these estimates with full accuracy are used for the simulations.

The output dynamics of the basic HIV model exhibits some robustness to the precision of the estimates. The results for patient pt_1, pt_8 and pa_3 are shown to provide some evidence. The Matlab vpa () command which is a variable-precision floating-point arithmetic function was used to obtain 2 significant digits for the parameters of these patients. The results are as follows:

Patient pt_1

$\lambda = 433$
$\delta_T = 0.99$
$\beta = 0.00041$
$\mu_1 = 1$
$k = 1.7$
$\mu_2 = 0.4$
Patient pt_8 $\lambda = 32$
$\delta_T = 0.12$
$\beta = 0.000022$

$\mu_1 = 0.67$

$k = 166$

$\mu_2 = 1.4$

Patient pa_3 $\lambda = 19$

$\delta_T = 0.057$

$\beta = 0.00018$

$\mu_1 = 0.4$

$k = 25$

$\mu_2 = 0.33$

Fig. B.1, Fig. B.2 and Fig. B.3 show a comparative analysis of the output dynamics produced by the estimates with full precision and the ones with 2 significant digits. These graphs confirm that the output dynamics of the model exhibit some robustness to the precision chosen for the estimates because the trajectories are relatively close to each other.

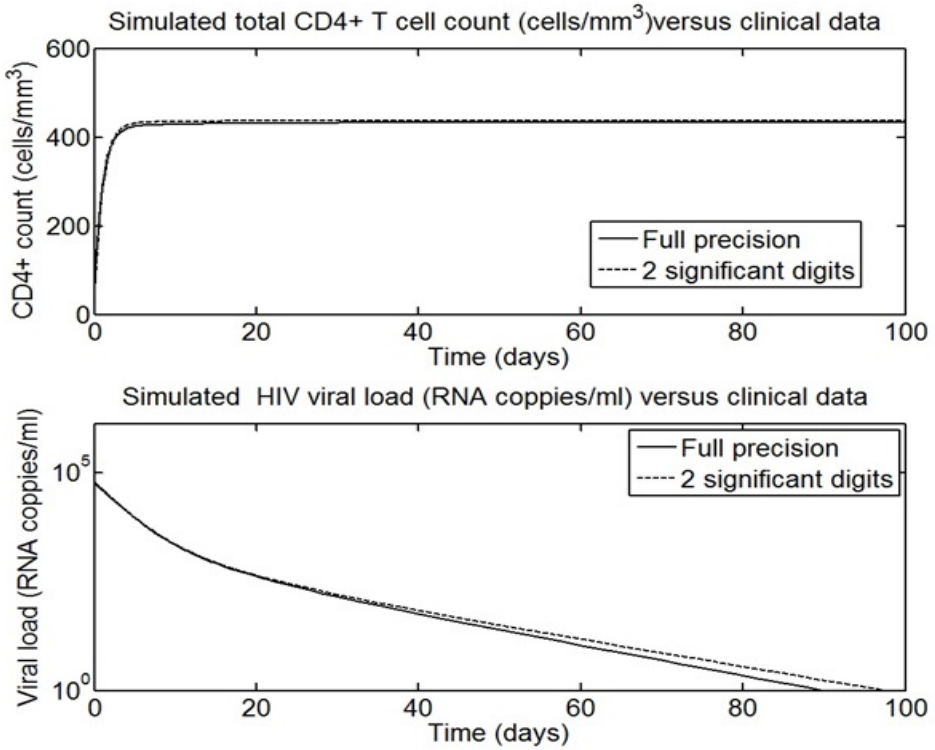

FIGURE B.1: Comparison of the time evolution of the estimated dynamics of CD4+ T cell count and HIV load with different precision. Results for pt_1. l (6.7).

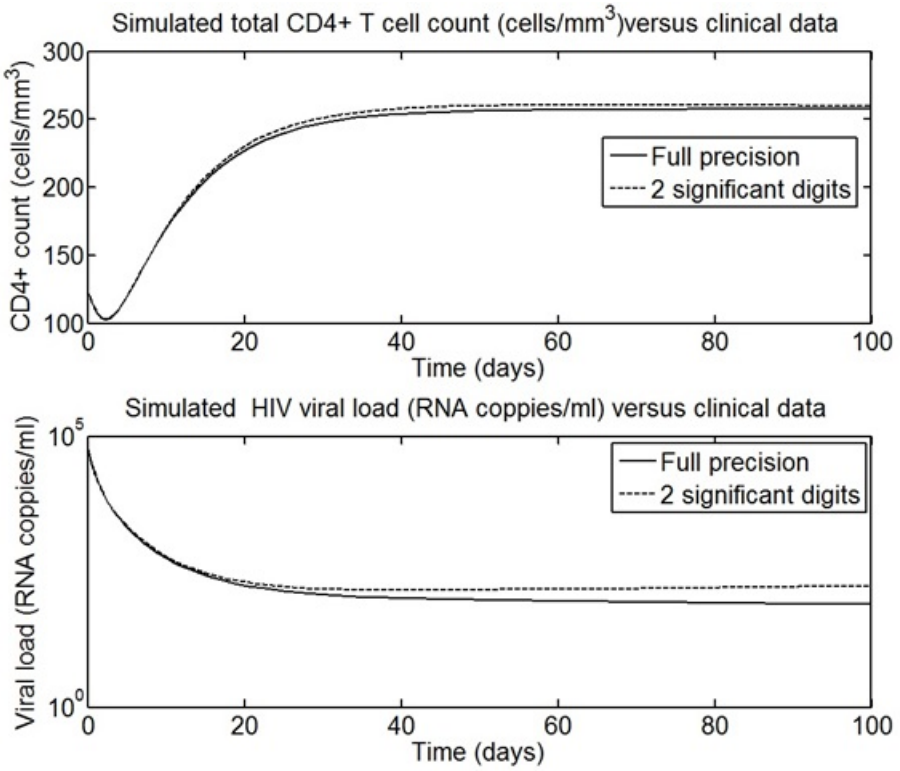

FIGURE B.2: Comparison of the time evolution of the estimated dynamics of CD4+ T cell count and HIV load with different precision. Results for pt_8. l (6.7).

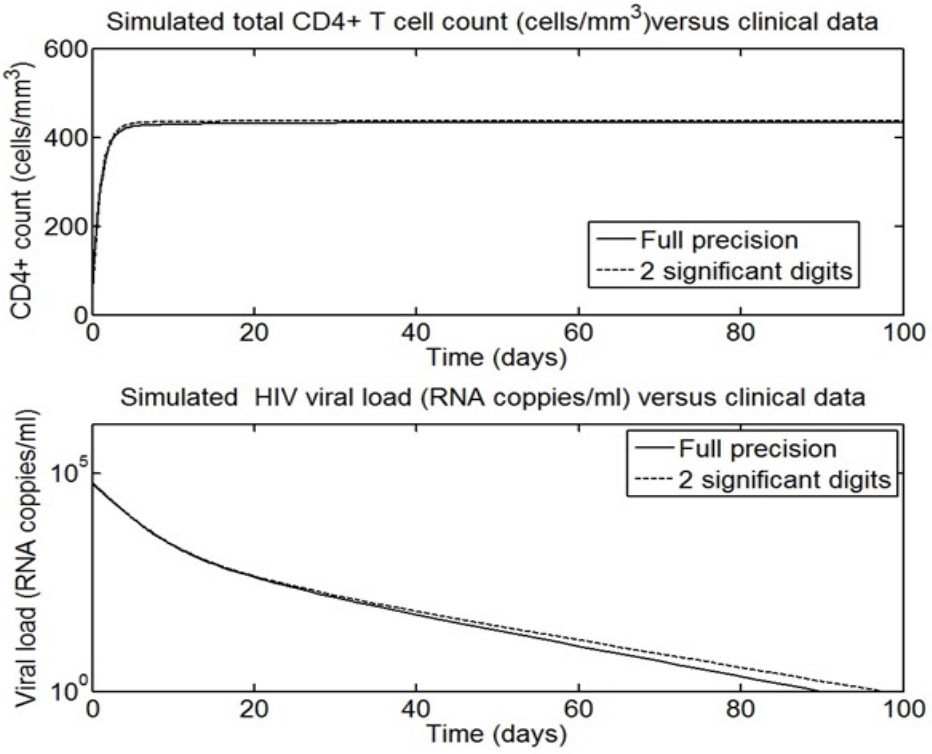

FIGURE B.3: Comparison of the time evolution of the estimated dynamics of CD4+ T cell count and HIV load with different precision. Results for pa_3. l (6.7).

Bibliography

[1] R. J. De Boer, M. Oprea, R. Antia, K. Murali-Krishna, R. Ahmed, and A. S. Perelson, "Recruitment times, proliferation, and apoptosis rates during the cd8+ t-cell response to lymphocytic choriomeningitis virus," *Journal of Virology*, vol. 75, no. 22, pp. 10 663–10 669, 2001. [Online]. Available: http://jvi.asm.org/content/75/22/10663.abstract

[2] E. West, B. Youngblood, W. Tan, H. Jin, K. Araki, G. Alexe, B. Konieczny, S. Calpe, G. Freeman, C. Terhorst, W. Haining, and R. Ahmed, "Tight regulation of memory cd8+ t cells limits their effectiveness during sustained high viral load," *Immunity*, vol. 35, no. 2, pp. 285 – 298, 2011.

[3] G. Franklin, J. Powell, and A. Emami-Naeini, *Feedback control of dynamic systems*, ser. Alternative Etext Formats. Pearson, 2010, no. v. 10. [Online]. Available: https://books.google.co.uk/books?id=J-spAQAAMAAJ

[4] H. Shanechi, "Continuous and discrete control systems modeling, identification, design, and implementation, john dorsey, 2002, mcgraw hill, new york, 727 pages. isbn 0-07-248308-3," *International Journal of Adaptive Control and Signal Processing*, vol. 18, no. 5, pp. 487–488, 2004. [Online]. Available: http://dx.doi.org/10.1002/acs.818

[5] N. S. Nise, *Control systems engineering /*, 6th ed. Singapore :: Wiley (Asia) Pte,, c2011., previous ed.: Hoboken, N.J., c2008.

[6] V. I. Utkin, *Sliding modes and their application to variable structure systems.* Moscow: MIR Publication House, 1978.

[7] V. Utkin, "Variable structure system with sliding mode," *IEEE Trans. on Control Systems Technology*, vol. 10, no. 6, pp. 780–792, 1977.

[8] J. Y. Hung, W. Gao, and J. C. Hung, "Variable structure control: A survey," *IEEE Trans. on Industrial Electronics*, vol. 40, no. 1, pp. 2–22, 1993.

[9] N. Burroughs, B. Oliveira, A. Pinto, and H. Sequeira, "Sensibility of the quorum growth thresholds controlling local immune responses. math. comput." *Math. Comput. Model.*, vol. 47, p. 714725, 2008.

[10] C. Edwards and S. K. Spurgeon, *Sliding mode control: theory and applications*. CRC Press, 1998.

[11] W. Chen and M. Saif, "Adaptive actuator fault detection, isolation and accommodation in uncertain systems," *Int. J. Control*, vol. 80, no. 1, pp. 45–63, 2007.

[12] M. Blanke, M. Kinnaert, J. Lunze, and M. Staroswiecki, *Diagnosis and Fault-tolerant Control*. Berlin: Springer, 2003.

[13] A. T. Azar and Q. Zhu, *Advances and applications in sliding mode control systems*. Springer, 2015.

[14] J. Slotine and W. Li, "Applied nonlinear control, prentice-hall, englewood cliffs, nj, 1991," 1998.

[15] H.-M. Chen, J.-C. Renn, and J.-P. Su, "Sliding mode control with varying boundary layers for an electro-hydraulic position servo system," *The International Journal of Advanced Manufacturing Technology*, vol. 26, no. 1-2, pp. 117–123, 2005.

[16] lyas Eker, "Second-order sliding mode control with experimental application," {*ISA*} *Transactions*, vol. 49, no. 3, pp. 394 – 405, 2010. [Online]. Available: http://www.sciencedirect.com/science/article/pii/S0019057810000297

[17] V. Utkin and J. Shi, "Integral sliding mode in systems operating under uncertainty conditions," in *Decision and Control, 1996., Proceedings of the 35th IEEE Conference on*, vol. 4, Dec 1996, pp. 4591–4596 vol.4.

[18] H. K. Khalil and J. Grizzle, *Nonlinear systems*. Prentice hall Upper Saddle River, 2002, vol. 3.

[19] C. Edwards, A. Akoachere, and S. K. Spurgeon, "Sliding-mode output feedback controller design using linear matrix inequalities," *IEEE Trans. on Automat. Control*, vol. 46, no. 2, pp. 115–119, 2001.

[20] G. Bartolini, A. Ferrara, E. Usai, and V. Utkin, "On multi-input chattering-free second-order sliding mode control," *Automatic Control, IEEE Transactions on*, vol. 45, no. 9, pp. 1711–1717, 2000.

[21] J. A. Burton and A. S. I. Zinober, "Continuous approximation of variable structure control," *Int. J. Systems Sci.*, vol. 17, pp. 876–885, 1986.

[22] M.-S. Chen, Y.-R. Hwang, and M. Tomizuka, "A state-dependent boundary layer design for sliding mode control," *IEEE Transactions on Automatic Control*, vol. 47, no. 10, pp. 1677–1681, Oct 2002.

[23] H. Lee and V. I. Utkin, "Chattering suppression methods in sliding mode control systems," *Annual Reviews in Control*, vol. 31, no. 2, pp. 179 – 188, 2007. [Online]. Available: http://www.sciencedirect.com/science/article/pii/S1367578807000363

[24] C. Edwards and S. K. Spurgeon, "Sliding mode stabilisation of uncertain systems using only output information," *Int. J. Control*, vol. 62, no. 5, pp. 1129–1144, 1995.

[25] V. I. Utkin and A. S. Poznyak, "Adaptive sliding mode control with application to super-twist algorithm: Equivalent control method," *Automatica*, vol. 49, no. 1, pp. 39 – 47, 2013. [Online]. Available: http://www.sciencedirect.com/science/article/pii/S0005109812004694

[26] C. Edwards, S. K. Spurgeon, and R. G. Hebden, "On the design of sliding mode output feedback controllers," *Int. J. Control*, vol. 76, no. 9, pp. 893–905, 2003.

[27] T. Floquet, C. Edwards, and S. K. Spurgeon, "On unknown input sliding mode observers," in *Proceedings of IEEE International Workshop on Varaibe Structure System-VSS'06*, Sardinia, Italy, 2006.

[28] C. P. Tan and C. Edwards, "Sliding mode observers for robust detection and reconstruction of actuator sensor faults," *Int. J. Robust Nonlinear Control*, vol. 13, no. 5, pp. 443–463, 2003.

[29] R. J. D. Boer and A. S. Perelson, "Quantifying t lymphocyte turnover," *Journal of Theoretical Biology*, vol. 327, no. 0, pp. 45 – 87, 2013.

[30] A. S. Perelson and R. Ribeiro, "Modeling the within-host dynamics of HIV infection," *BMC Biology*, vol. 11, no. 1, p. 96, 2013. [Online]. Available: http://www.biomedcentral.com/1741-7007/11/96

[31] K. Bluestone, J.A. amd Herold and G. Eisenbarth, "Genetics,pathogenesis and clinical interventions intype1diabetes." *Nature*, vol. 464, p. 12931300, 2010.

[32] C. T. Bergstrom and R. Antia, "How do adaptive immune systems control pathogens while avoiding autoimmunity?" *Trends in Ecology & Evolution*, vol. 21, no. 1, pp. 22 – 28, 2006.

[33] A. Arazi, W. F. P. III, R. M. Ribeiro, A. S. Perelson, and N. Hacohen, "Human systems immunology: Hypothesis-based modeling and unbiased data-driven approaches," *Seminars in Immunology*, vol. 25, no. 3, pp. 193 – 200, 2013, system Immunology.

[34] R. M. Ribeiro, L. Qin, L. L. Chavez, D. Li, S. G. Self, and A. S. Perelson, "Estimation of the initial viral growth rate and basic reproductive number during acute HIV-1 infection," *Journal of Virology*, vol. 84, no. 12, pp. 6096–6102, 2010. [Online]. Available: http://jvi.asm.org/content/84/12/6096.abstract

[35] M. A. Stafford, L. COREY, Y. Cao, E. S. Daar, D. D. HO, and A. S. Perelson, "Modeling plasma virus concentration during primary HIV infection," *Journal of Theoretical Biology*, vol. 203, no. 3, pp. 285 – 301, 2000. [Online]. Available: http://www.sciencedirect.com/science/article/pii/S0022519300910762

[36] J. M. Conway and A. S. Perelson, "Post-treatment control of hiv infection," *Proceedings of the National Academy of Sciences*, vol. 112, no. 17, pp. 5467–5472, 2015. [Online]. Available: http://www.pnas.org/content/112/17/5467.abstract

[37] K. Murphy, P. Travers, M. Walport, and C. Janeway, *Janeway's immunobiology*, 8th ed. Garland Science, New York, 2012.

[38] R. Antia, C. Bergstrom, S. S. Pilyungin, S. M. Kaech, and R. Ahmed, "Models of cd8+ responses: 1. what is the antigen-independent proliferation program," *Journal of Theoretical Biology*, vol. 221, no. 4, pp. 585 – 598, 2003.

[39] R. De Boer, D. Homann, and A. S. Perelson, "Different dynamics of cd4+ and cd8+ t cell responses during and after acute lymphocytic choriomeningitis virus infection," *The Journal of Immunology*, vol. 171, no. 8, pp. 3928–3935, 2003.

[40] H. K. Alexander and L. M. Wahl, "Self-tolerance and autoimmunity in a regulatory T cell model," *Bulletin of Mathematical Biology*, vol. 73, no. 1, pp. 33–71, 2011.

[41] F. M. Burnet, *The Clonal Selection Theory of Acquired Immunity.* Cambrige: Cambridge University, 1959.

[42] T. Veiga-Parga, S. Sehrawat, and B. T. Rouse, "Role of regulatory t cells during virus infection," *Immunological reviews*, vol. 255, no. 1, pp. 182–196, 2013.

[43] V. P. Badovinac, K. A. N. Messingham, S. E. Hamilton, and J. T. Harty, "Regulation of CD8+ T cells undergoing primary and secondary responses to infection in the same host," *The Journal of Immunology*, vol. 170, no. 10, pp. 4933–4942, 2003.

[44] S. M. Kaech and R. Ahmed, "Memory CD8+ T cell differentiation: initial antigen encounter triggers a developmental program in naive cells," *Nature immunology*, vol. 2, no. 5, pp. 415–422, 2001.

[45] V. P. Badovinac, B. B. Porter, and J. T. Harty, "Programmed contraction of CD8+ T cells after infection," *Nature immunology*, vol. 3, no. 7, pp. 619–626, 2002.

[46] R. J. D. Boer and A. Perelson, "Towards a general function describing t cell proliferation," *Journal of Theoretical Biology*, vol. 175, no. 4, pp. 567 – 576, 1995.

[47] P. Kim, P. P. Lee, and D. Levy, "Basic principles in modeling adaptive regulation and immunodominance," in *Mathematical Methods and Models in Biomedicine.* Springer, 2013, pp. 33–57.

[48] C. L. Althaus, V. V. Ganusov, and R. J. De Boer, "Dynamics of CD8+ T cell responses during acute and chronic lymphocytic choriomeningitis virus infection," *The Journal of Immunology*, vol. 179, no. 5, pp. 2944–2951, 2007.

[49] C. L. Althaus and R. J. De Boer, "Implications of CTL-Mediated killing of HIV-Infected cells during the non-productive stage of infection," *PLoS ONE*, vol. 6, no. 2, p. e16468, 02 2011.

[50] S. Sakaguchi, N. Sakaguchi, I. M. Asano, M., and M. Toda, "Immunological self-tolerance maintained by activated t-cells expressing il-2 receptor alpha-chains (cd25). breakdown of a single mechanism of self-tolerance causes various autoimmune diseases." *J. Immunol.*, vol. 155, no. 1, p. 11511164, 1995.

[51] S. Iwami, Y. Takeuchi, Y. Miura, T. Sasaki, and T. Kajiwara, "Dynamical properties of autoimmune disease models: tolerance, flare-up, dormancy." *J. of Theoretical Biology*, vol. 246, pp. 646–659, 2007.

[52] S. Iwami, Y. Takeuchi, K. Iwamoto, and M. Naruo, Y.and Yasukawa, "A mathematical designof vector vaccine against autoimmune disease." *J.Theor.Biol.*, vol. 256, p. 382392, 2009.

[53] M. Simonov, R. A. Rawlings, N. Comment, S. E. Reed, X. Shi, and P. W. Nelson, "Modeling adaptive regulatory t-cell dynamics during early hiv infection," *PLoS ONE*, vol. 7, no. 4, p. e33924, 04 2012.

[54] D. S. Callaway and A. S. Perelson, "Hiv-1 infection and low steady state viral loads," *Bulletin of Mathematical Biology*, vol. 64, no. 1, pp. 29–64, 2002.

[55] R. J. De Boer, "Which of our modeling predictions are robust?" *PLoS Comput Biol*, vol. 8, no. 7, p. e1002593, 07 2012. [Online]. Available: http://dx.doi.org/10.1371%2Fjournal.pcbi.1002593

[56] C. L. Althaus and R. J. De Boer, "Implications of ctl-mediated killing of hiv-infected cells during the non-productive stage of infection," *PLoS ONE*, vol. 6, p. e16468, 02 2011.

[57] S. G. Deeks and B. D. Walker, "Human immunodeficiency virus controllers: Mechanisms of durable virus control in the absence of antiretroviral therapy," *Immunity*, vol. 27, no. 3, pp. 406 – 416, 2007. [Online]. Available: http://www.sciencedirect.com/science/article/pii/S1074761307004141

[58] M. Elemans, N.-K. S. Al Basatena, and B. Asquith, "The efficiency of the human CD8+ T cell response: How should we quantify it, what determines it, and does it matter?" *PLoS Comput Biol*, vol. 8, no. 2, p. e1002381, 02 2012.

[59] H. Wu, H. Zhu, H. Miao, and A. S. Perelson, "Parameter identifiability and estimation of HIV/AIDS dynamic models," *Bulletin of mathematical biology*, vol. 70, no. 3, pp. 785–799, 2008.

[60] A. S. Perelson and P. W. Nelson, "Mathematical analysis of HIV-1 dynamics in vivo," *SIAM Review*, vol. 41, pp. 3–44, 1998.

[61] C. J. Fox, P. S. Hammerman, and C. B. Thompson, "Fuel feeds function: energy metabolism and the t-cell response," *Nature Reviews Immunology*, vol. 5, no. 11, pp. 844–852, 2005.

[62] C. Edwards, S. K. Spurgeon, and R. J. Patton, "Sliding mode observers for fault detection and isolation," *Automatica*, vol. 36, no. 4, pp. 541–553, 2000.

[63] B. Xu, M. Sun, and W. Fan, "Dynamic-boundary-layer based nonlinear robust control for robotic systems," in *Electrical and Control Engineering (ICECE), 2010 International Conference on*, June 2010, pp. 5182–5185.

[64] F. Plestan, Y. Shtessel, V. Brgeault, and A. Poznyak, "New methodologies for adaptive sliding mode control," *International Journal of Control*, vol. 83, no. 9, pp. 1907–1919, 2010. [Online]. Available: http://www.tandfonline.com/doi/abs/10.1080/00207179.2010.501385

[65] S. Drakunov and V. Utkin, "Sliding mode observers. tutorial," in *Proc. of 34th IEEE CDC*, vol. 4, New Orleans, LA, 1995, pp. 3376–3378.

[66] C. Edwards and S. K. Spurgeon, "Discussion on: 'a sliding mode observer based FDI scheme for the ship benchmark'," *European Journal of Control*, vol. 6, pp. 585–586, 2000.

[67] A. R. Galimidi and B. R. Barmish, "The constrained Lyapunov problem and its application to robust output feedback stabilization," *IEEE Trans. on Automat. Control*, vol. 31, no. 5, pp. 410–419, 1986.

[68] G. Bartolini, A. Ferrara, and E. Usai, "Chattering avoidance by second-order sliding mode control," *IEEE Trans. on Automat. Control*, vol. 43, no. 2, pp. 241–246, 1998.

[69] J. Murray, *Mathematical Biology.* Springer, Berlin, 1989.

[70] G. Jianguo, L. Yuchao, Z. Jun, and W. Guoqing, "A new nonlinear sliding mode control system design," in *The 27th Chinese Control and Decision Conference (2015 CCDC)*, May 2015, pp. 4490–4493.

[71] P. Brown D., Rothery, *Models in biology: Mathematics, Statistics and computing.* J. Wiley and Sons, 1993.

[72] N. F. Britton, *Essentials of mathematical biology.* Berlin: Spinger, 2003.

[73] R. de Boer, *Theoretical Biology and Bioinformatics.* Utrecht University, 2013.

[74] M. D. Martin, S. A. Condotta, J. T. Harty, and V. P. Badovinac, "Population dynamics of naive and memory cd8 t cell responses after antigen stimulations in

vivo," *The Journal of Immunology*, vol. 188, no. 3, pp. 1255–1265, 2012. [Online]. Available: http://www.jimmunol.org/content/188/3/1255.abstract

[75] M. Elemans, N.-K. S. Al Basatena, N. R. Klatt, C. Gkekas, G. Silvestri, and B. Asquith, "Why don't CD8+ T cells reduce the lifespan of siv-infected cells in vivo?" *PLoS Comput Biol*, vol. 7, no. 9, p. e1002200, 09 2011.

[76] V. Ganusov, "Discriminating between different pathways of memory CD8+ T cell differentiation," *The Journal of Immunology*, vol. 179, no. 8, pp. 5006–5013, 2007.

[77] M. M. Peet, P. S. Kim, and P. P. Lee, "Biological circuit models of immune regulatory response: A decentralized control system." in *CDC-ECE*. IEEE, 2011, pp. 3020–3025.

[78] M. M. Delmastro-Greenwood and J. D. Piganelli, "Changing the energy of an immune response," *American journal of clinical and experimental immunology*, vol. 2, no. 1, p. 30, 2013.

[79] G. J. van der Windt, R. Ahmed *et al.*, "CD8 memory T cells have a bioenergetic advantage that underlies their rapid recall ability," *Proceedings of the National Academy of Sciences*, vol. 110, no. 35, pp. 14 336–14 341, 2013.

[80] M. B. Oldstone, M. Nerenberg, P. Southern, J. Price, and H. Lewicki, "Virus infection triggers insulin-dependent diabetes mellitus in a transgenic model: Role of anti-self (virus) immune response," *Cell*, vol. 65, no. 2, pp. 319 – 331, 1991. [Online]. Available: http://www.sciencedirect.com/science/article/pii/009286749190165U

[81] A. DeFranco, R. Locksley, and M. Robertson, "Immunity: The immune response in infectious and inflammatory disease." *New Science Press Ltd.*, 2007.

[82] K. Blyuss and L. Nicholson, "The role of tunable activation thresholds in the dynamics of autoimmunity," *J. Theor. Bio.*, vol. 308, pp. 45–55, 2012.

[83] J. Bluestone and Q. Tang, "How do cd4+cd25+ regulatory t cells control autoimmunity?" *Curr. Opin. Immunol.*, vol. 17, no. 1, p. 638642, 2005.

[84] A. Toda and C. Piccirillo, "Development and function of naturally occurring cd4+cd25+ regulatory t cells." *J. Leukoc. Biol.*, vol. 80, no. 1, p. 458470, 2006.

[85] S. Yamazaki, K. Inaba, K. Tarbell, and R. Steinman, "Dendritic cells expand antigen-specific foxp3+cd25+cd4+ regulatory t cells including suppressors of alloreactivity." *Immunol. Rev.*, vol. 12, p. 314329, 2006.

[86] K. Wing, Z. Fehervari, and S. Sakaguchi, "Emerging possibilities in the development and function of regulatory t cells." *Int. Immunol.*, vol. 18, no. 1, p. 9911000, 2006.

[87] N. Burroughs, M. Ferreira, B. Oliveira, and A. Pinto, "Autoimmunity arising from bystander proliferation of t cells in an immune response model," *Mathematical and Computer Modelling*, vol. 53, no. 78, pp. 1389 – 1393, 2011, ¡ce:title¿Mathematical Methods and Modelling of Biophysical Phenomena¡/ce:title¿. [Online]. Available: http://www.sciencedirect.com/science/article/pii/S0895717710000385

[88] M. Miyara and S. Sakaguchi, "Natural regulatory t cells: mechanisms of suppression." *TRENDS Mol. Med.*, vol. 132, no. 1, p. 108116, 2004.

[89] N. Misra, J. Bayry, S. Lacroix-Desmazes, M. Kazatchkine, and S. Kaveri, "Cutting edge: human cd4+cd25+ t cells restrain the maturation and antigen-presenting function of dendritic cells." *J. Immunol.*, vol. 172, no. 1, p. 46764680, 2004.

[90] C. Utzny and N. J. Burroughs, "Pertubation theory analysis of competition in a heterogenous population." *Physica D*, vol. 175, pp. 109–126, 2003.

[91] V. Ganusov, D. Barber, and R. De Boer, "Killing of targets by cd8¡sup¿+¡/sup¿ t cells in the mouse spleen follows the law of mass action," *PLoS ONE*, vol. 6, no. 1, p. e15959, 01 2011.

[92] Q. Tang and J. A. Bluestone, "Regulatory t-cell therapy in transplantation: Moving to the clinic," *Cold Spring Harbor Perspectives in Medicine*, vol. 3, no. 11, 2013.

[93] P. S. Kim, P. P. Lee, and D. Levy, "Emergent group dynamics governed by regulatory cells produce a robust primary t cell response," *Bulletin of mathematical biology*, vol. 72, no. 3, pp. 611–644, 2010.

[94] T. C. Wirth, M. D. Martin, G. Starbeck-Miller, J. T. Harty, and V. P. Badovinac, "Secondary cd8+ t-cell responses are controlled by systemic inflammation," *European Journal of Immunology*, vol. 41, no. 5, pp. 1321–1333, 2011.

[95] T. C. Wirth, J. T. Harty, and V. P. Badovinac, "Modulating numbers and phenotype of CD8+ T cells in secondary immune responses," *European journal of immunology*, vol. 40, no. 7, pp. 1916–1926, 2010.

[96] M. A. Nowak and C. R. M. Bangham, "Population dynamics of immune responses to persistent viruses," *Science*, vol. 272, no. 5258, pp. 74–79, 1996.

[97] B. B. Porter and J. T. Harty, "The onset of cd8+-t-cell contraction is influenced by the peak of listeria monocytogenes infection and antigen display," *Infection and Immunity*, vol. 74, no. 3, pp. 1528–1536, 2006.

[98] L. Jones and A. Perelson, "Opportunistic infection as a cause of transient viremia in chronically infected hiv patients under treatment with haart," *Bulletin of Mathematical Biology*, vol. 67, no. 6, pp. 1227 – 1251, 2005.

[99] B. Kohler, "Mathematically modeling dynamics of t cell responses: Predictions concerning the generation of memory cells," *Journal of Theoretical Biology*, vol. 245, no. 4, pp. 669 – 676, 2007.

[100] G. Bocharov, B. Ludewig, A. Bertoletti, P. Klenerman, T. Junt, P. Krebs, T. Luzyanina, C. Fraser, and R. M. Anderson, "Underwhelming the immune response: Effect of slow virus growth on CD8+-T-Lymphocyte responses," *Journal of Virology*, vol. 78, no. 5, pp. 2247–2254, 2004.

[101] B. Aloliwi and H. K. Khalil, "Robust adaptive output feedback control of nonlinear systems without persistence of excitation," *Automatica*, vol. 33, no. 11, pp. 2025–2032, 1997.

[102] G. B. Stan, F. Belmudes, R. Fonteneau, F. Zeggwagh, M.-A. Lefebvre, C. Michelet, and D. Ernst, "Modelling the influence of activation-induced apoptosis of CD4+ and CD8+ T-cells on the immune system response of a hiv-infected patient," *Systems Biology, IET*, vol. 2, no. 2, pp. 94–102, March 2008.

[103] J. M. Grayson, L. E. Harrington, J. G. Lanier, E. J. Wherry, and R. Ahmed, "Differential sensitivity of naive and memory CD8+ T cells to apoptosis in vivo," *The Journal of Immunology*, vol. 169, no. 7, pp. 3760–3770, 2002.

[104] H. K. Khalil, *Nonlinear Systems* (Third Edition). New Jersey: Prentice Hall, Inc., 2002.

[105] M. F. Chevalier and L. Weiss, "The split personality of regulatory t cells in hiv infection," *Blood*, vol. 121, no. 1, pp. 29–37, 2013.

[106] A. Y. Rudensky, "Regulatory t cells and foxp3," *Immunological Reviews*, vol. 241, no. 1, pp. 260–268, 2011. [Online]. Available: http://dx.doi.org/10.1111/j.1600-065X.2011.01018.x

[107] N. J. oughs, B. Oliveira, and A. A. Pinto, "Regulatory t cell adjustment of quorum growth thresholds and the control of local immune responses," *Journal of Theoretical Biology*, vol. 241, no. 1, pp. 134 – 141, 2006. [Online]. Available: http://www.sciencedirect.com/science/article/pii/S0022519305004959

[108] R. E. Billingham, L. Brent, P. B. Medawar *et al.*, "Actively acquired tolerance'of foreign cells." *Nature*, vol. 172, pp. 603–6, 1953.

[109] S. R. Guehler, R. J. Finch, J. A. Bluestone, and T. A. Barrett, "Increased threshold for tcr-mediated signaling controls self reactivity of intraepithelial lymphocytes," *The Journal of Immunology*, vol. 160, no. 11, pp. 5341–5346, 1998.

[110] M. A. Gronski, J. M. Boulter, D. Moskophidis, L. T. Nguyen, K. Holmberg, A. R. Elford, E. K. Deenick, H. O. Kim, J. M. Penninger, B. Odermatt *et al.*, "Tcr affinity and negative regulation limit autoimmunity," *Nature medicine*, vol. 10, no. 11, pp. 1234–1239, 2004.

[111] D. V. Prasad, S. Richards, X. M. Mai, and C. Dong, "B7s1, a novel {B7} family member that negatively regulates t cell activation," *Immunity*, vol. 18, no. 6, pp. 863 – 873, 2003. [Online]. Available: http://www.sciencedirect.com/science/article/pii/S107476130300147X

[112] J. Borghans, R. deBoer, E. Sercarz, and V. Kumar, "T cell vaccination and experimental autoimmune encephalomyelitis: a mathematical model." *J. Immunol.*, vol. 161, p. 10871093, 1998.

[113] M. S. Anderson and J. A. Bluestone, "The nod mouse: a model of immune dysregulation," *Annu. Rev. Immunol.*, vol. 23, pp. 447–485, 2005.

[114] F. S. Wong, I. Visintin, L. Wen, R. A. Flavell, and C. A. Janeway, "Cd8 t cell clones from young nonobese diabetic (nod) islets can transfer rapid onset of diabetes in nod mice in the absence of cd4 cells." *The Journal of experimental medicine*, vol. 183, no. 1, pp. 67–76, 1996.

[115] A. D. Bitmansour, D. C. Douek, V. C. Maino, and L. J. Picker, "Direct ex vivo analysis of human cd4+ memory t cell activation requirements at the single clonotype level," *The Journal of Immunology*, vol. 169, no. 3, pp. 1207–1218, 2002. [Online]. Available: http://www.jimmunol.org/content/169/3/1207.abstract

[116] H. Smith and P. D. Leenheer, "Virus Dynamics: A Global Analysis," *SIAM J. Appl. Math*, vol. 63, no. 4, pp. 1313–1327, 2003.

[117] L. B. Nicholson, A. C. Anderson, and V. K. Kuchroo, "Tuning t cell activation threshold and effector function with cross-reactive peptide ligands," *International immunology*, vol. 12, no. 2, pp. 205–213, 2000.

[118] D. M. Fields, B.N. Knipe, Ed., *Fields virology*, 5th ed. Philadelphia: Wolters Kluwer Health/Lippincott Williams & Wilkins, c2007, vol. 2, 2107-2214.

[119] N. Smith, P. Mlcochova, S. Watters, M. Aasa-Chapman, N. Rabin, S. Moore, S. Edwards, J. Garson, P. Grant, R. Ferns, A. Kashuba, N. Mayor, J. Schellekens, S. Marsh, A. McMichael, A. Perelson, D. Pillay, N. Goonetilleke, and R. Gupta, "Proof-of-principle for immune control of global hiv-1 reactivation in vivo," *Clinical Infectious Diseases*, 2015. [Online]. Available: http://cid.oxfordjournals.org/content/early/2015/03/16/cid.civ219.abstract

[120] X. Wei, S. K. Ghosh, M. E. Taylor, V. A. Johnson, E. A. Emini, P. Deutsch, J. D. Lifson, S. Bonhoeker, M. A. Nowak, and B. H. Hahn, "Viral dynamics in human immunodeficiency virus type 1 infection." *Nature*, vol. 373, pp. 117–122, 1995.

[121] R. M. Ribeiro, N. M. Dixit, and A. S. Perelson, "13 modelling the in vivo growth rate of hiv: implications for vaccination," in *Multidisciplinary Approaches to Theory in Medicine*, ser. Studies in Multidisciplinarity, R. Paton and L. A. McNamara, Eds. Elsevier, 2005, vol. 3, pp. 231 – 246. [Online]. Available: http://www.sciencedirect.com/science/article/pii/S1571083106800171

[122] R. J. De Boer, "Understanding the failure of cd8+ t-cell vaccination against simian/human immunodeficiency virus," *Journal of Virology*, vol. 81, no. 6, pp. 2838–2848, 2007.

[123] D. E. Kirschner and G. F. Webb, "A mathematical model of combined drug therapy of HIV infection," *Journal of Theoretical Medecine*, vol. 1, no. 1, pp. 25 – 34, 1997.

[124] H. Chang, H. Shim, and J. Seo, "Control of immune response of hiv infection model by gradual reduction of drug dose," in *Decision and Control, 2004. CDC. 43rd IEEE Conference on*, vol. 1, Dec 2004, pp. 1048–1054 Vol.1.

[125] H.-D. Kwon, "Optimal treatment strategies derived from a {HIV} model with drug-resistant mutants," *Applied Mathematics and Computation*, vol. 188, no. 2, pp. 1193 – 1204, 2007. [Online]. Available: http://www.sciencedirect.com/science/article/pii/S0096300306014639

[126] R. Zurakowski and A. R. Teel, "A model predictive control based scheduling method for HIV therapy," *Journal of Theoretical Biology*, vol. 238, no. 2, pp. 368 – 382, 2006. [Online]. Available: http://www.sciencedirect.com/science/article/pii/S0022519305002067

[127] H. Chang and A. Astolfi, "Immune response enhancement via controlled drug scheduling," in *Decision and Control, 2007 46th IEEE Conference on*, 2007, pp. 3919–3924.

[128] B. Costa and J. Lemos, "Nonlinear feedback control of a HIV-1 infection model," in *Control Automation (MED), 2011 19th Mediterranean Conference on*, June 2011, pp. 79–84.

[129] M. Brandt and G. Chen, "Feedback control of a biodynamical model of hiv-1," *Biomedical Engineering, IEEE Transactions on*, vol. 48, no. 7, pp. 754–759, July 2001.

[130] S. Sam Ge, Z. Tian, and T. Lee, "Nonlinear control of a dynamic model of HIV-1," *Biomedical Engineering, IEEE Transactions on*, vol. 52, no. 3, pp. 353–361, March 2005.

[131] F. A. Alazabi and M. A. Zohdy, "Nonlinear uncertain hiv-1 model controller by using control lyapunov function," *International J. of Modern Nonlinear Theory and App.*, vol. 1, pp. 33 – 39, 2012.

[132] A. L. Knorr and R. Srivastava, "Evaluation of HIV-1 kinetic models using quantitative discrimination analysis," *Bioinformatics*, vol. 21, no. 8, pp. 1668–1677, 2005. [Online]. Available: http://bioinformatics.oxfordjournals.org/content/21/8/1668.abstract

[133] F. Menezes Campello de Souza, "Modeling the dynamics of hiv-1 and cd4 and cd8 lymphocytes," *Engineering in Medicine and Biology Magazine, IEEE*, vol. 18, no. 1, pp. 21–24, Jan 1999.

[134] M. Brandt and G. Chen, "Feedback control of a biodynamical model of hiv-1," *Biomedical Engineering, IEEE Transactions on*, vol. 48, no. 7, pp. 754–759, 2001.

[135] G. E. L. van den Berk, P. H. J. Frissen, R. M. Regez, and P. J. G. M. Rietra, "Evaluation of the rapid immunoassay determine hiv 1/2 for detection of antibodies to human immunodeficiency virus types 1 and 2," *Journal of Clinical Microbiology*, vol. 41, no. 8, pp. 3868–3869, 2003. [Online]. Available: http://jcm.asm.org/content/41/8/3868.abstract

[136] M. R. Zarrabi, M. H. Farahi, and S. Effati, "Using sliding mode control in stability treatment of HIV disease," *Advanced Modeling and Optimization*, vol. 14, no. 1, pp. 165–173, February 2012.

[137] X. Xia, "Estimation of HIV/AIDS parameters," *Automatica*, vol. 39, no. 11, pp. 1983 – 1988, 2003. [Online]. Available: http://www.sciencedirect.com/science/article/pii/S0005109803002206

[138] H. Wu, "Statistical methods for HIV dynamic studies in AIDS clinical trials," *Statistical Methods in Medical Research*, vol. 14, no. 2, pp. 171–192, 2005.

[139] S. Gadhamsetty, A. Mare, J. Beltman, and de Boer R.J., "A general functional response of cytotoxic T lymphocyte-mediated killing of target cells," *Biophysical Journal*, vol. 106, no. 8, pp. 1780 – 1791, 2014.

[140] V. Müller, A. F. M. Marée, and R. J. De Boer, "Small variations in multiple parameters account for wide variations in HIV –1 set–points: a novel modelling approach," *Proceedings of the Royal Society of London B: Biological Sciences*, vol. 268, no. 1464, pp. 235–242, 2001.

[141] A. M. Jeffrey and X. Xia, *Identifiability of HIV/AIDS model In: W.Y. Tan, H. Wu (Eds.), Deterministic and Stochastic Models of AIDS Epidemics and HIV Infections with Intervention.* Singapore: World Scientific, 2005.

[142] N. K. Vaidya, R. M. Ribeiro, C. J. Miller, and A. S. Perelson, "Viral dynamics during primary simian immunodeficiency virus infection: Effect of time-dependent virus infectivity," *Journal of Virology*, vol. 84, no. 9, pp. 4302–4310, 2010.

[143] E. Hernandez-Vargas and R. Middleton, "Modeling the three stages in {HIV} infection," *J. Theo. Bio.*, vol. 320, no. 0, pp. 33 – 40, 2013.

[144] R. Kaul, F. A. Plummer, J. Kimani, T. Dong, P. Kiama, T. Rostron, E. Njagi, K. S. MacDonald, J. J. Bwayo, A. J. McMichael, and S. L. Rowland-Jones, "Hiv-1-specific mucosal CD8+ lymphocyte responses in the cervix of hiv-1-resistant prostitutes in nairobi," *The Journal of Immunology*, vol. 164, no. 3, pp. 1602–1611, 2000.

[145] J. Murray, *Mathematical Biology.* Springer, Berlin., 1989.

[146] T. C. Friedrich, L. E. Valentine, L. J. Yant, E. G. Rakasz, S. M. Piaskowski, J. R. Furlott, K. L. Weisgrau, B. Burwitz, G. E. May, E. J. León *et al.*, "Subdominant cd8+ t-cell responses are involved in durable control of aids virus replication," *Journal of virology*, vol. 81, no. 7, pp. 3465–3476, 2007.

[147] J. E. Schmitz, M. J. Kuroda, S. Santra, V. G. Sasseville, M. A. Simon, M. A. Lifton, P. Racz, K. Tenner-Racz, M. Dalesandro, B. J. Scallon, J. Ghrayeb, M. A. Forman, D. C. Montefiori, E. P. Rieber, N. L. Letvin, and K. A. Reimann, "Control of viremia in simian immunodeficiency virus infection by cd8+ lymphocytes," *Science*, vol. 283, no. 5403, pp. 857–860, 1999. [Online]. Available: http://science.sciencemag.org/content/283/5403/857

[148] M.-J. Mhawej, C. Brunet-Franois, R. Fonteneau, D. Ernst, V. Ferr, G.-B. Stan, F. Raffi, and C. H. Moog, "Apoptosis characterizes immunological failure of HIV infected patients," *Control Engineering Practice*, vol. 17, no. 7, pp. 798 – 804, 2009.

[149] World Health Organization, "HIV/AIDS fact sheet n 360," http://www.who.int/mediacentre/factsheets/fs360/en/, Tech. Rep., November 2015.

[150] M. M. Lederman, E. Connick, A. Landay, D. R. Kuritzkes, J. Spritzler, M. S. Clair, B. L. Kotzin, L. Fox, M. H. Chiozzi, J. M. Leonard *et al.*, "Immunologic responses associated with 12 weeks of combination antiretroviral therapy consisting of zidovudine, lamivudine, and ritonavir: results of aids clinical trials group protocol 315," *Journal of Infectious Diseases*, vol. 178, no. 1, pp. 70–79, 1998.

[151] H. Chang and A. Astolfi, "Estimation of immune states in HIV dynamics," in *Decision and Control, 2008. CDC 2008. 47th IEEE Conference on*, Dec 2008, pp. 1759–1764.

[152] P. S. Rivadeneira, C. H. Moog, G. B. Stan, V. Costanza, C. Brunet, F. Raffi, V. Ferr, M. J. Mhawej, F. Biafore, D. A. Ouattara, D. Ernst, F. R, and X. Xia, "Mathematical

modeling of HIV dynamics after antiretroviral therapy initiation: a clinical research study," *AIDS Research and Human Retroviruses*, vol. 30, no. 9, pp. 831–834, 2014.

[153] Q. Sun, L. Min, and Y. Kuang, "Global stability of infection-free state and endemic infection state of a modified human immunodeficiency virus infection model," *Systems Biology, IET*, vol. 9, no. 3, pp. 95–103, 2015.

[154] H. Liang, H. Miao, and H. Wu, "Estimation of constant and time-varying dynamic parameters of HIV infection in a nonlinear differential equation model," *The annals of applied statistics*, vol. 4, no. 1, p. 460, 2010.

[155] D. A. Ouattara, M.-J. Mhawej, and C. H. Moog, "Clinical tests of therapeutical failures based on mathematical modeling of the HIV infection," *Automatic Control, IEEE Transactions on*, vol. 53, no. Special Issue, pp. 230–241, Jan 2008.

[156] H. Wu, H. Xue, and A. Kumar, "Numerical discretization-based estimation methods for ordinary differential equation models via penalized spline smoothing with applications in biomedical research," *Biometrics*, vol. 68, no. 2, pp. 344–352, 2012.

[157] D. A. Ouattara, "Mathematical analysis of the HIV-1 infection : parameter estimation, therapies effectiveness and therapeutical failures," in *Engineering in Medicine and Biology Society, 2005. IEEE-EMBS 2005. 27th Annual International Conference of the*, Jan 2005, pp. 821–824.

[158] S. Bonhoeffer, R. M. May, G. M. Shaw, and M. A. Nowak, "Virus dynamics and drug therapy," *Proceedings of the National Academy of Sciences*, vol. 94, no. 13, pp. 6971–6976, 1997.

[159] E. Connick, M. M. Lederman, B. L. Kotzin, J. Spritzler, D. R. Kuritzkes, M. S. Clair, A. D. Sevin, L. Fox, M. H. Chiozzi, J. M. Leonard *et al.*, "Immune reconstitution in the first year of potent antiretroviral therapy and its relationship to virologic response," *Journal of Infectious Diseases*, vol. 181, no. 1, pp. 358–363, 2000.

[160] P. S. Rivadeneira, C. H. Moog, G. B. Stan, C. Brunet, F. Raffi, V. Ferré, V. Costanza, M. J. Mhawej, F. Biafore, D. A. Ouattara *et al.*, "Mathematical modeling of HIV dynamics after antiretroviral therapy initiation: A review," *BioResearch open access*, vol. 3, no. 5, pp. 233–241, 2014.

[161] A. Hartmann, S. Vinga, and J. M. Lemos, "Identification of hiv-1 dynamics - estimating the noise model, constant and time-varying parameters of long-term clinical data," in *Proceedings of the International Conference on Bioinformatics Models, Methods and Algorithms (BIOSTEC 2012)*, 2012, pp. 286–289.

[162] X. Xia, "Brief estimation of HIV/AIDS parameters," *Automatica*, vol. 39, no. 11, pp. 1983–1988, Nov. 2003. [Online]. Available: http://dx.doi.org/10.1016/S0005-1098(03)00220-6

[163] A. S. Perelson, A. U. Neumann, M. Markowitz, J. M. Leonard, and D. D. Ho, "Hiv-1 dynamics in vivo: Virion clearance rate, infected cell life-span, and viral generation time," *Science*, vol. 271, no. 5255, pp. 1582–1586, 1996.

[164] H. Liang and H. Wu, "Parameter estimation for differential equation models using a framework of measurement error in regression models," *Journal of the American Statistical Association*, 2012.

List of Publications

Journal papers

1. **Anelone, Anet J.N., Spurgeon, Sarah K., Modelling and simulation of the dynamics of the antigenspecific T cell response using variable structure control theory, 2016, PLOS ONE 11(11): e0166163. doi: 10.1371/journal.pone.0166163**

Abstract: Experimental and mathematical studies in immunology have revealed that the dynamic response of antigen-specific CD8+ T cells to vigorous infection is regulated by an immune response program. Interestingly, this program can be conveniently modelled using a sigmoidal or a discontinuous function. This paper hypothesizes strong synergies between the immune response program and the variable structure control (VSC) paradigm. This motivate the use of techniques from variable structure control theory to analytically assess the dynamical properties and robustness of the immune response dynamics. In particular, the context of the memory CD8+ T cell response following chronic Lymphocytic Choriomeningitis Virus infection is considered and analytical tools from VSC are utilized to estimate the level of CD4+ T cell help required to sustain the expansion of secondary effector CD8+ T cells. Moreover, a VSC approach is used to predict the dynamics of the CD4+ T cell help mechanism. These results suggest that the magnitude of CD4+ T cell help increases dynamically to sustain CD8+ T cell expansion and to overcome the down-regulation signals induced by antigen persistence and high virus load. Together, the findings demonstrate that studying the immune system using variable structure control theory provides a new framework for to analyse experimental observations and assist design of treatment strategies.

2. **Anelone, Anet J.N., Spurgeon, Sarah K., Prediction of the Containment of HIV Infection by Antiretroviral Therapy - a Variable Structure Control Approach, IET Systems Biology, 2016, DOI: 10.1049/iet-syb.2016.0028**

Abstract: It is demonstrated that the reachability paradigm from Variable Structure Control (VSC) theory is a suitable framework to monitor and predict the progression of the Human Immunodeficiency Virus (HIV) infection following initiation of antiretroviral therapy. A manifold is selected which characterises the desirable infection-free steady state. A model of HIV infection together with an associated reachability analysis which considers the action of antiretroviral drugs is used to formulate a dynamical condition for the containment of HIV infection on the desirable manifold. This condition is tested using data from two different HIV clinical trials which contain measurements of the CD4+ T cell count and HIV load in the peripheral blood collected from HIV infected individuals for the six month period following initiation of antiretroviral therapy. The biological rates of the model are estimated using the multi-point identification method and data points collected in the initial period of the trial. Using the parameter estimates and the numerical solutions of the model, the predictions of the reachability analysis are shown to be consistent with the subsequent clinical diagnosis at the conclusion of the trial. The methodology captures the dynamical characteristics of eventual successful, failed and marginal outcomes. The findings evidence that the reachability analysis is an appropriate tool to monitor and develop personalized antiretroviral treatment.

Conference papers

3. **Anelone, Anet J.N., Orlov, Yury, Spurgeon, Sarah K., Synergies between the dynamics of the immune response of T cells and the variable structure control paradigm, Recent Advances in Sliding Modes (RASM), 2015 International Workshop on , vol., no., pp.1,6, 9-11 April 2015**

Abstract: This paper argues that strong synergies exist between the Variable Structure Control (VSC) paradigm and the dynamical behaviour of the immune response of T cells following vigorous infection. Sharp changes in T cell population kinetics in response to an infection have been revealed by experimental studies. Striking similarities are shown to exist between the phase portrait of a classical VSCS and the phase portrait of an accurate model of the T cell response with an on/off activation function. The robustness properties of the T cell response dynamics described in

current experimental and mathematical studies are evaluated using Lyapanov stability theory and numerical simulations. The findings demonstrate that the T cell dynamics following vigorous infection behave as a closed-loop system under variable structure control. This control law effectively determines the immunological control structure and the metabolic energy regime required to ensure that the dynamics of the responding T cells maintain a healthy state. The VSC paradigm thus provides a mechanism to understand the transition from health to disease.

4. **Anelone, Anet J.N., Oza, Harsal B., Spurgeon, Sarah K., The immune system: A variable structure control perspective, Proceedings of the 19th IFAC World Congress, 24-29 August 2014, Cape Town, South Africa.**

Abstract: A healthy immune system exhibits robustness to disease where the robust stability and performance depends on the immune response mechanism. This paper presents an analysis of the immune system from the viewpoint of variable structure control. The immune response function is regarded as a switch. The influence of candidate personal immune response functions inspired by both experimental and mathematical work from immunology on capturing this crucial dynamics is reviewed. Motivated by this analysis and knowledge of variable structure control, a discontinuous switch which yields more realism and an improvement in the stability and robustness of the immune system has been designed and studied. In particular, surfaces which are functions of immune cell concentrations are identified. These form analogous functions to the well-known sliding mode surfaces which are known to represent a special class of variable structure control. These functions can be seen from the biological viewpoint as system properties which the healthy immune system appears to drive to zero, a well-known characteristic of the sliding mode paradigm.

5. **Anelone, Anet J.N., Orlov, Yury, Spurgeon, Sarah K., Modelling the self-tolerance mechanisms of T cells: An adaptive sliding mode control approach, Control (CONTROL), 2014 UKACC International Conference on, vol., no., pp.573,578, 9-11 July 2014 doi: 10.1109/CONTROL.2014.6915203**

Abstract: The response of the immune system to self or foreign tissues induce dynamics which lead to health or disease. The maintenance of the healthy state by the inhibition of undesirable responses to self-tissues is a key property of the naturally

occurring robust feedback mechanism seen within a healthy immune system. In this paper, Variable Structure Control (VSC) theory is used to design an adaptive sliding mode control to model the observed self-tolerance exhibited by a healthy immune system. A suitable sliding manifold and corresponding reachability condition are formulated based on knowledge of the healthy tolerance steady-state. Unlike existing candidate immune response functions, the proposed control function exhibits robust performance commensurate with the self-tolerance mechanisms of the immune system which have been observed experimentally.